UNIVERSIDAD NACIONAL DE EDUCACIÓN A DISTANCIA

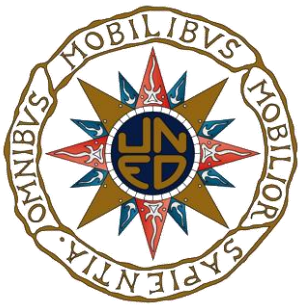

TESIS DOCTORAL

VALORIZACIÓN DEL GLICEROL MEDIANTE PROCESOS CATALIZADOS POR NANOPARTÍCULAS METÁLICAS SOPORTADAS

Esteban Gallegos Suárez

Ldo. en Ciencias Químicas

Departamento de Química Inorgánica y Química Técnica

Facultad de Ciencias

Madrid, 2015

Departamento de Química Inorgánica y Química Técnica
Facultad de Ciencias

VALORIZACIÓN DEL GLICEROL MEDIANTE PROCESOS CATALIZADOS POR NANOPARTÍCULAS METÁLICAS SOPORTADAS

Esteban Gallegos Suárez

Ldo. en Ciencias Químicas

Memoria para optar al grado de
Doctor en Ciencias Químicas,

dirigida por

Dr. D. Antonio Guerrero Ruiz
Catedrático Dpto. De Química Inorgánica y Técnica
Facultad de Ciencias
(UNED)

Dra. Dª. Inmaculada Rodríguez Ramos
Profesora Investigación del Instituto de Catálisis y Petroleoquímica
(CSIC)

Agradecimientos

En primer lugar quiero agradecer enormemente a mis directores de Tesis, la Dra. Inmaculada Rodríguez Ramos y el Dr. Antonio Guerrero Ruiz, por darme la oportunidad de poder realizar esta tesis doctoral en su grupo de investigación. Ellos han sido el pilar de este proyecto y por ello quiero agradecerles la confianza depositada en mí, la cercanía y el trato recibido durante todos estos años que han hecho que me sienta como en casa. Gracias por la paciencia y dedicación prestada en todo momento que han hecho posible que al final esta tesis sea la meta y una gran victoria.

Al Dr. Adolfo Arcoya, por todos los buenos consejos y ánimos que me ha dado y por todos los buenos ratos que hemos pasado a lo largo de estos años. Han sido muchas las conversaciones compartidas durante los desayunos. A la Dra. Belén Bachiller Baeza por su ayuda y por enseñarme la inmensa mayoría de las técnicas experimentales que fueron tan necesarias para el desarrollo de este trabajo.

Quiero agradecer a la Facultad de Ciencias de la Universidad Nacional de Educación a Distancia por la beca de Formación de Profesorado Universitario que me concedieron ya que gracias a la cual he podido desarrollar esta tesis doctoral.

No me puedo olvidar de la gente de la UNED, de los doctores Esther, Eva, María y Jesús. Gracias a todos por ayudarme y por poner cada uno su granito de arena en este proyecto. Han sido muchos los momentos compartidos y de cada uno de vosotros me llevo algún buen recuerdo. Quiero agradecerle especialmente al Dr. Ángel Maroto, el cariño y los sabios consejos que me ha dado en cada una de las visitas a la UNED. Además, agradecerle que me dejase entrar en su grupo “cuarentones” para pasar algún que otro domingo ciclando por aquí y por allá.

Tampoco me puedo olvidar de quienes me introdujeron en el mundo científico cuando andaba por Granada: los doctores Paco Pepe, Agustín y Paco Carrasco. Ellos me abrieron las puertas de este mundo y me “engañaron” para que realizase la tesis doctoral. Sin ellos nunca

hubiese llegado a Madrid. Quiero también dar las gracias a mis dos compañeros de Granada, al mosquetero Juan Francisco y a un gran amigo, Sergio Morales, por tantos buenos ratos que pasamos juntos tanto dentro como fuera del laboratorio. Fuero muchas rumbas las que nos marcamos por aquellos entonces.

Quiero expresar mi más profundo agradecimiento a los compañeros del grupo GDMCH. A los que se fueron o pasaron por aquí como Laura, Ana Belén, Hanane, Nora, Cedric, Pablo, Cecilia y Miguel. De todos guardo un buen recuerdo de su estancia por los laboratorios. Y a los que están por aquí: Mariví (buen recuerdo en Sitges), Alba, Maika, Annie, Wendy y Adrián. Ellos son los que me sufren y me aguantan todos los días, tanto los buenos como los malos. En especial, quiero agradecerle a mi compañero y amigo José Luis el compañerismo y la amistad que me ha brindado todo este tiempo. Han sido muchos almuerzos, muchas alegrías (y no tan buenas) y algún que otro carnaval los que hemos vivido juntos. Sólo nos falta ir a pescar un día a esas playas de Cádiz. Y no me puedo olvidar de mi compañera y amiga María Almohalla. Gracias por cruzarte en mi camino y hacer mi estancia en Madrid más agradable. No podré olvidar las experiencias vividas en los congresos que hemos compartido juntos.

No me puedo olvidar de la gente que me ha rodeado estos años en el trabajo, mi Ana Iglesias, que me ha aconsejado y enseñado multitud de cosas, los compañeros de las comidas y a toda la gente que me ha ayudado, como el grupo de la unidad de apoyo y el taller de mantenimiento. A Laura Pascual por enseñarme con mucha paciencia la microscopía electrónica de transmisión y al Dr. Marcos Fernández por esos días de sincrotrón y por sus clases magistrales enseñándome multitud de cosas tanto químicas como no tan químicas. También quiero agradecerles a Álvaro y Patricio, mis compañeros de quinielas, los momentos compartidos y espero que algún día podamos irnos a tomar una cerveza con el dinero ganado.

Gracias a los dos centros receptores de mis estancias, al Professor Kan Li y al Professor Alexandre Goguet por dejarme entrar en sus laboratorios y darme la oportunidad de conocer a todas las personas que trabajaban por aquellas tierras lejanas. Han sido dos grandes

experiencias que me han hecho madurar tanto científicamente como personalmente y además me llevo muchos amigos que siempre estarán presentes como Smith, Rami, Kevin, Nati, Rebecca, Fadzlie y Lars. Una mención especial tengo que dedicar a mi compañero y amigo el Dr. Francisco García. Poco se puedo decir de Paco, salvo que siga siendo siempre la misma persona que brilla por sí solo.

También quiero dar las gracias a mis amigos porque todos ellos han marcado mi forma de ser y de todos ellos he aprendido multitud de cosas. Gracias al Dr. Espi (me adelantaste en conseguir el título de Dr.) y a Josele, por todos los años de carrera y por aquellas tardes jugando y bebiendo que nunca podré olvidar. A la quilla Anabel, a Susana y al pequeñajo Alejandro, que aunque han llegado más tarde, no por ello se les quiere menos. A mis magníficos cuñados Ana y Pablo. Para ellos no tengo palabras, sólo decirles que nos vemos en el campo base del Everest.

Por último quiero dedicar esta tesis a mi familia, en especial a mis padres que tanto me han dado y enseñado desde pequeño. Gracias a ellos he podido defender esta tesis doctoral. No me puedo olvidar de mi hermano, al que tanto quiero a pesar de que el destino interponga kilómetros entre nosotros. Él me ha enseñado a luchar y sufrir para terminar consiguiendo la victoria. Y por último, la persona más importante y piedra angular de toda esta tesis. Gracias a María por ser esa piedra angular, por ayudarme día a día y por hacer que cada día sea un día especial.

Después de estos cinco años, considero que he aprendido y evolucionado mucho como persona y como científico y eso ha sido gracias a cada uno de los mencionados. Por eso quiero decir una vez más MUCHAS GRACIAS a todos y espero que esto sea el principio de un gran final.

A mis padres,

a mi hermano y

a María

“Lo consiguieron porque no sabían que era imposible”

Jean Cocteau

“La única lucha que se pierde es la que se abandona”

Ernesto *Che* Guevara

Tabla de contenidos

Tabla de contenidos

Capítulo 0

Resumen / summary

Contenido del capítulo

0.1. Resumen

Actualmente los niveles de contaminación generados por el ser humano están llegando a unos límites peligrosos para nuestro planeta. Esta contaminación está provocando el cambio climático, que tiene consecuencias directas en la vida cotidiana de las personas. En este contexto, los combustibles fósiles son un producto indispensable para el confort humano y su uso origina grandes cantidades de residuos contaminantes. Además estos combustibles fósiles no son renovables y existe mucha preocupación por su agotamiento. Por ello se están buscando sustitutos que sean de origen renovable y sostenible. Un buen candidato es el biodiesel, combustible procedente de la biomasa que se obtiene mediante la transesterificación de los ácidos grasos que contienen los aceites vegetales y animales. Pero el uso del biodiesel tiene como principales inconvenientes su precio, que actualmente no es competitivo y el subproducto que se origina (el glicerol) que actualmente no tiene suficientes aplicaciones en el mercado y por ello se almacena.

Por eso, el motivo de esta tesis doctoral se centra en la revalorización del glicerol para dar salida comercial a este subproducto que se puede valorizar y con ello poder abaratar el precio del biodiesel, haciéndolo más competitivo comparado con los combustibles de origen fósil. Dentro de los posibles procesos para transformar el glicerol en productos de mayor valor añadido, en esta tesis nos hemos centrado en dos reacciones en concreto. La hidrogenolisis del glicerol desarrollada en el capítulo 4 y el reformado con vapor de agua que se introduce en el capítulo 5.

La elección de la reacción de hidrogenolisis del glicerol es consecuencia de la importancia de los productos que se obtienen como son el 1,2-propanodiol, el 1,3-propanodiol y el etilenglicol. Estos compuestos tienen sus principales aplicaciones en el campo de la fabricación de polímeros, donde se consumen

cantidades del orden de miles de toneladas por año. Según la bibliografía, la reacción de hidrogenolisis del glicerol es catalizada por metales que sean capaces de activar la molécula del hidrógeno como son el Ni, Ru, Pt y Pd. Además, según el mecanismo de la reacción, la presencia de una fase ácida es favorable en cuanto al aumento de la selectividad y la actividad de la reacción hacia 1,2-propanodiol. Con estos objetivos en mente, en el capítulo 4 de esta tesis doctoral se puede encontrar los resultados más relevantes obtenidos respecto a esta reacción. Para llevar a cabo la reacción se han sintetizado catalizadores de Ru soportados en carbón activo, el cual fue modificado mediante tratamientos ácidos para introducir grupos oxigenados que aportaran acidez al sistema. Además, para evaluar si existen diferencias en la actividad de los catalizadores en función de la sal metálica precursora, se han estudiado las diferencias entre el uso del $RuCl_3 \cdot 3H_2O$ y el $Ru(NO)(NO_3)_3$.

Con el objetivo de comparar los resultados obtenidos y evaluar la influencia del soporte en la reacción, se sintetizaron catalizadores de Ru soportados en grafito de alta superficie, nanotubos de carbono y una zeolita KL. Estos soportes van a introducir modificaciones tanto electrónicas como estructurales en las partículas de Ru, lo cual producirá modificaciones en la actividad y selectividad en la reacción de hidrogenolisis del glicerol. Para confirmar estas modificaciones del Ru, se realizó un estudio detallado de quimisorción de CO acoplado a la microcalorimetría. Esta técnica nos permite identificar la distribución y fortaleza de los sitios activos superficiales ayudando a entender los resultados experimentales obtenidos.

Por otra parte, se ha estudiado la reacción del reformado del glicerol con vapor de agua. Como producto de esta reacción se obtiene el hidrógeno, gas de gran interés actual ya que multitud de expertos coinciden en considerar el hidrógeno como el combustible del futuro para ser usado en las pilas de combustible. Actualmente el hidrógeno se obtiene del reformado del gas natural, pero se están

buscando nuevas materias primas de procedencia renovable y sostenible para producir el hidrógeno. En esta línea, el glicerol reúne los requisitos para ser el precursor de hidrógeno de origen sostenible y renovable.

El reformado con vapor de agua es la reacción que transforma el glicerol en hidrógeno, obteniendo 7 moles de hidrógeno por cada mol de glicerol convertido. Los catalizadores más empleados para esta reacción son los constituidos por una fase activa de Ni soportados en óxidos inorgánicos. El principal problema de estos catalizadores es que sufren fenómenos de sinterización y desactivación por coque. En el capítulo 5 de esta tesis doctoral se han propuesto dos diseños distintos de catalizadores de Ni que pretenden mejorar los ya existentes. En primer lugar se han sintetizados catalizadores de Ni mediante el método de Pechini, incorporando las fases activas en la porosidad que presentan las fibras cerámicas *hollow fibre*. Estas fibras tienen una porosidad característica donde el catalizador ha sido depositado en su interior con el objetivo de controlar el tamaño de partícula. Se ha demostrado que el uso de estos reactores *hollow fibre* mejora la actividad de la reacción comparado con el catalizador operando en el tradicional reactor de lecho fijo.

Por otra parte, se han preparado catalizadores de Ni mediante el método de microemulsión para obtener un óxido mixto Ni-Ce con estructura tipo fluorita. Con esta síntesis se pretende mantener el Ni disperso dentro de la matriz de CeO_2 protegiendo así al Ni a los fenómenos de sinterización. Además se realizó un estudio detallado con ayuda de la microscopía electrónica de transmisión para entender la interacción existente entre ambas fases y comprender la evolución de los residuos de carbono generados tras la reacción del reformado.

0.2. Summary

Nowadays, the environment is being degraded for the pollution produced by the human. The contamination level in the environment is high enough to become a big problem for human's lives. In this context, the use of fossil fuel produces a huge amount of contamination products. Moreover, this fossil fuel is not renewable and it is being depleted. New generation of viable fuels are needed, where biodiesel could be a possible renewable and sustainable alternative. The biodiesel comes from the transesterification of vegetable and animal oils with alcohols using KOH or NaOH as a catalyst. But currently the price of the biodiesel is not competitive with diesel from fossil fuel. Furthermore, byproduct, glycerol, is generated during the biodiesel production process and this compound has not yet enough application in the industry. For that reason the glycerol has to be stored and this could be a further problem.

The motivation of this thesis is focused on developing process for adding value to the glycerol, in order to achieve a competitive price of biodiesel in the market. In the scientific publications are reported several reactions for transforming the glycerol into different valuable products, but in this thesis we are focused on the hydrogenolysis of glycerol (chapter 4) and glycerol steam reforming (chapter 5).

The main products obtained in the hydrogenolysis of glycerol are 1,2-propanediol, 1,3-propanediol and ethylene glycol. These products are typically used to synthesize different kind of polymers, being the requirements of this industry in the order of miles of tons of these products per year. For these reasons, hydrogenolysis of glycerol is an attractive reaction with applied relevance in this context. The catalysts used for this reaction are based on a metal phase that can activate the hydrogen molecule. The main active metals are Ni, Ru, Pd and Pt, but

also the presence of acid functionalities is recommended, in order to improve the activity and selectivity towards 1,2-propanediol. In the chapter 4 of this thesis is summarized the most relevant results obtained related with this topic. The hydrogenolysis of glycerol was done using catalysts based on Ru supported on activated carbon. A nitric acid treatment was performed over some activated carbon supports with the aim of introducing oxygen surface groups, which can exhibit acid character. Furthermore, two different metal precursors ($RuCl_3 \cdot 3H_2O$ and $Ru(NO)(NO_3)_3$) were used to synthetize the catalysts in order to evaluate the influence of these precursors in the catalytic activity.

In addition, aiming to evaluate the influence of the support in the hydrogenolysis of glycerol, high surface area graphite, carbon nanotube and KL zeolite were used as Ru supports. Structural and electronic properties of the Ru particles were modified by interaction with these supports, and the effects of these modifications on the activity and selectivity of the resulting catalysts were evaluated. Moreover, to detect and to determine the influence of the support over the Ru particle, a microcalorimetric study of CO chemisorption over the Ru crystallites was accomplished. This technique provides insights into the nature, number and adsorption strength distribution of surface sites exposed by the Ru catalysts, relating these with the catalytic findings.

Chapter 5 summarizes the results of glycerol steam reforming reaction. The main aim of this reaction is to produce hydrogen from glycerol. Hydrogen is considered by experts an important energy carrier for the near future, because it can be produced from renewable sources and it is reactant for the electricity production in the fuel cells. At present, hydrogen is mainly produced from natural gas by reforming processes, but new sources are being searched to obtain hydrogen from

renewable and sustainable sources. In this perspective, glycerol is revealed as a good source to produce green hydrogen because glycerol comes from biomass.

Glycerol steam reforming reaction produces 7 mol of hydrogen per mol of glycerol using a heterogeneous catalyst. The most popular catalysts used are based on Ni metal phase supported on inorganic oxides. But these catalysts normally suffer of deactivation concerns: by sintering of the Ni particles or by coke depositions. To improve the behavior of Ni catalysts, in this thesis two different approaches for the non-conventional synthesis of catalysts were evaluated. A series of NiO/MgO/CeO_2 materials were synthesized by sol-gel method (Pechini method) with different Ni loading and with the same Ce/Mg ratio. The best catalyst formulation was deposited into the finger-like region and sponge-like region of asymmetric and symmetric hollow fiber supports. When the catalysts are deposited in this specific porosity the Ni particle size can be controller. Also it is demonstrated that the use of the hollow fiber reactor improves the activity of the catalysts compared with traditional fix-bed reactor.

On the other hand, microemulsion method was used to obtain a series of mixed oxide Ni-Ce catalysts with fluorite structure. In these catalysts, Ni is situated in a specific location inside the fluorite structure of the CeO_2 to hinder Ni particles sintering. Also it has been evaluated how the interactions between Ni-Ce phases, studied by transmission electron microscopy and energy dispersive X-ray spectroscopy, take place. Moreover, the evolution of the carbon deposited during reaction was analyzed to understand the influence of these deposits in the catalyst stability.

Capítulo 1

Introducción

Contenido del capítulo

1. Introducción

1.1. Biomasa y biodiésel

A comienzos del siglo XXI se impone la conservación del medio ambiente como objetivo principal de todos los países desarrollados o en vías de desarrollo. Este medio ambiente viene deteriorándose desde mediados del siglo XVIII como una consecuencia de la revolución industrial, donde la acción del ser humano ha generado una gran cantidad de residuos contaminantes. Estos residuos crecen de forma exponencial en los países más desarrollados con el consecuente deterioro de nuestro planeta, el cual ha aumentado hasta límites tan preocupantes que se teme por la supervivencia de la humanidad. Algunas de las consecuencias más impactantes de este gran desarrollo tecnológico e industrial y de nuestra forma de vida, a día de hoy, son el agotamiento de los recursos naturales, el calentamiento global del planeta y los comienzos de un posible cambio climático. Por estas razones existe un gran afán por la investigación y desarrollo de nuevos procesos y sistemas tecnológicos con el objetivo de minimizar y/o reparar el daño continuado que se está realizando a nuestro planeta. Un buen ejemplo es el cambio de los modelos energéticos, donde el desarrollo de energías sostenibles y renovables [1, 2, 3] permitirá la implantación de nuevas fuentes de energía y así sustituir el uso de los combustibles fósiles. Estos, como es bien sabido, son un recurso natural que está en vías de agotamiento y su utilización masiva origina la emisión de una gran cantidad de gases contaminantes, lo que conlleva el deterioro del medioambiente mediante los efectos conocidos como lluvias ácidas, efecto invernadero, disminución de la capa de ozono y más recientemente el cambio climático, por el cual nuestro planeta sufre un sobrecalentamiento. Además la extracción de estos combustibles fósiles provoca una disminución de la cantidad total de carbono existente en la corteza terrestre, así como un gran deterioro e impacto

medioambiental como consecuencia de las grandes infraestructuras necesarias para la extracción del petróleo, que cada vez son más complejas y agresivas para la naturaleza.

Por lo tanto, como resultado de todos los factores expuestos, en la actualidad están emanando nuevas fuentes de energía de origen renovable que pretenden sustituir las fuentes de energía tradicionales que son tan contaminantes. Actualmente del consumo energético mundial solo un 14% proviene de fuentes renovables, el resto procede de los combustibles fósiles y de las centrales nucleares. En este último caso, el inconveniente del uso de las centrales nucleares radica en los residuos radiactivos que se generan, los cuales son difíciles de tratar y/o almacenar y peor aún, en los peligros asociados con estos métodos de obtención de energía, que en ocasiones pueden producir catástrofes mundiales como ocurrió en Chernobyl en 1986 y más recientemente en Fukushima en 2011. Respecto a los combustibles fósiles, además de los problemas de contaminación ya mencionados, hay que sumar que son un recurso natural en proceso de agotamiento donde los datos estadísticos estiman (aunque estos son muy cambiantes) que las reservas naturales durarán 218 años para el carbón, 41 años en el caso del petróleo y 63 años para el gas natural [4].

Con este panorama, los investigadores están planteando y desarrollando nuevas alternativas energéticas para asegurar un futuro limpio y sin escasez de recursos. En este escenario aparece la biomasa como un posible candidato para la sustitución de los combustibles fósiles, ya que la biomasa es un recurso de origen renovable que en su generación consume dióxido de carbono y agua usando como fuente de energía la luz solar y produciendo oxígeno como subproducto [5]. Por tanto el balance total del carbono es neutro, es decir, que el combustible final

procedente de la biomasa al consumirse produce CO_2 que previamente ha sido consumido. Dentro de la biomasa los productos de mayor interés debido a su contenido energético son, por orden decreciente de energía, los terpenos, los aceites vegetales, las ligninas y los azúcares. La abundancia de los terpenos es bastante reducida en la naturaleza, por eso los productos que mayor interés energético adquieren son los aceites vegetales y la lignocelulosa [5,6].

En este sentido los aceites vegetales, conjuntamente con ciertas grasas animales y algunos restos de aceites usados industrialmente, son la materia prima para la industria del biodiésel. Ya en el siglo XIX Rudolf Diésel (1858-1913) creador del motor de combustión interna y del combustible diésel probó como combustible en su motor un aceite vegetal (concretamente el aceite de cacahuete) debido a su alto contenido energético y obtuvo un comportamiento energético al quemar el aceite bastante prometedor. Sin embargo, el principal problema que encontraron en el uso directo de los aceites vegetales es su alta viscosidad, lo que causa problemas de deposición de coque, obturación de los inyectores, problemas de polimerización y/o reacción con los lubricantes del motor, etc. Pero Rudolf, hace ya 100 años, dijo textualmente "*The use of vegetable oils for engine fuels may seem insignificant today. But such oils may in course of time be as important as petroleum and the coal tar products of the present time*" [7]. Para solventar los problemas anteriormente expuestos y poder usar como combustible en los motores de combustión los aceites vegetales y animales, aparece la industria del biodiésel, que transforma los ácidos grasos de origen natural en hidrocarburos similares a los encontrados en el diésel procedente del petróleo. Para obtener este biocombustible se parte de esos aceites, vegetales y animales, que por la reacción de transesterificación con alcoholes de cadena corta (generalmente metanol) y usando catalizadores básicos como NaOH o KOH, produce la reacción para obtener el biodiésel y como subproducto el glicerol [8, 9]

(Esquema 1). El principal problema de esta síntesis es que la presencia de agua o de ácidos grasos libres en el aceite vegetal produce la reacción de saponificación bajando mucho el rendimiento global de la reacción [8].

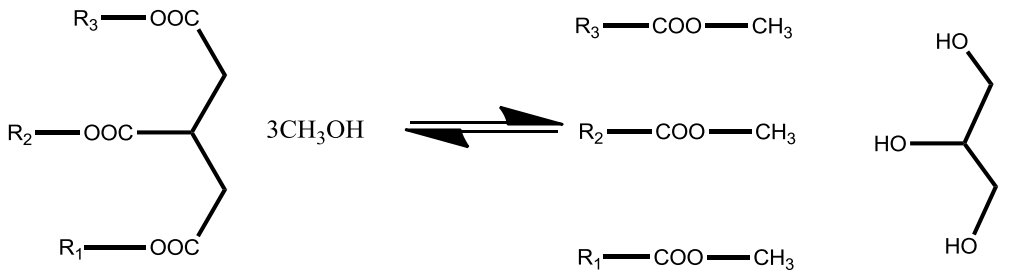

Esquema 1.- Proceso de síntesis de biodiésel

Al comparar la cantidad de energía que genera el biodiésel respecto al diésel procedente del petróleo los resultados obtenidos muestran que es un 10% menor aunque contradictoriamente el biodiésel presenta un índice de cetano mayor que el diésel normal. Concretamente el biodiésel tiene un índice de cetano comprendido entre 51 – 70, pudiendo llegar hasta un valor de 87 en función de la procedencia del aceite vegetal de partida. Por el contrario, el diésel normal tiene un valor comprendido entre 40 y 52, siendo estas diferencias consecuencia de su composición, donde el diésel está compuesto en un 75% de la mezcla por hidrocarburos de 8 a 12 átomos de carbono, siendo la mayoría de los hidrocarburos lineales, ramificados y cicloalcanos, y el 25% restante está formado por compuestos aromáticos. En el caso del biodiésel en su mayoría está compuesto de cadenas lineales con 10 a 24 átomos de carbono [8], donde estos hidrocarburos lineales tienen un mayor contenido en hidrógeno lo que se transforma en un mayor valor energético, pero su mayor viscosidad, como consecuencia de presencia de hidrocarburos más largos, produce que el rendimiento total en el motor de combustión sea menor comparado con el diésel normal.

Pero asumiendo este menor rendimiento energético total del biodiésel, el uso de este biocombustible presenta numerosas ventajas entre las que cabe destacar que los gases emitidos en su combustión contienen menor proporción de monóxido de carbono, que la cantidad de hidrocarburos que no se llegan a quemar en la combustión disminuye drásticamente respecto al diésel normal y que no contienen compuestos sulfurados. Como inconveniente el biodiésel presenta una mayor cantidad de compuestos de óxidos de nitrógeno que son generados en su combustión pero el hecho de no presentar compuestos sulfurados permite el uso de otros catalizadores más eficientes para la eliminación de estos NO_x [4].

Aunque actualmente el precio del barril de petróleo ha caído hasta valores cercanos a 43 $, expertos como el secretario general de la OPEP (Organización de Países Exportadores de Petróleo) estiman que el precio del barril sufrirá un "efecto rebote" llegando a precios cercanos a los 200 $ por barril. Con estos pronósticos el precio del biodiésel, que hoy en día no es competitivo comparado con los combustibles fósiles, puede empezar a competir en el mercado a consecuencia de dicho incremento y más en un futuro donde las reservas de petróleo se agotan y cada vez la extracción del crudo es más compleja y en lugares más inhóspitos . En la Figura 1 observamos esta evolución del precio del barril crudo de petróleo donde existe un constante aumento desde 1994, salvo dos hechos puntuales, el reciente desplome ya mencionado y cuyo alcance temporal es difícil de extrapolar y otro hecho similar ocurrido a finales del 2008 donde hubo otro desplome del precio del barril. Por lo tanto, si se consigue un desarrollo y/u optimización de la tecnología necesaria para la producción de biodiésel y si esta tendencia del aumento del precio del barril de petróleo se produce, el precio del biodiésel podrá ser rentable en un futuro no muy lejano. Hoy día el biodiésel es de 1.5 a 2 veces más caro que el diésel normal, pero con las mejoras del proceso de producción y si

se amplía el campo de materias primas a no solo aceites comestibles, sino a otros aceites como los procedentes de Mahua, Karanja o Jatropha este precio disminuiría considerablemente [4].

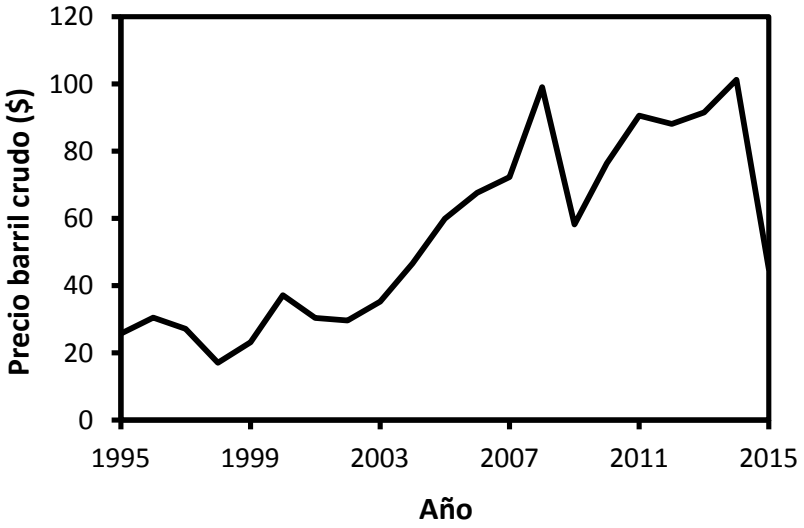

Figura 1.- Precio del barril de crudo (Datos suministrados por NASDAQ)

1.2. Glicerol

El glicerol puede ser una ficha clave en esta disminución del precio del biodiésel. Si repasamos previamente un poco la historia del glicerol, el nombre de glicerol fue dado en 1811 por el químico Michel Eugene Chevreul (Francés) de la palabra griega "*glykos*" que significa dulce. Pero fue el suizo Carl Wilhelm Scheele en 1783 quien descubrió el glicerol cuando estaba tratando unos aceites naturales con materiales alcalinos, obteniéndolo como un subproducto que desechó [10]. Anteriormente a la aparición de la industria del biodiésel, el glicerol se obtenía a partir del propileno (derivado del petróleo) en un proceso que consta de tres etapas y cuyo producto intermedio es la epiclorhidrina, que mediante hidrólisis da lugar al glicerol [11].

El primer uso industrial del glicerol fue para la creación de explosivos como por ejemplo la nitroglicerina. Hoy en día, el glicerol se está usando como sustituto del etilenglicol y sorbitol debido a las analogías en propiedades químicas que presentan estos tres compuestos. Como sustituto del etilenglicol se usa en la industria de los alimentos, en producción de fármacos y en la elaboración de detergentes, cosméticos y anticongelantes. Y como sustituto del sorbitol sus usos más frecuentes son para elaboración de pasta de dientes, conservantes de comida, humectantes y edulcorantes [5]. Esta demanda de glicerol como sustituto del etilenglicol y sorbitol es consecuencia de la disminución de su precio en el mercado internacional, que es una derivación directa de las grandes cantidades de glicerol existentes procedentes de la industria del biodiésel. En la Figura 2 se muestra la producción actual de biodiésel en Estados Unidos y como se puede observar existe

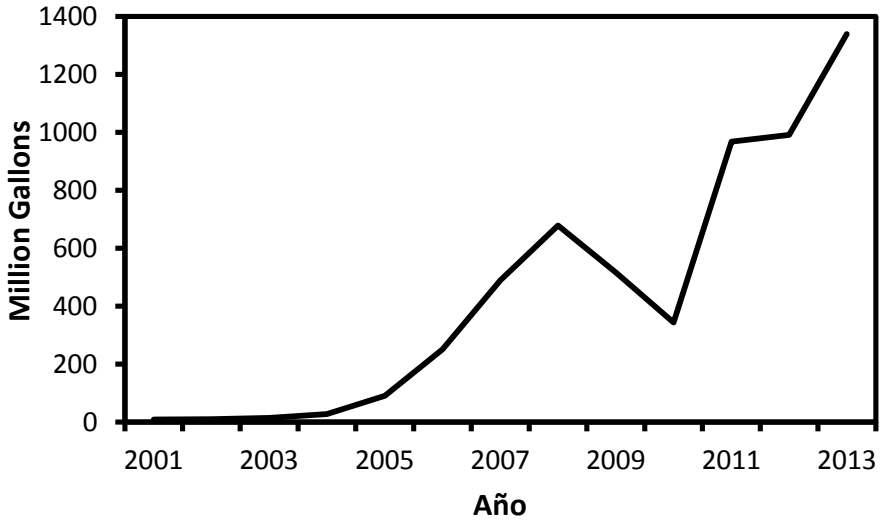

Figura 2.- Producción de biodiésel en U.S.A. (Datos suministrados por US EIA)

un aumento muy acentuado en los últimos años, llegando en 2013 a producirse 1350 millones de galones de biodiésel (5110 millones de litros). Según la estequiometría de esta reacción (esquema 1) existe un rendimiento a glicerol de un

10% en peso, por lo que esto supone millones de toneladas de glicerol crudo disponibles que se almacenan y cuyo refinado para poder ser usado como glicerol puro cuesta del orden de 1 \$ kg^{-1} [12]. Este almacenamiento de glicerol está produciendo que su precio se desplome en los mercados internacionales, de hecho entre los años 2000 y 2005 el precio de la tonelada de glicerol estaba comprendido entre 1130 y 1680 \$, mientras que en el intervalo del 2006 al 2010 el precio descendió a la mitad (entre 560 y 790 \$ por tonelada) [13]. Por eso, un método atractivo para rentabilizar la industria del biodiésel y hacer de este último un sustituto real de los combustibles fósiles es añadir valor al glicerol, subproducto que, como vimos en el esquema 1, es generado tras la transesterificación de los aceites vegetales. De acuerdo con esto, en el mundo científico actual se pueden encontrar multitud de publicaciones que tratan de encontrar nuevas aplicaciones para el glicerol, mediante su transformación en otros productos de mayor valor añadido [14, 15, 16, 17]. En el esquema 2 se recogen las principales rutas de transformación del glicerol. Entre estas rutas catalíticas de valorización del glicerol destaca su oxidación [18] mediante el empleo de catalizadores heterogéneos con el objetivo principal de producir la dihidroxiacetona [19] o el ácido glicérico y el gliceraldehido [20, 21] donde incluso se están aplicando otras técnicas no tan convencionales como son las electrocatalíticas [22] para obtener el ácido glicérico.

Otras rutas importantes son la deshidratación para producir acroleína [10, 23, 24], la eterificación del glicerol para obtener di- o tri-gliceroles [25] o la esterificación, por ejemplo, con ácido acético para obtener el mono- o diacetato de glicerolin [26],o con urea para obtener el glicerol carbonato [27].

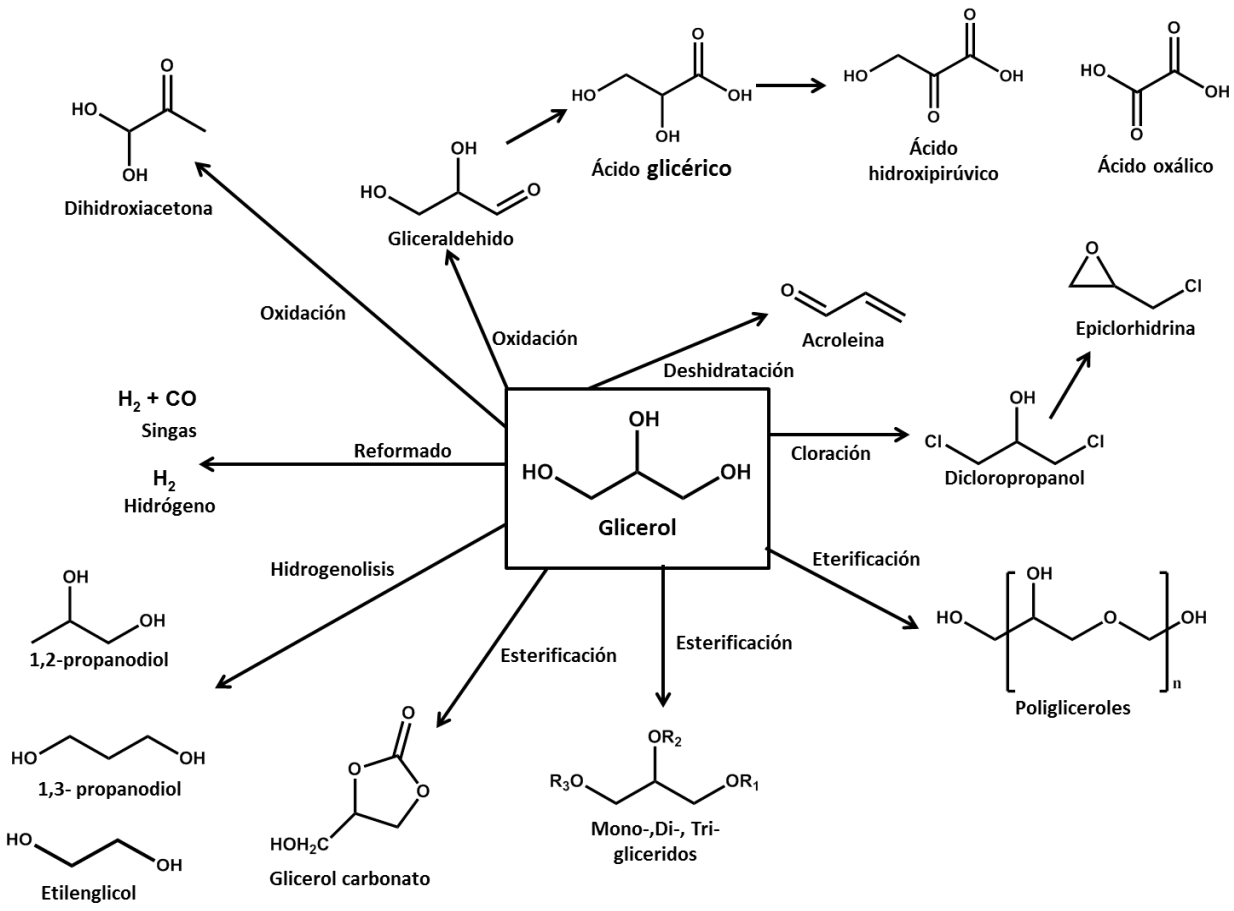

Esquema 2. Posibles rutas catalíticas para la valorización del glicerol.

1.3. Hidrogenolisis del glicerol

Las reacciones de hidrogenolisis constituyen una rama importante de las rutas catalíticas del glicerol, cuyos productos principales son la formación del 1,2-propanodiol (1,2-DPO), 1,3-propanodiol (1,3-PDO) y el producto de ruptura por un enlace carbono-carbono, etilenglicol. Estos compuestos químicos son de gran interés debido a su aplicación en distintos procesos industriales, por ejemplo el 1,3-PDO se usa como monómero de policondensación para la producción de plásticos con propiedades especiales como son el poliéster, poliéteres y poliuretanos. Entre ellos, un plástico que está adquiriendo una gran importancia y que es fabricado por las empresas Shell y DuPont, es el que se obtiene cuando se usa como monómero el 1,3-PDO y se hace reaccionar con el polipropileno

tereftalato, formándose un poliéster biodegradable que presenta un gran potencial para la industria textil y para la fabricación de carpetas. En la actualidad la producción mundial de 1,3-PDO es de 10^5 toneladas por año que se obtiene por hidroformilación del óxido de etileno (derivado del petróleo) [28].

El 1,2-PDO es un reactivo químico no tóxico cuyo principal uso es como compuesto de partida para la fabricación de resinas de poliéster. Otras aplicaciones del 1,2-PDO son como agente anticongelante y como aditivo para la fabricación de pinturas, detergentes líquidos, cosméticos, comidas, etc. La producción mundial de 1,2-PDO es de 1.4 millones de toneladas al año, obteniéndose fundamentalmente mediante la hidratación del óxido de propileno (derivado del petróleo) [29]. Finalmente, el etilenglicol tiene una producción mundial de 7 millones de toneladas al año y se obtiene por hidratación de etileno, siendo sus aplicaciones más destacadas como anticongelante y como materia prima para la síntesis de polietileno tereftalato [29].

Debido a todas las aplicaciones que presentan estos tres compuestos químicos derivados del glicerol es muy importante el desarrollo de nuevos catalizadores para optimizar la reacción de hidrogenolisis del glicerol (Esquema 2). Además el sintetizar estos compuestos mediante dicha reacción significaría obtenerlos mediante materia prima no derivada del petróleo transformando el proceso de producción en un proceso no agresivo para el medioambiente. Si a este factor le añadimos que el glicerol es un subproducto almacenado procedente del biodiésel, su transformación hacia estos compuestos podría abaratar los costes de producción del biodiésel para su posible implantación en la sociedad.

Las reacciones de hidrogenolisis del glicerol se llevan a cabo, generalmente, en presencia de hidrógeno a elevadas presiones (entre 2 y 8 MPa) y a temperaturas

moderadas (393 – 523 K). Por eso los catalizadores que se usan en esta reacción tienen que ser capaces de activar la molécula del hidrógeno. Como es bien conocido, los metales nobles presentan esta capacidad y por ello suelen ser la fase activa más empleada en estas reacciones, siendo los metales más estudiados el Pt, Pd, Ru y Rh depositados en diversidad de soportes. En líneas generales, el Pt y Pd presentan poca actividad para esta reacción, mientras que el Ru presenta un buen comportamiento catalítico [30, 31] siendo el de mejor comportamiento el Rh [32, 33]. El principal problema del uso del Rh es su alto precio 49 \$ g^{-1}, por eso se están desarrollando catalizadores usando como metal noble el rutenio, ya que este presenta un precio mucho más reducido en el mercado de metales preciosos (1.8 \$ g^{-1}).

Aunque aún no se ha establecido un mecanismo de reacción definitivo para la hidrogenolisis del glicerol, el más aceptado para catalizadores monometálicos se basa en una primera etapa de deshidrogenación del glicerol, obteniéndose un producto intermedio que sufre una deshidratación, para finalmente producirse la hidrogenación que da lugar al 1,2-PDO. En el caso de la formación del etilenglicol lo que ocurre es la reacción retro-aldólica con la ruptura del enlace C-C [34]. Pero aún no se ha desarrollado un catalizador monometálico eficaz y para mejorar la actividad algunos autores han introducido cocatalizadores o promotores que modifican tanto la actividad como la selectividad de esta reacción. Están descritas en la bibliografía dos posibles rutas catalíticas alternativas (ruta ácida y ruta básica) para esta reacción que implican el uso de estos cocatalizadores o promotores. Entre los cocatalizadores ácidos usados, los más destacados son el óxido de zirconio sulfonado, zeolitas ácidas, óxido de niobio y sales de heteropoliácidos [35, 36], en el caso de catalizadores sólidos, y la adición en fase homogénea de ácidos como H_2SO_4 o HCl. Pero los mejores cocatalizadores sólidos de tipo ácido descritos son

las resinas de intercambio iónico, como por ejemplo la Amberlite-15 [37, 38]. El principal problema de dicha Amberlite-15 es que no soporta temperaturas elevadas, por ello se están desarrollando nuevas Amberlites, como la Amberlite-70 que presenta una mayor estabilidad térmica, obteniéndose buenos resultados tanto de conversión como en selectividad hacia el 1,2-PDO [39]. El mecanismo más aceptado para la catálisis ácida se fundamenta en una primera etapa de deshidratación, donde el cocatalizador ácido desempeña dicha función, para obtener la acroleína que posteriormente sería hidrogenada sobre los sitios activos del catalizador metálico para obtener el 1,2PDO [40].

En cuanto al empleo de cocatalizadores básicos, se ha estudiado el uso de LiOH, NaOH y CaO junto a catalizadores formados por una fase activa de Ru o Pt soportados en materiales de carbón o en óxido de titanio. Los resultados obtenidos con estos catalizadores, en presencia de las bases, muestran que se mejoran mucho la conversión del glicerol y la selectividad hacia 1,2-PDO. Además disminuyen significativamente la selectividad hacia etilenglicol, siendo el LiOH la base que mejores resultados catalíticos proporciona [41, 42, 43]. En cuanto al mecanismo propuesto para el medio básico, la primera etapa es la deshidrogenación producida por la base, seguido de la deshidratación y posterior hidrogenación para obtener el 1,2-PDO. El principal motivo por el cual se obtienen bajas selectividades hacia el etilenglicol es porque la reacción retro-aldólica no se puede dar en medio básico.

También se han añadido en la formulación de los catalizadores heterogéneos óxidos metálicos junto a los metales nobles. Por ejemplo, a los metales nobles más activos, Rh y Ru, se le han añadido óxidos de los metales de transición como el Mn, V y Zr que empeoran la actividad, mientras que los óxidos de Re, Mo y W la mejoran, siendo el óxido de Re el que mejores propiedades

presenta para la transformación del glicerol en 1,2-PDO y 1,3-PDO [33, 44].

Finalmente se han empleado metales no nobles como Ni, Cu y Co ya que estos metales también son capaces de activar la molécula de hidrógeno, requisito necesario para que se produzca esta reacción. Aunque generalmente estos metales presentan una actividad mucho menor que la que tienen los metales nobles, su menor precio y su mayor resistencia al envenenamiento por impurezas trazas los convierte en catalizadores de gran importancia. Entre estos metales, el Cu es el más empleado ya que tiene una alta selectividad hacia 1,2-PDO, cuando por ejemplo se presenta en catalizadores de cobre-cromita [40], en Cu-ZnO [45] o en sistemas ternarios como Cu/Zn/Al [46].

1.4. Reformado de glicerol con vapor de agua

El reformado de glicerol es una de las rutas catalíticas de valorización del glicerol que más interés está adquiriendo dentro de la comunidad científica cuyo objetivo es la trasformación del glicerol en hidrógeno o gas de síntesis [47, 48, 49]. Dentro de las distintas reacciones posibles, el reformado de glicerol con vapor de agua ("*Glycerol Steam Reforming*") es la reacción que mayor interés ha despertado en la comunidad científica. El principal motivo del auge de esta reacción es porque se obtiene el hidrógeno como producto principal. En este contexto, el hidrógeno es considerado por numerosos expertos como una molécula con un papel muy importante como vector energético en el sector de la energía del futuro [50, 51]. Además el hidrógeno es un reactivo usado en multitud de procesos químicos como por ejemplo la purificación de los combustibles fósiles, la síntesis del amoniaco, la producción de metanol, etc. [52]. El hidrógeno es un combustible limpio que no genera CO_2, lo cual evitaría los problemas de contaminación derivados del CO_2 como son el efecto invernadero y el calentamiento global del planeta. Además el

hidrógeno puede transformarse fácilmente en energía eléctrica mediante las celdas o pilas de combustible siendo el contenido energético del hidrógeno (122 $kJ \cdot g^{-1}$) 2.75 veces superior al que presentan los hidrocarburos [53]. Pero actualmente los principales problemas que presenta el uso del hidrógeno como vector energético son derivados de su obtención, ya que es un compuesto que no existe en la naturaleza en estado puro (su mayor parte está contenido en el agua). Además están los problemas asociados a su transporte y a su almacenamiento. El hidrógeno es un gas muy ligero y difícilmente licuable (en condiciones de temperatura y presión atmosférica) lo que hace que su transporte sea complicado, sobre todo cuando se pretende usar el hidrógeno como combustible para los vehículos. El almacenamiento para uso en automoción requiere de depósitos que soporten alta presión, lo que implica el uso de depósitos que son muy pesados comparados con los tanques de combustibles líquidos que se usan actualmente. Por ello se está desarrollando mucho la tecnología derivada del hidrógeno, por ejemplo en el campo del almacenamiento, donde se están buscando nuevos métodos para almacenarlo [54]. En este sentido se está investigando el uso de recipientes más resistentes y más ligeros, adsorción en hidruros metálicos o como hidrógeno licuado en tanque criogénicos o más recientemente adsorbido en complejos organometálicos [55].

Actualmente el hidrógeno se obtiene mediante el reformado de gas natural (fuente de origen fósil) en un proceso que emplea catalizadores heterogéneos a elevadas temperaturas. Por eso la reacción del reformado de glicerol con vapor de agua tiene un gran interés como consecuencia de la necesidad de encontrar nuevas fuentes de hidrógeno de procedencia limpia, es decir, que no sean contaminantes ni perjudiciales para nuestro planeta. Dentro de las posibles reacciones de reformado de glicerol, el reformado con vapor de agua es la reacción que más cantidad de

hidrógeno produce, siendo la relación producida de 7 moles de hidrógeno por cada mol de glicerol transformado. Normalmente se considera que el proceso consta de dos etapas de reacción. La primera etapa (eq. 1) es conocida como la pirólisis del glicerol, donde la molécula de reactivo se fragmenta para obtener monóxido de carbono e hidrógeno. En una segunda etapa (eq. 2) ocurre la reacción de "*water-gas shift*" donde el monóxido de carbono interacciona con el vapor de agua para obtener hidrógeno y dióxido de carbono. El balance total de la reacción (eq. 3) es la producción de 3 moles de dióxido de carbono y 7 moles de hidrógeno, en un proceso global fuertemente endotérmico.

$$C_3H_8O_3 \rightarrow 3CO + 4H_2 \qquad \Delta H° = 250\,kJ/mol \qquad \text{(eq.1)}$$

$$3CO + 3H_2O \rightarrow 3CO_2 + 3H_2 \qquad \Delta H° = -41\,kJ/mol \qquad \text{(eq.2)}$$

$$C_3H_8O_3 + 3H_2O \rightarrow 3CO_2 + 7H_2 \qquad \Delta H° = 128\,kJ/mol \qquad \text{(eq.3)}$$

Además del reformado de glicerol con vapor de agua, existen otras reacciones que transforman el glicerol en hidrógeno y en gas de síntesis. Las que más destacan son la pirólisis, el reformado acuoso del glicerol ("*Aqueous phase reforming*") y el reformado autotérmico de glicerol, siendo esta última reacción una variante del ya mencionado reformado con vapor de agua.

Si comparamos estas reacciones y empezando por la pirolisis del glicerol, esta consiste en un craqueo térmico en atmósfera libre de oxígeno obteniendo como principales productos el hidrógeno y el monóxido de carbono (gas de síntesis). El principal problema de este proceso es que la reacción es fuertemente endotérmica ($\Delta H° = 250\,kJ/mol$), lo que conlleva la necesidad de un gran aporte energético. Esto supone elevar la temperatura por encima de los 973 K en la mayoría de los casos. Otro gran inconveniente de esta reacción es la aparición de subproductos

procedentes de reacciones de deshidratación de glicerol, como son la hidroxiacetona o 3-hidroxipropanal, o reacciones de deshidrogenación de glicerol donde aparece el gliceraldehido. La presencia de estos compuestos en el medio de reacción combinados con las elevadas temperaturas necesarias para la pirolisis suelen conllevar la formación de coque o depósitos de carbón sólido sobre el catalizador, lo que normalmente es la principal causa de la desactivación en estos sistemas catalíticos [49, 56].

El reformado de glicerol en fase líquida (*Aqueous Phase Reforming*) es una variante que pretende evitar la etapa previa de vaporización del glicerol que se lleva a cabo en el reformado con vapor de agua. Lo que se pretende en este reformado es disminuir el coste energético que conlleva el calentar la disolución de glicerol hasta fase vapor. En términos generales, las condiciones experimentales para esta reacción oscilan entre 453 – 553 K de temperatura de reacción y a una presión comprendida entre 25 – 40 bar [47]. Estas temperaturas son más baja que las típicas usadas para el reformado con vapor de agua (que oscilan entre los 673 – 1073 K) lo que conlleva un gran ahorro energético, pero el sistema de reacción tiene que ser capaz de trabajar a dicha presión lo cual implica un coste adicional. Por otra parte, los catalizadores que se emplean en esta reacción (suelen ser catalizadores de Pt o Ni soportados en alúmina) suelen ser afectados por las condiciones de reacción sufriendo procesos de desactivación por sinterización, reoxidación y/o envenenamiento por adsorción de productos obtenidos por reacciones secundarias. Estas reacciones secundarias hacen que el rendimiento a hidrógeno final sea menor que el obtenido cuando se realiza el reformado con vapor de agua, ya que en estas reacciones secundarias se originan distintos hidrocarburos de hasta 3 átomos de carbono. [57]. Por este motivo, existen estudios para mejorar la actividad y

estabilidad de los catalizadores mediante el control del tamaño de partícula [58] o usando aleaciones y aditivos [59, 60].

Por último hay que mencionar el reformado autotérmico o reformado con oxidación parcial de glicerol como una reciente alternativa para la producción de hidrógeno. En este reformado lo que se realiza es la introducción de oxígeno en cantidades pequeñas para llevar a cabo la combustión parcial del glicerol que es un proceso fuertemente exotérmico. Este calor desprendido en la oxidación parcial ayuda a compensar el aporte energético necesario para llevar a cabo el reformado con vapor de agua. Además con esta oxidación se evita los fenómenos de deposición de coque como consecuencia de la atmósfera oxidante [47]. Pero si comparamos la producción final de hidrógeno respecto al reformado con vapor de agua, el hecho de consumir parte del glicerol para transformarlo en calor, agua y dióxido de carbono hace que el rendimiento final sea menor que el encontrado en el reformado con vapor de agua [48].

Por eso el reformado de glicerol con vapor de agua es la reacción más estudiada ya que el rendimiento hacia hidrógeno es mayor que en el resto de reacciones y es para esta reacción donde se están desarrollando catalizadores cada vez más eficientes. Un análisis más detallado de los catalizadores empleados en la reacción del reformado del glicerol nos muestra que dichos catalizadores están constituidos por una fase activa metálica soportada generalmente sobre óxidos inorgánicos como Al_2O_3, SiO_2, CeO_2, ZrO_2, etc [47, 49]. Los metales que presentan actividad catalítica en esta reacción son, según un orden decreciente de producción de hidrógeno, Rh ≈ Ru > Ni > Ir > Co > Pt > Pd. A pesar de esta clasificación, la mayoría de los estudios realizados se centran en catalizadores basados en níquel y platino debido a las propiedades que presentan estos elementos. En el caso

particular del níquel, este metal tiene la propiedad de ser activo para la disociación de los enlace O-H, C-H y C-C, además de ser activo en la reacción de "*water-gas shift*" para transformar el CO en CO_2 y así producir más hidrógeno. De acuerdo con estas propiedades el níquel disocia la molécula de glicerol mediante un mecanismo que aún no está totalmente definido, pero basado en reacciones sucesivas de deshidrogenación y decarbonilación del glicerol transformándolo en CO e H_2 [61]. El CO producido es convertido en CO_2 mediante especies oxidadas de $Ni(OH)_2$ y/o NiOOH, que existen en la superficie del catalizador, como consecuencia de la reacción con el vapor de agua. Pero los grandes inconvenientes que presenta el níquel son su capacidad para producir metano a partir de la ruptura del enlace C-O en presencia de hidrógeno, la facilidad de sinterización de las partículas metálicas bajando mucho la cantidad de níquel expuesta en superficie para reaccionar y la desactivación por formación de coque y filamentos de carbono [62, 63]. En el caso de los catalizadores de Pt, se ha observado que el glicerol se descompone limpiamente en la superficie del Pt, mediante reacciones sucesivas de deshidrogenación y decarbonilación [48, 64]. Al igual que en el caso del níquel, el Pt presenta buena actividad para la disociación de los enlaces O-H, C-H y C-C. Además el platino presenta una baja actividad para la disociación del enlace C-O en presencia de H_2, evitando así la reacción secundaria de producción de metano o de productos de polimerización resultantes de la reacción de Fischer-Tropsch. El gran inconveniente que presentan estos catalizadores de platino es su baja actividad para la reacción de "*water-gas shift*", lo que conlleva obtener mucho CO, y bajar la producción de hidrógeno de 7 a 4 moles por mol de glicerol transformado. Resulta por tanto el Pt un catalizador más eficiente para producir "*syngas*" que como catalizador de producción de hidrógeno [64]. Un buen sustituto de los catalizadores de Pt, son los catalizadores que usan como fase activa el Ru, ya que

los resultados experimentales realizados con catalizadores de Ru muestran que el Ru presenta las mismas propiedades del Pt respecto a la disociación de los enlaces O-H, C-H y C-C y además es activo para la reacción de *water-gas-shift* [65]. Esto supone elevar el rendimiento de producción de hidrógeno y evitar la producción de CO, que es tan indeseada cuando se pretende usar el hidrógeno en las pilas de combustible.

Respecto a los soportes de los catalizadores, las propiedades ácido-base influyen tanto en la morfología de las partículas metálicas como en la estabilidad del glicerol. En concreto, los soportes con propiedades muy ácidas tienden a producir la deshidratación del glicerol, dando lugar a compuestos que pueden polimerizar y quedar adsorbidos en la superficie del sólido, los cuales tienden a evolucionar formando coque que envenena el sistema catalítico e incluso puede llegar a producir la obstrucción del sistema [64]. Por el contrario, el uso de soportes básicos, como el MgO, tampoco aseguran un mejor comportamiento catalítico, ya que pueden producir dificultades a la hora de la reducción de la fase metálica activa. En concreto se ha reportado que en catalizadores de Ru soportados en MgO, las especies RuO_x son difíciles de reducir siendo inactivas para el reformado de glicerol [66]. Si se compara la estabilidad inducida por un soporte ácido frente a otro de carácter básico se ha descrito que ambos soportes presentan velocidades de desactivación similares. Esto se ha explicado como una posible reducción parcial de los óxidos que facilitan la formación de hidrocarburos indeseados que quedan adsorbidos en la superficie del catalizador evolucionando a distintos compuestos de polimerización, que a su vez son los precursores que originan la formación de coque [67, 68]. Con el fin de mejorar las propiedades de los soportes, existen numerosos estudios donde utilizan soportes dopados con óxidos de cerio, lantano y circonio que reducen la acidez del soporte (generalmente Al_2O_3) mejorando así la

producción global de hidrógeno y la estabilidad del catalizador [69, 70]. Estos óxidos de metales de transición tienen propiedades redox que actúan como fuente de oxigeno mejorando con ello la disociación del agua, disminuyendo la producción de metano, evitando la formación de coque y mejorando la reacción de "*water-gas shift*" [71].

Para mejorar el sistema del reformado del glicerol con vapor de agua se han desarrollado principalmente dos variables. La primera es el uso de adsorbentes para la captura del CO_2 producido. Este concepto se fundamenta en el proceso conocido como "*sorption-enhanced reaction process*"(SERP), que es usado para mejorar el rendimiento y obtener hidrógeno de mayor calidad [72]. Los estudios realizados en reactores de lecho fijo mediante la mezcla física del catalizador y adsorbente (generalmente es el carbonato de calcio o una dolomita) presentan la ventaja de producir hidrógeno más puro (parte del CO_2 es adsorbido) y mejorar el rendimiento por desplazamiento del equilibrio (principio de Le Chatelier). Así como consecuencia de retirar el CO_2 del medio de reacción se produce un desplazamiento del equilibrio de la reacción de "*water-gas shift*" [73, 74]. El gran inconveniente de estos sistemas es que el adsorbente presenta una capacidad de adsorción limitada y una vez saturado los procesos de regeneración son tratamientos térmicos a alta temperatura, que en la mayoría de las ocasiones producen importantes modificaciones estructurales en el catalizador [75].

La segunda variable es la combinación de la reacción del reformado con membranas selectivas de hidrógeno. Hay pocos estudios realizados por el momento en este campo, pero el objetivo es usar las membranas densas de Pd o aleaciones con otros metales para separar y obtener hidrógeno libre de otros productos de la reacción, especialmente libre de CO que no es apto para la

alimentación de las celdas de combustible. A parte de producir hidrógeno puro, otra gran ventaja de usar las membranas de Pd en esta reacción es el desplazamiento de las reacciones que se produce según el principio de Le Chatelier, por retirada de hidrógeno del medio [76]. Este desplazamiento produce un aumento de la actividad de los catalizadores y cambios en la selectividad de la reacción evitando la formación de hidrocarburos que son los precursores del coque [77, 78]. Este coque es uno de los principales motivos de envenenamiento y desactivación de los catalizadores, como ya se ha visto en esta introducción. Pero el inconveniente del uso de las membranas de Pd, a parte del coste de estos sistemas, es que el coque producido durante la reacción también envenena la membrana de Pd y la temperatura de trabajo no puede ser superior a los 773 K ya que temperaturas superiores no son factibles para las membranas de Pd [77, 78, 79]. Por eso la búsqueda de un catalizador que opere a bajas temperaturas y que no genere coque es necesaria para el desarrollo de estos sistemas.

1.5. Bibliografía

[1] Eltawil, M. A.; Zhengming, Z.; Yuan, L. *Renewable and Sustainable Energy Reviews* 2009, 13, 2245.

[2] Baños, R.; Manzano-Agugliaro, F.; Montoya, F. G.; Gil, C.; Alcayde, A.; Gómez, J. *Renewable and Sustainable Energy Reviews* 2011, 15, 1753.

[3] Erdinc, O.; Uzunoglu, M. *Renewable and Sustainable Energy Reviews* 2012, 16, 1412.

[4] Agarwal, A. K. *Progress in Energy and Combustion Science* 2007, 33, 233.

[5] Corma, A.; Iborra, S.; Velty, A. *Chemical Reviews* 2007, 107, 2411.

[6] Huber, G. W.; Iborra, S.; Corma, A. *Chemical Reviews* 2006, 106, 4044.

[7] Meher, L.; Vidyasagar, D.; Naik, S. *Renewable and Sustainable Energy Reviews* 2006, 10, 248.

[8] Issariyakul, T.; Dalai, A. K. *Renewable and Sustainable Energy Reviews* 2014, 31, 446.

[9] Ma, F.; Hanna, M. A. *Bioresource Technology* 1999, 70, 1.

[10] Behr, A.; Eilting, J.; Irawadi, K.; Leschinski, J.; Lindner, F. *Green Chemistry* 2008, 10, 13.

[11] Kent, J. A. *Kent and Riegel's handbook of industrial chemistry and biotechnology*; Eleventh Edition ed.; Springer, 2007; Vol. Volumen 1.

[12] Corma, A.; Huber, G. W.; Sauvanaud, L.; O'Connor, P. *Journal of Catalysis* 2008, 257, 163.

[13] Quispe, C. A. G.; Coronado, C. J. R.; Carvalho Jr, J. A. *Renewable and Sustainable Energy Reviews* 2013, 27, 475.

[14] Zhou, C.-H.; Beltramini, J. N.; Fan, Y.-X.; Lu, G. Q. *Chemical Society Reviews* 2008, 37, 527.

[15] Alonso, D. M.; Wettstein, S. G.; Dumesic, J. A. *Chemical Society Reviews* 2012, 41, 8075.

[16] Zhou, C. H.; Zhao, H.; Tong, D. S.; Wu, L. M.; Yu, W. H. *Catalysis Reviews* 2013, 55, 369.

[17] Serrano-Ruiz, J. C.; Luque, R.; Sepulveda-Escribano, A. *Chemical Society Reviews* 2011, 40, 5266.

[18] Katryniok, B.; Kimura, H.; Skrzynska, E.; Girardon, J.-S.; Fongarland, P.; Capron, M.; Ducoulombier, R.; Mimura, N.; Paul, S.; Dumeignil, F. *Green Chemistry* 2011, 13, 1960.

[19] Liu, S.-S.; Sun, K.-Q.; Xu, B.-Q. *ACS Catalysis* 2014, 4, 2226.

[20] Wu, G.; Wang, X.; Huang, Y. a.; Liu, X.; Zhang, F.; Ding, K.; Yang, X. *Journal of Molecular Catalysis A: Chemical* 2013, 379, 185.

[21] Skrzyńska, E.; Wondołowska-Grabowska, A.; Capron, M.; Dumeignil, F. *Applied Catalysis A: General* 2014, 482, 245.

[22] Kim, H. J.; Lee, J.; Green, S. K.; Huber, G. W.; Kim, W. B. *Chemsuschem* 2014, 7, 1051.

[23] Wang, Z.; Wang, L.; Jiang, Y.; Hunger, M.; Huang, J. *ACS Catalysis* 2014, 4, 1144.

[24] Chai, S.-H.; Wang, H.-P.; Liang, Y.; Xu, B.-Q. *Green Chemistry* 2007, 9, 1130.

[25] Gholami, Z.; Abdullah, A. Z.; Lee, K. T. *Applied Catalysis A: General* 2014, 479, 76.

[26] Liu, X.; Ma, H.; Wu, Y.; Wang, C.; Yang, M.; Yan, P.; Welz-Biermann, U. *Green Chemistry* 2011, 13, 697.

[27] Jagadeeswaraiah, K.; Kumar, C. R.; Prasad, P. S. S.; Loridant, S.; Lingaiah, N. *Applied Catalysis A: General* 2014, 469, 165.

[28] Nakagawa, Y.; Tomishige, K. *Catalysis Science & Technology* 2011, 1, 179.

[29] A. Chauvel , G. L.; TECHNIP, Ed. 1989; Vol. 2, Major oxigenated, chlorinated and nitrated derivatives, p 21

[30] Bolado, S.; Treviño, R. E.; García-Cubero, M. T.; González-Benito, G. *Catalysis Communications* 2010, 12, 122.

[31] Feng, J.; Fu, H.; Wang, J.; Li, R.; Chen, H.; Li, X. *Catalysis Communications* 2008, 9, 1458.

[32] Furikado, I.; Miyazawa, T.; Koso, S.; Shimao, A.; Kunimori, K.; Tomishige, K. *Green Chemystry* 2007, 9, 582

[33] Shinmi, Y.; Koso, S.; Kubota, T.; Nakagawa, Y.; Tomishige, K. *Applied Catalysis B: Environmental* 2010, 94, 318.

[34] Montassier, C.; Ménézo, J. C.; Hoang, L. C.; Renaud, C.; Barbier, J. *Journal of Molecular Catalysis* 1991, 70, 99.

[35] Balaraju, M.; Rekha, V.; Prasad, P. S. S.; Devi, B. L. A. P.; Prasad, R. B. N.; Lingaiah, N. *Applied Catalysis A: General* 2009, 354, 82.

[36] Alhanash, A.; Kozhevnikova, E. F.; Kozhevnikov, I. V. *Catalysis Letters* 2008, 120, 307.

[37] Kusunoki, Y.; Miyazawa, T.; Kunimori, K.; Tomishige, K. *Catalysis Communications* 2005, 6, 645.

[38] Miyazawa, T.; Kusunoki, Y.; Kunimori, K.; Tomishige, K. *Journal of Catalysis* 2006, 240, 213.

[39] Miyazawa, T.; Koso, S.; Kunimori, K.; Tomishige, K. *Applied Catalysis A: General* 2007, 329, 30.

[40] Dasari, M. A.; Kiatsimkul, P.-P.; Sutterlin, W. R.; Suppes, G. J. *Applied Catalysis A: General* 2005, 281, 225.

[41] Feng, J.; Wang, J.; Zhou, Y.; Fu, H.; Chen, H.; Li, X. *Chemistry Letters* 2007, 36, 1274.

[42] Maris, E.; Ketchie, W.; Murayama, M.; Davis, R. *Journal of Catalysis* 2007, 251, 281.

[43] Maris, E.; Davis, R. *Journal of Catalysis* 2007, 249, 328.

[44] Amada, Y.; Watanabe, H.; Tamura, M.; Nakagawa, Y.; Okumura, K.; Tomishige, K. *The Journal of Physical Chemistry C* 2012, 116, 23503.

[45] Wang, S.; Liu, H. *Catalysis Letters* 2007, 117, 62.

[46] Meher, L. C.; Gopinath, R.; Naik, S. N.; Dalai, A. K. *Industrial Engineering Chemistry Research* 2009, 48, 1840.

[47] Lin, Y.-C. *International Journal of Hydrogen Energy* 2013, 38, 2678.

[48] Vaidya, P. D.; Rodrigues, A. E. *Chemical Engineering & Technology* 2009, 32, 1463.

[49] Tran, N. H.; Kannangara, G. S. K. *Chemical Society Reviews* 2013, 42, 9454.

[50] Andrews, J.; Shabani, B. *International Journal of Hydrogen Energy* 2012, 37, 1184.

[51] Veziroğlu, T. N.; Şahi˙n, S. *Energy Conversion and Management* 2008, 49, 1820.

[52] Montini, T.; Singh , R.; Das , P.; Lorenzut, B.; Bertero , N.; Riello, P.; Benedetti, A.; Giambastiani, G.; Bianchini, C.; Zinoviev, S.; Miertus, S.; Fornasiero , P. *Chemsuschem* 2010, 3, 619

[53] Balat, M. *International Journal of Hydrogen Energy* 2008, 33, 4013.

[54] Züttel, A. *Naturwissenschaften* 2004, 91, 157.

[55] Suh, M. P.; Park, H.J.; Prasad, T.; Lim, D.W. *Chemical Reviews* 2012, 112, 782.

[56] Valliyappan, T.; Bakhshi, N. N.; Dalai, A. K. *Bioresource Technology* 2008, 99, 4476.

[57] El Doukkali, M.; Iriondo, A.; Cambra, J. F.; Gandarias, I.; Jalowiecki-Duhamel, L.; Dumeignil, F.; Arias, P. L. *Applied Catalysis A: General* 2014, 472, 80.

[58] Lehnert, K.; Claus, P. *Catalysis Communications* 2008, 9, 2543.

[59] Iriondo, A.; Cambra, J. F.; Barrio, V. L.; Guemez, M. B.; Arias, P. L.; Sanchez-Sanchez, M. C.; Navarro, R. M.; Fierro, J. L. G. *Applied Catalysis B: Environmental* 2011, 106, 83.

[60] Dietrich, P.; Wu, T.; Sumer, A.; Dumesic, J.; Jellinek, J.; Delgass, W. N.; Ribeiro, F.; Miller, J. *Topics in Catalysis* 2013, 56, 1814.

[61] Pompeo, F.; Santori, G. F.; Nichio, N. N. *Catalysis Today* 2011, 172, 183.

[62] Wu, G.; Zhang, C.; Li, S.; Han, Z.; Wang, T.; Ma, X.; Gong, J. *ACS Sustainable Chemistry & Engineering* 2013, 1, 1052.

[63] Vicente, J.; Montero, C.; Ereña, J.; Azkoiti, M. J.; Bilbao, J.; Gayubo, A. G. *International Journal of Hydrogen Energy* 2014, 39, 12586.

[64] Pompeo, F.; Santori, G.; Nichio, N. N. *International Journal of Hydrogen Energy* 2010, 35, 8912.

[65] Grenoble, D.C., Estadt, M.M., Ollis, D.F. *Journal of Catalysis* 1981, 67, 90.

[66] Hirai, T.; Ikenaga, N.-o.; Miyake, T.; Suzuki, T. *Energy & Fuels* 2005, 19, 1761.

[67] Soares, R. R.; Simonetti, D. A.; Dumesic, J. A. *Angewandte Chemie International Edition* 2006, 45, 3982.

[68] Chiodo, V.; Freni, S.; Galvagno, A.; Mondello, N.; Frusteri, F. *Applied Catalysis A: General* 2010, 381, 1.

[69] Montini, T.; Singh , R.; Das , P.; Lorenzut, B.; Bertero , N.; Riello, P.; Benedetti, A.; Giambastiani, G.; Bianchini, C.; Zinoviev, S.; Miertus, S.; Fornasiero , P. *Chemsuschem* 2010, 3, 619.

[70] Iriondo, A.; Barrio, V. L.; Cambra, J. F.; Arias, P. L.; Güemez, M. B.; Navarro, R. M.; Sánchez-Sánchez, M. C.; Fierro, J. L. G. *Topics in Catalysis* 2008, 49, 46.

[71] Zhang, B.; Tang, X.; Li, Y.; Xu, Y.; Shen, W. *International Journal of Hydrogen Energy* 2007, 32, 2367.

[72] Hufton, J. R.; Mayorga, S.; Sircar, S. *AIChE Journal* 1999, 45, 248.

[73] Dou, B.; Dupont, V.; Rickett, G.; Blakeman, N.; Williams, P. T.; Chen, H.; Ding, Y.; Ghadiri, M. *Bioresource Technology* 2009, 100, 3540.

[74] He, L.; Parra, J. M. S.; Blekkan, E. A.; Chen, D. *Energy & Environmental Science* 2010, 3, 1046.

[75] Dou, B.; Rickett, G. L.; Dupont, V.; Williams, P. T.; Chen, H.; Ding, Y.; Ghadiri, M. *Bioresource Technology* 2010, 101, 2436.

[76] Silva, J.M., Soria, M.A., Madeira, L.M. *Journal of Power Sources* 2015, 273, 423.

[77] Lin, K.H., Lin, W.H., Hsiao, C.H., Chang, H.F., Chang, A.C.C. *International Journal of Hydrogen Energy* 2012, 37, 13770.

[78] Chang,, A.C.C., Lin, W.H., Lin, K.H., Hsiao, C.H., Chen, H.H. *International Journal of Hydrogen Energy* 2012, 37, 13110.

[79] Iulianelli, A., Seelam, P.K., Liguori, S., Longo, T., Keiski, R. *International Journal of Hydrogen Energy* 2011, 36, 3827.

Capítulo 2

Objetivos

De acuerdo con la introducción desarrollada el objetivo de esta tesis doctoral es la revalorización del glicerol, un subproducto de la industria del biodiésel que hoy en día se almacena y que representa un futuro problema si la industria del biodiésel evoluciona según los datos previstos. Dentro de la multitud de reacciones posibles para revalorizar el glicerol, en esta tesis doctoral nos hemos centrado en dos reacciones, la hidrogenolisis del glicerol y su reformado con vapor de agua.

En cuanto a la hidrogenolisis del glicerol, los principales objetivos que se han planteado son:

1. Teniendo en cuenta que la reacción de hidrogenolisis del glicerol es sensible a la acidez del sistema en general y del soporte en particular, se ha seleccionado el carbón activado como soporte de la fase activa para modificarlo químicamente mediante tratamientos con ácidos que introducen grupos oxigenados superficiales, los cuales aportan acidez al sistema necesaria para llevar a cabo la reacción. Usando estos soportes, se pretende evaluar la actividad de las nanopartículas de rutenio soportadas, tanto en un carbón activado purificado como en los modificados con la incorporación de centros ácidos, en la citada reacción de hidrogenolisis del glicerol. También se evaluará la importancia del precursor metálico usado en la preparación de los catalizadores de Ru, estudiando la actividad final de las fases activas generadas a partir de dos sales precursoras distintas, el cloruro de rutenio y el nitrosilnitrato de rutenio.

2. También se estudiará la influencia del soporte de los catalizadores de Ru en la hidrogenolisis del glicerol, en cuanto a la importancia que la estructura, la textura y la acidez del soporte tienen en el mecanismo de dicha reacción. Así se pretenden analizar comparativamente diversos soportes con estructuras diferentes como son: un carbón activado con una estructura microporosa turbostratica no

grafitizable y con grupos oxigenados superficiales, un grafito de alta superficie que expone muchos bordes de láminas grafíticas, unos nanotubos de carbono multipared, que presentan carácter electrodonor y que pueden modificar las propiedades electrónicas del metal, y una zeolita básica (KL) con una estructura cristalina bien definida, lo que nos permitirá obtener partículas metálicas con diferentes geometrías y propiedades electrónicas.

En todos los casos se realizará un estudio de caracterización muy exhaustivo mediante la calorimetría de quimisorción de CO, con el fin de conocer los efectos de los diferentes materiales de carbón, de los diversos precursores del Ru y de las posibles disposiciones en la estructura porosa del soporte, sobre la morfología de las nanopartículas metálicas y sus propiedades superficiales. De esta forma obtendremos información de cómo afectan estos parámetros sobre la fortaleza y distribución de los sitios activos metálicos expuestos en la superficies de nuestros catalizadores. También se estudiará cómo afecta la modificación superficial del soporte al introducir grupos oxigenados, sobre el tipo de sitios activos metálicos que se generan.

En cuanto a la reacción del reformado del glicerol con vapor de agua, dado que existen multitud de experimentos realizados con catalizadores de níquel soportados en muy diversos soportes, entre ellos el óxido de cerio, los principales objetivos planteados en esta tesis doctoral son dos:

1. El primero consiste en el uso de un soporte especial como son las fibras cerámicas *hollow fibre*, que poseen una estructura porosa característica, para comparar la acción de un catalizador en un reactor tradicional de lecho fijo respecto de cuando trabaja en un reactor *hollow fibre*. Con ello se pretenden constatar si la porosidad de diferentes fibras cerámicas afecta en la reacción del reformado del

glicerol. Además se prepararán catalizadores compuestos por tres fases (níquel, magnesio y óxido de cerio), sintetizados por un método de deposición de sol-gel (Pechini), con lo cual pretendemos conseguir la deposición integrada del catalizador dentro de la porosidad de las fibras cerámicas.

2. También planteamos preparar catalizadores de níquel con óxido de cerio, pero sintetizados mediante un método de microemulsión, en un solo paso, que da lugar a un óxido mixto con estructura tipo fluorita. Se plantea estudiar la actividad y estabilidad en la reacción del reformado del glicerol de varias composiciones o relaciones Ni/Ce. Con el fin de conocer mejor los mecanismos de desactivación se estudiarán los catalizadores mediante microscopia electrónica de transmisión (TEM), oxidación a temperatura programada (TPO) y espectroscopia de fotoemisión de rayos X (XPS). Con ello pretendemos seguir la evolución del metal níquel, del óxido de cerio y de los posibles depósitos de carbono generados durante la reacción.

Capítulo 3

Materiales y métodos de caracterización

Contenido del capítulo

3. Materiales y métodos de caracterización

3.1. Materiales

En esta tesis doctoral hay dos grupos diferentes de catalizadores estudiados. Los catalizadores basados en Ru, que son los usados para la reacción de hidrogenolisis del glicerol, y los catalizadores basados en Ni, que han sido los empleados para el reformado del glicerol con vapor de agua.

3.1.1. Soportes y fase activa para la hidrogenolisis del glicerol

Un aspecto muy importante en el desarrollo de los catalizadores es la elección del soporte. Para el caso de la reacción de hidrogenolisis del glicerol, los soportes fundamentalmente empleados en esta tesis doctoral han sido distintos tipos de materiales de carbón. El motivo por el cual se han elegido los materiales de carbón como soporte radica en la gran versatilidad que presentan estos materiales, tanto en sus características texturales, área superficial y porosidad, como en su naturaleza química superficial. Ésta, además, puede ser modificada mediante distintos tratamientos químicos con objeto de introducir diferentes grupos superficiales que doten al material de unas características deseadas en cuanto a acidez, hidrofilicidad y carga superficial [1, 2].

Entre la variedad de posibilidades de modificación de un soporte carbonoso, en esta tesis doctoral se ha elegido introducir grupos superficiales de oxígeno, para lo cual existen varios métodos o procedimientos experimentales. Entre estos cabe distinguir entre los basados en un tratamiento en atmósfera oxidante (dióxido de carbono, oxígeno, ozono) y los originados por un tratamiento en disolución acuosa con agentes oxidantes (peróxido de hidrógeno, ácido nítrico, persulfato amónico)[1, 2, 3, 4]. Con estos tratamientos se consigue introducir una variedad de funciones

químicas en la superficie del material de carbón, como ácidos carboxílicos, anhídridos, lactonas, fenoles, quininas, peróxidos y éteres cíclicos, los cuales van a aportar carácter ácido al soporte [5].

Entre los diversos materiales de carbón existentes se han seleccionado un carbón activado de hueso de aceituna (ICASA, Córdoba), un grafito de alta superficie (TIMCAL) y nanotubos de carbono comerciales (NANOCYL). Con el fin de alterar las propiedades superficiales del carbón activado, se procedió a un tratamiento de oxidación superficial mediante el método del tratamiento con una disolución de ácido nítrico, al 10% en volumen, a la temperatura de reflujo de la disolución durante 24 h.

Para la elección de la fase activa para realizar la citada reacción de hidrogenolisis del glicerol, basándonos en la bibliografía encontrada y ya descrita en el capítulo de introducción, se ha seleccionado el rutenio como metal catalítico. El método para preparar los catalizadores ha sido el método de impregnación a humedad incipiente con la sal precursora disuelta en el mínimo volumen de una disolución al 50% de acetona en agua. En nuestro caso, y con el objetivo de ver si existen diferencias catalíticas en función del compuesto de rutenio utilizado en la preparación de los catalizadores, se han usado dos precursores metálicos diferentes. Estos han sido el tricloruro de rutenio y el nitrosil nitrato de rutenio.

3.1.2. Soportes y fase activa para el reformado del glicerol

Esta reacción de gran interés científico se ha llevado a cabo con multitud de soportes y fases activas, como ya se ha descrito en la introducción. En esta tesis doctoral se ha seleccionado el óxido de cerio como aditivo fundamental de la formulación de los catalizadores debido a sus propiedades, entre las que cabe

destacar su eficacia en las reacciones de reformado. Así este óxido de cerio tiene la capacidad de actuar como sistema tampón de oxígeno mediante un proceso de almacenamiento y transferencia de oxígeno, consecuencia de su capacidad redox para mantener en el sistema el equilibrio Ce^{3+}/Ce^{4+} [6]. Esto produce una mayor resistencia a la formación de coque [7], ya que las vacantes de oxígeno en la superficie del CeO_2 favorecen la reacción de water-gas-shift, como consecuencia de una mayor interacción del vapor de agua con el soporte, y una mayor facilidad para llevar a cabo la oxidación del CO quimisorbido [6, 8]. Además el carácter básico del CeO_2 inhibe las reacciones de deshidratación que conllevan a productos que suelen evolucionar generando el coque [9].

Entre las fases activas usadas en el reformado de glicerol, el Ni es una de las más empleadas debido a sus propiedades para catalizar esta reacción, como ya se recogió en la introducción. Con el objetivo de mejorar las propiedades de los catalizadores basados en Ni y CeO_2 en esta tesis doctoral se han desarrollado dos metodologías distintas para la preparación de los catalizadores. La primera es el uso de un catalizador de Ni soportado en CeO_2 que ha sido dopado con MgO. El motivo de añadir este óxido radica en las propiedades que presenta, ya que su incorporación reduce la generación de coque debido a su carácter básico, que desfavorece las reacciones de deshidratación. También la presencia de MgO favorece la dispersión del Ni, lo que afecta negativamente al mecanismo de formación de productos de desactivación (como las nanofibras de carbono) y mejora la selectividad bajando la producción de metano [9, 10].En un segundo caso, se ha procedido a preparar los catalizadores de Ni-CeO_2 usando un método de síntesis algo más complejo basado en una microemulsión en fase inversa. Lo que se pretende con este procedimiento es obtener una red cristalina donde algunos átomos de Ce están intercambiados por átomos de Ni, sin distorsionar

significativamente la estructura tipo fluorita del CeO_2. Para conseguir esto la cantidad máxima de incorporación de Ni en la estructura del CeO_2 debe estar entre 12-16%, con lo que se consigue además una alta dispersión de Ni [11]. El objetivo de la preparación del catalizador por este método es, además de obtener una alta dispersión del Ni, evitar los posibles fenómenos de sinterización del Ni al estar este Ni en posiciones concretas de la estructura fluorita formando un óxido mixto Ni-Ce.

3.2. Métodos de caracterización

3.2.1. Adsorción física de nitrógeno a 77 K

Con esta técnica se puede determinar la superficie específica, distribución y tamaño de poro de un material poroso basándose en fenómenos de adsorción de gases y líquidos en la interfase entre el sólido problema (adsorbente) y el fluido con el que se realiza la adsorción (adsorbato). En esta técnica el adsorbato se introduce poco a poco, con sucesivos incrementos de la presión de equilibrio del adsorbente, sobre el sólido hasta formar y completar una monocapa. El grosor de dicha monocapa va aumentando al incrementar la presión hasta llegar a la presión de saturación del adsorbente, a la cual el adsorbato condensa como líquido. La información obtenida a partir de la cantidad de adsorbente introducido permite, mediante el empleo de modelos matemáticos, determinar el área del sólido y el tamaño y distribución de los poros. Esta técnica es usada para la caracterización de sólidos microporosos (<2 nm) y mesoporosos (2-50 nm) [12].

Para realizar el experimento se emplea aproximadamente 200 mg de muestra que se desgasifica a 473 K. El área superficial se determina cuando se representa la isoterma de adsorción de N_2 a 77 K y se aplica el método matemático de Brunauer-Emmet-Teller (BET) considerando el área de la molécula de N_2 de

0,162 nm^2 [13]. Para el cálculo del tamaño y volumen de poro se emplea el método BJH a partir de la curva de desorción del N_2 [14]. El equipo automático empleado para realizar estas medidas es un Micromeritics ASAP 2010/2000.

3.2.2. Difracción de rayos X

La difracción de rayos X (XRD) es una técnica que se fundamenta en el uso de una radiación monocromática de rayos X que al aplicarla sobre una muestra sólida da lugar, como consecuencia del ordenamiento de los planos cristalinos espaciados regularmente en dicha muestra, a un patrón de líneas de difracción específico de cada material; correspondiendo cada línea a un espaciado entre planos concretos y específicos del material [15]. Para poder obtener dicho espaciado se usa la ecuación de Bragg ($n\lambda = 2d_{hkl}\sin\theta$), con lo que sabiendo el ángulo de incidencia de la radiación y la longitud de onda de la misma podemos calcular el espaciado (d_{hkl}).

Para llevar a cabo el experimento, se sitúa una pequeña cantidad de muestra (50-100 mg) en un portamuestras, que se coloca en el equipo. Las condiciones experimentales usadas con nuestros materiales fueron 45 kV, 40 mV y una velocidad de barrido de 0,04º por segundo, entre 4º y 90º de ángulo de Bragg (2θ). El equipo empleado fue un difractómetro de rayos X Polycristal X'Pert Pro PANalytical, equipado con un monocromador de grafito y usando la radiación Cu Kα (λ= 1,5406 Å).

3.2.3. Termogravimetría y oxidación a temperatura programada

Estas técnicas se basan en la medida de la variación de masa de la muestra cuando esta se somete a un programa de temperatura en una atmósfera controlada. Lo que ofrece esta técnica cuando se aplica a carbones en atmósfera inerte es una idea de los grupos funcionales inestables térmicamente y de los compuestos

adsorbidos presentes en los materiales medidos. El sistema de medida empleado es una balanza electrónica de dos brazos, que como consecuencia de la pérdida de masa se produce una desviación de uno de los brazos que es compensada por una corriente eléctrica aplicada a un imán permanente. La amplificación de esta señal eléctrica, previamente calibrada, nos da la información de la pérdida de peso [16].

Para llevar a cabo la calibración se pone la celda de medida (consistente en una cesta de cuarzo) en el sistema y se purga con He (50 mL min^{-1}) hasta señal constante. En esta atmósfera este será nuestro cero. A continuación se introduce una pesa patrón de 100 mg dentro de la cestilla y se vuelve a purgar el sistema con He, quedando así calibrado el sistema con un segundo punto. En los experimentos la cantidad de masa de muestra situada en la cesta fue de unos 100 mg aproximadamente y antes de empezar el programa de temperatura el sistema debe ser purgado con He durante 2 h para asegurar una atmósfera perfectamente inerte. El programa de temperatura empleado consta de un incremento de temperatura hasta 373 K a una velocidad de 10 K min^{-1} y manteniendo esta temperatura durante 30 min. Con ello pretendemos eliminar el agua adsorbida. Seguidamente se aumenta la temperatura hasta 1123 K a una velocidad de 8 K min^{-1}.

En el caso de la oxidación a temperatura programada (TPO), la cual se realiza para determinar la cantidad de depósitos de carbón generados durante la reacción en un catalizador, la única diferencia experimental es que la atmósfera de He se cambia por una atmósfera oxidante, para lo cual se hace pasar un caudal de aire sintético (100 mL min^{-1}) permanentemente por el sistema. Al igual que el caso anterior antes de calibrar y realizar el calentamiento hay que esperar un tiempo para asegurar que la atmósfera reactiva está estabilizada. Con esta técnica se analiza la estabilidad del material a la oxidación en función de la temperatura.

3.2.4. Desorción a temperatura programada

Esta técnica es complementaria a las termogravimetrias y nos permite completar la caracterización superficial de los materiales [17, 18]. El objetivo de la técnica es seguir la desorción de las especies presentes en una superficie, bien sean previamente quimisorbidas o bien que provengan de la descomposición de especies químicas térmicamente inestables. Para ello la muestra se somete a un programa de temperatura en atmósfera inerte o en vacío al mismo tiempo que se analiza la fase gaseosa que se va produciendo. El equipo de trabajo consta de un horno programable, donde se sitúa la muestra dentro de un tubo de cuarzo, y de un detector conectado a la salida de dicho tubo con el que se analizan los gases producidos. En este caso dicho detector es un espectrómetro de masas cuadrupolar. Dado que el equipo trabaja en condiciones de vacío se puede considerar que no hay reacciones secundarias y por lo tanto que los gases analizados en el espectrómetro de masas proceden sólo de la muestra.

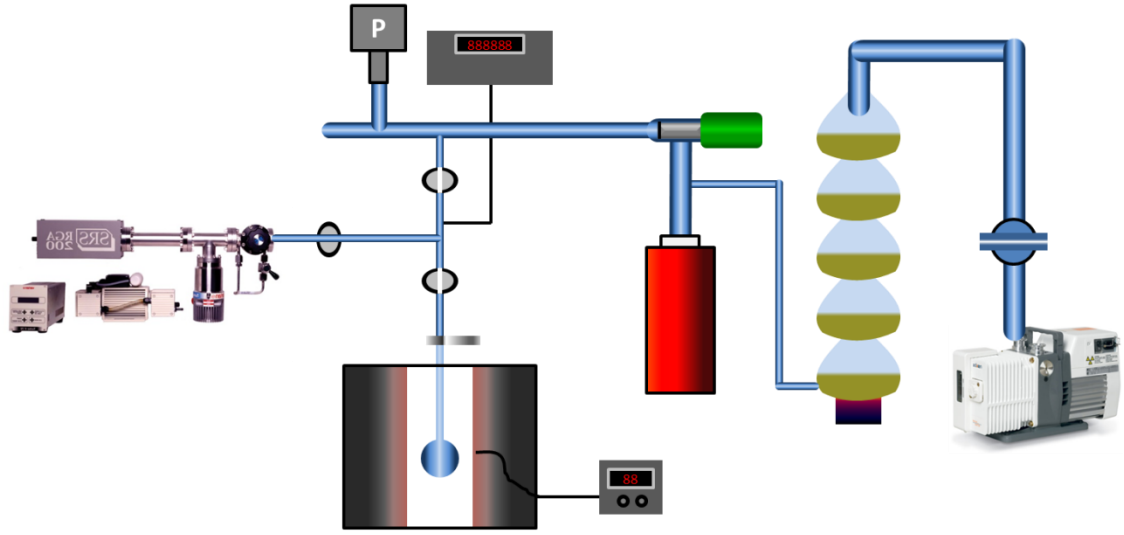

Figura 1. Equipo de desorción a temperatura programada

Para realizar el experimento en el equipo esquematizado en la Figura 1, se dispone de un bulbo de cuarzo adaptado para conectarlo al equipo, en el cual se introducen aproximadamente 30 mg de muestra y se hace vacío durante 30 min para la desorción del agua fisisorbida. A continuación se procede a calentar la muestra a una velocidad constante de 8 K min^{-1} hasta los 1123 K, analizando online los compuestos que se desorben/descomponen mediante el espectrómetro de masas. El equipo empleado consiste en un horno con un controlador de temperatura electrónico, en el cual se sitúa el reactor de cuarzo, y que está conectado a un sistema de vacío y a su vez a un espectrómetro de masas cuadrupolar (modelo SRS RGA200), lo que permite la identificación en continuo de los gases desorbidos.

3.2.5. Reducción a temperatura programada

Con esta técnica (abreviada TPR) se determina la temperatura a la que se produce la reducción del catalizador cuando se aumenta la temperatura en una atmósfera reductora (en nuestro caso una atmósfera de H_2) [19]. Los gases consumidos y producidos, durante la reducción, se analizan en continuo mediante un cromatógrafo de gases lo que permite observar la variación de la concentración de H_2 y simultáneamente observar la aparición de otros compuestos, como por ejemplo los procedentes de la descomposición del precursor o de la descomposición de grupos térmicamente inestables. Cuando se representa el consumo de hidrógeno en función de la temperatura se obtiene el perfil de reducción del catalizador.

Para llevar a cabo el experimento se coloca 100 mg de muestra (la cantidad dependerá de la carga de metal) en un reactor tubular de cuarzo con forma de U y a continuación se pasa un flujo de 30 mL min^{-1} de una mezcla al 5% H_2 en He.

Cuando el sistema se estabiliza se eleva la temperatura con una velocidad de calentamiento de 8 K min^{-1} desde temperatura ambiente hasta los 1073 K. El equipo empleado está formado por el reactor de cuarzo introducido en un horno programable (regulador de temperatura RKC rex-P90 y termopar tipo K) y un sistema de gases controlados por controladores de flujo másico (Brooks 5850 TR). La salida de los gases del reactor están acoplados a un cromatógrafo de gases (Varian 3400) equipado con un detector de conductividad térmica y usando las columnas Chromosorb 102 y Porapack Q para la separación de H_2, CO, CO_2 y CH_4 principalmente.

3.2.6. Microcalorimetría de quimisorción de CO

Esta técnica es la combinación de dos técnicas, la quimisorción volumétrica de CO y la microcalorimetría. La quimisorción de CO nos permite determinar la cantidad de gas sonda (CO) necesaria para formar una monocapa de gas quimisorbido en la superficie metálica del catalizador. En este caso la monocapa hace referencia a la capa de moléculas sonda que forma un enlace entre un átomo o molécula del gas reactivo (adsorbato) con cada uno de los átomos del metal expuestos en la superficie de las partículas metálicas (normalmente asociados con los centros catalíticamente activos). Con esta información se puede calcular la dispersión (D), que representa el número de átomos superficiales relativos al número de átomos totales del metal en la muestra [20]. La dispersión se define como $D = \frac{M_s}{M_t}$, donde M_s es el número de átomos metálicos en superficie y M_t es el número de átomos metálicos totales. Conocido el valor de dispersión D, y suponiendo que las partículas metálicas son esféricas se puede calcular el tamaño medio de partícula:

$$D = \frac{N_s}{N_v}\frac{6}{\bar{d}}$$

donde, N_s es el número de átomos superficiales por unidad de área de metal en la superficie (densidad superficial de sitios) y N_v es la concentración atómica o número de átomos por unidad de volumen.

La microcalorimetría de adsorción permite además calcular la cantidad de calor que se desprende al adsorberse una cantidad dada de molécula sonda (CO en este caso) sobre una muestra en cada dosis. Representando el calor diferencial de adsorción (por ejemplo en julios por mol de gas adsorbido) frente a la cantidad adsorbida por gramo de catalizador se obtiene el perfil de microcalorimetría de adsorción. El valor de la monocapa de CO (cantidad de CO quimisorbida) se puede hacer corresponder con la cantidad de gas adsorbido que tiene un calor de adsorción mayor a 40 kJ/mol, ya que por debajo de este valor los calores de adsorción se consideran consecuencia de fenómenos de adsorción física [21]. Para la comparación de los distintos catalizadores se calcula el cubrimiento (θ), que se define como la fracción de monocapa de gas quimisorbido. Entonces se representa el calor de adsorción frente a la fracción de cubrimiento conseguida en cada dosis o punto. Con el análisis de este perfil calorimétrico, característico de cada catalizador, obtenemos información acerca del tipo y número de centros de adsorción, así como de la distribución energética de éstos.

En el sistema experimental esquematizado en la Figura 2, se introduce la muestra dentro de un bulbo de adsorción, en una cantidad de 200 mg aproximadamente. Se procede primero a la reducción del catalizador en un flujo de H_2 (30 mL min^{-1}) calentando hasta la temperatura adecuada y manteniendo la temperatura durante 2 h. Posteriormente se procede a la desgasificación en alto vacío durante 16 h a la misma temperatura de reducción para posteriormente dejar enfriar hasta temperatura ambiente. El siguiente paso es trasladar el bulbo a la

célula del calorímetro, donde se deja en vacío dinámico hasta la estabilización de la señal del calorímetro (unos 90 minutos generalmente), es decir, hasta que no existe flujo de calor entre la celda de referencia y la celda de medida ya que ambas están a una temperatura concreta y exactamente igual (en nuestro caso 330 K). A continuación se inicia la quimisorción de CO introduciendo sucesivos pulsos de gas sonda al bulbo de adsorción, con presiones iniciales que varían desde 0.2 a 9 Torr. Para un pulso en concreto, la adsorción se considera completa cuando el flujo térmico del calorímetro y la presión permanecen constantes.

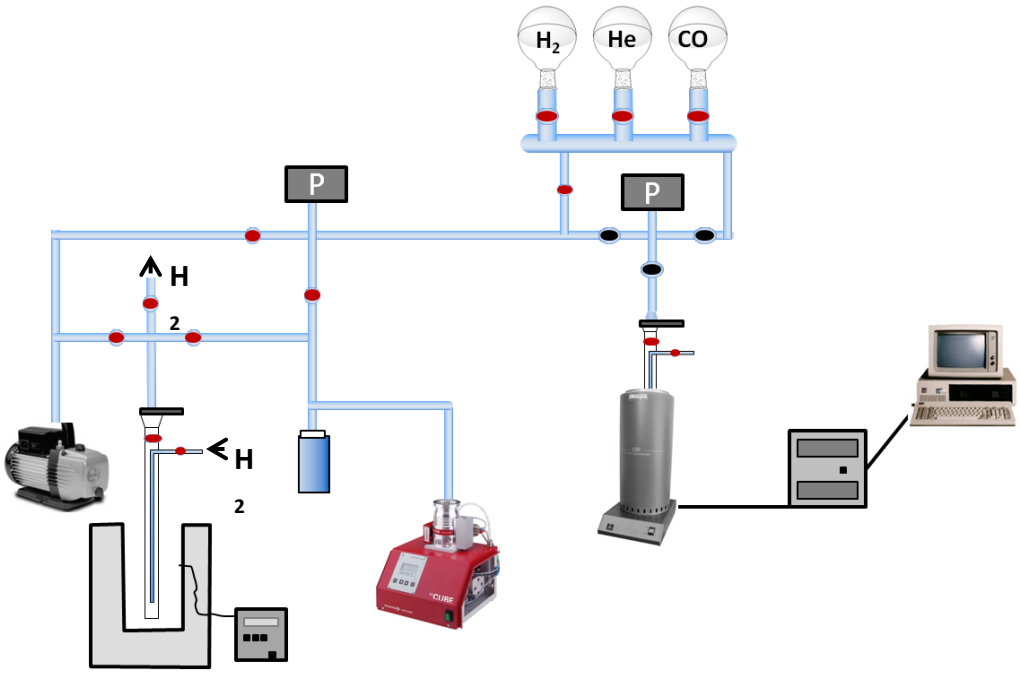

Figura 2. Equipo volumétrico y de microcalorimetría de quimisorción de CO

El sistema experimental para realizar las microcalorimetrías de quimisorción de CO consta de un equipo volumétrico de adsorción construido en vidrio Pyrex y un microcalorímetro del tipo Tian-Calvet (C80 II-Setaram) con una unidad de control CS32. El equipo volumétrico consta de dos bombas (una rotatoria y una bomba turbomolecular), una trampa de nitrógeno líquido para mejorar el vacío, un

conjunto de llaves automáticas, un medidor de cátodo frio (Alcatel CF2P) para medir la presión residual, cuando se realiza el alto vacío, y un medidor de capacitancias (Baratron MKS) para controlar los pulsos del gas sonda con un rango de trabajo de 1-10 Torr y una precisión de 10^{-3} Torr.

3.2.7. Espectroscopía de fotoemisión de rayos X

El fundamento teórico de esta técnica (abreviada XPS) está basado en el efecto fotoeléctrico descubierto por Einstein en el año 1905 que, de forma simplificada, dice que cuando un haz de rayos X blandos monoenergéticos, de una energía mayor al enlace del electrón, incide sobre electrones de niveles atómicos profundos se produce la emisión de electrones con una energía cinética dada por la ecuación $E_c = h\nu - BE - \phi_s$, donde $h\nu$ es la energía del fotón incidente (normalmente Mg Kα = 1253,6 eV ó Al Kα = 1486,6 eV), E_c es la energía cinética del electrón emitido, BE es la energía de enlace del electrón y ϕ_s representa la función de trabajo del espectrómetro (energía necesaria para llevar el electrón desde el nivel de Fermi "virtual" hasta las condiciones de trabajo del espectrómetro). Esta técnica sirve para el análisis superficial por dos motivos, el primero porque la radiación penetra en la materia del orden de 1-10 μm, y segundo por el recorrido libre medio de los fotoelectrones antes de sufrir alguna colisión inelástica con los átomos del sólido está comprendida entre 0,4 y 4 nm, lo que provoca una pérdida de energía suficiente para que los fotoelectrones no puedan abandonar la muestra [22]. Por eso esta técnica nos da información únicamente de las capas atómicas más superficiales (entre 5 y 10 capas) del material sólido analizado.

Para realizar el experimento el material debe de pastillarse para proporcionar una superficie plana y lo más homogénea posible. Así se evitan también problemas de pérdida de material como consecuencia del alto vacío. La

muestra ya pastillada se coloca en el portamuestra y se introduce en la cámara de pretratamiento, donde se debe desgasificar hasta alcanzar un vacío próximo a $1{,}3 \cdot 10^{-6}$ Pa. En el último paso la muestra se transfiere a la cámara de análisis en la cual la presión se mantiene siempre por debajo de 10^{-9} Pa. Para realizar los análisis se ha empleado una radiación Kα del Mg, siendo el paso de energía de 50 eV. Con esta técnica se analizan los átomos, de forma semicuantitativa, presentes en la superficie del sólido, a partir de las áreas de los picos. Además se pueden identificar los estados de oxidación de los elementos analizados a partir de las posiciones exactas, separaciones y perfiles de los picos identificados.

El equipo empleado para estos análisis fue un espectrómetro ESCAPROBE-P de OMICROM equipado con un analizador de electrones semiesféricos EA-125 de 7 canales (con energía de paso de 2-200 eV) y una fuente de radiación de rayos X con ánodos de Mg y Al. En la cámara de pretratamiento se puede controlar la atmósfera y la temperatura, además tiene una toma de tierra que libera la acumulación de cargas positivas durante la adquisición de los espectros de muestras conductoras y para las muestras aislantes, el equipo dispone de un cañón de electrones que hace de neutralizador de carga.

3.2.8. Microscopía electrónica de transmisión, microscopía electrónica de transmisión de barrido y espectroscopía de energía dispersiva de rayos X

La microscopía electrónica de transmisión es una técnica ampliamente usada para la caracterización estructural y química de los materiales, ya que se produce información directa sobre la morfología, distribución de tamaños de partícula, composición química e identificación de fases cristalinas aplicable a un gran rango de materiales [23]. El fundamento de la técnica, básicamente, consiste

en la obtención de un haz de electrones acelerados que, mediante un conjunto de lentes electromagnéticas, se enfoca en la muestra problema produciendo una interacción entre los electrones y la muestra. En función de cómo se modula el haz podemos obtener la microscopía electrónica de transmisión (Transmission Electron Microscopy, TEM) cuando se proyecta un haz paralelo a la muestra, o la microscopía electrónica de transmisión de barrido (Scanning Transmission Electron Microscopy, STEM) cuando el haz se converge en un punto del orden de 1nm y con este haz se produce un barrido de la muestra. Para la microscopía TEM los electrones que se usan para generar la imagen son los electrones transmitidos que no sufren interacción con la materia, mientras que para la microscopía STEM los electrones que se usan para generar la imagen son aquellos que se dispersan como consecuencia del choque de los primeros con los átomos. A mayor número atómico de los elementos que componen la muestra mayor será la cantidad de electrones que son dispersados. También existe una relación directa entre ángulo de medida y número atómico, es decir, a mayor número atómico mayor es la cantidad de electrones dispersados a altos ángulos lo que genera un mayor contraste en la fotografía final.

A parte el microscopio puede estar dotado de un espectrómetro de energías dispersivas de rayos X (*Electron-Dispersive X-ray*, EDX) cuyo fundamento está basado en la interacción de los electrones con la materia, es decir, como consecuencia de la interacción existe una excitación de un electrón a estados energéticos superiores que al relajarse producen rayos X característicos de cada elemento, los cuales son recogidos y analizados por el sistema EDX. Esto permite conocer la composición elemental del área estudiada e incluso se puede hacer mapas de composición "mapping" cuando se acopla el modo de análisis de barrido STEM con el EDX.

Para llevar a cabo el análisis de catalizadores, que previamente deben ser reducidos, el procedimiento experimental consta de una primera etapa de molturación para dejar la muestra en un fino polvo que después es suspendido en un disolvente volátil (etanol). Se añaden un par de gotas a la rejilla de microscopía (Lacey carbon, 200 mesh, Aname) y esta se coloca en el brazo portamuestras para luego proceder a introducirla en el microscopio para su desgasificación y posterior análisis. El microscopio empleado en estos estudios fue un JEOL 2100F electron-gun microscope con un sistema EDX INCAX-Sight de Oxford Instruments que opera a 200 kV con una resolución máxima de 0.17 nm y con un tamaño mínimo de convergencia del haz de 0.2 nm para el modo STEM.

Para el cálculo de la distribución y tamaño medio de partícula se realiza un conteo de partículas, como mínimo 150, y se aplica la ecuación $d_{TEM} = \sum n_i d_i^3 / \sum n_i d_i^2$, donde n_i es el número de partículas de tamaño d_i. Esta ecuación se utiliza cuando existen partículas de formas similares, pero con distintos tamaños. El valor medio obtenido, d_{TEM}, puede usarse para comparar con otras técnicas que estiman el tamaño medio de partícula a partir del área superficial del metal, como es el caso de la quimisorción [24].

3.2.9. Microscopía electrónica de barrido

El microscopio electrónico de barrido es muy similar al microscopio electrónico de transmisión ya que ambos usan un haz de electrones generado por un cañón de electrones y tiene lentes electromagnéticas para focalizar y colimar el haz de electrones hacia la muestra problema [25]. La principal diferencia que existe entre ambos microscopios radica en la forma de focalizar el haz y producir la magnificación de la imagen lo que da lugar a obtener información distinta a la conseguida por el TEM, ya que el SEM permite conocer la morfología superficial

obteniendo profundidad de campo. El haz de electrones se focaliza en un punto de tamaño comprendido entre 0.4 nm y 5 nm (en función de la calidad del microscopio y del tipo de análisis) y luego se realiza un barrido sobre la superficie del material. Otra importante diferencia son los electrones que se usan para formar la imagen, ya que en el SEM se usan los electrones secundarios y electrones retrodispersados que se emiten cuando la muestra es irradiada con el haz incidente, mientras que en el TEM son electrones transmitidos o dispersados.

Un requisito importante que tiene que cumplir la muestra en SEM es que tiene que ser conductora, para muestras no conductoras se pueden analizar metalizando la muestra, es decir, se recubre la superficie con una pequeña capa de un metal conductor, siendo el más utilizado el Au. Al igual que en el TEM, se le puede acoplar el sistema de detección de rayos X (EDS) para realizar análisis de la composición del material.

En nuestro caso para estudiar las muestras estas se recubren con una fina capa de Au en vacío durante 3 min a 20 mA (en un equipo EMITECH model K550 LV). Una vez metalizadas se llevan al microscopio electrónico de barrido, Jeol modelo JSM-5610 LV, capaz de operar entre 0.5 – 35 kV obteniendo una magnificación comprendida entre 50 y 300000 aumentos.

3.3. Bibliografía

[1] Stavinskaya, O. N.; Oranskaya, E. I.; Imshennik, V. K. *Carbon* 2001, 39, 291.

[2] Moreno-Castilla, C.; Ferro-Garcia, M. A.; Joly, J. P.; Bautista-Toledo, I.; Carrasco-Marin, F.; Rivera-Utrilla, J. *Langmuir* 1995, 11, 4386.

[3] Moreno-castilla, C.; Carrasco-marín, F.; Maldonado-hódar, F. J.; Rivera-utrilla, J. *Carbon* 1998, 36, 145.

[4] Serp, P.; Hierso, J. C.; Feurer, R.; Kihn, Y.; Kalck, P.; Faria, J. L.; Aksoylu, A. E.; Pacheco, A. M. T.; Figueiredo, J. L. *Carbon* 1999, 37, 527.

[5] Serp, P.; Figueiredo, J. L. *Carbon Materials for catalysis*; John Wiley & sons: New Jersey, 2009.

[6] de Lima, S. M.; Silva, A. M.; da Cruz, I. O.; Jacobs, G.; Davis, B. H.; Mattos, L. V.; Noronha, F. B. *Catalysis Today* 2008, 138, 162.

[7] Zhang, B.; Tang, X.; Li, Y.; Cai, W.; Xu, Y.; Shen, W. *Catalysis Communications* 2006, 7, 367.

[8] Srisiriwat, N.; Therdthianwong, S.; Therdthianwong, A. *International Journal of Hydrogen Energy* 2009, 34, 2224.

[9] Ni, M.; Leung, D. Y. C.; Leung, M. K. H. *International Journal of Hydrogen Energy* 2007, 32, 3238.

[10] Carrero, A.; Calles, J. A.; Vizcaíno, A. J. *Chemical Engineering Journal* 2010, 163, 395.

[11] Barrio, L.; Kubacka, A.; Zhou, G.; Estrella, M.; Martínez-Arias, A.; Hanson, J. C.; Fernández-García, M.; Rodriguez, J. A. *The Journal of Physical Chemistry C* 2010, 114, 12689.

[12] Martín-Martínez, J. M. *Adsorción física de gases y vapores por carbones*; Universidad de Alicante: Alicante, 1990.

[13] Brunauer, S.; Emmett, P. H.; Teller, E. *Journal of the American Chemical Society* 1938, 60, 309.

[14] Barrett, E. P.; Joyner, L. G.; Halenda, P. P. *Journal of the American Chemical Society* 1951, 73, 373.

[15] Jenkins, R.; Snyder, R. L. *Introduction to X-ray powder diffractometry* New York, 1996.

[16] Otake, Y.; Jenkins, R. G. *Carbon* 1993, 31, 109.

[17] Donnet, J. B. *Carbon* 1968, 6, 161.

[18] Nevskaia, D. M.; Santianes, A.; Muñoz, V.; Guerrero-Ruíz, A. *Carbon* 1999, 37, 1065.

[19] Arnoldy, P.; Moulijn, J. A. *Journal of Catalysis* 1985, 93, 38.

[20] Yang, C. H.; Goodwin Jr, J. G. *Reaction Kinetics and Catalysis Letters* 1982, 20, 13.

[21] Maroto-Valiente, A.; Rodríguez-Ramos, I.; Guerrero-Ruiz, A. *Thermochimica Acta* 2001, 379, 195.

[22] Wagner, C. D.; Riggs, W. M.; Davis, L. E.; Moulder, J. F. *Handbook of X-ray photoelectron spectroscopy* Eden Prairie, Minnesota, 1979.

[23] Willians, D. B.; Barry-Carter, C. Transmission electron microscopy I, Basics New York, 1996.

[24] Borodziński, A.; Bonarowska, M. *Langmuir* 1997, 13, 5613.

[25] Faraldos, M.; Goberna, C. Técnicas de análisis y caracterización de materiales Madrid, 2003.

Capítulo 4

Hidrogenolisis del glicerol

Contenido del capítulo

4.1 Resumen de los artículos relativos a la hidrogenolisis del glicerol

Como ya se vio en la introducción, la reacción de hidrogenolisis del glicerol es de gran interés por los productos que se obtienen (1,2-propanodiol y etilenglicol). Para llevar a cabo esta reacción es necesaria la presencia de catalizadores, siendo los más habituales los catalizadores heterogéneos formados por una fase activa metálica soportada. Por otra parte, según el esquema de reacción propuesto por varios autores, esta reacción es favorecida por la presencia de centros ácidos, que producen la deshidratación del glicerol. Por lo tanto se han desarrollado varios catalizadores heterogéneos usando como soporte diferentes materiales de carbón y como fase metálica el rutenio, ya que este metal ha presentado buena actividad en trabajos ya reportados en la bibliografía. Para la síntesis de los catalizadores se han usado dos sales metálicas precursoras, el $RuCl_3 \cdot 3H_2O$ y el $Ru(NO)(NO_3)_3$ con la finalidad de evaluar si existen diferencias catalíticas entre ellas.

Se han seleccionado como soportes varios materiales de carbón, por la posibilidad de modificar fácilmente la química de sus superficies para así poder adaptarlas en función de los requisitos de nuestra reacción. En concreto, se ha seleccionado un carbón activado, que una vez limpiado de restos de impurezas inorgánicas, ha sido tratado químicamente con una disolución de ácido nítrico para su modificación superficial, incorporándole grupos oxigenados que aportan cierto carácter ácido a la superficie. Ambos soportes (carbón activado limpio de impurezas y el tratado con ácido nítrico) se usaron como soporte para la síntesis de catalizadores, mediante el método de impregnación a humedad incipiente, y usando dos precursores de rutenio anteriormente mencionados ($RuCl_3 \cdot 3H_2O$ y

$Ru(NO)(NO_3)_3$). Por otra parte, se utilizaron el grafito de alta superficie y los nanotubos de carbono como soportes, ya que estos materiales poseen un alto grado de grafitización por lo que son capaces de donar electrones a la fase metálica obteniendo especies electrónicamente enriquecidas ($Ru^{\delta-}$). Según la bibliografía estas especies electronegativas favorecen la formación de 1,2-propanodiol, pero también favorecen la ruptura del enlace C-C, lo que origina la formación de productos indeseados, siendo el mayoritario el metano. Al igual que en el caso anterior, se usó el método de impregnación a humedad incipiente para la síntesis y solo la sal de $RuCl_3 \cdot 3H_2O$ como precursor metálico, ya que dicha sal presentó los mejores resultados en el primer estudio realizado.

Por otro lado y para comparar con los soportes de carbón, se seleccionó una zeolita no ácida (en concreto la zeolita KL) como soporte para depositar el Ru. En este caso se usó la misma sal precursora ($RuCl_3 \cdot 3H_2O$) pero usando para la síntesis del catalizador el método del intercambio iónico. En este método se prepara una suspensión de la zeolita en agua y a continuación se le añade gota a gota la disolución que contiene la sal de rutenio. Mediante este método se obtiene un catalizador con sitios ácidos de Brönsted originados durante la reducción de las especies de cloruro de rutenio enlazadas en la estructura de la zeolita.

La actividad catalítica de todos estos catalizadores fue evaluada en la reacción de hidrogenolisis del glicerol a 453 K y 8 MPa de hidrógeno en un reactor de tipo "*bach*" con agitación. Además, para entender las diferencias encontradas en la actividad, los catalizadores fueron caracterizados mediante termogravimetría, espectroscopía de fotoemisión de rayos X, microscopía electrónica de transmisión y desorción a temperatura programada. Además se realizó un estudio exhaustivo de los catalizadores mediante microcalorimetría de quimisorción de CO.

En el caso de los catalizadores soportados sobre los carbones activados (purificado y modificado con grupos de oxígeno) se observó mediante microscopía electrónica de transmisión que las partículas de Ru soportadas en el carbón activado oxidado son de mayor tamaño que en el carbón purificado. Sin embargo, esta diferencia de tamaño de partícula de Ru no tiene ningún efecto en la naturaleza de los sitios activos superficiales de las partículas metálicas determinados mediante la calorimetría de quimisorción de CO. Además se estudió mediante termogravimetría y desorción a temperatura programada la cantidad y naturaleza de los grupos oxigenados superficiales que el tratamiento con ácido nítrico originó. Por otra parte, el uso del precursor $Ru(NO)(NO_3)_3$ que posee cierto carácter oxidante, también modifica la superficie del carbón activado introduciendo grupos oxigenados superficiales adicionales, los cuales aportan acidez al medio. Pero estos grupos oxigenados son grupos carboxílicos, de baja estabilidad térmica, y durante el proceso de reducción del rutenio son destruidos en parte. Por ello se realizó un ensayo de reacción usando el catalizador soportado en carbón activado original y añadiéndole una alícuota de carbón activado modificado, observándose que la selectividad y la conversión mejoran por la presencia de los grupos ácidos.

La calorimetría de quimisorción de CO es una técnica capaz de determinar la naturaleza, el número y la distribución en fortaleza de los sitios activos superficiales. Esta técnica nos puede ayudar a entender las diferencias encontradas en la actividad de los catalizadores procedentes de las distintas sales metálicas precursoras. En el caso de los catalizadores procedente de la sal $RuCl_3 \cdot 3H_2O$, se observa una distribución más heterogénea de sitios activos con unos calores iniciales a bajas coberturas de CO excepcionalmente altos. Sin embargo, los catalizadores procedentes del complejo $Ru(NO)(NO_3)_3$ tienen una distribución más homogénea de sitios activos superficiales, con unas entalpias más altas a coberturas

de CO medias, comparados con los catalizadores de $RuCl_3 \cdot 3H_2O$. Este fenómeno se atribuye a la presencia de especies cloruro que permanecen ancladas después de la reducción de los catalizadores a baja temperatura (523 K). Dichas especies modifican la quimisorción de CO tanto por impedimento estérico, como por modificación electrónica de los átomos de Ru que estén próximos. Por otra parte, la modificación superficial de los carbones activados mediante tratamientos oxidantes, no producen alteraciones en la distribución de sitios activos superficiales detectados por la quimisorción de CO.

Finalmente, la comparación de la actividad catalítica de las muestras preparadas usando los distintos tipos soportes de carbón (carbón activado purificado, grafito de alta superficie y nanotubos de carbono) y la zeolita KL, nos revela aspectos significativos de los distintos tipos de mecanismos posibles en la reacción de hidrogenolisis del glicerol. En el caso del catalizador de Ru en zeolita KL con acidez tipo Brönsted, las partículas de Ru presentan cierto carácter electrodeficiente determinado por quimisorción de CO. Estos centros electrodeficientes unido a los centros ácidos que presenta la zeolita favorecen la formación del 1,2-propanodiol, ya que producen la deshidratación del glicerol para dar el acetol, intermedio detectado en este catalizador. Por otra parte, las propiedades electrodonadoras de los soportes de grafito de alta superficie y los nanotubos de carbono originan especies $Ru^{\delta-}$ que como ya se dijo favorecen la formación del 1,2-propanodiol, pero además la ruptura del enlace C-C. Pero sin la presencia de los centros ácidos en estos catalizadores, se produce la catálisis monofuncional en los centros metálicos favoreciendo la ruptura del enlace C-C. Esto origina que el producto mayoritario sean los compuestos de ruptura del glicerol como son el etilenglicol o el metano.

4.2 Effect of the functional groups of carbon on the surface and catalytic properties of Ru/C catalysts for hydrogenolysis of glycerol

E. Gallegos-Suárez[1,2], M. Pérez-Cadenas[2], A. Guerrero-Ruiz[2,3], I. Rodríguez-Ramos[1,3] and A. Arcoya[1,3]

Applied Surface Science 287 (2013)108-116

[1]Instituto de Catálisis y Petroleoquímica, CSIC, Marie Curie nº 2, L-10, 28049 Madrid, Spain.
[2]Departamento de Química Inorgánica y Técnica, Facultad de Ciencias, UNED, Paseo Senda del Rey nº 9, 28040 Madrid, Spain.
[3]Unidad Asociada UNED ICP-CSIC, Group Design and Applied Heterogeneous Catalysis.

4.2.0 ABSTRACT

Ruthenium catalysts supported on activated carbons, original (AC) and treated with nitric acid (AC-Ox) were prepared by incipient wetness impregnation from either chloride (Cl) or nitroxyl nitrate (n) precursors. These catalysts were characterized by TG, XPS, TEM, TPD-MS and CO adsorption microcalorimetry and evaluated in the hydrogenolysis of glycerol in the liquid phase, at 453 K and 8 MPa. Studies by TEM show that ruthenium particles supported on AC-Ox are larger than on AC, without any effect of the nature of the metal precursor. However, adsorption of CO on the ex-chloride catalysts is inhibited in comparison with that of the ex-nitroxyl nitrate catalysts. Catalysts characterization by TG, TPD-MS and XPS reveals that the nitric acid treatment and the nitroxyl nitrate precursor generate oxygenated groups on the carbon surface, which provide acid properties to the catalysts, although they are partly destroyed during the reduction treatment applied to the catalysts. The sequence of the overall TOF, Ru(Cl)/AC < Ru(n)/AC < Ru(Cl)/AC-Ox ≈ Ru(n)/AC-Ox, reasonably parallels the population increase of surface acid groups. Participation of the -COOH groups in the transformation of glycerol into 1,2-propanediol is verified by using the admixture Ru(Cl)/AC+AC-Ox as catalyst. In this case, since AC-Ox was not thermally treated and no loss of oxygenated groups occurred, TOF and selectivity towards 1,2-propanediol improve in comparison with those of the more active catalysts.

4.2.1 INTRODUCTION

Glycerol is one of the ten top building blocks in the biorefinery feedstocks [1] because it appears as an important byproduct in the biodiesel industry [2]. Since the selectivity of the process towards glycerol is 10% and the biodiesel production is growing, the surplus glycerol needs to be transformed into other more valuable products. With this aim, important catalytic processes, such as dehydration to acrolein [3, 4], oxidation for producing dihydroxyacetone [5, 6] or glyceric acid [7, 8] and degradation until hydrogen production by steam reforming [9, 10, 11, 12] among other, have been developed.

In order to obtain raw materials for synthesis of polymers, plastics, pharmaceuticals, farming products and automotive fuels, some glycols such as 1,2-propanediol, 1,3-propanediol and ethylene glycol are highly demanded [13, 14, 15]. In this context hydrogenolysis of glycerol for producing those valuable products is an alternative process to the more conventional routes based on the hydration of either propylene or ethylene oxides [16, 17, 18]. Hydrogenolysis of glycerol has been performed on various supported noble metals, Rh and Ir-based catalysts being the most active [19, 20, 21, 22, 23, 24, 25, 26] as it occurs for other reactions involving hydrogen [27, 28]. However, Rh and Ir-based catalysts were not suitable to the glycerol conversion to 1,2-propanediol because of high reaction rate of the consecutive hydrogenolysis of 1,2-propanediol. Regarding the glycerol hydrogenolysis to 1,2-propanediol, ruthenium is one of the most suitable active components for the catalysts [29] but it simultaneously induces the C-C cleavage leading to lower chain products, even methane [30]. In contrast, copper presents low hydrogenolysis activity but it is highly selective toward the target product 1,2-propanediol, due to its intrinsic ability to selectively cleave the C-O bond [31,

32, 33]. Selectivity towards 1,2-propanediol over Ru-supported catalyst has been improved by using additives as CaO or NaOH [34] K, Cu and Mo [35] sulfurized metal catalysts [30] bimetal catalysts like Ru-Pt, Ru-Au and Ru-Cu [36, 37] or admixtures of Ru and Pt supported catalysts [38]. On the other hand ruthenium supported catalysts over inorganic materials as SiO_2, Al_2O_3, ZrO_2 [39], TiO_2 [40, 41], hydrotalcite [42], bentonite [43] and also on carbon nanotubes [44] are reported to be highly active and selective toward 1,2-propanediol and the performances usually related to the occurrence of acid sites at the support surface. In this sense it has been also claimed that ion-exchanged resins (Amberlysts) used as co-catalysts, promote the hydrogenolysis activity of Ru/carbon supported catalysts, improve the selectivity towards 1,2-propanediol from glycerol and minimize formation of undesired products [45, 46, 47, 48]. Although several reaction schemes have been proposed to explain the increase of selectivity observed, one of the more accepted reaction mechanisms in these last references and reviews [49, 50, 51, 52, 53] consists of two steps: dehydration of the –triol molecule and the subsequent hydrogenation of produced intermediates. The first step takes place on surface acid sites and the second one occurs on metallic surface centers [29]. This means that a bifunctional catalyst is required. Bearing this idea in mind we have prepared Ru/C supported catalysts, but using a carbon support previously treated with nitric acid to generate oxygenated groups at the surface. Among them, carboxyl groups behave as acidic species, which could enhance the hydrogenolysis activity of Ru/C catalysts in the transformation of glycerol into 1,2-propanediol. The catalysts were prepared using two different ruthenium precursors, chloride and nitroxyl nitrate, and were characterized by different physical techniques and some chemical titrations. These materials were tested in the hydrogenolysis of glycerol with the aim of to correlate

the catalytic performance with the presence of carboxyl groups at the carbon surface.

4.2.2. EXPERIMENTAL

4.2.2.1. Catalysts preparation

An activated-carbon produced from olive stones (Oleicola el Tejar, Córdoba Spain) with 1.25-0.8 mm particle sizes and 1190 m^2g^{-1} specific surface area, was used as row material for preparing catalyst supports. A portion of the as received material was treated with hydrochloric acid solution 10% (v/v) at 373 K for 24 h for removing residual inorganic components. After filtering and washing with distiller water until complete removal of detectable solved metallic ions, the solid was dried and labeled as AC (S_{BET} = 1190 $m^2 g^{-1}$). In order to functionalize the surface of this activated carbon with carboxyl groups and thus provide acid properties to the support, a portion of AC was treated with nitric acid solution 10% (v/v) at 348 K for 24 h and successively washed and dried. This sample was labeled as AC-Ox (S_{BET} = 1160 m^2 g^{-1}).

Catalysts were prepared by incipient wetness impregnation trying to obtain 4 wt% Ru incorporated to the supports. Two Ru precursors $RuCl_3 \cdot xH_2O$ ($1<x<3$) (denoted "Cl") and $Ru(NO)(NO_3)_3$ (denoted "n") were used. These metal precursors were solved, in both cases, into water/ethanol (1/1) solution. After evaporation of the solvent from the impregnated supports by keeping the solids overnight in an open recipient at room temperature, the samples were dried at 393 K for 24 h and then reduced under hydrogen flow (30 mL min^{-1}) at 523 K for 2 h. In order to avoid reoxidation of ruthenium, the reduced catalysts were

immediately transferred to the reactor suspended in a 10% glycerol aqueous solution and/or stored under inert atmosphere.

4.2.2.2. Materials characterization

Reducibility of the catalysts was determined by temperature programmed reduction (TPR) under flow of 100 mL min^{-1} of a 5% H_2/Ar mixture, heating at 8 K min^{-1} from room temperature up to 873 K. Oxygen groups at the carbon surface were quantified by thermogravimetric analysis in a CI Electronics microbalance (MK2-MC5). The samples were treated in flowing helium (50 mL min^{-1}) for 2 h at 373 K and then heated at 10 K min^{-1} up to 1023 K. The thermal stability and chemical nature of the groups exposed at the catalyst surfaces were evaluated by temperature programmed desorption coupled with mass spectrometry analysis (TPD-MS) measurements, under vacuum, in a conventional volumetric apparatus connected to a SRS RGA-200 mass quadrupole spectrometer. The samples were outgassed at room temperature for 2 h and then heated up to 1023 K at 10 K min^{-1}. Precise metal content of the catalysts was determined by thermogravimetric analysis, burning the carbon in flowing pure air (50 mL min^{-1}) at 1073 K, and then weighing the RuO_2 residual product.

Metal surface of the catalysts was studied by microcalorimetry of CO chemisorption in order to gain information about the nature, number and strength of the adsorption sites. Measurements were performed in a Tian Calyet heat-flow microcalorimeter (Setaram C-80 II) operated isothermally at 330 K and connected to a glass vacuum-dosing-apparatus, following the methodology described in detail elsewhere [54]. Metal dispersion was calculated from the CO uptake at the monolayer, considering that this is attained when the evolved CO adsorption heat falls to the physisorption values (40 kJ mol^{-1}) and assuming a molar stoichiometry

CO/Ru = 1/1. The mean metal crystallite size was calculated from the dispersion values assuming the spherical model, d (nm) = 1.32/D_{CO}. The catalyst surface was also examined by X-ray photoelectron spectroscopy (XPS) in an ESCAPROBE P spectrometer from OMNICROM equipped with an EA-125 hemispherical multichannel electronics analyzer. The excitation source was Mg using the Kα line ($h\nu$ = 1253.6 eV, 300 W) and the pressure in the analysis chamber was kept below 10^{-9} Pa during measurements. Accurate binding energies (BE) were determined by charge referencing with the C1s peak at 284.6 eV. The error in the binding energy and line width measurements was lower than 0.2 eV.

Analysis of the catalysts by transmission electron microscopy (TEM) was carried out in a JEOL 2100 F electron gun microscope provided with a X-ray energy dispersive spectroscopy system (XEDS). The samples were milled and suspended in ethanol by ultrasonic treatment and a drop of the fine suspension was placed on a carbon-coated copper grid of 200 mesh to be loaded into the microscope. Average particle size (d_{TEM}) was calculated as

$$d_{TEM} = \Sigma n_i d_i^3 / \Sigma n_i d_i^2$$

where n_i is the number of particles with d_i diameter.

4.2.2.3. Catalytic activity measurement

Hydrogenolysis of glycerol was carried out in a 160 mL stainless-steel autoclave PARR 3350, at 453 K, 8 MPa and 500 rpm stirring. The reactor was filled with 100 mL of 10 wt% glycerol aqueous solution with 0.450 g of the reduced catalyst in suspension. The system was flushed several times with high purity He and then H_2 was admitted. Subsequently the reactor was heated to the reaction temperature and pressurized with H_2 up to the working pressure, which remained

constant along the 24 h of experiment. At the end of the run the autoclave was cooled down to room temperature, the gas phase collected in a gasbag and the liquid filtered in order to separate the spend catalyst. The liquid samples were analyzed by gas chromatography in a Varian 3400 equipment, which is provided with a FID detector and a Supercowax 10 column (30m x 0.53mm x 1μm) for product separations. The samples for analysis were prepared by dilution of 300 μL of the reaction products with 700 μL of water and 100 μL of 1,4-butanediol as internal standard. Samples of 0.4 μL of this solution were injected into the chromatograph column. Repeated kinetic experiments supplied conversion and selectivity data that were reproducible to within ±3%.

4.2.3. RESULTS AND DISCUSSION

4.2.3.1. Catalysts characterization

Figure 1 shows the TPR profiles of the carbon-supported Ru samples. These profiles display two broad and intense regions of hydrogen consumptions. The first one, at temperature below 600 K, corresponds to the decomposition-reduction of the ruthenium precursors while the second one, above 600 K, is related to other phenomena at the catalyst surface that require hydrogen consumption, as it will be seen below. For catalysts ex-chloride the peak at low temperature is really formed by two overlapped reduction peaks, which usually have been related to the two reduction steps of the ruthenium chloride precursor, i.e. $Ru^{3+} \rightarrow Ru^{2+} \rightarrow Ru^{0}$ [55, 56, 57]. In the case of Ru(Cl)/AC they appear at 430 K and 470 K, while for Ru(Cl)/AC-Ox they were registered at 457 K and 520 K, the former being a shoulder of the latter. In both cases the peak registered above 600 K may be related to hydrogen consumption in the partial gasification of carbon, very probably around the metal particles [55] as suggested by the fact that methane (dot line in

the Figure 1) is observed at the exit gas. For catalysts prepared from $Ru(NO)(NO_3)_3$ the TPR profiles show a reduction peak at around 500 K. It is remarkable that the hydrogen consumption for these latter is higher than that expected for the complete reduction of ruthenium. Since the catalysts were not subjected to calcination treatment the additional consumption of hydrogen has to be related to the decomposition/reduction of the nitroxyl nitrate anionic groups, which occurs simultaneously to that of the ruthenium reduction. According to the TPR experiments 523 K was the temperature selected for the reduction treatments of the catalysts. Further TPR measurements performed on catalyst samples reduced at 523 K revealed no hydrogen consumption, which indicates that ruthenium was completely reduced, and also the NO_x surface species have been removed.

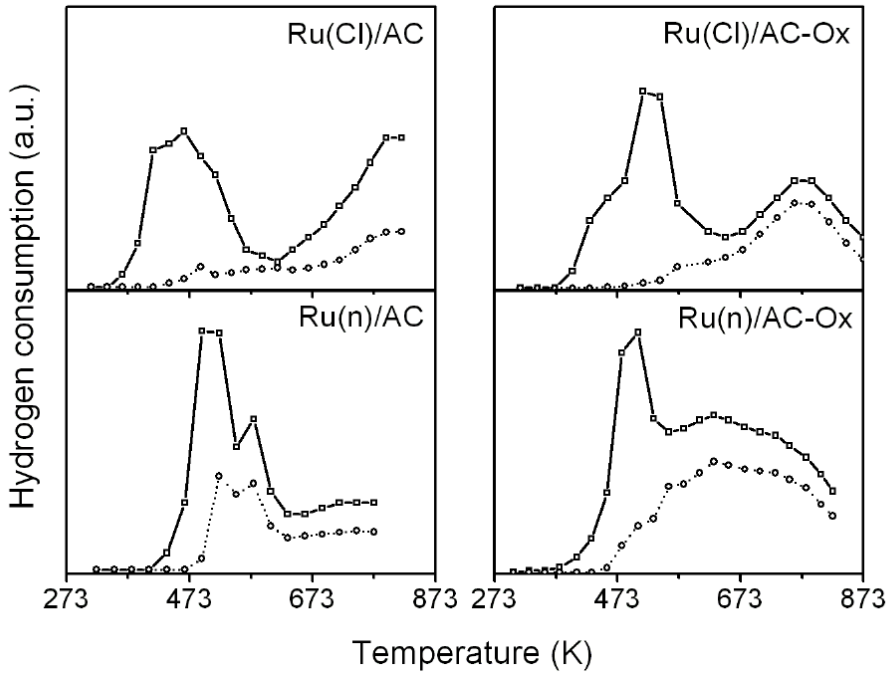

Figure 1. TPR profiles for the catalysts. Solid line: hydrogen consumption; dot line: methane production.

Study of the catalysts by TPD-MS after the reduction step was performed in order to determine the number and nature of the oxygenated groups at the catalyst surface. Figure 2 shows the concentration profiles of CO, CO_2 and H_2O removed

from the catalysts reduced at 523 K as a function of the temperature. For comparative purposes the TPD profiles of the non-pretreated supports are also included. The surface oxygen groups decompose upon heating in an inert atmosphere, the more acidic groups (carboxylic, lactonic and anhydride) evolving as CO_2 between 373 and 723 K and the less acidic ones (phenolic and carbonylic groups) evolving as CO above 723 K [58, 59].

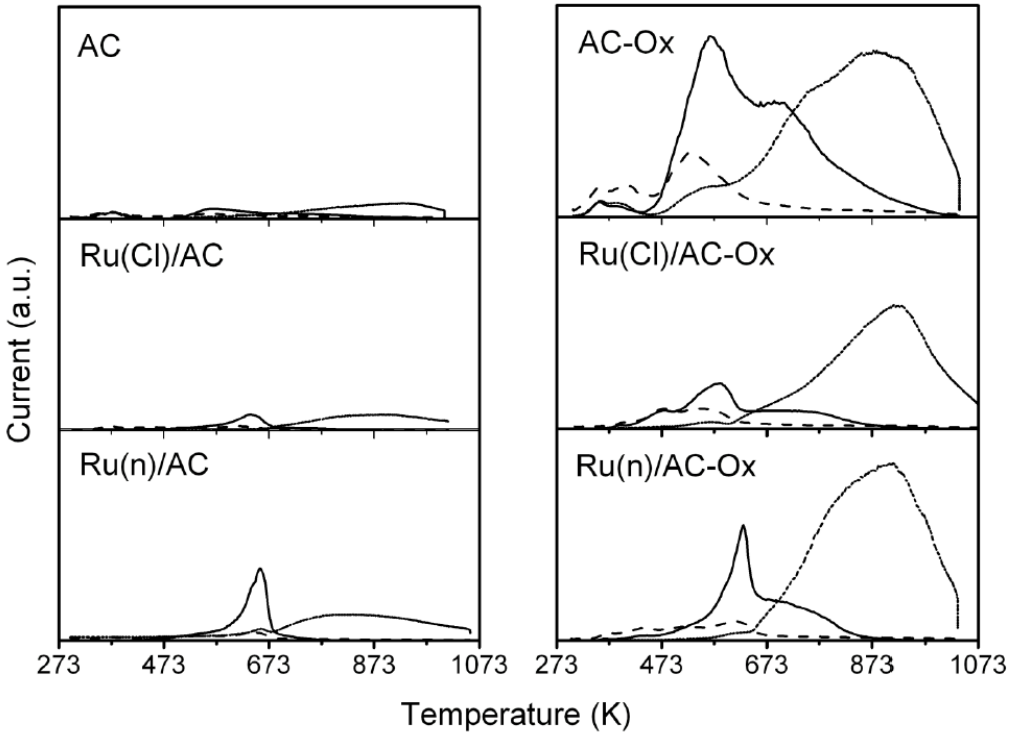

Figure 2. TPD-MS profiles of gases removed from the supports and catalysts: CO_2(solid line), CO (dot line) and H_2O (dash line).

Quantitative evaluation of the functional groups from the TPD-MS analysis is reported in Table 1 for the two supports and the reduced catalysts. As seen, the amounts of CO_2 and CO desorbed are considerably higher on the oxidized activated carbon, thus functional groups were formed on the surface of the original activated carbon. Furthermore, the oxidation treatment increases the CO_2 releasing groups in a higher proportion than the CO releasing groups. As for the reduced

catalysts is concerned, Figure 2 indicates absence of oxygen surface groups that decompose below the reduction temperature (523 K) whatever the support is. At temperatures above 523 K, it is feasible to distinguish the nature of the functional groups as a function of the precursor. Thus, ex-chloride catalysts, Ru(Cl)/AC and Ru(Cl)/AC-Ox, display the same content of oxygen groups evolving at temperatures above 523 K as their respective supports for the oxygen groups that decompose as CO and a little bit lower to the oxygen groups that decompose as CO_2, due to reduction treatment at 523 K. However, ex-nitroxyl catalysts, Ru(n)/AC and Ru(n)/AC-Ox, evidence a population of oxygen groups above 523 K higher than that of the respective supports. Therefore, new oxygen groups are formed by effect of the strong oxidant character of the nitroxyl nitrate precursor, which are added to those previously present on the respective supports. According to this information the population of oxygen groups on the surface of the reduced catalysts increases in the order Ru(Cl)/AC < Ru(n)/AC < Ru(Cl)/AC-Ox < Ru(n)/AC-Ox.

Table 1. Quantitative determination from TPD-MS analysis of surface oxygen groups for supports and the catalysts after reduction at 523 K.

Sample	mmol CO_2 g^{-1}	mmol CO g^{-1}
AC	0.19	0.99
Ru(Cl)-AC	0.14	1.01
Ru(n)-AC	0.36	1.79
AC-Ox	1.75	5.71
Ru(Cl)-AC-Ox	0.59	5.36
Ru(n)-AC-Ox	0.86	7.50

Metal loading, dispersion and average metal particle sizes obtained from both CO chemisorptions and TEM measurements, are given in Table 2. Representative images of the catalysts by TEM are shown in Figure 3. From Table 2

it should be noted that the metal particle sizes for samples prepared with AC-Ox are higher than those supported on AC, as measured either by CO adsorption or by TEM. On the other hand, the values of average particle size, measured by TEM over ex-chloride samples are similar to those of the ex-nitroxyl nitrate counterpart, in spite of the fact that the former exhibit dispersion values (D) determined from CO chemisorption lower than the latter. This finding indicates that the average ruthenium particle size does not depend on the nature of the metal precursor but rather on the previous treatment given to the support. Histograms of particle size distribution in Figure 3 illustrate this assertion.

Table 2. Characterization measurements of the catalysts.

Catalyst or support	Metal loading (%)	CO Uptake ($\mu mol/g_{cat}$)	D_{CO} (%)	d_{CO} (nm)	d_{TEM} (nm)
Ru(Cl)/AC	3.9	75	19	6.8	2.9
Ru(n)/AC	4.1	177	44	3.0	2.7
Ru(Cl)/AC-Ox	3.5	52	15	8.8	3.5
Ru(n)/AC-Ox	4.0	140	35	3.7	3.7

D_{CO}, metal dispersion; d_{CO}, average particle size as determined from CO chemisorption measurements; d_{TEM}, average particle size as determined by TEM.

The lower CO adsorption capability of the ex-chloride catalysts can be attributed to the presence of residual surface chloride species, as evidenced for instance by XPS analysis (Cl $2p_{3/2}$ = 198.4 eV) where no quantifiable trace amounts were detected. This observation, in agreement with earlier studies [60, 61] and other information [41] evidences that chloride surface species were not fully removed during the reduction treatment given to these catalysts at 523 K. Moreover, chloride species anchored at the surface can inhibit the adsorption of CO by steric blocking of Ru surface sites and simultaneously decrease the CO

chemisorption enthalpy as consequence of the formation of electron deficient ruthenium surface species [62]. On the other hand, the oxygenated groups that partially cover the surface of carbon in samples supported on AC-Ox and participate in the genesis of the metal particles, favor also their sintering when they decompose by the thermal treatment [55]. In this way the ruthenium particles on this support (samples Ru(Cl)/AC-Ox and Ru(n)/AC-Ox) are larger than those on the AC support (samples Ru(Cl)/AC and Ru(n)/AC). It should be noted that in all the cases the metal nanoparticles are homogeneously distributed at the support surface (Figure 3).

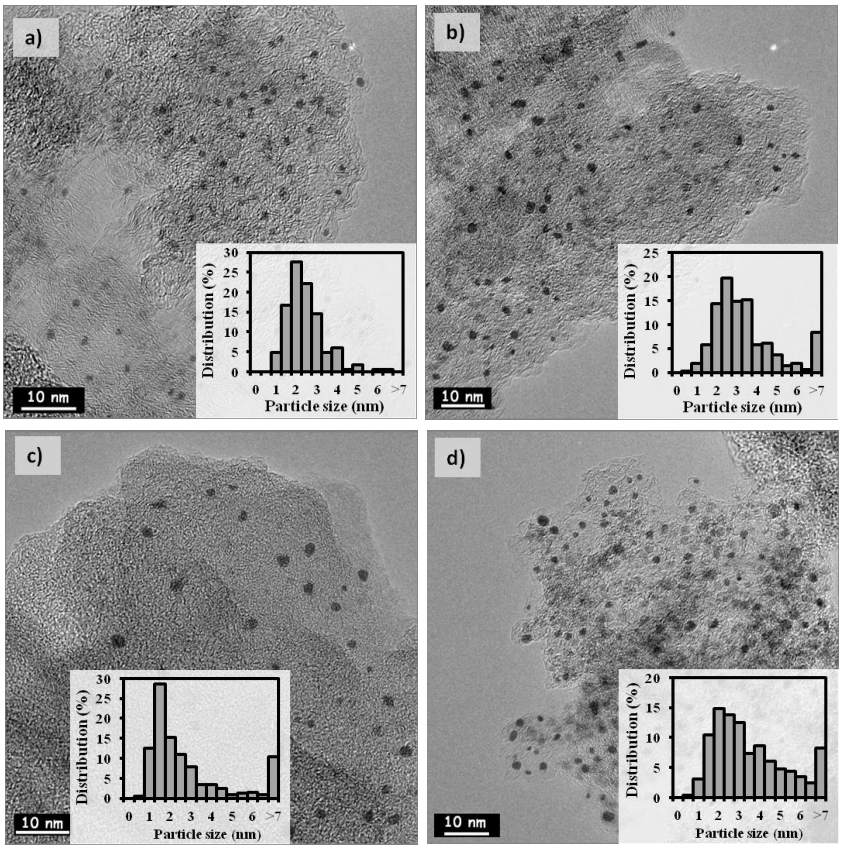

Figure 3. Images by TEM and particle size distribution of the catalysts: (a) Ru(Cl)/AC, (b) Ru(Cl)/AC-Ox, (c) Ru(n)/AC and (d) Ru(n)/Ac-Ox.

Figure 4 shows the adsorption heat of CO (Q_{ad}) as a function of the coverage degree of the metal surface for all the reduced catalysts. As shown, the calorimetric profiles of catalysts prepared from the same metal precursor are very similar, without any appreciable effect of the previous treatment given to the support. The ex-chloride catalysts exhibit an initial adsorption heat of 128 kJ mol^{-1}, which quickly

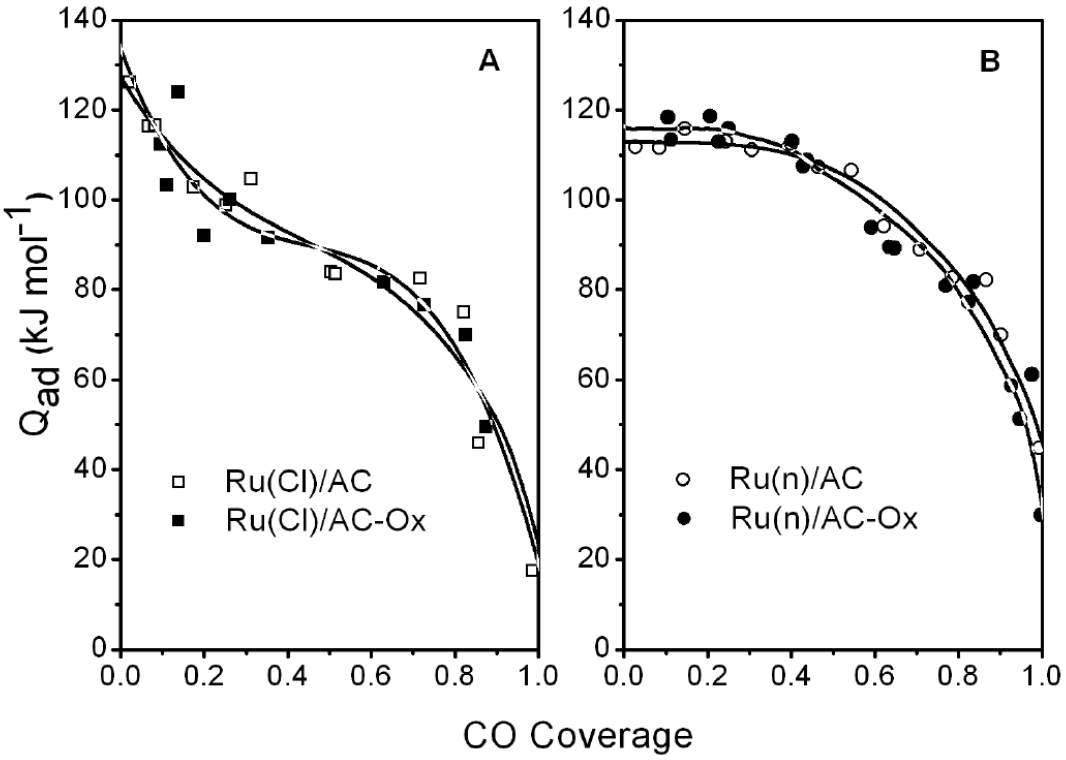

Figure 4. Microcalorimetric profiles of CO adsorption of the catalysts. (A) Samples prepared from $RuCl_3 \cdot xH_2O$ nad (B) samples prepared from $Ru(NO)(NO_3)_3$.

fall to 80 kJ mol^{-1} for a coverage degree as low as 0.5. For samples prepared from nitroxyl nitrate precursor the initial adsorption heat is lower (around 118 kJ mol^{-1}) but, in contrast, it reveals a long plateau until 0.5 coverage degree, thus suggesting a more homogeneous surface of these latter. These calorimetric profiles, which were extensively analyzed in a previous paper [62] indicate that the number of the surface adsorption sites as well as the strength and mode of the CO adsorption are more depending on the metal precursor identity than on the oxidation treatment

given to the carbon support. In other words, the nature of the metal species formed at the surface does not seem to be conditioned by the oxidation treatment given previously to the support, which only favors the growth of the ruthenium crystals. The quick decreasing of the adsorption heat values observed for the ex-chloride catalysts is consistent with the probable existence of electron-deficient metal species at the surface, above suggested, on which a weaker strength for the CO adsorption would be expected.

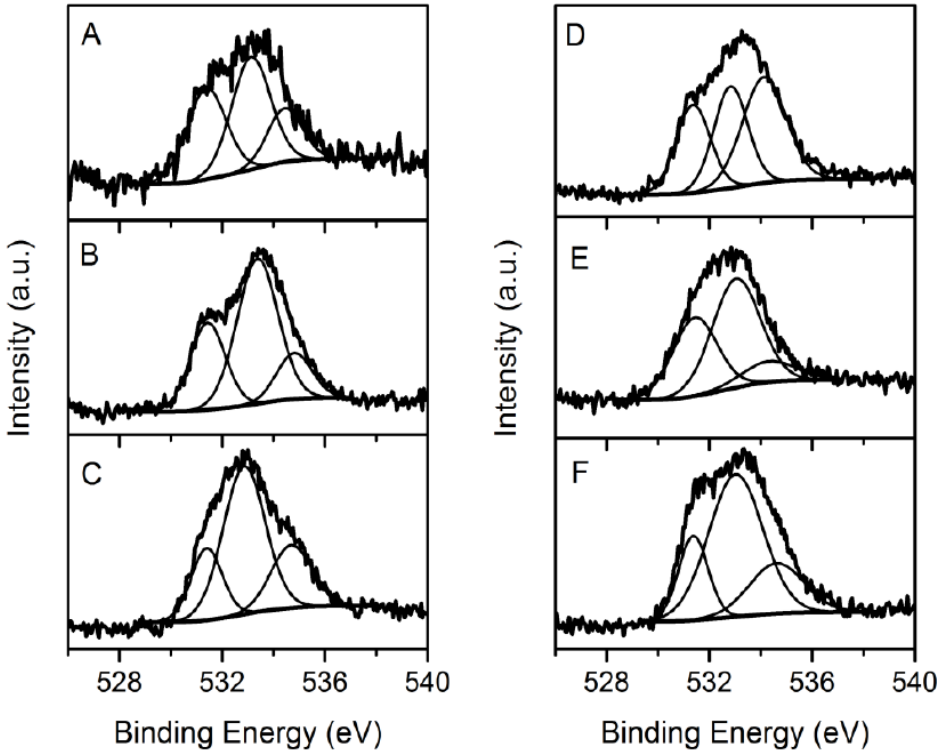

Figure 5. XPS spectra of the supports and catalysts showing the deconvolution of the O 1s peak: (A) AC, (B) Ru(Cl)/AC, (C) Ru(n)/AC, (D) AC-OX, (E) Ru(Cl)/AC-Ox and (F) Ru(n)/AC-Ox.

The chemical nature of the oxygenated surface groups above suggested was determined by XPS measurements. The XPS spectra of the supports and catalysts showing the deconvolution of the O 1s peak are given in Figure 5. From these the O/C surface atomic ratios and the percentages of the different oxygenated groups

at the surface (carboxyl, carbonyl and hydroxyl groups) were calculated and summarized in Table 3**.** The relative amounts of the O and C elements were calculated from the corresponding peak areas divided by the sensitivity factors (1.00 for C 1s and 2.85 for O 1s). The fraction of each surface oxygen groups was obtained by deconvolution of the O 1s peak in three components, namely, carbonyl oxygen (peak at 531.4 eV), oxygen atoms in C–O bonds, like hydroxyl and ether groups (peak at 532.6 eV) and oxygen atoms in acidic carboxyl groups (peak at 534.6 eV).

Table 3. XPS results of the supports and catalysts. Atomic ratios and percentage of oxygenated groups at the surface.

Support or catalyst	O/C (atom/atom)	-C=O (%)	-C-OH (%)	-COOH (%)	BE Ru $3p_{3/2}$ (eV)	Ru/C (atom/atom)	
						Bulk	XPS
AC	0.087	38	37	25			
Ru(Cl)/AC	0.100	32	58	10	462.5	0.005	0.002
Ru(n)/AC	0.127	23	55	21	462.7	0.005	0.024
AC-Ox	0.249	26	33	41			
Ru(Cl)/AC-Ox	0.138	28	48	23	462.9	0.004	0.001
Ru(n)/AC-Ox	0.174	23	44	33	462.8	0.005	0.011

Oxygenated groups at the surface: -COOH, carboxyl groups; -C=O, carbonyl groups:

-C-OH, hydroxyl and ether groups

As observed the wet oxidation of AC with nitric acid (sample AC-Ox) introduces new oxygen groups on the carbon surface, preferably carboxylic acid groups (-COOH). When comparing the values of the O/C atomic ratio for the reduced catalysts and supports it is worth to note that those corresponding to the ex-chloride catalysts are smaller (or similar in the case of AC) than those of the supports. The O/C atomic ratio for the sample Ru(Cl)/AC-Ox is lower than that of the AC-Ox support, but very similar to that found for Ru(n)/AC which, on the

other hand, is higher than the one of the AC-support. In comparison with the other catalysts the sample Ru(n)/AC-Ox exhibits the highest population of oxygen at the surface, most them being carboxylic acid species (-COOH). All these observations confirm that the nitric acid treatment and the use of nitroxyl nitrate precursor introduce oxygen groups on the carbon surface, being majority the carboxylic acid groups. They also show that part of the oxygenated groups generated on the support by the nitric acid treatment are destroyed during the reduction step of the catalysts, while the oxygenated groups formed from Ru-nitroxyl nitrate are more resistant. All these observations are in agreement with the TPD-MS measurements above discussed.

The values of binding energy of Ru $3p_{3/2}$ (Ru $3d_{5/2}$ is overlapped by C1s) registered for the reduced catalyst after exposure to air range from 462.5 to 462.9 eV. These values could be reasonably ascribed to anhydrous RuO_2, in accordance with the values reported for these species [63, 64, 65] and evidence the surface oxidation of the reduced catalysts. As for the Ru/C surface atomic ratio is concerned, comparison of the XPS values with the corresponding bulk values in Table 3 indicates that Ru in samples ex-nitroxyl nitrate is preferentially deposited outside the support, in contract with that observed for the ex-chloride catalysts. It seems that the adsorption sites at the external surface of the carbon grains interact with the nitroxyl nitrate precursor more strongly than with the chloride precursor.

4.2.3.2. Hydrogenolysis of glycerol

The overall activity of the catalysts and selectivity towards the main reaction products in the hydrogenolysis of glycerol at 453 K and 8 MPa, after 24 h of reaction, are summarized in Table 4. Results obtained at lower temperatures were not considered, due to the low reaction rates achieved. In all cases the major

products were ethylene glycol (EG) and 1,2-propanediol (1,2-PDO). Other products (OP) such as 1-propanol, 2-propanol, propane, ethanol, methanol, ethane and methane were identified either in the liquid phase or in the gas phase. Trace amounts of 1,3-propanediol (1,3-PDO) and acetol were also found. Activity was calculated as glycerol molecules converted per gram of catalyst and per minute, while selectivity towards a product i is defined as molecules of i formed per glycerol molecule converted. The catalytic activity per active site or turnover frequency (TOF) was calculated using the number of surface Ru sites as measured by CO chemisorption.

Table 4. Activity and selectivity of the catalysts in the hydrogenolysis of glycerol at 453 K and 8 MPa, after 24 h of reaction time.

Catalyst	*X* (%)	Activity (μmol g_{cat}^{-1} min^{-1})	TOF (h^{-1})	Selectivity (%)		
				1,2-PDO	EG	OP
Ru(Cl)/AC	11	19.0	16	14	63	24
Ru(n)/AC	36	62.0	21	10	41	49
Ru(Cl)/AC-Ox	17	29.2	34	11	43	46
Ru(n)/AC-Ox	42	72.2	31	8	30	62
Ru(Cl)/AC+ AC-Ox	26	44.7	36	15	21	64

In order to compare the performance of the catalysts, it is important to remind that impurities of the commercial carbon used as support were removed by the hydrochloric acid treatment and, therefore, differences in the catalytic action of the samples have to be related to the respective metal precursor used and the treatment given to the support. Also control blank experiments with the bare supports were conduced and in no case EG or 1,2-PDO were detected as reaction products.

Results in Table 4 show that regardless of the support used the ex-nitroxyl nitrate catalysts, Ru(n)/AC and Ru(n)/AC-Ox, are much more active than the corresponding ex-chloride catalysts, Ru(Cl)/AC and Ru(Cl)/AC-Ox, due in part to the higher dispersion of the former. Moreover, the TOFs of catalysts prepared from different Ru precursor but with the same support are very similar, the TOF of catalyst supported on AC-Ox being higher than those of the corresponding samples based on the AC support. These findings reveal, on one hand, that surface ruthenium atoms free of chloride species in ex-chloride catalysts have the same catalytic activity as those in the corresponding ex-nitroxyl catalyst and, on the other hand, surface metal atoms on the oxidized carbon (AC-Ox) are more active than the counterparts supported on the untreated carbon (AC).

As for the reaction product composition is concerned, selectivity towards ethylene glycol (S_{EG}) strongly decreases in the order Ru(Cl)/AC > Ru(n)/AC ≈ Ru(Cl)/AC-Ox > Ru(n)/AC-Ox, from 62% to 30%. Selectivity toward 1,2-propanediol (S_{PDO}) decreases in parallel with S_{EG}, but only from 14% to 8%. On the contrary, selectivity towards other products (S_{OP}), which are mostly undesired, markedly increases in the opposite trend, from 24% to 62%. Note, on the other hand, that catalysts Ru(n)/AC and Ru(Cl)/AC-Ox at different conversion levels (36% and 17%, respectively) show very similar selectivity values, while Ru(Cl)/AC and Ru(Cl)/AC-Ox or Ru(n)/AC and Ru(n)/AC-Ox, at nearer conversion levels, exhibit different selectivities.

Comparison of our kinetic results with those reported in the literature for other ruthenium supported catalysts is neither easy nor immediate, due to the important differences in the formulation of the catalysts and in the experimental conditions used in the catalytic tests. Even so, activity and selectivity values in Table 4 agree with the results reported in the literature for other Ru/C supported

catalysts tested at 453 K [30, 45]. They contrast, however, with the higher selectivity values towards 1,2-PDO obtained at 473 K by using high concentration solutions of glycerol [66] and with those obtained using other supports [39, 40, 41].

Since the turnover frequency improves when the surface population of carboxyl functional groups increases (see Tables 1 and 3) it is reasonable to believe that transformation of glycerol over our catalysts occurs through the mechanism proposed by Miyazawa et al. [29] involving metal and acid sites, following the scheme of parallel and consecutive reactions given in Figure 6. In this reaction scheme dehydration of glycerol to acetol or 3-hydroxypropionaldehyde occurs on acid sites, with the consecutive hydrogenation of these intermediates over metal sites to be desorbed as 1,2-PDO and 1,3-PDO, respectively. In parallel, ethylene glycol is formed by dehydrogenation of glycerol to glyceraldehyde on metal sites, which is transformed into ethylene glycol, on the same metal sites, by successive retro-aldol and hydrogenation reactions. These parallel routes of reaction have been verified by different author [47, 66] and the bifunctional mechanism frequently invoked to explain results of hydrogenolysis of glycerol over metal catalysts ([67, 68], among other).

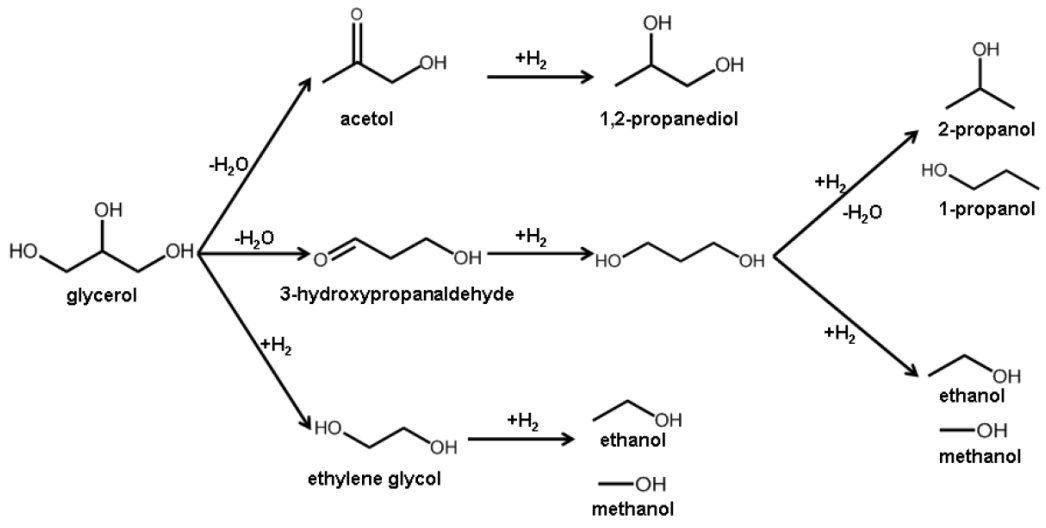

Figure 6. Reaction scheme for the hydrogenolysis of glycerol in the liquid phase.

Following the reaction scheme in Figure 6, the highest selectivity towards ethylene glycol (62%) over Ru(Cl)/AC catalyst could be related to a low population of acid groups in comparison with that of metal sites, so that the reactions proceeding on metal sites (EG formation) are majority. Decreasing of S_{EG} in the order Ru(Cl)/AC > Ru(n)/AC ≈ Ru(Cl)/AC-Ox > Ru(n)/AC-Ox, as the population of acid groups increases, is clearly consistent with the enhancement of the transformation routes of glycerol through acetol and 3-hydroxypropionaldehyde on acid sites. In this context it is remarkable that catalysts Ru(n)/AC and Ru(Cl)/AC-Ox containing similar concentration of –COOH groups, give much the same selectivity values at very different conversions, while Ru(Cl)/AC and Ru(Cl)/AC-Ox or Ru(n)/AC and Ru(n)/AC-Ox, exhibit very different selectivities at nearer conversion levels, in accord with the respective concentration of –COOH acidic groups. Undesired by-products such as 1-propanol, 2-propanol, ethanol and methane can be formed from 1,3-PDO, EG and 1,2-PDO. Indeed, degradation of these three compounds occurs over Ru/C catalysts with the reactivity order 1,3-PDO > EG > 1,2-PDO [29, 47]. Thereby, the high reactivity of 1,3-PDO could explain the low concentration of this product observed under our experimental conditions (~1%) and selectivities toward degradation products around 60%.

In order to a better insight about the effect of the functional groups of carbon on the transformation of glycerol, an additional experiment was done using an admixture catalyst comprised of the less active sample Ru(Cl)/AC (450 mg) and an aliquot of 500 mg of the AC-Ox support (2 mEq H^+ per g of carbon). As shown in Table 4 the activity and the TOF values of the admixture Ru(Cl)/AC+AC-Ox are more than twice those of Ru(Cl)/AC and also higher than those of Ru(Cl)/AC-Ox. Moreover, reactions involving acid sites seem to be more favored on the admixture catalyst. In this sense selectivity towards 1,2-PDO remains practically invariable

with respect to that of Ru(Cl)/AC (15% vs. 14%) but it is higher than that of Ru(Cl)/AC-Ox (8%), while S_{EG} decreases to 21%. From a kinetic point of view, this means that activity to 1,2-PDO of the admixture catalyst (6.7 μmol g_{cat}^{-1} min) is improved with respect to that of Ru(Cl)/AC and Ru(Cl)/AC-Ox (2.6 and 3.2 μmol g_{cat}^{-1} min^{-1}, respectively) while activity to ethylene glycol slightly decreases with respect to that of Ru(Cl)/AC-Ox (from 12.0 μmol g_{cat}^{-1} min^{-1} to 9.4 μmol g_{cat}^{-1} min^{-1}). Notwithstanding, transformation of glycerol into undesired products on the admixture Ru(Cl)/AC+AC-Ox is highly favored.

Bearing in mind all these results it is clear that the admixture Ru(Cl)/AC+AC-Ox is more effective than the Ru(Cl)/AC-Ox catalyst, because the acid functional groups were not removed from the AC-Ox support and, therefore, their concentration is higher than on Ru(Cl)/AC-Ox (Table 3). These findings evidence that acid sites formed at the carbon surface from either the nitroxyl nitrate precursor or by effect of the nitric acid treatment play a positive role in the transformation of glycerol into 1,2-propanediol, but only part of these acid sites are stable at the reduction temperature. Hence, in order to improve the production of 1,2- propanediol over Ru/C catalysts promoted by acid functional groups in treated carbon, the admixture comprised of Ru(Cl)/AC catalyst and AC-Ox support is preferred to the Ru(Cl)/AC-Ox catalyst. Additional studies are required, however, to minimize formation of undesired products and know the effect of the different experimental parameters on the product distribution, namely, the catalyst weigh, the ratio of Ru(Cl)/AC to AC-Ox, the reaction temperature as well as the reaction time, among other.

4.2.4. CONCLUSIONS

Characterization measurements and performances in the hydrogenolysis of glycerol of the prepared catalysts, Ru(Cl)/AC, Ru(n)/AC, Ru(Cl)/AC-Ox and Ru(n)/AC-Ox, are analyzed and discussed. The nitric acid treatment generates oxygenated groups of different nature on the carbon surface and nitroxyl nitrate, as ruthenium precursor, also originates incorporation of some oxygen species on the supports. Nevertheless, part of the more acidic groups (carboxylic, lactonic and anhydride groups) decompose during the reduction of the catalysts at 523 K, the groups formed from nitroxyl nitrate precursor being more stable than those originated by the nitric acid treatment. Catalysts supported on treated activated carbon, Ru(Cl)/AC-Ox and Ru(n)/AC-Ox, exhibit ruthenium particles larger than catalysts supported on untreated activated carbon, without any effect of the nature of the precursor. Chlorine species anchored at the surface of the ex-chloride catalysts block part of the Ru sites and inhibit the adsorption capacity of the metal surface.

The overall activity of the catalysts in the hydrogenolysis of glycerol increases in parallel with the concentration of surface acid groups. These groups improve formation of 1,2-propanediol through a two-step reaction mechanism involving metal and acid sites, in the detriment of the formation of ethylene glycol on metal sites. However, the enhancement of overall TOF, which is related to the population increase of surface acidic groups, is largely the result of the higher C=O and/or C-C cleavage activity that produces degradation of glycerol and of their hydrogenolysis products.

4.2.5. REFERENCES

[1] S. Fernando, S. Adhikari, C. Chandrapal, N. Murali, Biorefineries: Current status, challenges, and future direction, Energy & Fuels 20 (2006) 1727-1737.

[2] H. Fukuda, A. Kondo, H. Noda, Biodiesel fuel production by transesterification of oils, J. Biosci. Bioeng. 92 (2001) 405-416.

[3] A. Corma, G.W. Huber, L. Sauvanaud, P. O'Connor, Biomass to chemicals: Catalytic conversion of glycerol/water mixtures into acrolein, reaction network, J. Catal. 257 (2008) 163-171.

[4] E. Tsukuda, S. Sato, R. Takahashi, T. Sodesawa, Production of acrolein from glycerol over silica-supported heteropoly acids, Catal. Comm. 8 (2007) 1349-1353.

[5] S. Hirasawa, H. Watanabe, T. Kizuka, Y. Nakagawa, K. Tomishige, Performance, structure and mechanism of Pd–Ag alloy catalyst for selective oxidation of glycerol to dihydroxyacetone, J. Catal. 300 (2013) 205-216.

[6] S. Hirasawa, Y. Nakagawa, K. Tomishige, Selective oxidation of glycerol to dihydroxyacetone over a Pd–Ag catalyst. Catal. Sci. Technol. 2 (2012) 1150-1152.

[7] W.C. Ketchie, Y.L. Fang, M.S. Wong, M. Murayama, R.J. Davis, Influence of gold particle size on the aqueous-phase oxidation of carbon monoxide and glycerol, J. Catal. 250 (2007) 94-101.

[8] S. Carrettin, P. McMorn, P. Johnston, K. Griffin, C.J. Kiely, G.J. Hutchings, Oxidation of glycerol using supported Pt, Pd and Au catalysts, Phys. Chem. Chem. Phys. 5 (2003) 1329-1336.

[9] A. Gallo, C. Pirovano, M. Marelli, R. Psaro, V. Dal Santo, Hydrogen production by glycerol steam reforming with Ru-based catalysts: A study on Sn doping, Chem. Vapor Deposition J. 16 (2010) 305-310.

[10] P.D. Vaidya, A.E. Rodrigues, Glycerol reforming for hydrogen production: A review, Chem. Eng. Tech. 32 (2009) 1463-1469.

[11] M. Crisan, M. Zaharescu, V. D. Kumari, M. Subrahmanyam, D. Crisan, N. Dragan, M. Raileanua, M. Jitianu, A. Rusu, G. Sadanandam, J. K. Reddy, Sol–gel

based alumina powders with catalytic applications, Appl. Surf. Sci. 258 (2011) 448-455.

[12] S. Liu, X. Wang, K. Wang, R. Lv, Y. Xu, ZnO/ZnS–PdS core/shell nanorods: Synthesis, characterization and application for photocatalytic hydrogen production from aglycerol/water solution, Appl. Surf. Sci. 283 (2013) 732-739.

[13] G.N. Bennett, K.Y. San, Microbial formation, biotechnological production and applications of 1,2-propanediol, Appl. Microbiol. Biotechnol. 55 (2001) 1-9.

[14] C. V. Rode, A.A. Ghalwadkar, R.B. Mane, A. M. Hengne, S.T. Jadkar, N.S. Biradar, Selective hydrogenolysis of glycerol to 1,2-propanediol: Comparison of batch and continuous process operations, Org. Process Res. Dev. 14 (2010) 1385-1392.

[15] H. Yue, Y. Zhao, X. Ma, J. Gong, Ethylene glycol: properties, synthesis, and applications, Chem. Soc. Rev. 41 (2012) 4218-4244.

[16] R. Jaganathan, R.V. Chaudhari, P.A. Ramachandran, Hydration of propylene oxide using ion-exchange resin catalyst in a slurry reactor, AIChE Journal 30 (1984) 1-7.

[17] L.K. Freidlin, V.Z. Sharf, Vapor-phase hydration of propylene oxide over tricalcium phosphate, Russ. Chem. Bull. 9 (1960) 170-174.

[18] D.F. Othmer, M.S. Thakar, Glycol Production-hydration of ethylene oxide, Ind. Eng. Chem. 50 (1958) 1235-1244.

[19] Furikado, T. Miyazawa, S. Koso, A. Shimao, K. Kunimori, K. Tomishige, Catalytic performance of Rh/SiO_2 in glycerol reaction under hydrogen, Green Chem. 9 (2007) 582- 588.

[20] Shimao, S. Koso, N. Ueda, Y. Shinmi, I. Furikado, K. Tomishige, Promoting effect of Re addition to Rh/SiO_2 on glycerol hydrogenolysis, Chem. Lett. 38 (2009) 540-541.

[21] Y. Shinmi, S. Koso, T. Kubota, Y. Nakagawa, K. Tomishige, Modification of Rh/SiO_2 catalyst for the hydrogenolysis of glycerol in water, Appl. Catal. B: Environmental 94 (2010) 318-326.

[22] Y. Nakagawa, Y. Shinmi, S. Koso, K. Tomishige, Direct hydrogenolysis of glycerol into 1,3-propanediol over rhenium-modified iridium catalyst, J. Catal. 272 (2010) 191-194.

[23] Y. Amada, S. Koso , Y. Nakagawa , K Tomishige, Hydrogenolysis of 1,2-propanediol for the production of biopropanols from glycerol, ChemSusChem, 3 (2010) 728-736.

[24] Y. Amada, Y. Shinmi, S. Koso, T. Kubota, Y. Nakagawa, K. Tomishige, Reaction mechanism of the glycerol hydrogenolysis to 1,3-propanediol over Ir–ReO_x/SiO_2 catalyst, Appl. Catal. B: Environmental 105 (2011) 117-127.

[25] Y. Nakagawa, X. Ning, Y. Amada, K. Tomishige, Solid acid co-catalyst for the hydrogenolysis of glycerol to 1,3-propanediol over Ir-ReO_x/SiO_2, Appl. Catal. A: General 433-434 (2012) 128-134.

[26] Y. Amada, H. Watanabe, M. Tamura, Y. Nakagawa, K. Okumura, K. Tomishige, Structure of ReO_x Clusters Attached on the Ir Metal Surface in Ir–ReO_x/SiO_2 for the Hydrogenolysis Reaction, J. Phys. Chem. C 116 (2012) 23503-23514.

[27] X. Hong, B. Li, Y. Wang, J. Lu, G. Hu, M. Luo, Stable Ir/SiO2 catalyst for selective hydrogenation of crotonaldehyde, Appl, Surf. Sci. 270 (2013) 388– 394.

[28] B. Li, X. Hong, J. Lin, G. Hu, Q. Yu, Y. Wang, M. Luo, J. Lu, Promoting effect of Ir on the catalytic property of Ru/ZnO catalysts for selective hydrogenation of crotonaldehyde, Appl. Surf. Sci. 280 (2013) 179-185.

[29] T. Miyazawa, Y. Kusunoki, K. Kunimori, K. Tomishige, Glycerol conversion in the aqueous solution under hydrogen over Ru/C + an ion-exchange resin and its reaction mechanism, J. Catal. 240 (2006) 213-221.

[30] C. Montassier, J.C. Ménézo, L.C. Hoang, C. Renaud, J. Barbier, Aqueous polyol conversions on ruthenium and on sulfur-modified ruthenium, J. Mol. Catal. 70 (1991) 99-110.

[31] M. Akiyama, S. Sato, R. Takahashi, K. Inui, M. Yokota, Dehydration–hydrogenation of glycerol into 1,2-propanediol at ambient hydrogen pressure, Appl. Catal. A: General 371 (2009) 60-66.

[32] Z. Huang, F. Cui, H. Kang, J. Chen, C. Xia, Characterization and catalytic properties of the CuO/SiO2 catalysts prepared by precipitation-gel method in the hydrogenolysis of glycerol to 1,2-propanediol: Effect of residual sodium, Appl. Catal. A: General 366 (2009) 288-298.

[33] E.S. Vasiliadou, A.A. Lemonidou, Investigating the performance and deactivation behaviour of silica-supported copper catalysts in glycerol hydrogenolysis, Appl. Catal. A: General 396 (2011) 177-185.

[34] E. Maris, R. Davis, Hydrogenolysis of glycerol over carbon-supported Ru and Pt catalysts, J. Catal. 249 (2007) 328-337.

[35] X. Liao, K. Li, X. Xiang, S.G. Wang, X. She, Y. Zhu, Y. Li, Mediatory role of K, Cu and Mo over Ru/SiO2 catalysts for glycerol hydrogenolysis, J. Ind. Eng. Chem. 18 (2012) 818-821.

[36] E. Maris, W. Ketchie, M. Murayama, R. Davis, Glycerol hydrogenolysis on carbon-supported PtRu and AuRu bimetallic catalysts, J. Catal. 251 (2007) 281-294.

[37] Z. Wu, Y. Mao, X. Wang, M. Zhang, Preparation of a Cu–Ru/carbon nanotube catalyst for hydrogenolysis of glycerol to 1,2-propanediol via hydrogen spillover, Green Chem. 13 (2011) 1311-1316.

[38] D. Roy, B. Subramaniam, R.V. Chaudhari, Aqueous phase hydrogenolysis of glycerol to 1,2-propanediol without external hydrogen addition, Catal Today 156 (2010) 31–37.

[39] E.S. Vasiliadou, E. Heracleous, I.A. Vasalos, A.A. Lemonidou, Ru-based catalysts for glycerol hydrogenolysis - Effect of support and metal precursor, Appl. Catal. B: Environmental 92 (2009) 90-99.

[40] J. Feng, H. Fu, J. Wang, R. Li, H. Chen, X. Li, Hydrogenolysis of glycerol to glycols over ruthenium catalysts: Effect of support and catalyst reduction temperature, Catal. Commun. 9 (2008) 1458-1464.

[41] M. Balaraju, V. Rekha, B.L.A. Prabhavathi Devi, R.B.N. Prasad, P.S. Sai Prasad, N. Lingaiah, Surface and structural properties of titania-supported Ru catalysts for hydrogenolysis of glycerol, Appl. Catal. A: General 384 (2010) 107-114.

[42] S.H. Lee, D.J. Moon, Studies on the conversion of glycerol to 1,2-propanediol over Ru-based catalyst under mild conditions, Catal. Today 174 (2011) 10-16

[43] N. Hamzah, N.M. Nordin, A.H.A. Nadzri, Y.A. Nik, M.B. Kassim, M.A. Yarmo, Enhanced activity of Ru/TiO2 catalyst using bisupport, bentonite-TiO2 for hydrogenolysis of glycerol in aqueous media Appl. Catal. A: General 419-420 (2012) 133-141.

[44] J. Wang, S. Shen, B. Li, H. Lin, Y. Yuan, Ruthenium nanoparticles supported on carbon nanotubes for selective hydrogenolysis of glycerol to glycols. Chem. Lett. 38 (2009) 572-528.

[45] Y. Kusunoki, T. Miyazawa, K. Kunimori, K. Tomishige, Highly active metal–acid bifunctional catalyst system for hydrogenolysis of glycerol under mild reaction conditions, Catal. Comm. 6 (2005) 645-649.

[46] T. Miyazawa, S. Koso, K. Kunimori, K. Tomishige, Glycerol hydrogenolysis to 1,2-propanediol catalyzed by a heat-resistant ion-exchange resin combined with Ru/C, Appl. Catal. A: General 329 (2007) 30-35.

[47] T. Miyazawa, S. Koso, K. Kunimori, K. Tomishige, Development of a Ru/C catalyst for glycerol hydrogenolysis in combination with an ion-exchange resin, Appl. Catal. A: General 318 (2007) 244-251.

[48] S. Bolado, R.E. Treviño, M.T. García-Cubero, G. González-Benito, Glycerol hydrogenolysis to 1, 2 propanediol over Ru/C catalyst, Catal. Comm. 12 (2010) 122-126.

[49] A. Corma, S. Iborra, A. Velty, Chemical routes for the transformation of biomass into chemicals, Chem. Rev. 107 (2007) 2411-2502.

[50] J. N. Chheda, G,W. Huber, J.A. Dumesic, Liquid-phase catalytic processing of biomass-derived oxygenated hydrocarbons to fuels and chemicals, Angew. Chem. Int. Ed. 46 (2007) 7164-7183.

[51] Ch.H. Zhou, J.N. Beltramini, Y.X. Fana, G.Q. Lu, Chemoselective catalytic conversion of glycerol as a biorenewable source to valuable commodity chemicals, Chem. Soc. Rev. 37 (2008) 527-549.

[52] A. Behr, J. Eilting, K. Irawadi, J. Leschinski, F. Lindner, Improved utilization of renewable resources: New important derivatives of glycerol, Green Chem. 10 (2008) 13-30.

[53] Y. Nakagawa, K. Tomishige, Heterogeneous catalysis of the glycerol hydrogenolysis, Catal. Sci. Technol. 1 (2011) 179-190.

[54] A. Guerrero-Ruiz, A. Maroto-Valiente, M. Cerro-Alarcón, B. Bachiller-Baeza, I. Rodríguez-Ramos, Surface properties of supported metallic clusters as determined by microcalorimetry of CO chemisorption, Top. Catal. 19 (3) (2002) 303-311.

[55] A. Guerrero-Ruiz, P; Badenes, I. Rodríguez-Ramos, Study of some factors affecting the Ru and Pt dispersions over high surface area graphite-supported catalysts, Appl. Catal. A: General, 173 (1998) 313-321.

[56] J. Álvarez-Rodríguez, I. Rodríguez-Ramos, A. Guerrero-Ruiz, E. Gallegos-Suarez, A. Arcoya, Influence of the nature of support on Ru-supported catalysts for selective hydrogenation of citral, Chem. Eng. J. 204–206 (2012) 169-178.

[57] L.M. Gomez-Sainero, A. Cortes, X.L. Seoane, A. Arcoya, Hydrodechlorination of carbon tetrachloride to chloroform in the liquid phase with metal-supported catalysts. Effect of the catalyst components, Ind. Eng. Chem. Res. 39 (2000) 2849-2854.

[58] Y. Otake, and R.G. Jenkins, Characterization of oxygen-containing surface complexes created on a microporous carbon by air and nitric acid treatment. Carbon, 31 (1993) 109-121.

[59] J. L. Figueiredo, M.F.R. Pereira, M.M.A. Freitas, J.J.M. Órfão, Modification of the surface chemistry of activated carbons, Carbon 37 (1999) 1379-1389.

[60] A. Arcoya, A. Cortes, J.L.G. Fierro, X.L. Seoane, Comparative study of the deactivation of group-VIII metal-catalysts by thiophene poisoning in ethylbenzene hydrogenation, Stud. Surf. Sci. Catal. 68 (1991) 557-564.

[61] B. Bachiller-Baeza, A. Guerrero-Ruiz, I. Rodríguez-Ramos, Role of the residual chlorides in platinum and ruthenium catalysts for the hydrogenation of α,β-unsaturated aldehydes, Appl. Catal. A: General 192 (2000) 289-297.

[62] A. Guerrero-Ruiz, E. Gallegos-Suárez, L. Gonzalo-Chacón, I. Rodríguez-Ramos, Surface properties of Ru particles supported on carbon materials: A microcalorimetric study of the effects over the CO chemisorptions of residual anionic species, Therm. Acta 567 (2013) 112-117.

[63] B. Yang, Q. Lu, Y. Wang, L. Zhuang, J. Lu, P. Liu, J. Wang, R. Wang, Simple and low-cost preparation method for highly dispersed PtRu/C catalysts, Chem. Mater. 15 (2003) 3552-3557.

[64] R. Chetty, W. Xia, S. Kundu, M. Bron, T. Reinecke, W. Schuhmann, M. Muhler, Effect of reduction temperature on the preparation and characterization of Pt–Ru nanoparticles on multiwalled carbon nanotubes, Langmuir 25 (2009) 3853-3860.

[65] J. H. Ma, Y.Y. Feng, J. Yu, D. Zhao, A.J. Wang, B.Q. Xu, Promotion by hydrous ruthenium oxide of platinum for methanol electro-oxidation, J. Catal. 275 (2010) 34-44.

[66] M.A. Dasari, P.P. Kiatsimkul, W.R. Sutterlin, G.J. Suppes, Low-pressure hydrogenolysis of glycerol to propylene glycol, Appl. Catal. A: General 281 (2005) 225-231.

[67] A. Alhanash; E. F. Kozhevnikova, I. V. Kozhevnikov, Hydrogenolysis of glycerol to propanediol over Ru: polyoxometalate bifunctional catalyst, Catal. Lett. 120 (2008) 307-311.

[68] M. Balaraju, V. Rekha, P.S. Sai Prasad, B.L.A. Prabhavathi Devi, R.B.N. Prasad, N. Lingaiah, Influence of solid acids as co-catalysts on glycerol hydrogenolysis to propylene glycol over Ru/C catalysts, Appl. Catal. A: General 354 (2009) 82-87.

4.3 Surface properties of Ru particles supported on carbon materials: a microcalorimetric study of the effects over the CO chemisorptions of residual anionic species

A. Guerrero-Ruiz[1,2], E. Gallegos-Suárez[1,3], L. Gonzalo-Chacón[3] and I. Rodríguez-Ramos[3]

Thermochimica Acta 567(2013)11-117

1. Dpto. Química Inorgánica y Técnica, Fac. de Ciencias, UNED, c/Senda del Rey nº9, 28040 Madrid, Spain.
2. Grupo de Diseño y Aplicación de Catalizadores Heterogéneos, Unidad Asociada UNED-CSIC (ICP), Spain.
3. Instituto de Catálisis y Petroleoquímica, CSIC, c/Marie Curie 2, 28049 Madrid, Spain.

4.3.0 ABSTRACT

Chemisorption of CO combined with microcalorimetry has been applied to study the nature, number and adsorption strength distribution of surface sites exposed by carbon-supported Ru catalysts. A comparative analysis of the CO chemisorption on different Ru catalysts, prepared using two different metal precursors, $RuCl_3 \cdot xH_2O$ and $Ru(NO)(NO_3)_3$, has been carried out. An activated carbon and the corresponding derivative where oxygen surface groups were incorporated, as well as carbon nanotubes and a high surface area graphite, were used as catalytic supports. Based on previous temperature programmed reduction studies, all the catalysts were reduced under hydrogen flow at 523 K or at 573 K. The CO adsorption differential enthalpy profiles show that $Ru(NO)(NO_3)_3$ precursor produces more homogeneous surface site distribution in the Ru nanocrystals, in comparison with those prepared from $RuCl_3$, as well as higher values of enthalpies in the medium range of coverage. As a possible explanation for this effect, residual chloride species remaining after reduction treatment in the ex-chloride catalysts, that can be anchored to the Ru nanoparticles weakening the CO adsorption, have been considered. This behavior occurs for the three studied carbon supports. On the other hand, the oxygen surface groups incorporated on the activated carbon seem not to modify the CO adsorption properties of the catalysts, independently of the precursor employed.

4.3.1 INTRODUCTION

Adsorption calorimetry has been widely used to measure the energy of interaction of probe molecules with the surface of the catalysts, which is a parameter related with its surface structure [1]. Pioneers studies by Gravelle et al. have employed Tian-Calvet calorimeters to measure heats of hydrogen and CO chemisorptions on supported metal catalysts [2, 3, 4]. In this cases Ni and Ni-Cu supported nanoparticles where investigated, being demonstrated that CO chemisorption is an interesting tool for studying active metal surface sites. This is due, among others, to the well known CO molecule binding mechanism of chemisorption, which is highly sensitive to modifications of the electronic properties of the adsorbing sites and to the changes in surface topology [1, 5]. In many cases CO chemisorption calorimetric data are complementarily analyzed with spectroscopic techniques [6, 9], for instance Fourier-transformed Infrared Spectroscopy (FTIR), but when carbon materials are used as supports, the surface structure of the deposited nanometallic particles can be hardly characterized by these spectroscopic techniques, and chemisorption microcalorimetry rises as the more applicable technique.

On the other hand, the preparation and activation of carbon supported metal catalysts require a series of steps that merit a further understanding. The method of preparation and the metal precursor are some preliminary aspects to be considered, but also the activation steps are important, usually consisting in drying and reduction. Thus, if the reduction temperature is too high we can assure that the metallic surface sites are free of residual adsorbed species, but possibly we are producing particles larger in sizes than when we reduce at an adequate temperature. In general, choosing these reduction temperatures will be based on

previous temperature programmed reduction experiments, conducted over the dried materials. In summary, the generation of metallic nanoparticles over carbon materials, with more or less developed porosities and with various graphitic structures at their surface, is a relatively complex process from the chemical point of view [10]. Finally, it should not be forgotten the possibilities of specific interactions between the carbon supports, or some surface groups exposed at the surface of these materials, and the precursor compounds or even with the generated metallic nanoparticles.

In this paper we present a comparative study of different metal precursors of ruthenium used to synthesize metal catalysts on various carbon material supports (activated carbon, high-surface area graphite and carbon nanotubes) by means of CO adsorption microcalorimetry. Thus, the effects of the some carbon materials with different porous structure, crystallinity and electronic properties are comparatively evaluated. Also the effect of using different metal precursor and the introduction of oxygen surface groups into carbon material are studied in order to see some differences in the surface active metal sites.

4.3.2 EXPERIMENTAL

4.3.2.1 Catalysts Preparation

The support materials were activated carbon (produced at ICASA, Córdoba, Spain), high-surface-area graphite (TIMCAL, S_{BET} = 299 m^2 g^{-1}) and carbon nanotube (NANOCYL, S_{BET} = 285 m^2 g^{-1}). The original activated carbon was treatment with a 10% (v/v) chloride acid aqueous solution during 12 h at reflux temperature to remove inorganic impurities. Then the activated carbon was washed until pH 7. This support is denoted as AC (S_{BET} = 1190 m^2 g^{-1}). An aliquot of

the AC support was treated with a 10% (v/v) nitric acid aqueous solution at 348 K during 24 h to oxidize carbon surface. After treatment the activated carbon was washed until pH 7. This material is denoted AC-Ox (S_{BET} = 1160 $m^2 g^{-1}$).

All the catalysts were prepared by incipient wetness impregnation using a mixture of ethanol:water (1:1) as solvent of precursors. An exact amount of metal precursor was added in each case to obtain 4 wt% of Ru as final loading in the catalysts. Two metal precursors were used for the catalyst preparations, $RuCl_3$ and $Ru(NO)(NO_3)_3$. The catalysts synthesized with $RuCl_3$ are denoted with a "Cl" at the end of labels, and the catalysts synthesized using $Ru(NO)(NO_3)_3$ with a "N". The exact metal content of catalysts was determined gravimetrically by burning carbon in air at 1073 K for 24 h and weighing the residue (RuO_2).

4.3.2.2 Characterization techniques

The heats and enthalpies of CO chemisorption were measured in a differential and isothermal microcalorimeter of the Tian-Calvet type (C80 from SETARAM) working at 330 K and linked to a volumetric line that permitted the introduction of successive small amount of CO into the catalyst [11, 12]. For each adsorbed amount, the equilibrium pressure was measured by means of Baratron capacitance manometer (MKS Instruments). All the catalysts were first activated by reduction in H_2 during 2 h. The activated carbon (AC and AC-Ox) supported catalysts were reduced at 523 K and the other catalysts (HSAG and CNT) were reduced at 573 K. After reduction for 16 h, outgassing was performed at the same temperature as that used in reduction. Finally the samples were cooled until room temperature and transferred to the calorimeter, operated isothermically at 330 K, where using the volumetric system successive doses of CO were introduced. In each pulse both the equilibrium of CO pressure and of calorimetric thermal flow

were monitored. The metal dispersions (D) were calculated from the total CO adsorbed at the monolayer, considered to be attained when the evolved heat falls to the physisorption field (ca. 40 kJ·mol^{-1}), assuming an atomic stoichiometry of Ru/CO = 1/1 [13, 14]. The particle sizes (d_{CO}) were calculated from dispersion values, assuming spherical metal particles, using the equations d (nm) = ν/D (ν = 1.32 for Ru) [15].

TEM analysis was made using a JEOL 2100F field emission gun electron microscope operated at 200 kV. The TEM specimens were prepared by dispersing a small catalyst amount in ethanol and placing one drop of the dispersion on a lacey carbon film coated copper grid (3.0 mm, 200 mesh, Aname manufacturer) and allowing the solvent to evaporate. Over 200 individual metal particles were counted for each catalyst and the surface–weighted metal particle diameter d_s was calculated using the following equation [16].

$$d_s = \Sigma_i n_i d_i^3 / \Sigma_i n_i d_i^2$$

where n_i is the number of particles with diameter d_i.

4.3.3 RESULTS AND DISCUSSION

Table 1 summarizes the CO uptakes over the different catalysts, and the dispersions and particle sizes obtained from them assuming a Ru/CO = 1 stoichiometry.

For a certain carbon support, the amounts of adsorbed CO of catalysts synthesized using $RuCl_3$ are smaller than for the catalysts prepared from $Ru(NO)(NO_3)_3$. Furthermore the metallic dispersions determined from the CO adsorption are lower in the case of catalysts from $RuCl_3$ precursor, and

consequently the values of Ru particle sizes are higher; but these particles size determinations are in disagreement with TEM micrographs analysis (data included in the same table) for ex-chloride catalysts. Thus, when TEM particle sizes are examined it is seen that for all the activated carbon supported catalysts those values are in the same order, but these are close to those obtained by CO chemisorption only in the case of catalysts synthesized using $Ru(NO)(NO_3)_3$ as precursor. Similar result can be observed in the case of carbon nanotubes and high surface area graphite supported catalysts. As a tentative explanation taking into account the relative low temperature of reduction we have applied to the catalysts, it is considered possible that some chloride species can remain in the catalyst surfaces, as other authors have reported the detection of low levels of chlorines having high affinity on the Ru (100) surfaces [17]. Thus, residual chloride species anchored on Ru metal particles or close to them could block adsorption active sites and/or hinder the CO chemisorption.

Table 1. CO chemisorption and TEM data

Catalyst	Ru wt(%)	CO adsorption (μmol/g_{Cat})	D_{CO} (%)	d_{co} (nm)	d_{TEM} (nm)[a]
Ru/AC-Cl	3.9	75	19	6.8	3.5
Ru/AC-Ox-Cl	3.5	37	13	10.6	4.2
Ru/AC-N	4.1	177	44	3.0	3.9
Ru/AC-Ox-N	4.0	140	29	4.6	4.7
Ru/HSAG-Cl	3.8	97	26	5.1	1.9
Ru/HSAG-N	3.7	155	35	3.8	1.9
Ru/CNT-Cl	3.1	65	21	6.2	1.9
Ru/CNT-N	4.1	149	37	3.6	2.0

[a] $d_{TEM} = \sum n_i d_i^3 / \sum n_i d_i^2$

Figure 1 shows the differential enthalpies of CO adsorption as a function of surface coverage for all catalysts supported on activated carbons (original and oxidized one). The carbon monoxide coverage (θ) was determined as the ratio between adsorbed amount at a given point and the monolayer uptake of this sample, assumed to be when evolved differential enthalpy becomes lower than 40 $KJ \cdot mol^{-1}$. As can be appreciated in this figure, for a determined precursor, the two curves fully match each other for all CO surface coverage. This fact indicates that these catalysts exhibit at the metallic surfaces the same type of adsorption sites independently of the chemical properties of the support surface. Thus, the presence of surface oxygen groups on the AC-Ox support does not produce modifications in the energetic site distribution of the ruthenium nanoparticles, which is only a function of the metal precursor used in the preparation. In the case of ex-$RuCl_3$ catalysts, the profiles show high energetic actives sites at initial coverage, but quickly drop until 80 kJ at 0.5 CO coverage values. If we assume the presence of chloride species anchored on the Ru metal particles, this can have a double effect over the CO chemisorption. The first supposes a reduction in the CO uptake because this is hindered by the chloride anions occupying the surface metal sites, as it has been discussed above. The second effect can be a consequence of the electronegative character of the chloride anions which can withdraw electron density from Ru atoms giving them some electropositive character ($Ru^{\delta+}$). These electron deficient surface sites could have the property to make a stronger sigma bond with CO, but the pi back-bonding it is unfavourable, therefore due to the synergic character of the two contributions (pi and sigma) to the metal-CO molecule bond the overall metal-CO bond is weakened. This can be the reason causing that at medium and high coverage the values of adsorption enthalpies are lower in the case of catalysts prepared with $RuCl_3$. On the other hand, the profiles

of ex-Ru(NO)$(NO_3)_3$ catalysts in activated carbon reveal a long plateau at 118 kJ·mol^{-1} until 0.5 coverage. This finding indicates higher homogeneity of the surface

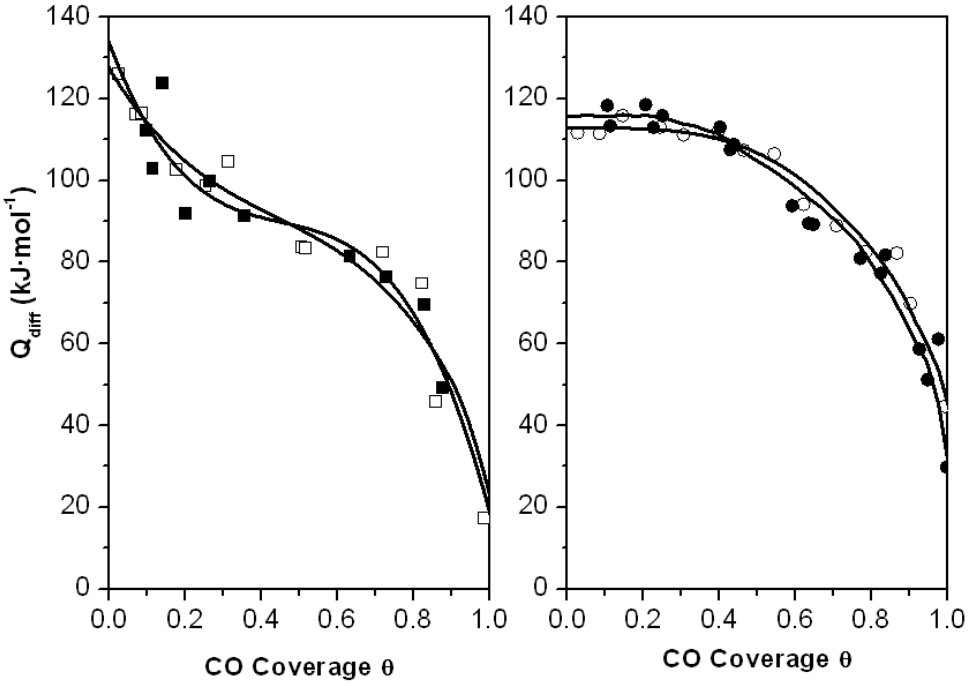

Figure 1. Differential enthalpies of CO adsorption at 330 K as a function of surface coverage for Ru/AC-Cl(□) and Ru/AC-Ox-Cl(■) in the left, and Ru/AC-N (○) and Ru/AC-Ox-N(●) in the right.

Ru atoms, which corresponds with active sites with more similar energy when bonded to CO molecules, in the case of ex-Ru(NO)$(NO_3)_3$ samples. These profiles and their values are near to those previously reported for catalysts prepared from Ru(NO)$(NO_3)_3$ and supported on high surface area graphites [18]. The higher initial values of differential chemisorption enthalpies obtained for ex-$RuCl_3$ samples can be assigned to the interaction of CO with special highly unsaturated metal atoms placed at corners or at edges of the Ru crystallites.

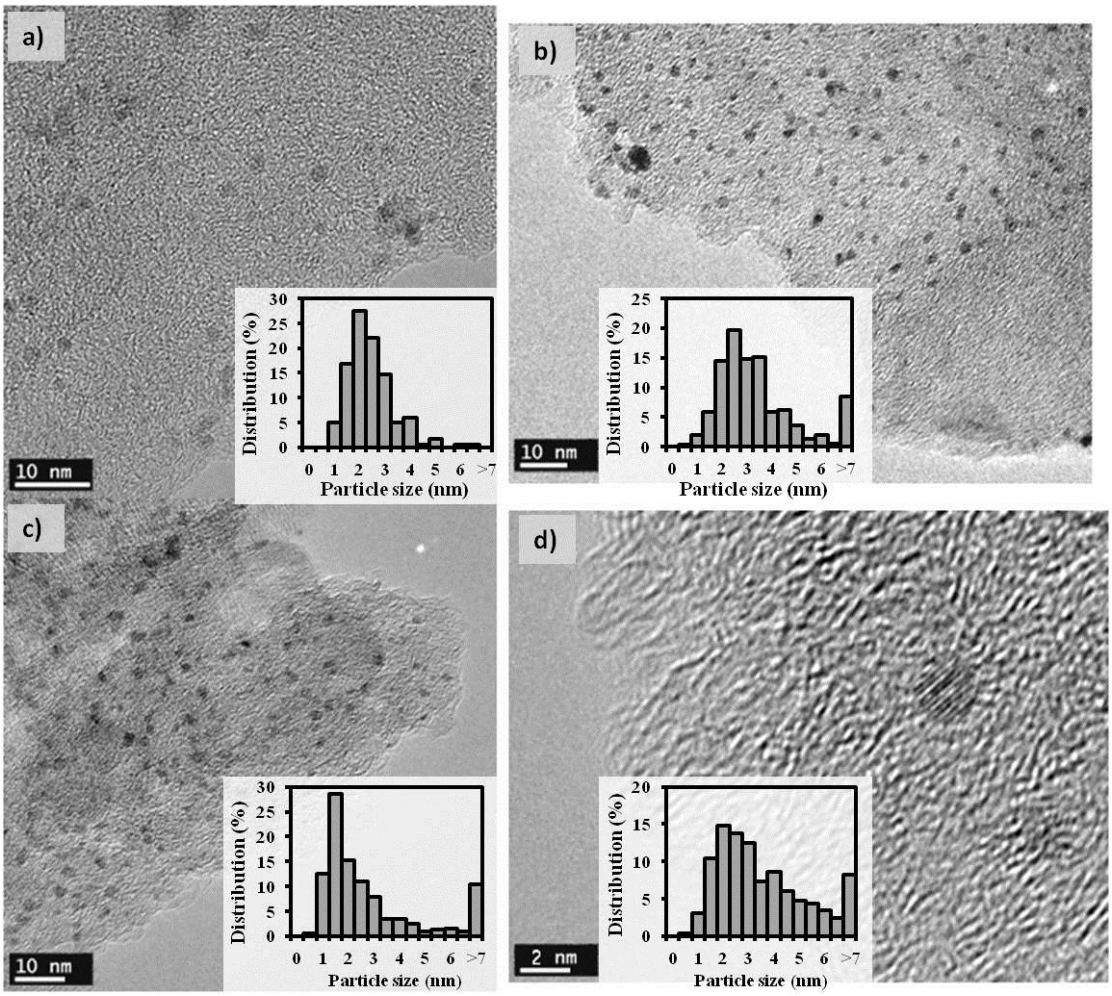

Figure 2.TEM micrographics and particle size distribution of a) Ru/AC-Cl, b) Ru/AC-Ox-Cl, c) Ru/AC-N and d) Ru/AC-OX-N.

Figure 2 shows TEM micrographs of activated carbon supported catalysts and their particle size distribution. As above indicated, for a certain support the average particle size determined by TEM for the catalysts prepared from the two precursors are close and the particle size distributions are very similar. However, for catalysts prepared with the same metal precursor there are differences as a function of the chemical properties of the activated carbon surface, this is, with or without surface oxygen groups. Thus, metal particle sizes of ruthenium supported on AC-Ox are a little bit larger than those over AC support. It is presumed that initially present oxygen groups which act anchoring in some extension Ru

precursors, are partially eliminated during the reduction treatment then conducing to some sintering of the generated Ru particles.

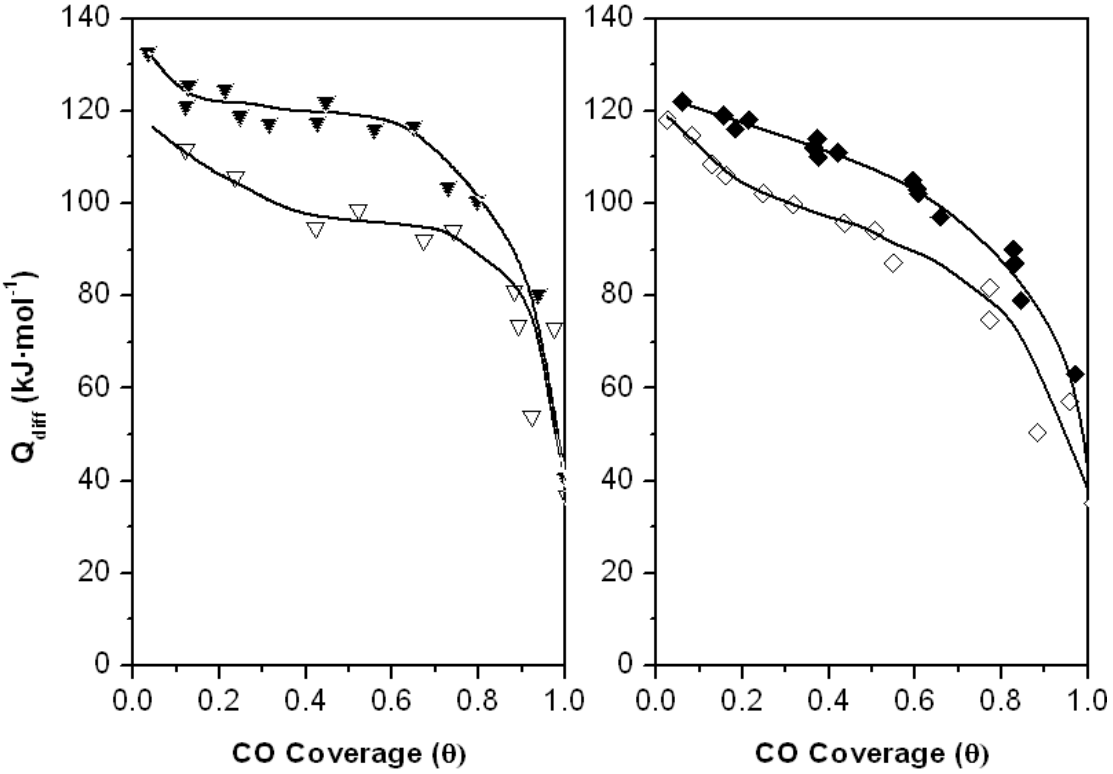

Figure 3. Differential enthalpies of CO adsorption at 330 K as a function of surface coverage for Ru/CNT-Cl (▽) and Ru/CNT-N (▼) in the left side and Ru/HSAG-Cl (◇) and Ru/HSAG-N (♦) in the right side.

For the HSAG and CNT supported Ru catalysts CO chemisorption uptakes are also lower when catalysts are prepared from $RuCl_3$ than from $Ru(NO)(NO_3)_3$. Moreover, CO enthalpy profiles (Figure 3) for both metal precursors confirm the same conclusion than with activated carbon. The catalysts prepared from $RuCl_3$ metal precursor display shapes of the calorimetric curves with lower values in all the range of CO coverage when compared with the ex- $Ru(NO)(NO_3)_3$ catalysts. Again the reason can be the presence of chloride spices anchored to Ru particles which weaken the enthalpies of CO adsorption on Ru particles. In the case of Ru-HSAG catalysts, the surface actives sites, as detected by interaction with CO,

are more heterogeneous and consequently the CO enthalpies decrease continuously along all values of surface coverage range. Contrarily for the CNT supported catalysts, the CO chemisorption enthalpies obtained when precursor is $Ru(NO)(NO_3)_3$, shows a plateau at 125 kJ·mol^{-1} from 0.1 until 0.6 CO coverage. This

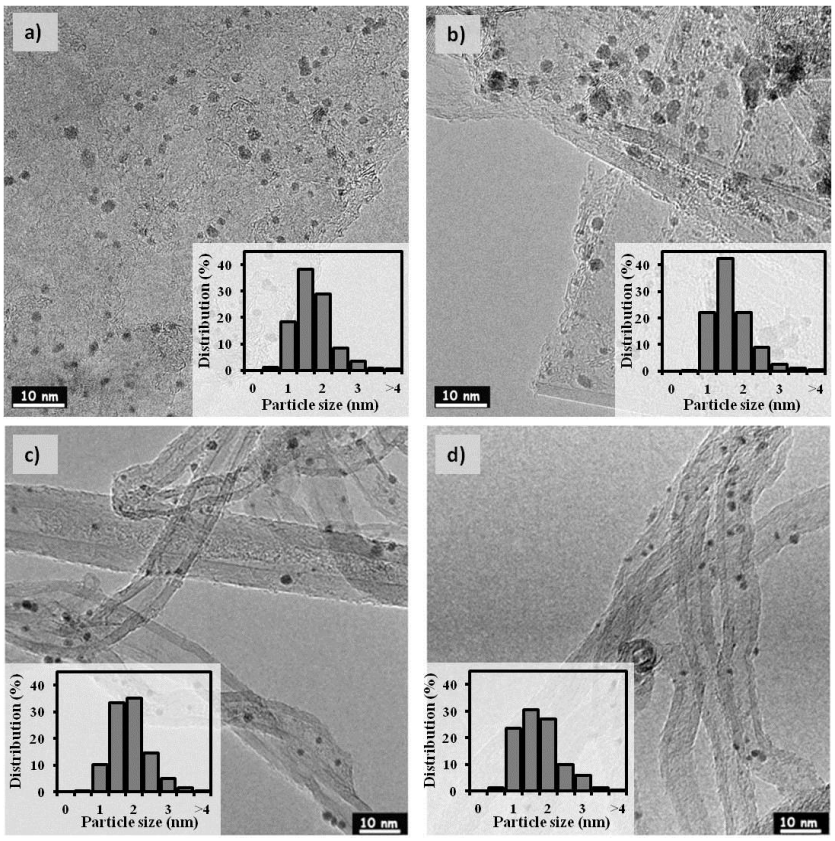

Figure 4. TEM micrographics and particle size distribution of a) Ru/HSAG-Cl, b) Ru/HSAG-N, c) Ru/CNT-Cl and d) Ru/CNT-N.

is a high energy of bond for CO molecules, which means that a strong interaction between CO and metal active sites in this catalyst takes place. Again the chloride catalyst displays weaker interaction with CO, and furthermore produces more heterogeneous surface metal particles. The higher initial values of differential chemisorption enthalpy obtained in Ru/CNT-N can be attributed to the interaction of CO with highly unsaturated metal atoms at corners and edges.

Figure 4 shows TEM micrographs of supported CNT and HSAG catalysts. The particles size determined by TEM (d_{TEM}) displayed in Table 1 are similar in all the catalysts and smaller than particle size obtained by CO chemisorption independently of the metal precursor. But for ex-$RuCl_3$ catalysts the differences in metal particle size obtained by CO chemisorption and from TEM are greater, which can be a consequence of the present of chloride species that reduced the CO chemisorption capacities, as discussed above. CO adsorption enthalpies on the different Ru catalysts are represented in Figure 5 to compare support effects. In the case of $RuCl_3$ precursor, all catalysts have the same values of adsorption enthalpies

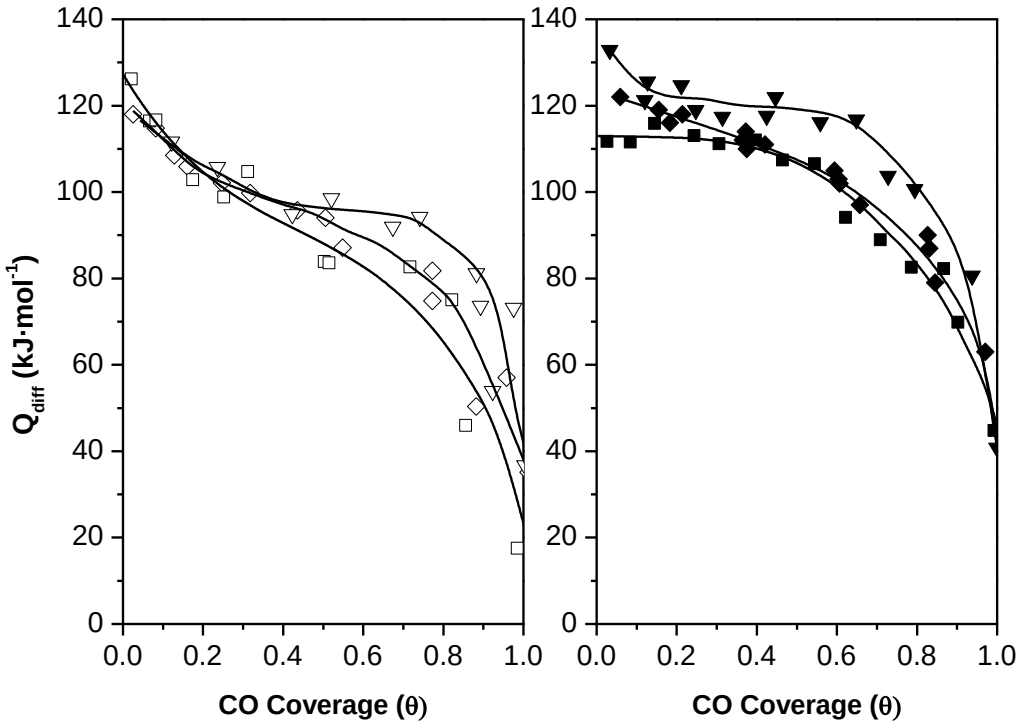

Figure 5. Differential enthalpies of CO adsorption at 330 K as a function of surface coverage for Ru/AC-Cl(□), Ru/HSAG-Cl(◊), Ru/CNT-C (▽) in the left side and Ru/AC-N(■), Ru/HSAG-N(♦) and Ru/CNT-N(▼) in the right side.

at low and medium CO coverage. For coverage values higher than 0.5 the Ru supported on CNT presents higher energies of interaction with CO than when supported on HSAG or on AC support. Also, when the metal precursor is

$Ru(NO)(NO_3)_3$ CNT support produce a catalyst with surface metal sites chemisorbing CO molecule with higher enthalpies, but in this case in the complete range of coverage. This finding can be explained if we assume that an electron donating support produces an enrichment of the electron density of metal atoms interacting with it, and also that CNTs have a higher graphitic character than HSAG or AC [19]. In fact the order of CO chemisorption enthapies Ru/CNT(N)>Ru/HSAG(N)>Ru/AC(N) could be related with the graphitic character of these carbon materials and their electron donating tendency. In the case of ex-$RuCl_3$ catalysts this effect does not occur, and only at higher CO coverage, when chloride species are no longer affecting the CO chemisorption, the support effect is apparent.

4.3.4 CONCLUSIONS

The comparative and systematic study of carbon supported Ru catalysts, by CO chemisorption coupled with calorimetry and TEM, has lead us to detect significant support effects on the surface properties of the metallic particles deposited on these materials. However, in the case of activated carbon, the presence of incorporated oxygen surface groups does not modify the CO adsorption enthalpies on the Ru surface sites. These facts can indicate that these metal-support interactions are of long distance range. Interestingly the presence of residual chloride species, when catalysts are prepared using $RuCl_3$ as precursor, produces important modifications in the chemisorption properties of the Ru nanoparticles.

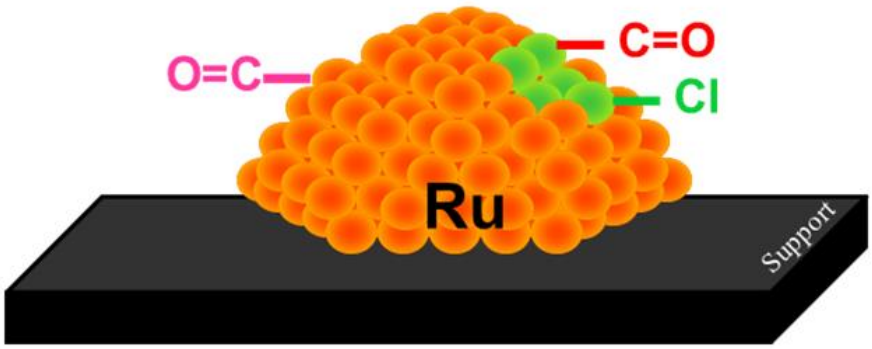

Figure 6. Proposed model to explain the differences of CO chemisorption enthalpies depending with the presence of residual chloride adatoms in the Ru nanoparticle surfaces.

Schematically the proposed mechanism of electronic modification of the Ru surfaces is presented in the Figure 6. In this picture some residual chloride species are anchored on the Ru particles blocking adsorption sites and altering the electronic properties of the neighbours Ru atoms. As a relevant effect of these surface ad-atoms they disrupt the synergetic bonds with CO decreasing systematically the chemisorption enthalpies.

4.3.5 REFERENCE

[1]. N. Cardona-Martinez, J.A. Dumesic, Applications of Adsorption Microcalorimetry to the Study of Heterogeneous Catalysis, in: H.P. D.D. Eley, B.W. Paul (Eds.), Advances in Catalysis, Academic Press, 1992, pp. 149-244.

[2]. J.J. Prinsloo, P.C. Gravelle, Volumetric and calorimetric study of the adsorption of hydrogen, at 296 K, on supported nickel and nickel-copper catalysts, J. Chem. Soc., Faraday Trans. 1, 76 (1980) 512-519.

[3]. J.J. Prinsloo, P.C. Gravelle, Volumetric and calorimetric study of the adsorption of hydrogen, at 296 K, on supported nickel and nickel-copper catalysts containing preadsorbed carbon monoxide. J. Chem. Soc., Faraday Trans. 1, 76 (1980) 2221-2228.

[4]. J.J. Prinsloo, P.C. Gravelle, Calorimetric study of the adsorption of carbon monoxide, at 296 K, on supported nickel and nickel-copper catalysts, J. Chem. Soc., Faraday Trans. 1, 78 (1980) 273-281.

[5]. A. Guerrero-Ruiz, A. Maroto-Valiente, M. Cerro-Alarcón, B. Bachiller-Baeza, I. Rodríguez-Ramos, Surface Properties of Supported Metallic Clusters as Determined by Microcalorimetry of CO Chemisorption, Top. Catal. 19 (2002) 303-311.

[6]. A. Guerrero-Ruiz, S.W. Yang, Q. Xin, A. Maroto-Valiente, M. Benito-González, I. Rodriguez-Ramos, Comparative Study by Infrared Spectroscopy and Microcalorimetry of the CO Adsorption over Supported Palladium Catalysts. Langmuir 16 (2000) 8100-8106.

[7]. A. Maroto-Valiente, I. Rodríguez-Ramos, A. Guerrero-Ruiz, Determination of the surface states of metallic clusters supported on alumina using microcalorimetry of CO adsorption, Thermochim. Acta, 379 (2001) 195-199.

[8]. O. Dulaurent, K. Chandes, C. Bouly, D. Bianchi, Heat of adsorption of carbon monoxide on a Pd/Rh three-way catalyst and on a Rh/Al2O3 solid, J. Catal. 192 (2000) 262-272.

[9]. S.W. Yang, A. Maroto-Valiente, M. Benito-Gonzalez, I. Rodriguez-Ramos, A. Guerrero-Ruiz, Methane combustion over supported palladium catalysts: I. Reactivity and active phase, Appl. Catal. B- Environ. 28 (2000) 223-233.

[10]. L.R. Radovic, F. Rodriguez-Reinoso, Carbon materials in catalysis, in: P.A. Thrower (Ed.), Chemistry and Physics of Carbon, Vol. 25, CRC Press, Norfolk, 1996, pp. 243-358.

[11]. A. Guerrero-Ruiz, P. Badenes, I. Rodríguez-Ramos, Study of some factors affecting the Ru and Pt dispersions over high surface area graphite supported catalysts, Appl. Catal. A- Gen. 173 (1998) 179-187.

[12]. Y.J. Zhang, A. Maroto-Valiente, I. Rodríguez-Ramos, Q. Xin, A. Guerrero-Ruiz, Synthesis and characterization of carbon black supported Pt-Ru alloy as a model catalyst for fuel cells, Catal. Today, 93 (2004) 619-626.

[13]. E. Miyazaki, Chemisorption of diatomic molecules (H2, N2, CO) on transition d-metals, J. Catal. 65 (1980) 84-94.

[14]. T. Narita, H. Miura, K. Sugiyama, T. Matsuda, R. D. Gonzalez, The effect of reduction temperature on the chemisorptive properties of Ru/SiO2: Effect of chlorine, J. Catal. 103 (1987) 492-495.

[15]. Anderson, J.R., Structure of Metallic Catalysts, Academic Press ed., New York, 1975.

[16]. G. Bergeret and P. Gallezot, Particle Size and Dispersion Measurements, in: G. Ertl, H. Knözinger, F. Schüth, J. Weitkamp (Eds.), Handbook of Heterogeneous Catalysis, Wiley-VCH, 2008, pp. 738-765.

[17]. K. Lu, B.J. Tatarchuk, Activated chemisorption of hydrogen on supported ruthenium: I. Influence of adsorbed chlorine on accurate surface area measurements, J. Catal, 106 (1987) 166-175.

[18]. M. Cerro-Alarcón, A. Maroto-Valiente, I. Rodríguez-Ramos, A. Guerrero-Ruiz, Surface sites on Carbon -supported Ru, Co and Ni nanoparticles as determined by microcalorimetry of CO adsorption, Thermochim. Acta, 434 (2005) 100-106.

[19]. P. Gallezot, D. Richard, Selective hydrogenation of α,β-unsaturated aldehydes, Catal. Rev. 40 (1998) 81-126002E

4.4 Comparative study of the hydrogenolysis of glycerol over Ru-based catalysts supported on activated carbon, graphite, carbon nanotubes and KL-zeolite

E. Gallegos-Suárez[1,2], A. Guerrero-Ruiz[2,3], I. Rodríguez-Ramos[1,3], A. Arcoya[1,3]

Chemical Engineering Journal 262(2015)326-333

[1]Instituto de Catálisis y Petroleoquímica, CSIC, Marie Curie nº 2, L-10, 28049 Madrid, Spain.

[2]Departamento de Química Inorgánica y Técnica, Facultad de Ciencias, UNED, Paseo Senda del Rey nº 9, 28040 Madrid, Spain.

[3]Unidad Asociada UNED ICP-CSIC, Group Design and Applied Heterogeneous Catalysis.

4.4.0 ABSTRACT

Supported ruthenium catalysts were prepared by incipient wetness impregnation of three different carbon materials: activated carbon (AC), high surface area graphite (HSAG) and multiwalled carbon nanotubes (CNT). Another catalyst was prepared by treating KL zeolite with $RuCl_3.xH_2O$ in aqueous solution. All these samples were characterized by temperature programmed reduction (TPR), CO chemisorption coupled with microcalorimetry and transmission electron microscopy (TEM). The reduced catalysts were tested in the hydrogenolysis of glycerol in the liquid phase, under a reaction pressure of 8 MPa and isothermally at the reaction temperature of 453 K. The CO microcalorimetry measurements evidenced that electron donor properties of graphite and carbon nanotubes promote formation of electron-rich metal species ($Ru^{\delta-}$) in Ru/HSAG and Ru/CNT catalysts, which not only favors formation of 1,2-propanediol from glycerol but also enhances the successive C-C cleavage, with formation of undesired products, mainly methane. For Ru/KL the occurrence of Brönsted acid sites, resulting of the reduction of the chlorinated ruthenium species bonded to the zeolite framework, was verified by temperature programmed desorption (TPD) of NH_3. Furthermore, observations by TEM of the Ru/KL catalyst showed an important population of metal nanoparticles lower than 1 nm, part of which exhibits electron deficient character as indicated by the CO microcalorimetry. As a consequence, the transformation of glycerol into 1,2-PDO over Ru/KL seems to be promoted through formation of the intermediate acetol on acid sites, while for the scarcely acid Ru-carbon catalyst conversion of glycerol occurs mainly on metal sites, ethylene glycol being the preferred hydrogenolysis product.

4.4.1 INTRODUCTION

The high selectivity towards glycerol in the biodiesel manufacture and the rapid development of the commercial processes in the last years has generated an oversupply of this byproduct with low price in the market. Glycerol is a potentially renewable resource susceptible of being transformed into high value-added products through very different catalytic processes such as dehydration to acrolein, oxidation for producing dihydroxyacetone or glyceric acid, among others [1, 2, 3]. Hydrogen production by steam reforming [4] and hydrogenolysis to obtain 1,2-propanediol, ethylene glycol or lactic acid are also important routes for revaluating glycerol. Ethylene glycol (EG) and the valuable 1,2-propanediol (1,2-PDO) are used in the manufacture of polymers, resins, functional fluids, foods and cosmetics, while lactic acid is important for the food and beverage industry.

Hydrogenolysis of glycerol is generally performed over supported metal catalysts, ruthenium being one of the most suitable active components to obtain 1,2-PDO [5, 6] although it promotes excessive C–C cleavage and the subsequent formation of undesired products, mainly methane. Selectivity toward 1,2-PDO is improved, however, by using additives [7, 8] sulfurized catalysts [9] bimetal catalysts [10, 11] or by adding acid co-catalysts to the reaction system [12, 13].

Interesting results in the hydrogenolysis of glycerol have been reported employing supports of different nature in the formulation of the catalysts [14, 15, 16, 17] however, since the catalytic tests were carried out generally under very different experimental conditions, the results are hardly comparable. Notwithstanding, comparative studies about the effect of the support are rather scant. In this regard Feng et al. [18] studied the influence of SiO_2, NaY, γ-Al_2O_3, activated carbon and TiO_2 as supports of ruthenium and found that activity

increases in the order Ru/SiO_2 < Ru/NaY< Ru/γ-Al_2O_3< Ru/C< Ru/TiO_2, while selectivity towards 1,2-PDO follows the trend Ru/SiO_2 > Ru/γ-Al_2O_3 > Ru/C > Ru/NaY > Ru/TiO_2. For Cu/ZnO supported on various different carriers they also observed important differences in selectivity [19]. Vasiliadou et al. [20] reported a direct correlation between acidity and yield to the hydrogenolysis products of glycerol over Ru/SiO_2, Ru/Al_2O_3 and Ru/Zr_2O_3. It has been also noticed [21] that Pt/TiO_2 is more selective towards C_3 products than Pt/Al_2O_3 or Pt/Al_2O_3-SiO_2 in the conversion of glycerol, because TiO_2 leads to the most stable metallic phase. It is worth mentioning, on the other hand, that studies about conversion of glycerol into acrolein [22] or into fuel additives [23] over several free metal zeolites of different structure evidenced that the selectivity of the reactions is governed by the structure and acidity of the zeolites. Likewise, it has been stated the important role of the respective structure of ferrite, ZSM-23, Y-zeolite, mordenite and theta-1 on the selectivity towards propionaldehyde in the dehydration of 1,2PDO [24].

In this context, taking into account that the acidity and structure of the supports can play an important role on the performance of the supported ruthenium catalysts in the hydrogenolysis of glycerol, we have prepared and studied four Ru catalysts supported on activated carbon (AC), high surface area graphite (HSAG), multiwall carbon nanotubes (CNT) and KL-zeolite, respectively. To our knowledge this latter has not been used hitherto in that reaction. Activated carbons have a non-graphitizable turbostratic microstructure which results in a large propensity for oxygen chemisorption and usually present surface oxygenated groups of acid character [25]. On the other hand, graphite and carbon nanotubes may exhibit electron donor character that can modify the properties of the supported metal nanoparticles and they can be also functionalized in order to change their surface chemical properties [26, 27, 28, 29]. The very well-known crystalline structure of the

basic KL-zeolite enables, on the other hand, to obtain supported metal catalysts with different geometrical and electronic properties depending on the preparation method used for incorporating the metal to the support [30]. The different catalysts were characterized by temperature programmed reduction (TPR), transmission electron microscopy (TEM) and CO chemisorption coupled with microcalorimetry. The catalysts behavior was tested in the hydrogenolysis of glycerol in the liquid phase and the kinetic results are related to the electronic properties of the supports. In the case of the Ru/KL catalyst, the location of the metal in the zeolite structure is also considered.

4.4.2 EXPERIMENTAL

4.4.2.1 Catalysts preparation

Four different materials were used as supports of the catalysts: KL-zeolite ($K_9Al_9Si_{27}O_{72}$, Union Carbide, SK-45, S_{BET} = 245 $m^2\ g^{-1}$); commercial activated-carbon, produced from olive stones (Oleicola el Tejar, Córdoba Spain, S_{BET} = 1190 $m^2\ g^{-1}$); high surface area graphite (TIMCAL, S_{BET} = 299 $m^2\ g^{-1}$) and multiwall carbon nanotube (NANOCYL, S_{BET} = 285 $m^2\ g^{-1}$). Prior to the catalyst preparation the KL-zeolite was calcined at 873 K. The as received activated-carbon was treated with hydrochloric acid solution 10% (v/v) at 373 K for 24 h to remove residual inorganic materials and then it was successively washed with deionized water at reflux temperature and dried at 393 K.

From the carbonaceous supports, activated carbon (AC), graphite (HSAG) and carbon nanotubes (CNT), the catalysts Ru/AC, Ru/HSAG and Ru/CNT were prepared by incipient wetness impregnation, using ruthenium chloride hydrate in H_2O:EtOH (1:1) solutions in the adequate concentration to incorporate 4 wt% Ru to

the support. The sample Ru/KL (2 wt% Ru) was prepared by adding drop wise an aqueous solution of the same precursor to the KL-zeolite in aqueous suspension (1 g of zeolite per 4 mL of water) under stirring at reflux temperature. Quantitative incorporation of the metal to the zeolite was evidenced by the complete bleaching of the suspension. After 24 h the slurry was successively filtered and the solid washed until complete removal of occluded ions. During that treatment no extraction of ruthenium was observed. After evaporation of the solvent at room temperature, all the samples were dried at 393 K for 24 h and then reduced under hydrogen flow (30 mL min^{-1}) at 523 K for 2 h. The catalysts were cooled down to room temperature under inert stream and immediately transferred to the autoclave.

4.4.2.2 Catalysts characterization

Ruthenium loading in catalysts Ru/AC, Ru/HSAG and Ru/CNT was measured by thermogravimetric analysis, burning a sample in flowing pure air (50 mL min^{-1}) at 1073 K and weighing then the residual product as RuO_2. For Ru/KL the metal content was determined by inductive coupled plasma. Crystallinity of the Ru/KL catalyst was checked by X-ray diffraction in a Seifert C-3000 powder diffractometer using CuKα radiation at 40 mA and 40 kV, with slits of 1^o, 0.1^o. Temperature programmed reduction measurements were performed in a flow system with a thermal conductivity detector, heating the sample from room temperature to 873 K at 8 K min^{-1}, under a flow of 5% of hydrogen in argon (30 mL min^{-1}). The metal surface of the catalysts was studied by microcalorimetry of CO chemisorption in a Tian Calvet heat-flow microcalorimeter (Setaram C-80 II) isothermally operated at 330 K and connected to a glass vacuum-dosing-apparatus. The number of exposed metal atoms was calculated from the CO uptake at the

monolayer assuming an atomic stoichiometry CO/Ru = 1/1. Monolayer was considered to be attained when the evolved heat falls to the physisorption field (40 kJ mol^{-1}). From the number of exposed metal atoms (Ru_S) and the ruthenium loading in the catalyst (Ru_l), metal dispersion (D_{CO}) is defined as $D_{CO} = 100\ Ru_S/Ru_l$.

Information about the supported metal particles was acquired by TEM in a JEOL 2100F field emission gun electron microscope provided with a X-ray energy dispersive spectroscopy system (XEDS) with a spatial resolution limit of 0.5 nm and a magnification of 1000000X-1500000X. The catalyst samples were suspended and dispersed by ultrasonic treatment in ethanol and a drop of this fine suspension was placed on a carbon-coated copper grid of 200 meshes, allowing the solvent to evaporate.

Surface acidity of the Ru/KL and Ru/AC catalysts was determined by temperature programmed desorption (TPD) of NH_3 in a flow system with thermal conductivity detector. For this purpose the catalyst sample, previously saturated with ammonia gas, was heated from 373 to 823 K at 10 K min^{-1} and the desorbed NH_3 collected with a 0.01 M HCl solution.

4.4.2.3 Catalytic activity measurements

Hydrogenolysis of glycerol was carried out in a 160 mL stainless-steel autoclave for 24 h, at 453 K, 8.0 MPa and 500 rpm stirring. The reactor was filled with 100 mL of 10 wt% glycerol aqueous solution and 450 mg of catalyst. The sealed reactor was purged several times with high purity helium and afterward with H_2. Subsequently the vessel was heated up to the reaction temperature and then pressurized with H_2 at the working pressure, which remained constant during the experiment. At the end of the run the autoclave was cooled down to room

temperature, the gas phase collected in a gasbag and the liquid filtered in order to separate the spend catalyst. The liquid samples were analyzed by gas chromatography in a device with a FID detector and a Supercowax 10 column (30m x 0.53mm x 1μm). Samples for analysis were prepared by dilution of 300 μL of the reaction product with 700 μL of water and 100 μL of 1,4-butanediol as internal standard. Samples of 0.4 μL of this solution were injected into the chromatograph. Reproducibility of the experiments was within ±3%.

4.4.3 RESULTS AND DISCUSSION

4.4.3.1 Catalysts characterization

Metal loading from thermogravimetric or ICP analysis and dispersion from CO chemisorption (D_{CO}) for all the samples are given in Table 1. The average metal particle size as calculated from CO chemisorption (d_{CO}) and TEM (d_{TEM}) is also included. As shown composition of the sample Ru/KL matches the theoretical one and corroborates the quantitative incorporation of Ru into the zeolite.

The TPR profiles of the precursors of the catalysts are depicted in Figure 1. Below 550 K the profiles of the Ru/HSAG and Ru/NTC catalysts essentially exhibit two well-defined partially overlapped single reduction peaks at nearly the same temperatures, 399 – 406 K the first peak and 474 – 476 K the second one, which are usually related to the two reduction steps of the $RuCl_3$ species: $Ru^{3+} \rightarrow Ru^{2+} \rightarrow Ru^0$ [31]. These two reduction steps are also suggested by the profile of the Ru/AC catalyst, however, in comparison with the two profiles above mentioned, the first reduction peak is shifted to 414 K and, moreover, it appears as a shoulder of the broad reduction peak at 464 K. A similar reduction profile was already registered for other Ru/carbon catalysts [32] and it would indicate that the preferential

location of Ru within the carbon grains [33] disturbs the consecutive reduction of the metal species.

Table 1. Characterization measurements of the catalysts.

Catalyst	Metal loading (%)	D_{CO} (%)	d_{CO} (nm)	d_{TEM} (nm)
Ru/AC	3.9	19	6.8	2.9
Ru/HSAG	3.8	26	5.1	2.3
Ru/CNT	3.6	21	6.2	2.4
Ru/KL	2.0	22	6.0	2.5

D_{CO}, metal dispersion as calculated from the CO chemisorption measurements; d_{CO}, average ruthenium particle size calculated from the D_{CO} values assuming the spherical model, d_{CO} (nm) = 100 · 1.32/ D_{CO}; d_{TEM}, average ruthenium particle size as determined by TEM.

The TPR profiles of the three carbon-supported Ru catalysts show additional hydrogen consumptions above roughly 570 K. According to the results of the simultaneous chromatographic analysis of the exit gas of the TPR equipment these signals are related to both the surface group decomposition and the partial gasification of the supports to produce methane [34]. In this regard, the hydrogen consumption registered in that region of temperatures, in the order Ru/AC >> Ru/HSAG >> Ru/CNT, parallels the concentration of oxygen surface groups of the supports [35]. Moreover, as the carbon-structure becomes more graphitic, the reactivity of the surface decreases following the same order.

The TPR profile of Ru/KL only exhibits two reduction peaks. In comparison with the above discussed profiles, the first peak, at 395 K, is shifted to lower temperature, whereas the second one, at 523 K, appears at higher temperature. This profile is comparable to that reported by Pârvulescu et al. [36] for ex-chloride Pt/KL catalysts in where the reducibility of the metal is greatly influenced by the pore

structure of the zeolite and the depth of penetration of the metal precursor. In this sense, it was suggested that the hydrogen consumption at the higher temperature is associated to the reduction of the hardly reducible ruthenium particles inside the zeolite channels, while the reduction peak at the lower temperature corresponds to easily reducible species mainly located outside the zeolite as large particles. The shoulder at 361 K in this latter is consistent with the two successive reduction steps of Ru^{3+} to Ru^{0}.

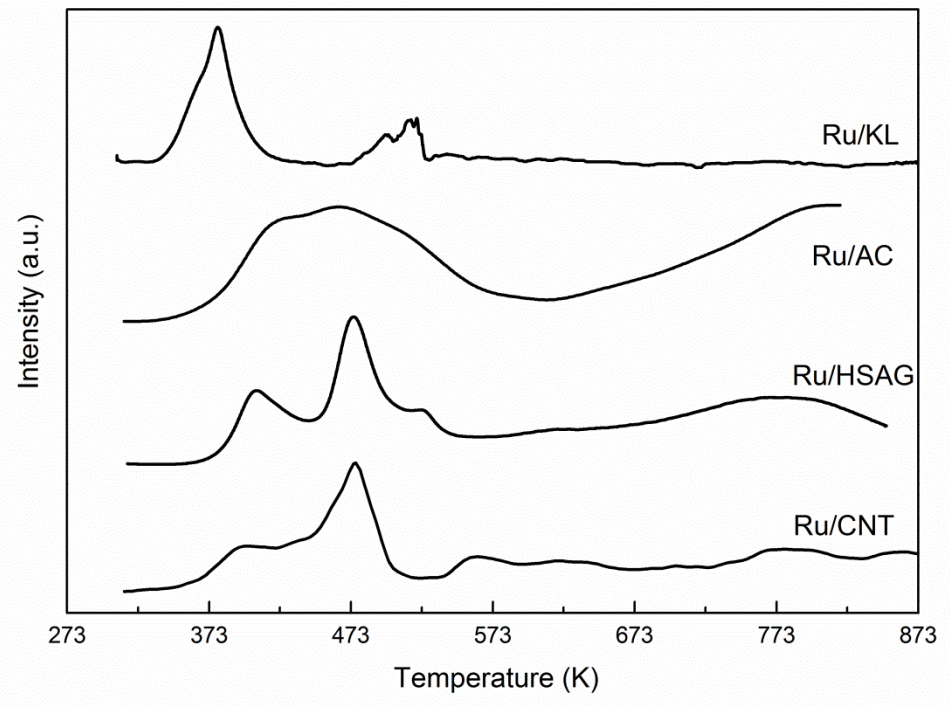

Figure 1. TPR profiles of the catalysts.

The results of CO chemisorption in Table 1 indicate that ruthenium is moderately dispersed in all the catalysts. Furthermore, in all the cases the Ru particle size calculated from CO chemisorption (d_{CO}) is higher than the corresponding value determined from TEM (d_{TEM}). For Ru/KL this observation is consistent with the occurrence of electron deficient metal species ($Ru^{\delta+}$) stabilized by Brönsted acid sites, which were generated during the reduction of the chlorinated ruthenium species bonded to the zeolite framework. In this regard, it

should be noted that ruthenium chloride ($RuCl_3 \cdot x\ H_2O$) in aqueous solutions, at reflux temperature, forms several ruthenium chloroaquo complexes, preferentially of cationic nature, ($[Ru(H_2O)_6]^{n+}$) [37] which are incorporated to the framework by ion exchange of the exchangeable K^+ ions of the zeolite, but also on Al sites and on the framework silanols, in such a way that Si-O-$RuCl_2$, Al-O-$RuCl_2$ and Si-O-$Ru(OH)_xCl_{2-x}$ species are formed [36, 38]. As result of the subsequent reduction of all these complexes bonded to the zeolite, formation of reduced ruthenium nanoparticles accompanied of the corresponding Brönsted acid sites in the framework takes place, in spite of the initial basic character of the KL zeolite. In fact, acidity of Ru/KL, as measured by TPD of NH_3, was 116 μEq g^{-1}. The Brönsted acid sites, in the close proximity of Ru nanoparticles, can stabilize electron deficient metal species ($Ru^{\delta+}$). Formation of $Ru^{\delta+}$ in a similar sample was evidenced and discussed elsewhere [30] from the shift, from 2124 cm^{-1} to 2146 cm^{-1}, of the CO-FTIR band associated to the CO stretching frequency of polycarbonyl species on ruthenium having a lower electron density than Ru^0, i.e. $Ru^{\delta+}(CO)_x$. Over these electron deficient ruthenium sites the CO adsorption can be weakened [39] and produces adsorption heats lower than 40 kJ mol^{-1}, value at which we consider the monolayer is already attained, from what the determined amount of adsorbed CO accounts only the stronger Ru surface sites. Therefore, the number of Ru surface sites measured by this way would be underestimated on the Ru/KL sample. Conversely, acidity of the sample Ru/AC arising from the residual oxygen groups at the carbon surface after reduction (cetonic, lactonic and anhydride groups) is much lower (6 μEq g^{-1}). For Ru/HSAG and Ru/CNT the occurrence of Brönsted acid sites is even lower and the electron donor character of the respective supports stands out [27, 31, 40]. Therefore, for the carbon supported catalysts it is probable that the overestimated values of d_{CO} might be the result of an steric blocking of part

of the surface ruthenium atoms by effect of residual chloride species [41, 42] which were not completely removed during the reduction step of the catalyst, as it was previously evidenced by XPS analysis for other ex-chloride Ru supported catalysts (Cl $2p_{3/2}$ = 198.4 eV) [43]. In addition, the discrepancies between the d_{CO} and the d_{TEM} values can not only be interpreted as due to a support effect or to the presence of residual inhibiting chloride species but also as an adsorption stoichiometry of CO over Ru involving more than one Ru surface atoms per chemisorbed CO molecule.

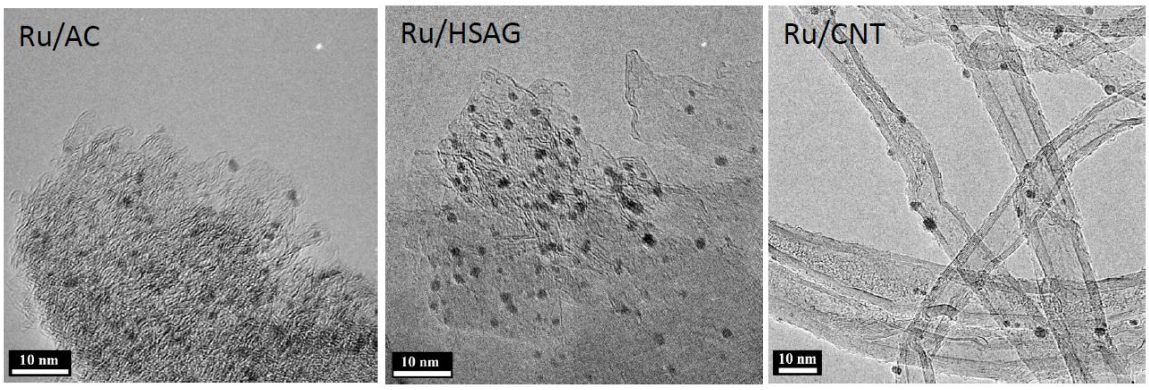

Figure 2. Representative TEM images of the catalysts Ru/AC, Ru/HSAG and Ru/CNT

Representative TEM images of the catalysts Ru/AC, Ru/HSAG and Ru/CNT are shown in Figure 2, while those corresponding to Ru/KL are given in Figure 3. Histograms showing the metal particle size distribution for all the samples are displayed in Figure 4. The average metal particle size in Table 1 was calculated from the micrographs as $d_{TEM} = \sum n_i d_1^3 / \sum n_i d_1^2$. At least 150 particles were counted to obtain each distribution histogram.

The TEM images in Figure 2 show very well dispersed rounded ruthenium nanoparticles, with a narrow size distribution (1.5-2.5 nm) for Ru/HSAG and Ru/CNT and a little wider range (1-4 nm) for Ru/AC. For Ru/CNT, furthermore, the metal particles look like they were mainly outside the nanotubes [44]. Micrographs of sample Ru/KL (Figure 3) exhibit a larger range of metal nanoparticle sizes, with

the major part lower than 3 nm, the 23% of the total nanoparticles being lower than 1 nm, as deduced from the corresponding histogram in Figure 4. This is an important remark because taking into account the dimensions of the cages and windows of the zeolite (0.48 nm x 1.24 nm x 1.07 nm and 0.71 nm x 0.78 nm, respectively) and in agreement with the TPR results of this sample, one can assume that important part of ruthenium has to be outside the support, but other minor fraction could be inside the channels as clusters small enough to reside in the cages

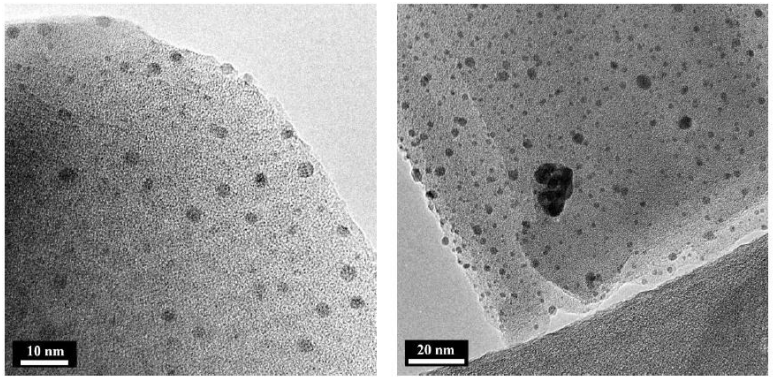

Figure 3. TEM micrographs of the Ru/KL catalysts.

without blocking them. In fact the specific surface area of this catalyst (235 $m^2 g^{-1}$) is very similar to that of the as received zeolite (245 $m^2 g^{-1}$). On the other hand, since the average metal particle size from the TEM measurements was calculated to be 2.5 nm, it can be estimated that up to 20 wt% of ruthenium loading could be located within the zeolite, as it occurs for other mesoporous molecular sieves containing ruthenium ex-chloride [45]. This means that about 40% of the exposed metal surface of ruthenium could be inside the zeolite channels, in accordance with the TPR profile. The assumption about the metal location is strengthened by the results of a separate XPS analysis in where comparison of the *Ru*/*Si* XPS atomic ratio (0.200) with the corresponding value of the bulk atomic ratio (0.018) evidences that ruthenium is preferentially deposited outside the zeolite, in contrast with that observed for Ru/AC, where Ru is essentially located inside the carbon grains [28].

Information about the strength and energetic distribution of the surface adsorption sites on the catalysts is supplied by the microcalorimetric profiles of CO adsorption given in Figure 5. The different shape of the profiles indicates that the strength and mode of adsorption of the CO molecule as well as the energetic distribution of the adsorption sites on the catalysts are highly influenced by the nature of the supports. The sample Ru/KL shows an initial adsorption heat (Q_{ad}) of 108 kJ mol^{-1}, which remains practically unalterable until a coverage degree (θ) of 0.5 and then it declines. The long plateau of this calorimetric profile indicates high homogeneity of the surface Ru atoms, which corresponds with active sites with more similar energy when bonded to CO molecules. This observation agrees with the above suggestion that around 40% of the ruthenium surface sites stems from external surface of 1 nm ruthenium particles located within the zeolite.

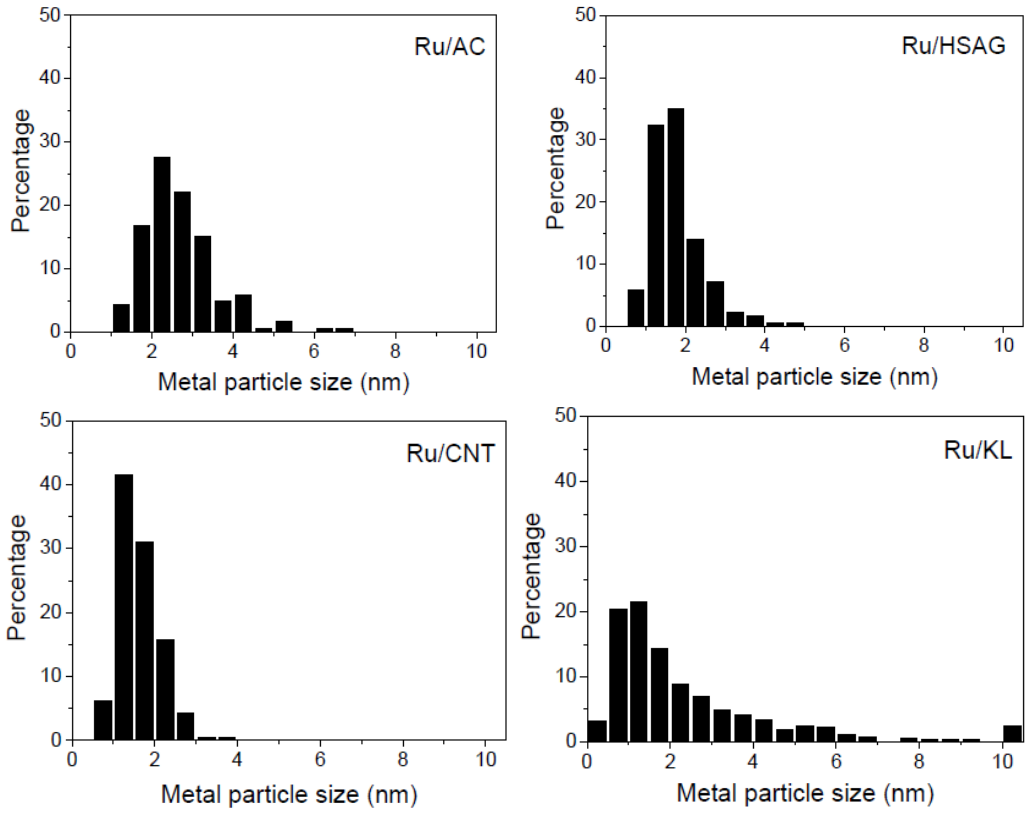

Figure 4. Histograms showing the metal particle size distribution of the catalysts calculated from the TEM analysis.

For Ru/AC, Ru/HSAG and Ru/CNT the initial adsorption heats, around 120-128 kJ mol^{-1}, are higher than that of Ru/KL but, in contrast, they progressively fall to physisorption values, although with some differences, revealing a relatively heterogeneous surface sites energy distribution for these samples. The higher initial adsorption heats found for the carbon supported catalysts can be attributed to the interaction of CO with highly unsaturated metal atoms at corners and edges. In addition, the high initial adsorption heats evolved from the three samples can be

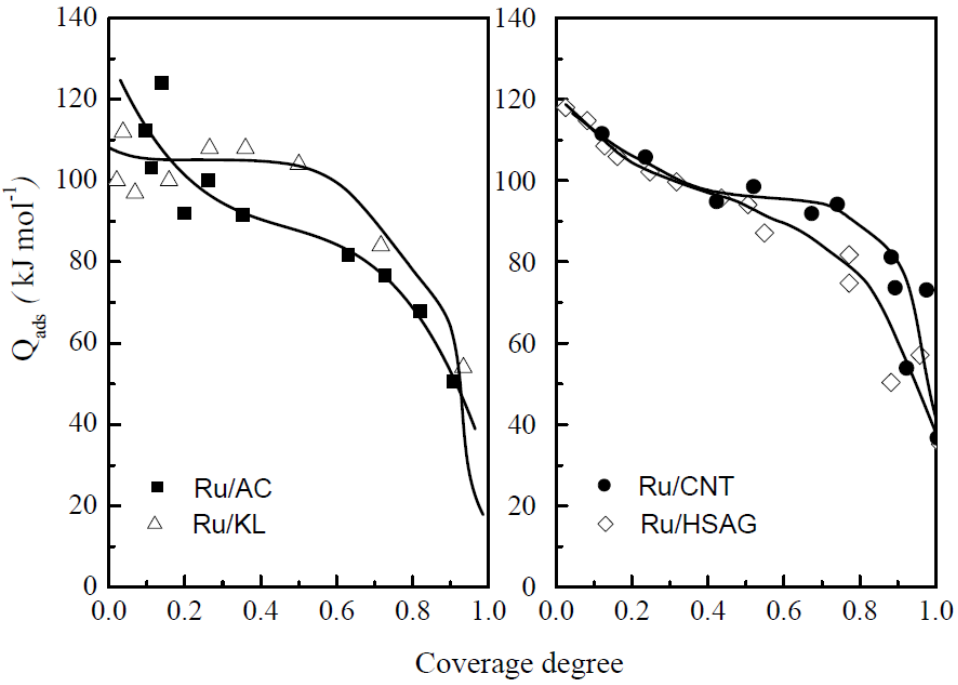

Figure 5. Microcalorimetric profiles of CO adsorption for the catalysts.

attributed to the formation of bridged CO species above suggested from the discrepancy between the metal particle sizes obtained from CO adsorption and those obtained from TEM (Table 1). It is worth noticing that for coverage degrees of 0.2 and higher the CO adsorption heats on Ru/HSAG and Ru/CNT are higher than on Ru/AC, while for $\theta > 0.4$ the sample Ru/CNT shows the highest values. These features can be due to the graphitic-character of the supports used. As a result of this latter, electron transfer to the metal nanoparticles located in the close

proximity of edges and corner of the graphitic structure of the supports could stabilize electron rich ruthenium species ($Ru^{\delta-}$) [34, 46]. In this sense, it should be noted that the order of the CO chemisorption heats for the high coverage degrees, Ru/CNT > Ru/HSAG > Ru/AC, parallels the graphitic character of the respective supports and their electron donor tendency [44].

4.4.3.2 Hydrogenolysis of glycerol

Kinetic results of the catalysts in the hydrogenolysis of glycerol at 453 K and 8 MPa, after 24 h of reaction are summarized in Table 2. The major products were ethylene glycol (EG) and 1,2 propane-diol (1,2-PDO) which are, in addition, the most valuable ones. By-products including mono-alcohols and undesired gaseous products mainly methane, were obtained. Trace amounts of acetol and 1,3-PDO were also observed in some cases. For comparative purposes activity (*A*) is referred to ruthenium loading per g of catalyst (mol of glycerol converted per g of metal per h) while the overall "site time yield" (*STY*) is reported as the average transformation rate of glycerol per surface metal atom calculated, this latter, from the CO chemisorption measurements. Selectivity towards a product *i* is defined as molecules of glycerol transformed into *i* per cent molecules of glycerol converted.

Inspection of the results in Table 2 evidences that Ru/CNT and Ru/HSAG are the most active catalysts (A= 80 and 71 mmol g_{Ru}^{-1} h^{-1}, respectively) but they are highly selective towards degradation products mainly methane (50% and 41%, respectively) in the detriment of the more valuable ones. The least active catalyst Ru/AC (A= 29.1 mmol g_{Ru}^{-1} h^{-1}) is highly selective towards EG (S_{EG}= 63%) and moderately selective towards 1,2-PDO (S_{PDO} =14%), while Ru/KL is barely more active than this latter but in return it exhibits the highest selectivity towards

1,2-PDO (S_{PDO} = 32%), the highest one towards PDO + EG (80%) and the lowest selectivity towards undesired products (20%).

Table 2. Activity and selectivity of the catalysts in the hydrogenolysis of glycerol, at 453 K and 8 MPa, after 24 h of reaction time.

Catalyst	*X* (%)	*A*	*STY*	Selectivity (%)			
				1,2-PDO	EG	Methane	Other
Ru/AC	11.0	29.1	15	14	63	8	16
Ru/HSAG	26.0	70.7	28	16	32	50	2
Ru/CNT	28.0	80.0	39	22	35	41	2
Ru/KL	7.5	38.0	16	32	48	15	5

X, conversion; *A*, activity (mmol glycerol converted $g_{Ru}^{-1}h^{-1}$); *STY*, Site Time Yield (h^{-1}); 12-PDO, 1,2-propanodiol; EG, ethylene glycol; others, is the sum of selectivities toward propanol, ethanol, methanol and trace amounts of acetol and 1,3-PDO.

All these results evidence an important influence of the intrinsic properties of the supports on the performance of Ru in the catalytic transformation of glycerol, in which the differences of selectivity observed go beyond that expected from the differences of conversion reached in the range 7.5% - 28.0%. Note in this sense, that catalysts Ru/AC and Ru/KL at low conversion levels (11.0% and 7.5%, respectively) with analogous *STY* values (15 h^{-1} and 16 h^{-1}) exhibit very different selectivities towards 1,2-PDO (14% and 32%) and EG (63 % and 48%, respectively). Even the composition of the fraction of undesired products (methane and mono-alcohols) is neatly different. In a same way, Ru/HSAG and Ru/CNT, for conversion values very close (26% and 28%) show different *STY* values (28 h^{-1} and 39 h^{-1}) and also different selectivities towards 1,2-PDO (16 % and 22 %) and towards methane (50 % and 41 %) but the same values towards EG (32% and 35%). Conversely, Ru/AC and Ru/HSAG for different conversion values give similar selectivities towards 1,2-PDO (14% and 16%) but very different values of both *STY* (15 h^{-1} and 28 h^{-1}) and selectivities towards EG (63% and 32%) and methane (8% and 50%). The

results listed in Table 2 are, on the other hand, within the ranges of activity and selectivity reported for other Ru-supported catalysts tested at somewhat comparable reaction conditions [5, 45]**.** The *STY* values are also within the broad range 0.005 s^{-1} - 0.13 s^{-1} recently reported for a series of TiO_2 supported Ru-Cu bimetallic catalysts [8] in spite of the fact that these latter were obtained under other very different reaction conditions (473 K, 2.5 MP, 50 mL of 20% wt/wt aq. glycerol, 650 mg catalyst).

It has been stated that transformation of glycerol into 1,2-PDO and 1,3-PDO over Ru-supported catalysts containing acid sites follows a scheme of parallel and consecutive reactions [5] in where the intermediates acetol (Eq.1) and 3-hydroxypropionaldehyde (Eq. 2) are formed by dehydration on acid sites, while the subsequent hydrogenation of such intermediates into 1,2 PDO and 1,3-PDO, respectively, takes place on metal sites [47].

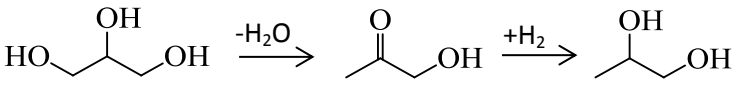

(Eq. 1)

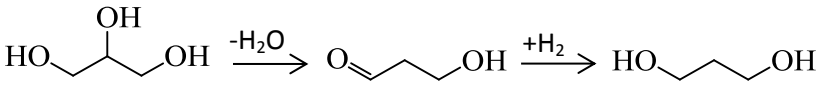

(Eq. 2)

In parallel, glycerol is transformed into ethylene glycol plus methanol via glyceraldehyde on metal sites (Eq. 3). From all these reaction products degradation products are formed by successive C-C and C-O cleavage, mainly from 1,3-PDO, which is more reactive than 1,2-PDO and EG [45].

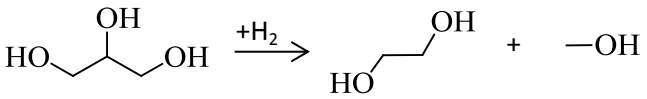

(Eq. 3)

According to these reactions, the highest selectivity towards 1,2-propanediol over Ru/KL may be related to the Brönsted acid sites existing in this catalyst, which promote preferential formation of the intermediate acetol respect to that of glyceraldehyde. This selectivity enhancement agrees with those reported for other moderately acidic catalysts [16, 20, 48] in contrast with the negative effect reported recently for the catalytic system based on Ru/HZSM-5 [49] where the ability of Ru to cleave C-C bonds is increased by the large population of acid sites [21]**.** Moreover, and from a geometrical point of view, it is feasible that the performance of Ru/KL is conditioned by the size, shape and location of ruthenium particles in the zeolite framework, because the smallest metal nanoparticles (< 1nm) we observed by TEM can hinder the free transit of glycerol through the channels thus controlling its transformation. Indeed, the molecular diameters of glycerol (0.63 nm) and 1,2-PDO (0.61 nm) [50] are only slightly lower than the windows of the zeolite (0.71 x 0.78 nm). It is worth to mention also that a possible effect of residual basic sites in the Ru/KL framework cannot be ruled out, although it would stay masked by the acidity generated during the preparation of the catalyst. Regarding to the sample Ru/AC, the higher selectivity towards ethylene glycol we found, in accordance with the reaction scheme in Figure 6, may be attributed to the very low acid-sites/metal-sites ratio, as it was already argued [33].

The samples Ru/HSAG and Ru/CNT, in comparison with Ru/AC (STY = 15 h^{-1}) show an enhanced hydrogenolysis activity (STY = 28 h^{-1} and 39 h^{-1}, respectively) which is manifested mainly through the transformation of glycerol into gaseous degradation products, basically methane (S_{OP}= 52% and 43, respectively). Formation of 1,2-PDO is also increased and, since neither acids sites nor hydroxyl groups that favor formation of this target product [51] are present in these catalysts, it is reasonable to believe that formation of 1,2-PDO occurs on the

ruthenium particles, through a metal-catalyzed route. This proposal agrees with the results obtained by Balaraju et al. [14] suggesting that hydrogenolysis of glycerol over Ru/TiO_2 occurs on metal sites, via dehydration to acetol and the subsequent hydrogenation to 1,2-propanediol. In our case, furthermore, it seems that the occurrence of electron rich Ru species ($Ru^{\delta-}$), above evidenced in Ru/HSAG and Ru/CNT, favors the cleavage of the C-O bond and promotes excessive hydrogenolysis reaction, thus converting propylene glycol into lower alcohols and gases, mainly methane.

4.4.4 CONCLUSIONS

The role of the supports on the activity and selectivity of the catalysts Ru/AC, Ru/KL, Ru/HSAG and Ru/CNT for the hydrogenolysis of glycerol is comparatively analyzed and discussed. For the scarcely acid Ru/AC catalyst conversion of glycerol into ethylene glycol on metal sites is preferred. For Ru/KL the occurrence of acid sites arising from the reduction of the ruthenium species bonded to the zeolite, increases the hydrogenolysis activity and improves the selectivity towards 1,2 PDO via formation of the intermediate acetol on acid sites. For Ru/HSAG and Ru/CNT the electron donor character of the respective supports stabilizes electron-rich Ru nanoparticles that, in comparison with Ru/AC, favor formation of 1,2-propanediol on metal sites but simultaneously enhances the successive C-C cleavage of glycerol and the subsequent formation of undesired products, in agreement with the extent of the graphitic character of the supports (CNT > HSAG).

4.4.5 REFERENCES

[1] C. Zhou, J.N. Beltramini, Y.X. Fana, G.Q. Lu, Chemoselective catalytic conversion of glycerol as a biorenewable source to valuable commodity chemicals, Chem. Soc. Rev. 37 (2008) 527-549.

[2] A. Behr, J. Eilting, K. Irawadi, J. Leschinski, F. Lindner, Improved utilisation of renewable resources: New important derivatives of glycerol, Green Chem. 10 (2008) 13-30.

[3] C.A.G. Quispe, C.J.R. Coronado, J. A. Carvalho Jr., Glycerol: Production, consumption, prices, characterization and new trends in combustion, Renew. Sust. Energ. Rev. 27 (2013) 475-493.

[4] C. Wang, B. Dou, H. Chen, Y.C. Song, Y.J. Xu, X. Du, T.T. Luo, C. Tan. Hydrogen production from steam reforming of glycerol by Ni-Mg-Al based catalysts in a fixed-bed reactor. Chem. Eng. J 220 (2013) 133-142

[5] T. Miyazawa, Y. Kusunoki, K. Kunimori, K. Tomishige, Glycerol conversion in the aqueous solution under hydrogen over Ru/C + an ion-exchange resin and its reaction mechanism, J. Catal. 240 (2006) 213-221.

[6] S. Bolado, R.E. Treviño, M.T. García-Cubero, G. González-Benito, Glycerol hydrogenolysis to 1, 2 propanediol over Ru/C catalyst, Catal. Comm. 12 (2010) 122-126.

[7] X. Liao, K. Li, X. Xiang, S.G. Wang, X. She, Y. Zhu, Y. Li, Mediatory role of K, Cu and Mo over Ru/SiO_2 catalysts for glycerol hydrogenolysis, J. Ind. Eng. Chem. 18 (2012) 818-821.

[8] J.B. Salazar, D.D. Falcone, H.N. Pham, A.K. Datye, F.B. Passos, R.J. Davis, Selective production of 1,2-propanediol by hydrogenolysis of glycerol over bimetallic Ru–Cu nanoparticles supported on TiO_2, Appl. Catal. A: General 482 (2014) 137-144

[9] C. Montassier, J.C. Ménézo, L.C. Hoang, C. Renaud, J. Barbier, Aqueous polyol conversions on ruthenium and on sulfur-modified ruthenium, J. Mol. Catal. 70 (1991) 99-110.

[10] E. Maris, W. Ketchie, M. Murayama, R. Davis, Glycerol hydrogenolysis on carbon-supported PtRu and AuRu bimetallic catalysts, J. Catal. 251 (2007) 281-294.

[11] Z. Wu, Y. Mao, X. Wang, M. Zhang, Preparation of a Cu–Ru/carbon nanotube catalyst for hydrogenolysis of glycerol to 1,2-propanediol via hydrogen spillover, Green Chem. 13 (2011) 1311-1316.

[12] Y. Kusunoki, T. Miyazawa, K. Kunimori, K. Tomishige, Highly active metal-acid bifunctional catalyst system for hydrogenolysis of glycerol under mild reaction conditions, Catal. Comm. 6 (2005) 645-649.

[13] T. Miyazawa, S. Koso, K. Kunimori, K. Tomishige, Development of a Ru/C catalyst for glycerol hydrogenolysis in combination with an ion-exchange resin, Appl. Catal. A: General 318 (2007) 244-251.

[14] J. Wang, S. Shen, B. Li, H. Lin, Y. Yuan, Ruthenium nanoparticles supported on carbon nanotubes for selective hydrogenolysis of glycerol to glycols, Chem. Lett. 38 (2009) 572-573.

[15] M. Balaraju, V. Rekha, B.L.A. Prabhavathi Devi, R.B.N. Prasad, P.S. Sai Prasad, N. Lingaiah, Surface and structural properties of titania-supported Ru catalysts for hydrogenolysis of glycerol, Appl. Catal. A: General 384 (2010) 107-114.

[16] S.H. Lee, D.J. Moon, Studies on the conversion of glycerol to 1,2-propanediol over Ru-based catalyst under mild conditions, Catal. Today 174 (2011) 10-16.

[17] N. Hamzah, N.M. Nordin, A.H.A. Nadzri, Y.A. Nik, M.B. Kassim, M.A. Yarmo, Enhanced activity of Ru/TiO_2 catalyst using bisupport, bentonite-TiO_2 for hydrogenolysis of glycerol in aqueous media, Appl. Catal. A: General 419-420 (2012) 133-141.

[18] J. Feng, H. Fu, J. Wang, R. Li, H. Chen, X. Li, Hydrogenolysis of glycerol to glycols over ruthenium catalysts: Effect of support and catalyst reduction temperature, Catal. Commun. 9 (2008) 1458-1464.

[19] Y. Feng, H. Yin, A. Wang, L. Shen, L. Yu, T. Jiang. Gas phase hydrogenolysis of glycerol catalyzed by Cu/ZnO/MOx (MOx = Al_2O_3, TiO_2, and ZrO_2) catalysts. Chem. Eng. J. 168 (2011) 403-412.

[20] E.S. Vasiliadou, E. Heracleous, I.A. Vasalos, A.A. Lemonidou, Ru-based catalysts for glycerol hydrogenolysis - Effect of support and metal precursor, Appl. Catal. B: Environmental 92 (2009) 90-99.

[21] S.N. Delgado, D. Yap, L. Vivier, C. Especel, Influence of the nature of the support on the catalytic properties of Pt-based catalysts for hydrogenolysis of glycerol, J. Mol. Catal. A: Chem. 367 (2013) 89-98.

[22] A.S. de Oliveira, S.J.S. Vasconcelos, J.R. de Sousa, F. F. de Sousa, J.M. Filho, A.C. Oliveira, Catalytic conversion of glycerol to acrolein over modified molecular sieves: Activity and deactivation studies, Chem. Eng. J. 168 (2011) 765-774.

[23] H. Serafim, I.M. Fonseca, A.M. Ramos, J. Vital, J.E. Castanheiro. Valorization of glycerol into fuel additives over zeolites as catalysts. Chem. Eng. J. 178 (2011) 291-296

[24] D. Zhang, S. A.I. Barri, D. Chadwinck, Dehydration of 1,2-propanediol to propionaldehyde over zeolite catalysts, Appl. Catal. A: General 400 (2011) 148-155.

[25] T.J. Bandosz, Surface Chemistry of Carbon Materials, in: P. Serp, J.L. Figueiredo (Eds.), Carbon Materials for Catalysis, J. Wiley & Sons, Hoboken (NJ), 2009, pp. 5-92.

[26] K.L. Yeung, E.E. Wolf, A scanning tunneling microscopy study of the platinum catalysts particles supported on graphite, J. Vac. Sci. Technol. B, 9 (1991) 798-803.

[27] K.L. Yeung, E.E. Wolf, Scanning tunneling microscopy studies of size and morphology of Pt graphite catalysts, J. Catal. 135 (1992) 13-26.

[28] E. Castillejos-López, D.M. Nevskaia, V. Muñoz, I. Rodríguez-Ramos, A. Guerrero-Ruiz, Specific interactions between aromatic electrons of organic compounds and graphite surfaces as detected by immersion calorimetry, Langmuir 20 (2004) 1013-1015.

[29] A.B. Dongil, B. Bachiller-Baeza, A. Guerrero-Ruiz, I. Rodríguez-Ramos, A. Martínez-Alonso, J.M.D. Tascón, Surface chemical modifications induced on high surface area graphite and carbon nanofibers using different oxidation and functionalization treatments J. Colloid Interface Sci. 355 (2011) 179-189.

[30] J. Alvarez-Rodríguez, I. Rodríguez-Ramos, A. Guerrero-Ruiz, A. Arcoya, Surface changes in Ru/KL supported catalysts induced by the preparation method and their effect on the selective hydrogenation of citral, Appl. Catal. A: General 366 (2009) 114-121.

[31] J. Álvarez-Rodríguez, I. Rodríguez-Ramos, A. Guerrero-Ruiz, E. Gallegos-Suarez, A. Arcoya, Influence of the nature of support on Ru-supported catalysts for selective hydrogenation of citral, Chem. Eng. J. 204–206 (2012) 169-178.

[32] L.Mª. Gómez-Sainero, A. Cortés, X.L. Seoane, A. Arcoya, Hydrodechlorination of carbon tetrachloride to chloroform in the liquid phase with metal-supported catalysts. Effect of the catalysts component, Ind. Eng. Chem. 39 (2000) 2849-2854

[33] E. Gallegos-Suarez, M. Pérez-Cadenas, A. Guerrero-Ruiz, I. Rodriguez-Ramos, A. Arcoya, Effect of the functional groups of carbon on the surface and catalytic properties of Ru/C catalysts for hydrogenolysis of glycerol, Appl. Surf. Sci. 287 (2013) 108-116.

[34] A. Guerrero-Ruiz, P. Badenes, I. Rodríguez-Ramos, Study of some factors affecting the Ru and Pt dispersions over high surface area graphite-supported catalysts, Appl. Catal. A: General, 173 (1998) 313-321.

[35] M. Soria-Sánchez, E. Castillejos-López, A. Maroto-Valiente, M.F.R. Pereira, J.J.M. Órfão, A. Guerrero-Ruiz, High efficiency of the cylindrical mesopores of MWCNTs for the catalytic wet peroxide oxidation of C.I. Reactive Red 241 dissolved in water, Appl. Catal. B: Environ. 121-122 (2012) 182-189.

[36] V.I. Pârvulescu, S. Coman, P. Palade, D. Macovei, C.M. Teodorescu, G. Filoti, R. Molina, G. Poncelet, F.E. Wagner, Reducibility of ruthenium in relation with zeolite structure, Appl. Surf. Sci. 141 (1999) 164-176.

[37] F. A. Cotton, G. Wilkinson, Advanced Inorganic Chemistry, J. Wiley & Sons, N.Y. 1988, p.1031.

[38] Y. Ying Liu, W. Zhao, S. Zhang, Y. Fang, XPS and EDX study on an Ru-KL zeolite hydrogenation catalyst, Appl. Surf. Sci. 59 (1992) 299-303.

[39] A. Maroto-Valiente, M. Cerro-Alarcón, , A. Guerrero-Ruiz, I. Rodríguez-Ramos, Effect of the metal precursor on the surface site distribution of Al_2O_3-supported

Ru catalysts: catalytic effects on the n-butane/H_2 test. Appl. Catal. A: General, 283 (2005) 23-32.

[40] M. Cerro-Alarcón, A. Maroto-Valiente, I. Rodríguez-Ramos, A. Guerrero-Ruiz, Surface study of graphite-supported Ru–Co and Ru–Ni bimetallic catalysts, Appl. Catal. A: General, 275 (2004) 257-269.

[41] B. Bachiller-Baeza, A. Guerrero-Ruiz, I. Rodríguez-Ramos, Role of the residual chlorides in platinum and ruthenium catalysts for the hydrogenation of α,β-unsaturated aldehydes, Appl. Catal. A: General 192 (2000) 289-297.

[42] A. Guerrero-Ruiz, E. Gallegos-Suárez, L. Gonzalo-Chacón, I. Rodríguez-Ramos Surface properties of Ru particles supported on carbon materials: A microcalorimetric study of the effects over the CO chemisorptions of residual anionic species, Therm. Acta 567 (2013) 112-117.

[43] A. Arcoya, A. Cortes, J.L.G. Fierro, X.L. Seoane, Comparative study of the deactivation of group-VIII metal-catalysts by thiophene poisoning in ethylbenzene hydrogenation, Stud. Surf. Sci. Catal. 68 (1991) 557-564.

[44] T. Trang Nguyen, P. Serp, Confinament of metal nanoparticles in carbon nanotubes, Chemcatchem. 5 (2013) 3595-3603.

[45] M. Hartmann, C. Bischof, Z. Luan, L. Kevan, Preparation and characterization of ruthenium clusters on mesoporous supports, Micropor. Mesopor. Mater. 44-45 (2001) 385-394.

[46] E. Asedegbega-Nieto, A. Guerrero-Ruíz, I. Rodríguez-Ramos, Study of CO chemisorption on graphite-supported Ru–Cu and Ni–Cu bimetallic catalysts, Thermochim. Acta 434 (2005) 113-118.

[47] M. Balaraju, V. Rekha, P.S. Sai Prasad, B.L.A. Prabhavathi Devi, R.B.N. Prasad, N. Lingaiah, Influence of solid acids as co-catalysts on glycerol hydrogenolysis to propylene glycol over Ru/C catalysts, Appl Catal. A: General 354 (2009) 82-87.

[48] L. Gonga, Y. Lua, Y. Dinga, R. Lina, J. Li, W. Donga, T. Wanga, W. Chena, Selective hydrogenolysis of glycerol to 1,3-propanediol over a Pt/WO_3/TiO_2/SiO_2 catalyst in aqueous media, Appl. Catal A: General 390 (2010) 119-126.

[49] Y. Li, L. Ma, H. Liu, D.He, Influence of HZSM-5 on the activity of Ru catalysts and product selectivity during the hydrogenolysis of glycerol, Appl. Catal. A: General 469 (2014) 45-51.

[50] S. Li, V.A. Tuan, J.L. Falconer, R.D. Noble, Separation of 1,3-propanediol from glycerol and glucose using a ZSM-5 zeolite membrane, J. Mem. Sci. 191 (2001) 53-59.

[51] C. Montassier, D. Giraud, J. Barbier, Polyol Conversion by Liquid Phase, Heterogeneous Catalysis over Metals, Stud. Surf. Sci. Catal. 41 (1988) 165.

Capítulo 5

Reformado de glicerol con vapor de agua

Contenido del capítulo

5.1 Resumen de los artículos relativos al reformado de glicerol con vapor de agua.

El reformado con vapor de agua del glicerol es una reacción química que pretende transformar este producto de desecho (glicerol) en una molécula de gran interés científico en los últimos años, como es el hidrógeno. Como ya se recogió en la introducción existe multitud de estudios relacionados con esta reacción, siendo lo más habitual el uso de catalizadores heterogéneos basados en una fase activa de Ni para llevar a cabo dicha transformación.

Trabajando en este contexto, en esta tesis doctoral se han planteado dos sistemas catalíticos no convencionales con el objetivo de mejorar el comportamiento de los catalizadores de Ni en la reacción del reformado del glicerol. En primer lugar se ha desarrollado un catalizador ternario de NiO, MgO y CeO_2 preparado mediante un método de sol-gel. Se realizó un estudio variando la cantidad de Ni desde un 5% hasta un 30% y manteniendo constante la relación Mg/Ce. La actividad catalítica fue probada en la reacción del reformado de glicerol con vapor de agua usando un reactor de lecho fijo. Para comprender las diferencias encontradas en la reacción, los catalizadores fueron caracterizados mediante adsorción de nitrógeno a 77 K, difracción de rayos X, reducción a temperatura programada, microscopía electrónica de transmisión y espectroscopia de energía dispersiva de rayos X.

El catalizador con un contenido de 20% de Ni presentó el mejor comportamiento catalítico, siendo el elegido para la síntesis de un novedoso reactor catalítico denominado "*hollow fibre reactor*". En este caso se usó dos tipos de *hollow fibre* cuya diferencia radica en su porosidad, siendo el reactor asimétrico *hollow fibre* el que presenta una estructura porosa denominada "*finger-like*" y el reactor

simétrico *hollow fibre* presenta una estructura porosa denominada *"sponge-like"*. El catalizador del 20% Ni fue depositado en dicha porosidad y la actividad catalítica de ambos reactores fue evaluada en el reformado de glicerol en el intervalo de temperatura comprendido entre 523 K y 823 K y usando una relación agua/glicerol de 16/1 (molar).

A la temperatura de 823 K se encuentra la máxima conversión de ambos reactores catalíticos, siendo de un 70% en el caso del asimétrico y un 46% para el reactor simétrico. Estos valores son 5 y 2 veces respectivamente superiores a la conversión obtenida cuando se usa el catalizador en un reactor de lecho fijo. Las diferencias encontradas en la actividad catalítica se deben a un efecto del tamaño de partícula de Ni y a la intensificación del contacto entre reactivo y catalizador como consecuencia del confinamiento del catalizador dentro de la estructura porosa del reactor *hollow fibre*.

Por otro lado, se sintetizaron catalizadores de Ni-Ce mediante el método de microemulsión variando el contenido en Ni. La actividad catalítica de estos materiales fue evaluada en la reacción del reformado de glicerol y comparada con un catalizador tradicional preparado mediante impregnación a humedad incipiente. Dicha actividad catalítica fue evaluada en un reactor de lecho fijo a la temperatura de 773 K y usando una disolución del 10% (wt) de glicerol en agua. El hecho de preparar los catalizadores mediante este método produce una mayor estabilidad en reacción comparada con el catalizador tradicional. Además se mejora la selectividad encontrando muy pocos productos indeseados, como son el metano o el monóxido de carbono.

Mediante este método de microemulsión se obtiene un óxido mixto el cual desempeña un papel importante en la actividad y estabilidad de los catalizadores.

Con el fin de profundizar en el papel catalítico del óxido mixto se realizó un estudio de los catalizadores mediante microscopía electrónica de barrido trasmisión y espectroscopía de energías dispersivas de rayos X. También se analizó en detalle los catalizadores después de reacción mediante oxidación a temperatura programada y espectroscopía de fotoemisión de rayos X para evaluar la naturaleza de los depósitos de carbono y establecer su relevancia química.

En particular, el catalizador que presenta una relación óptima de Ni:Ce, maximizando así la actividad y la estabilidad en la reacción del reformado de glicerol con vapor de agua, fue el catalizador con una relación 20:80 (Ni:Ce). Con esta relación se puede mantener controlado el tamaño de las partículas de Ni, minimizar la producción de coque y mantener una buena estabilidad catalítica a lo largo del tiempo de reacción. Además este catalizador evita las reacciones laterales indeseadas que bajan el rendimiento de producción de hidrógeno, como por ejemplo la producción de metano.

5.2 Ceramic hollow fibres catalytic enhanced reactors for glycerol steam reforming

E. Gallegos-Suárez[1,2], F.R. García-García[3], I. D. González-Jiménez[4], I. Rodríguez-Ramos[1], A. Guerreo-Ruiz[2] and K. Li[3]

Catalysis Today 233 (2014) 21-30

[1] Instituto de Catálisis y Petroleoquímica, C/Marie Curie 2, Cantoblanco-Madrid 28049, Spain

[2] Grupo de Diseño y Aplicación de Catalizadores Heterogéneos, UA: UNED-ICP/CSIC, Madrid, Spain

[3] Department of Chemical Engineering, Imperial College London, South Kensington Campus, London SW7 2AZ, UK

[4] Inorganic Chemistry and Catalysis, Debye Institute for Nanomaterial Science, Utrecht University, Sorbonelaan 16, Utrecht 3584 CA, The Netherlands

5.2.0 ABSTRACT

In this study, $NiO/MgO/CeO_2$ catalysts with Ni content from 5% to 30% were synthetized by sol-gel method and tested in a fixed-bed reactor (FBR) in the glycerol steam reforming (GSR) reaction. The catalysts were characterized by N_2 adsorption isotherms at -196°C (S_{BET}), X-ray diffraction (XRD), H_2 temperature programmed reduction (H_2-TPR), transmission electron microscopy (TEM) and energy dispersive X-ray (EDX). The 20% $NiO/MgO/CeO_2$ catalyst, which showed the highest catalytic activity in GSR reaction, was selected to be deposited in the finger-like region of the asymmetric Al_2O_3 hollow fibre and the sponge-like region of the symmetric Al_2O_3 hollow fibre in the development of the asymmetric hollow fibre reactor (AHFR) and symmetric hollow fibre reactor (SHFR), respectively. The impregnated ceramic substrates were characterized by scanning electron microscopy (SEM), EDX and TEM. The performances of the AHFR and SHFR were compared with that in a conventional FBR during the GSR reaction. Both AHFR and SHFR were operating at "dead-end" configuration in a temperature range from 250°C to 550°C, atmospheric pressure and in a reactant mixture of steam and glycerol (16:1 molar ratio). At 550°C the glycerol conversion in the AHFR and SHFR was 70% and 46%, respectively, which is 5 and 2 times higher than that obtained in the FBR. The different performance of the AHFR and SHFR could be explained due to the unlike catalyst particle size deposited in the asymmetric and symmetric substrates, 8 nm and 3 nm, respectively.

5.2.1 INTRODUCTION

The expansion of the biodiesel market involves the development of new approaches such as enhanced hollow fibre reactors which can efficiently transform the glycerol excess into more valuable products. Glycerol is by far the main by-product (10% w/w) obtained during the manufacturing of biodiesel through trans-esterification of vegetable oil and animal fats. Although glycerol is used in food, pharmaceutical, cosmetic and tobacco industries, its commercial market has been limited due to its low production a few years ago [1][2]. Nevertheless, since 1990 an increasing interest has been observed in the biodiesel as alternative and renewable fuel which has increased the annual production of glycerol. It is estimated that 4 billion gallons of glycerol will be produced by 2016 [3]. This represents an opportunity for new applications of the glycerol in the current market. In this contest, glycerol has been proposed as a promising renewable source of H_2 since it can be decomposed in the presence of H_2O to produce H_2:

$$C_3H_8O_3 + 3H_2O \rightarrow 3CO_2 + 7H_2 \quad \Delta H=128 \text{ kJ/mol} \qquad (1)$$

In addition, the CO_2 produced during the reaction is consumed for biomass growth which nearly closes the carbon loop. On the other hand, the chemical-physical properties of glycerol, liquid at room temperature and atmospheric pressure along with its non-toxicity possibly make it useful as a "storage-molecule" of H_2 [4].

The glycerol steam reforming (GSR) reaction has been extensively studied in the open literature over both noble and non-noble metal supported catalysts [5][6][7][8][9]. Nevertheless, it is still uncertain which could be the most suitable catalyst for industrial large scale applications. Among all the metal supported

catalysts reported, Pt, Ru, Pd and Ni based catalysts show the better catalytic activity and selectivity for hydrogen production due to their ability to cleave C-C, O-H and C-H rather than C-O bonds and removal of the adsorbed CO by water gas shift (WGS) reaction [10]. Despite the higher catalytic activity of noble-based catalysts, Ni-based catalysts are preferred due to the lower cost and higher availability. However, at the GSR reaction conditions, Ni-based catalysts could suffer deactivation due to both particle size sintering and carbon deposition. According to Swaan et al. the catalytic activity of Ni-based catalysts appears to be essentially dependent on the degree of reduction and dispersion of the Ni particles [11]. Likewise, Kumari et al. [12] who studied different Ni/SiO_2 based catalysts during the GSR reaction, found that the bigger the Ni particle size the lower the selectivity to carbon formation.

In attempts to improve catalytic properties of Ni-based catalysts, Ni has been dispersed on different oxide materials such as MgO, CeO_2, Al_2O_3, SiO_2, ZrO_2 and La_2O_3 [13][14][15]. In this respect, it has been reported that oxide supports such as ZrO_2, MgO and La_2O_3 could improve the catalytic activity and avoid carbon deposition due to their basic character. In this respect, Zhuang et al. have reported that carbon deposition can be avoided by adding CeO_2 into the catalytic system [16]. The reducibility and oxygen transfer capacity of the CeO_x accelerate the reaction between the steam and the adsorbed species on the Ni surface reducing the number of carbon species on the catalyst surface and in consequence the risk of their deactivation by carbon deposition.

Different catalytic multifunctional reactors have been described in the open literature in an attempt to improve the performance during the GSR reaction. Iulianelli [17] and Chang [18] have demonstrated the advantages of combining an

active Ni-based catalyst and an H_2 permselective membrane in a single unit over traditional FBR during the GRS reaction. As it is well known, catalytic membrane reactors (CMR) not only enhance the performance under a wide range of reaction conditions but also allow the H_2 separation/purification in a single step. Another procedure for shifting the thermodynamic equilibrium during the GSR reaction consists of blending the Ni-based catalyst with a CO_2 adsorbent in a so-called sorbent enhanced reactor (SER), thus the CO_2 produced can be selectively removed from the reaction medium [19]. Chen et al. obtained high purity hydrogen (99%) during the GSR reaction by in situ CO_2 capture in a SER which used Ni-Co as a catalyst and a dolomite as a selective adsorbed of CO_2 [20]. Although, both CMR and SER present important advantages over traditional FBR, it is important to be aware of the challenges of this technology. First, H_2 permeation through the high selective membrane increases the risk of carbon deposition in the CMR, since the reaction medium atmosphere becomes more oxidant [21][22][23]. Secondly, the high performance of the SER is limited by the saturation of the CO_2 adsorbent [24][25][26].

In this respect ceramic hollow fibres substrates, which can be used as a support of catalysts, are increasingly gaining the interest of the scientific community since they provide attractive alternatives in the development of novel multifunctional enhanced reactors for catalytic gas phase reactions [27][28][29][30]. In a previous study, both asymmetric and symmetric Al_2O_3 hollow fibres have been successfully employed as catalyst support in the development of a asymmetric (AHFR) and symmetric (SHFR) hollow fibre reactor, respectively [31]. It has been widely demonstrated in our previous work that deposition of catalysts either inside the finger-like region of the asymmetric Al_2O_3 hollow fibres or in the sponge-like region of the symmetric Al_2O_3 hollow fibres increases its catalytic efficiency [32].

These types of reactors, operated in a flow through mode, presents the advantage of providing intensive contact between reactants and catalysts, combined with a short residence time, allowing for a high selectivity and catalytic activity.

This paper described our understanding of the use of ceramic hollow fibre substrates as supports of catalysts in the development of new enhanced reactors. In order to better understand the influence of the support porous structure in the catalysts deposition, in this study both asymmetric and symmetric ceramic hollow fibre substrates have been studied. The GSR reaction was chosen as sample reaction to compare the performance of the new ceramic hollow fibre enhanced reactors with that in a conventional FBR. Before catalysts deposition into the ceramic hollow fibre substrates, a preliminary catalytic study in a fixed-bed reactor (FBR) was carried out with a series of $NiO/MgO/CeO_2$ catalysts with Ni content from 5% to 30% during the GSR reaction. The catalyst with the highest catalytic activity in the GSR reaction was selected to be deposited in the finger-like region of the asymmetric Al_2O_3 hollow fibre and the sponge-like region of the symmetric Al_2O_3 hollow fibre in the development of the asymmetric hollow fibre reactor (AHFR) and symmetric hollow fibre reactor (SHFR), respectively.

5.2.2 EXPERIMENTAL

5.2.2.1 Preparation of the $NiO/MgO/CeO_2$ catalysts

The $NiO/MgO/CeO_2$ catalysts were prepared using the sol-gel Pechini method. $Ni(NO_3)_2{\cdot}6H_2O$ (99% Acros Organics), $Mg(NO_3)_2{\cdot}6H_2O$ (98% BDH Laboratory Supplies) and $Ce(NO_3)_2{\cdot}3H_2O$ (99.0% Fluka Analytical) were dissolved in 100 mL deionised water. The amount of $Ni(NO_3)_2{\cdot}6H_2O$ was varied to produce $NiO/MgO/CeO_2$ with different NiO loading but with the molar ratio $MgO/CeO_2 = 0.880$. After all metal nitrates were fully dissolved, citric acid (99.0%

Sigma-Aldrich) was added to the solution with a molar ratio 2:1 between the citric acid and the metal ions. The process was continued by adding ethylene glycol into the solution with a molar ratio 1:1.2 between citric acid and ethylene glycol. The catalyst solutions were stirred for 3 h and later placed into an oven (Salvislab Thermocenter) for drying process at 115 ^{o}C for 24 h to form foamy dry gel. The dry gel was then calcined in a tubular furnace (Vecstar Furnaces,VCTF/SP) at 400 ^{o}C for an hour at 10 ^{o}C min^{-1}.

5.2.2.2 Characterization of the NiO/MgO/CeO_2 catalysts

The catalysts were characterized by N_2 adsorption isotherms at -196 ^{o}C (S_{BET}), X-ray diffraction (XRD), H_2 temperature programmed reduction (H_2-TPR), energy dispersive X-ray (EDX) and transmission electron microscopy (TEM).

The specific surface area of the fresh catalysts was measured by N_2 adsorption isotherms at -196 °C. An automatic TriStar 3000 volumetric system was used to obtain the gas adsorption isotherms. Prior to N_2 adsorption, the catalysts were degassed at 150 °C overnight. The BET model was used to obtain the specific surface area.

X-ray diffraction measurements were performed with a Bruker AXS D8 ADVANCE diffractometer with $Co_{K\alpha 1}$ source (λ = 0.178897 nm) in a wide angle range (from 30 to 90 in 2θ).

Temperature programmed reduction (TPR) was performed on a Micromeritics Autochem-II instrument equipped with a TCD detector. The samples (30 mg) were previously dried in Ar flow at 120 °C switched to 50 mL/min of 5% H_2/Ar (Linde). The temperature was raised from room temperature to 900 °C at 10 °C /min.

TEM analysis was made using a JEOL 2100F emission gun electron microscope operated at 200 kV equipped with an EDX detector. The TEM specimens were prepared by dispersing a small catalyst amount in ethanol and put one drop on a lacey carbon film coated copper grid (3.0 mm, 200 mesh, Aname).

5.2.2.3 Preparation and characterization of the Al_2O_3 hollow fibre

Symmetric and Asymmetric Al_2O_3 hollow fibre substrates have been prepared using phase-inversion techniques, followed by sintering at high temperatures. The detailed procedures in fabricating the substrates can be found elsewhere [33].

5.2.2.4 Fabrication of the AHFR and SHFR

Asymmetric and symmetric Al_2O_3 hollow fibres were loaded with 20% NiO/MgO/CeO_2 catalysts by sol-gel Pechini method in the development of the AHFR and SHFR, respectively. Prior to catalyst deposition, the hollow fibres were wrapped with the PTFE tape in order to prevent the catalyst solution from coming into contact with their outside surface. A homogeneous catalyst solution was later injected into the lumen of the Al_2O_3 hollow fibre substrates using a glass pipette, and this process was repeated several times. The Al_2O_3 hollow fibres were then dried in an oven (Salvislab Thermocenter) at 60 °C for 24 h and further dried at 115 °C to complete the polymerization of a polymeric resin precursor. The calcination process was later carried out by flowing 30 mL/min of air into the lumen-side of the Al_2O_3 hollow fibre at 400 °C for 1 h.

The catalyst loading in the Al_2O_3 hollow fibres was obtained by measuring the weight of the Al_2O_3 hollow fibre substrates before and after calcination steps

and was found to be around 25.4 mg and 21.1 mg for the asymmetric and symmetric hollow fibre, respectively.

The morphology and structure of hollow fibres after the catalyst deposition were studied using a scanning electron microscope (SEM, JEOL JSM-5610LV) equipped with an energy dispersive X-ray spectroscopy detector (EDX, INCA Energy by Oxford Instruments) which permit elemental analysis. The samples were gold coated under vacuum for 3 min at 20 mA (EMITECH Model K550 LV) before SEM and EDX analysis.

The average particle size of the 20% NiO/MgO/CeO_2 catalyst deposited in both asymmetric and symmetric substrates was estimated by TEM analysis using a JEOL 2100F emission gun electron microscope operated at 200 kV equipped with an EDX detector. The TEM specimens were prepared by dispersing a small catalyst amount of grilled hollow fibre in ethanol and placing one drop on a lacey carbon film coated copper grid.

5.2.2.5 Catalytic activity test

The catalytic activity measurements of the GSR reaction were tested in a fixed-bed reactor, AHFR and SHFR operating under atmospheric pressure over a temperature range from 300 ^{o}C to 550 ^{o}C. The feed mixture in all cases was 0.02 mL/min of 25% water solution of glycerol using an HPLC pump (Bath Univer series 1) and 60 mL/min of Ar as carrier gas.

The catalytic activity tests in the fixed-bed reactor were carried out using 60 mg of catalysts. The catalyst with a particle size of approximately 100 μm, was mixed with 2 g of SiC and packed into a 6 mm ID stainless steel reactor. The

packed-bed length was approximately 30 mm and the mass transfer limitation across the bed was negligible.

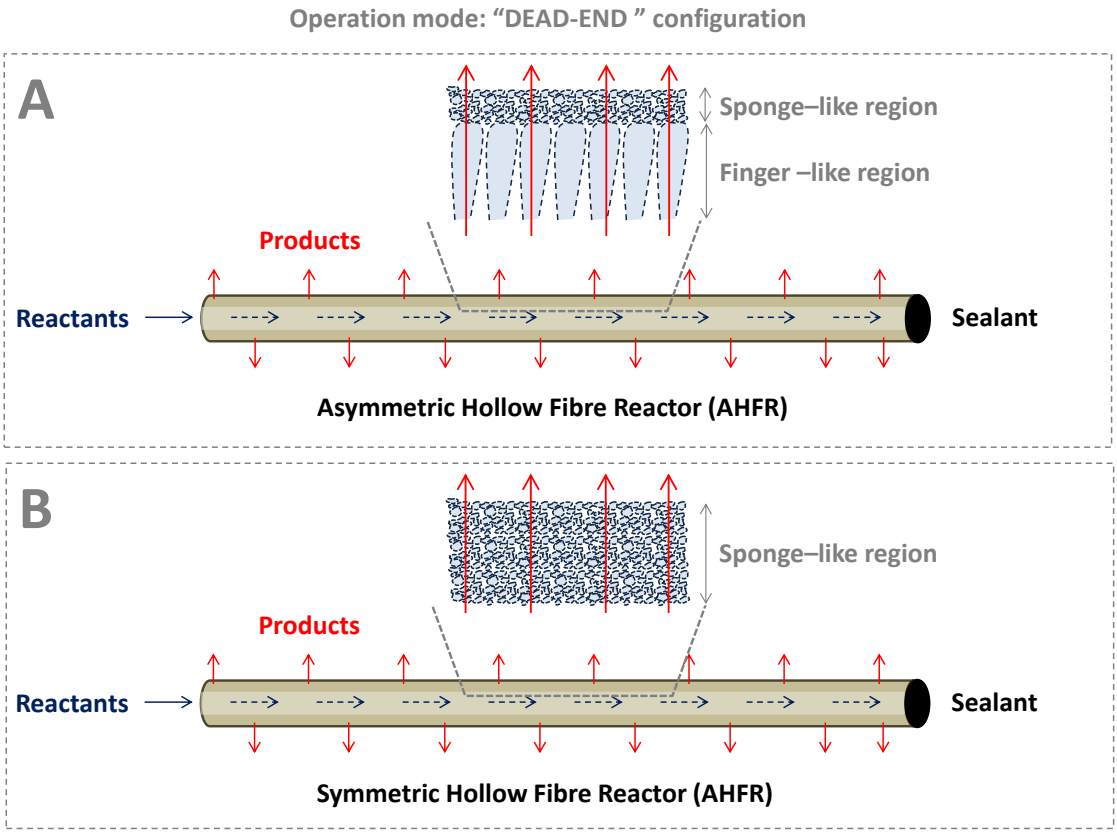

Figure 1. Asymmetric and symmetric Al_2O_3 hollow fibre reactors operating in a "dead-end" configuration, A and B, respectively.

The catalytic activity tests in both AHFR and SHFR were carried out in a "dead-end" configuration (Figure 1). The concentration of the products was measured using TCD gas chromatography (Varian-3900). Before the gasses were injected, a cold tramp was put in to prevent glycerol and water going into the GC. The GC injections for gas analysis were repeated three times to obtain more reliable results. The $C_3H_8O_3$ conversion is defined as follows:

$$X_{C_3H_8O_3(\%)}=\frac{[CO]_{out}+[CO_2]_{out}+[CH_4]_{out}}{3[C_3H_8O_3]_{in}}x100 \qquad (1)$$

And the H_2 yield is defined as follows:

$$Y_{H_2(\%)} = \frac{[H_2]_{out}}{7[C_3H_8O_3]_{in}} x100 \qquad (2)$$

5.2.3 RESULTS AND DISCUSSION

The XRD patterns of NiO/MgO/CeO_2 catalysts are shown in Figure 2A-E. All the catalysts presented show typical diffraction of cubic fluorite CeO_2. This diffraction had the reflection peaks at 2θ = 33.4º, 38.3º, 55.9º and 66.4º.

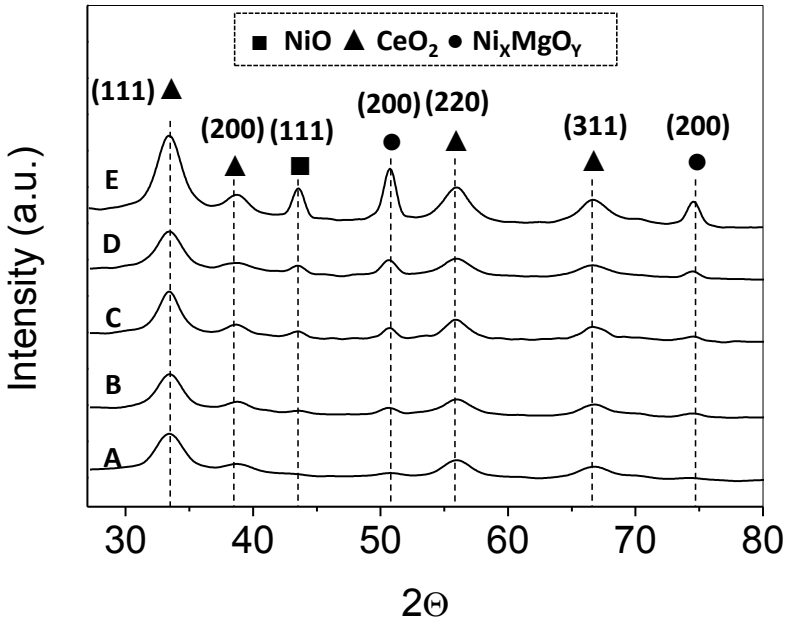

Figure 2. XRD patterns of NiO/MgO/CeO_2 catalysts: (A) 5% NiO/MgO/CeO_2, (B) 10% NiO/MgO/CeO_2, (C) 15% NiO/MgO/CeO_2, (D) 20% NiO/MgO/CeO_2 and (E) 30% NiO/MgO/CeO_2.

There are reflection peaks corresponding with the mixed oxide Ni_xMg_yO at 51º and 75º. The presence of this specie can be explained by a solid-state reaction between the corresponding oxides during the calcination step of the catalyst preparation procedure. This specie can be formed because the crystalline structure of NiO and MgO is cubic f.c.c, and the ionic radio of Ni^{2+} (0.070 nm) and Mg^{2+} (0.065 nm) are close [34]. The intensity of Ni_xMg_yO reflection peaks increases with Ni loading. There is no evidence of MgO phase for any of the samples, including

the catalyst with lower concentration of Ni. This result indicates that the MgO oxide present in that sample is either amorphous or the crystal size is too small to be detected.

Table 1. Physical properties of NiO/MgO/CeO_2 catalysts synthesized by sol–gel Pechini method.

Ni loading (wt %)	$S_{BET}(m^2/g)$	Particle size (nm)	
		NiO	CeO_2
5	74	8.6	6.7
10	77	8.8	6.4
15	68	12.3	6.6
20	86	16.5	5.3
30	76	15.1	5.3

Table 1 shows that the CeO_2 crystallite particle size decreases with the Ni loading due to NiO promoting thermal stability of CeO_2 particles, by inhibiting the growth of crystal during the calcination step [35]. Our result indicates that the mixed oxide Ni_xMg_yO acts as a structural promoter in the same way as NiO. The CeO_2 and the NiO crystallite particle sizes were determined from the XRD results by Scherrer analysis of the peaks (111) at 33.4° and (111) at 45.5°, respectively as shown in Table 1.

The effect of the Ni loading on the reduction properties of the different NiO/MgO/CeO_2 catalysts was studied by H_2-TPR. Figure 3 shows the deconvoluted H_2-TPR profiles of each catalyst. It can be seen in Figure 3 that all catalysts show a wide H_2-TPR profile, which indicates a broad particle size distribution of the NiO particles over the CeO_2/MgO support. The H_2-TPR profile of 5%, 10% and 15% NiO/MgO/CeO_2 catalysts have been deconvoluted in two main components, whereas for the 20% and 30% NiO/MgO/CeO_2 catalysts an additional third

component have been added. Similar treatment of the H_2-TPR profiles was reported by W. Gaowei et al. [36], which also fitted them into three different peaks using Gaussian-type functions. As it has been widely reported in the open literature, highly dispersed CeO_2 reduces at lower temperatures than bulk CeO_2, reduction temperature around 500^{o}C and 750 ^{o}C , respectively [37][38]. Likewise, the reduction of pure MgO does not occur at temperatures below 900 ^{o}C [39]. Hence, the first and second reduction component observed in all the catalysts studied can be ascribed to the reduction of the NiO well dispersed and NiO strongly interacting with the CeO_2/MgO support, respectively [40][41].

However, the fact that the first reduction component appears at a higher temperature range (from 385 ^{o}C to 426 ^{o}C) than that observed for pure NiO (from 370 ^{o}C to 400 ^{o}C) suggests that a weak interaction between the NiO well disperse and support CeO_2/MgO exists [39][42][43][44]. This interaction disappears as the Ni loading increases, which could be explained due the low interaction with the support of large NiO particles formed at high Ni loading [35]. Due to the fact that the reduction of NiO takes place in a single step, no intermediate Ni oxides are formed and the different NiO species present in the catalyst can be ascribed based on the reduction temperature [45]. In this respect, it is well established that the reduction of NiO particles in intimate contact with the oxide support occurs at temperatures higher than 500 ^{o}C [35][40][46]. Thus, the second reduction component at which occurs in the temperature range from 469 ^{o}C to 534 ^{o}C can be ascribed to the reduction of NiO particles strongly interacting with NiO-MgO support. Similar to the first reduction component, the reduction temperature decreases as the NiO particle size increases. According with Yang et al., at high temperature the reduction of the NiO in NiO/MgO/CeO_2 based catalysts is promoted by the presence of CeO_2 [46]. In this respect the CeO_2 not only inhibit the

diffusion of the NiO into the MgO lattice but also favour the reduction of the NiO by spillover of H_2 from the CeO_2 to the NiO phase [46][47].

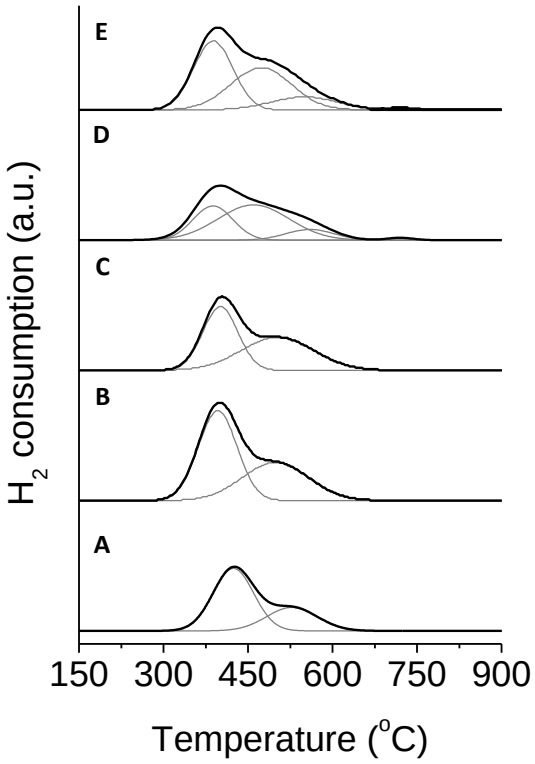

Figure 3. H_2-TPR profiles of $NiO/MgO/CeO_2$ catalysts in 5% H_2/Ar under a heating rate of 10 °C/min: (A) 5%$NiO/MgO/CeO_2$, (B) 10%$NiO/MgO/CeO_2$, (C) 15%$NiO/MgO/CeO_2$, (D) 20%$NiO/MgO/CeO_2$ and (E) 30%$NiO/MgO/CeO_2$.

To end with the H_2-TPR discussion, catalysts at 20% and 30% NiO show a third peak in the temperature range from 485 °C to 682 °C, which can be attributed due to the partial reduction the CeO_2 surface [48][49][50].

The catalytic behaviour of the different $NiO/MgO/CeO_2$ based catalysts during the GSR reaction using a conventional FBR it is shown in Figure 4. In order to properly compare each catalyst, the reaction conditions were fixed at $H_2O/C_3H_8O_3$ ratio 1/16 and WHSV = 5.27 h^{-1}. Thus, the $C_3H_8O_3$ conversion was below 100% in the temperature range studied.

It can be seen in Figure 4 that 15%, 20% and 30 % NiO/MgO/CeO_2 catalysts show the same $C_3H_8O_3$ conversion curve in the temperature range from 279 °C to 450 °C. This behaviour suggests that the three catalysts have the same type and number of active centres. Nevertheless, at reaction temperatures higher than 450 °C three different catalytic behaviours were observed. Whereas, the $C_3H_8O_3$ conversion for 20% NiO/MgO/CeO_2 catalyst increases as the temperature increases,

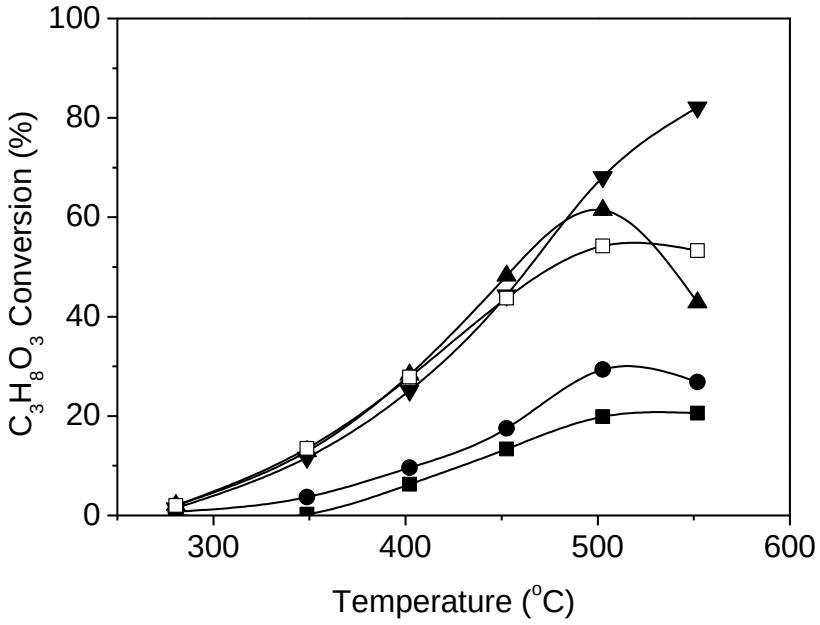

Figure 4. $C_3H_8O_3$ conversion as a function of the temperature in glycerol steam reforming reaction using a WHSV 5.3 h^{-1} in a fixed-bed reactor: (■) 5% NiO/MgO/CeO_2, (●) 10% NiO/MgO/CeO_2, (▲) 15% NiO/MgO/CeO_2, (▼) 20% NiO/MgO/CeO_2 and (□) 30% NiO/MgO/CeO_2.

it remains constant or decreases for 30% and 15% NiO/MgO/CeO_2 catalysts, respectively. Thus, at 550 °C the $C_3H_8O_3$ conversion for 20% NiO/MgO/CeO_2 catalyst is 82% which is 64% and 51% higher than that observed in the 30% and 15% NiO/MgO/CeO_2 catalysts, respectively. The differences observed at high reaction temperatures in the catalytic activity can be explained due to catalyst deactivation either by carbon deposition, particle sintering or both at the same

time. It has been widely reported in the open literature that there is a relation between the Ni particle size and the coke formation [13][51][52][53]. Moreover, Dieuzeide et al. have reported that carbon deposition could be related to the basic character of the catalyst [54]. Thus, higher content of MgO could minimize the carbon deposition, but if the goal is to enhance the catalytic activity during the GSR reaction, lower MgO ratios should be employed. This agrees with the fact that in the temperature range studied, the $C_3H_8O_3$ conversion for 5% and 10% NiO/MgO/CeO_2 catalysts is significantly lower than that observed for 15%, 20% and 30 % NiO/MgO/CeO_2 catalysts.

On the other hand, it is shown in Table 1 that the average particle size of 15%, 20% and 30 % NiO/MgO/CeO_2 catalysts is centred on 15 nm, whereas for the 5% and 10% NiO/MgO/CeO_2 catalysts, the average particle size is 8.6 nm and 8.8 nm, respectively. Thus, it is possible to establish a volcano curve relationship between the Ni particle size and catalytic activity observed during the GSR reaction. This behaviour, suggests that the GSR reaction could be sensitive to the Ni particle size. Similar results were reported by Gaowei et al., who found that the Ni particles with an average particle size of 11 nm showed the highest H_2 yield and stability during the GSR reaction than large Ni particles [36].

Based upon all this, the high catalytic activity of the 20% NiO/MgO/CeO_2 catalyst could be explained due to a combination of two different factors. First, an optimum catalyst particle size allows the $C_3H_8O_3$ carbon chain to be adsorbed on the metal surface. Secondly, the right MgO content which avoided the carbon deposition without compromising the catalytic activity. Finally, it is important to notice that high selectivity to H_2 was observed in all the catalysts studied at temperatures belong 500 °C. Although, CH_4 was observed at reaction temperatures

higher than 500 °C, its production was lower than 3%. Hence, all the catalysts studied have the capacity to efficiency transform the $C_3H_8O_3$ into CO_2 and H_2.

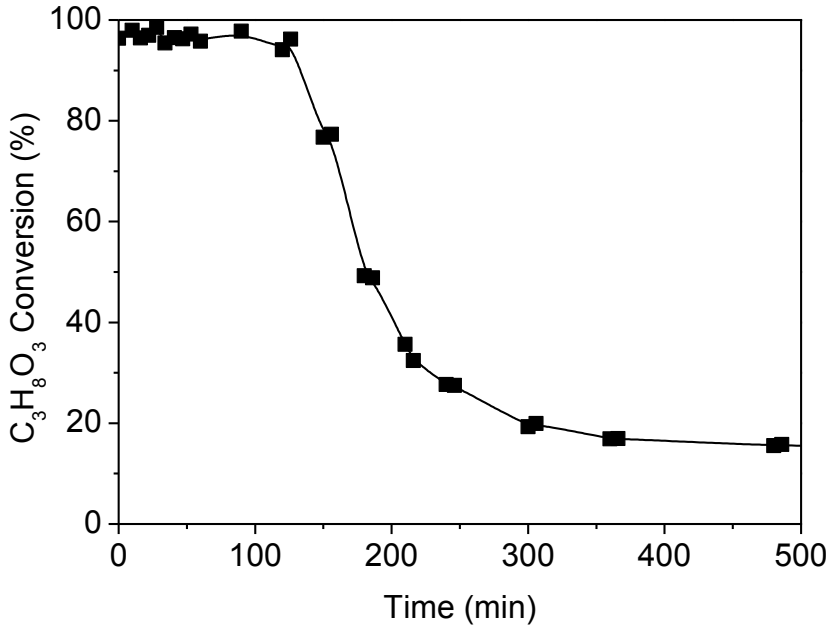

Figure 5. Stability test in over 20% NiO/MgO/CeO_2 catalyst at 550 °C for 500 minutes during the glycerol steam reforming reaction with a WSHV = 5.3 h^{-1} in a fixed-bed reactor.

The stability of the 20% NiO/MgO/CeO_2 catalyst during the GSR reaction was tested at 550 °C under atmospheric pressure and using a reactant mixture of steam and glycerol with a molar ratio 16:1. Figure 5 shows the evolution of the $C_3H_8O_3$ conversion profile during the first 500 min of reaction. Although 20% NiO/MgO/CeO_2 catalyst presented high catalytic activity and good stability during the first 120 min of reaction, the $C_3H_8O_3$ conversion dropped from 100% at 120 min to 16% at 400 min. Hence, in approximately 400min of reaction, the $C_3H_8O_3$ conversion decreased 84%. It is well accepted that Ni sintering and coke formation are the main causes of deactivation of Ni-based catalysts at high reaction temperatures [55][56][57]. In this respect, coke deposits on the surface of the 20% NiO/MgO/CeO_2 catalyst after the GSR reaction have been detected by EDX analysis (not shown here for brevity). Details regarding carbon deposition during

the GSR are commonly reported in the open literature [12][36][58]. According with Gaowei et al., who has studied the performance of Ni/Al_2O_3-based catalysts during the GSR reaction, large Ni particle size, low Ni dispersion or residual chloride are the main reasons for coke deposition and low reaction activity during the GSR reaction [36]. Likewise, Sadanandam et al. and Bobadilla et al. have found that the lower the surface-to-volume (S/V) ratio of the catalysts the lower the carbon gasification rate is, which decreases both the activity and stability of the Ni-based catalysts [12][58]. Based upon this, the fast deactivation of the 20%NiO/MgO/CeO_2 catalyst could be explained due to its low S/V ration (particle size approximately 100 μm).

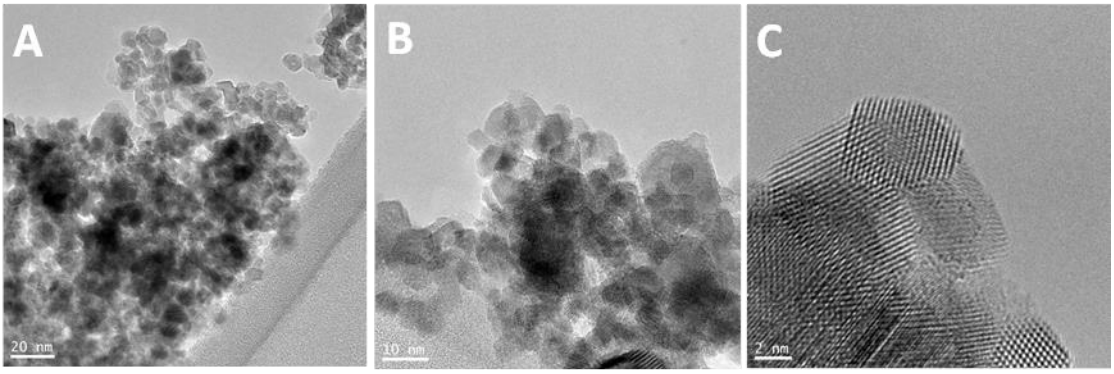

Figure 6. TEM images at different magnifications of the 20% NiO/MgO/CeO_2 catalyst.

Despite its low stability, 20% NiO/MgO/CeO_2 catalyst, which showed the highest catalytic activity in a GSR reaction, was selected to be deposited in both the finger-like region of the asymmetric Al_2O_3 hollow fibre and the sponge region of the symmetric Al_2O_3 hollow fibre in the development of the AHFR and SHFR, respectively.

Figure 6 shows a set of TEM pictures of the 20% NiO/MgO/CeO_2 catalyst at different magnifications. The sample is homogeneous and NiO particles are regularly distributed all around the MgO/CeO_2 support. An average particle size of

10.5 nm was observed, which agrees with the particle size calculated from the XRD results.

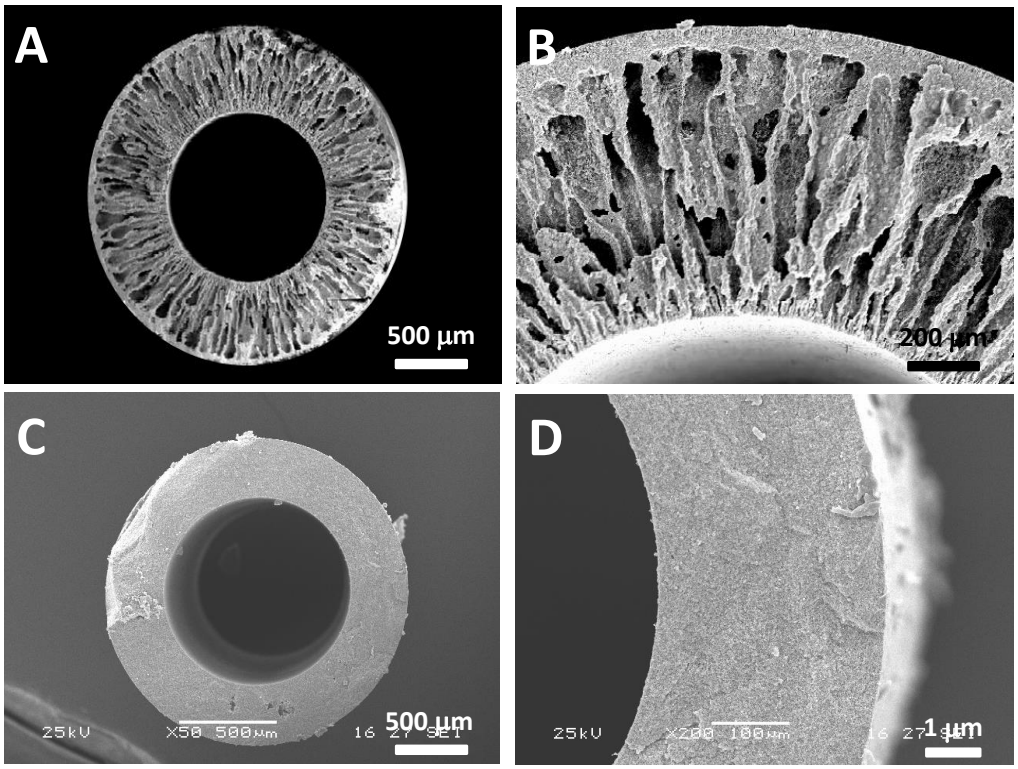

Figure 7. SEM pictures at different magnification of the cross section of a typical asymmetric and symmetric Al_2O_3 hollow fibre, A-B and C-D, respectively.

Figure 7 shows SEM pictures at different magnifications of the cross section of both ceramic tubular substrates employed in this study as a support of catalyst. The structure and morphology of a characteristic asymmetric Al_2O_3 hollow fibre (OD/ID = 1.9/1.0) is shown in Figures 7A and 7B. An asymmetric pore structure, which consists of a porous finger-like structure in the inner region (approximately 80% of its thickness) and a sponge-like structure in the outer region (the remaining 20% of its thickness), can be observed in both SEM images. Moreover, Figure 7B shows that the sponge-like region consists of a regular Al_2O_3 layer with a thickness of 100 µm whereas the finger-like region is made up of hundreds of conical micro-channels that are perpendicularly distributed around the lumen of the fibre. The conical micro-channels have a conical circular base between 10 µm to 50 µm and a

total length of 400 μm. On the other hand, Figures 7C and 7D show that the cross-section of a typical symmetric Al_2O_3 hollow fibre (OD/ID = 1.6/1.0) employed in the deployment of the SHFR consists of a regular sponge-like layer with an average thickness of 300 μm.

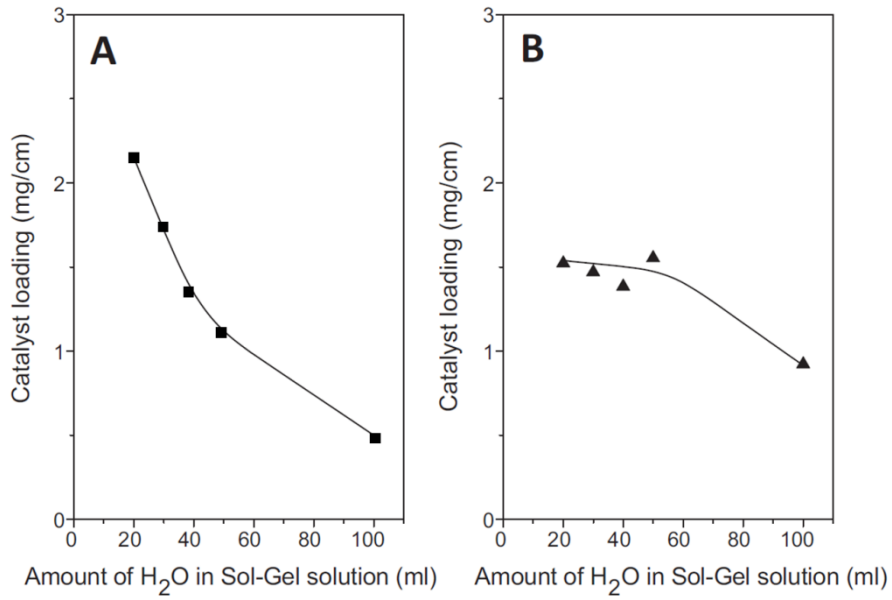

Figure 8. Catalyst loading deposited into the asymmetric and symmetric Al_2O_3 hollow fibre as a function of the amount of H_2O in the sol-gel solution, A and B, respectively.

The deposition of the 20% NiO/MgO/CeO_2 catalyst in both symmetric and asymmetric Al_2O_3 hollow fibre was carried out by sol-gel Pechini method [59]. It has been previously reported elsewhere [32] that the distribution of the catalyst either inside the finger-like conical micro-channels or in the sponge-like pores offers important advantages such as high catalytic efficiency along with a maximum selectivity. Thus, in order to optimize the catalyst loading in both ceramic substrates a preliminary catalyst impregnation study using different sol-gel solution concentrations was performed. The amount of catalyst deposited inside the finger-like and sponge-like region of the asymmetric and symmetric Al_2O_3 hollow fibre as a function of the solvent (water) present in the sol-gel

solution is shown in Figure 8A and B, respectively. As it was expected, the catalyst loading increased as the concentration of the sol-gel increases, i.e. when the sol-gel solution was prepare with 20 mL of H_2O the catalyst loading in the asymmetric Al_2O_3 hollow fibre was 2.3 mg/mL which is 4.6 time larger than when it is prepared with 100 mL of H_2O. Likewise, when the sol-gel solution was prepare with 20 mL of H_2O the catalyst loading in the symmetric Al_2O_3 hollow fibre was 1.6 time larger than when it is prepared with 100 mL of H_2O. However, the fact that the catalyst loading does not increase lineally with the concentration of the sol-gel solution indicates that other parameters such as surface tension of the sol-gel solution must play an important role during the impregnation process. In addition, it was reported in our previous work that the degree of dispersion of the catalyst within the Al_2O_3 hollow fibres is strongly dependent on the physical and chemical properties of the Al_2O_3 surface, which, in turn, are determined by the sintering temperature [28][60]. Based on this preliminary study, a sol-gel solution prepare with 20 mL of H_2O was employed for an optimal impregnation of the 20% $NiO/MgO/CeO_2$ catalyst in both asymmetric and symmetric hollow fibre in the development of the AHFR and SHFR, respectively.

The cross section of both symmetric and asymmetric Al_2O_3 hollow fibres after impregnation with 20% $NiO/MgO/CeO_2$ catalyst were studied by SEM-EDX surface mapping analysis. Figure 9 shows a uniform distribution of Ni, Ce and Mg ions on the cross section of both Al_2O_3 hollow fibre substrates. Although, the presence of C was observed due to traces of citric acid or ethylene glycol present in the sol-gel solution, it was very low. Hence, based upon these TEM pictures it can be concluded that the catalyst was successfully deposited by sol-gel Pechini method in both asymmetric and symmetric Al_2O_3 hollow fibre substrates.

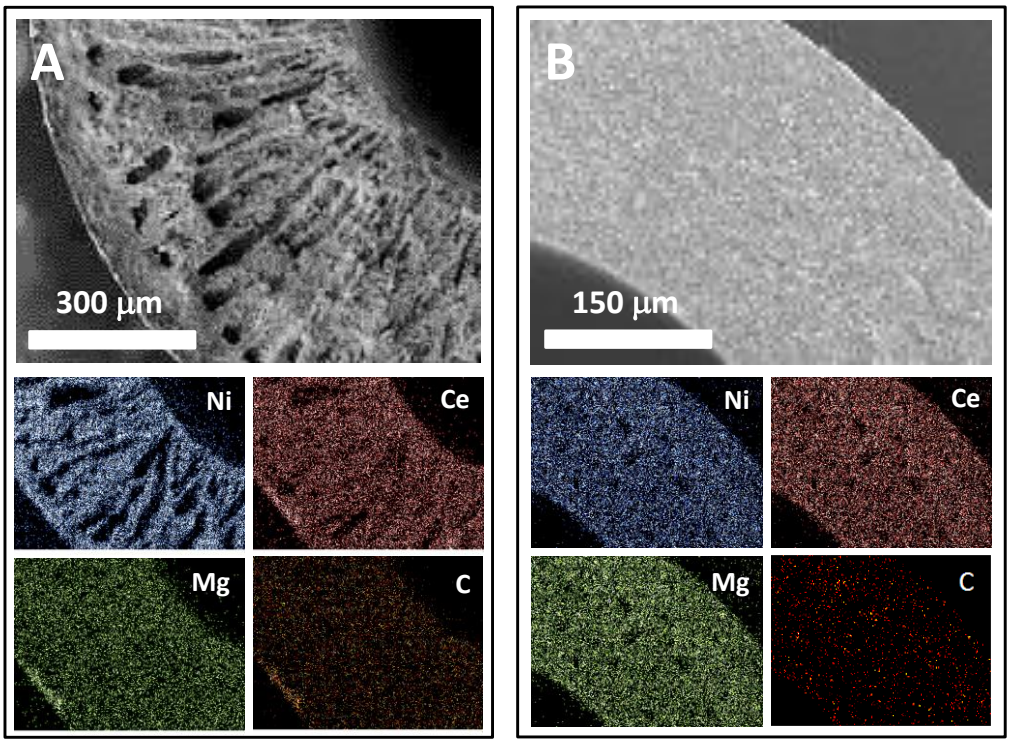

Figure 9. The SEM/EDX analysis surface mapping of the cross section of asymmetric and symmetric Al_2O_3 hollow fibre after impregnation with the 20% NiO/MgO/CeO_2 catalyst, A and B, respectively.

XRD analysis was carried out over both asymmetric and symmetric substrates after catalyst deposition in order to determinate the 20% NiO/MgO/CeO_2 catalyst average particle size (not shown here for brevity). Nevertheless, the reflection peaks corresponding to CeO_2, MgO and NiO were not observed by XRD due to the small amount of catalyst deposited in both Al_2O_3 hollow fibres which is under the limit of detection of the XRD technique. Thus, the average particle size of the 20% NiO/MgO/CeO_2 catalyst deposited in both asymmetric and symmetric substrates was estimated by TEM analysis. Figure 10 shows TEM pictures at different magnification of both ceramic hollow fibre substrates after catalyst deposition. It can be observed that 20% NiO/MgO/CeO_2 catalyst spherical particles are homogenously dispersed on both ceramics substrates. However, the average particle size of the catalyst deposited on the asymmetric hollow fibre is 2.6 times

larger than that observed on the symmetric hollow fibre, 8 nm and 3 nm, respectively. The difference in the average particle size could be explained due to the fact that the $NiO/MgO/CeO_2$ particles can grow larger during the polymerization step in the finger-like region than in the sponge-like region. Similar result were reported in our previous work, where 10% CuO/CeO_2 catalyst was deposited in two different pore structure ceramic hollow fibres and tested in water gas shift reaction [31].

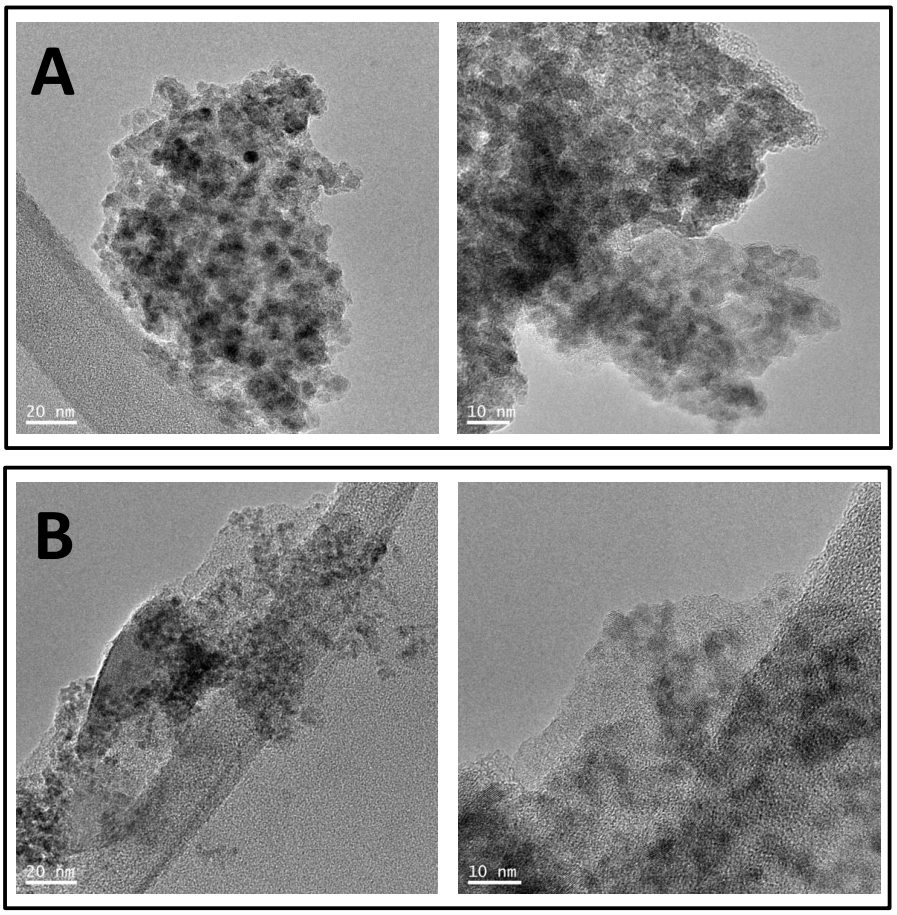

Figure 10. TEM images of the asymmetric (A) and symmetric (B) Al_2O_3 hollow fibre substrates impregnated with the 20% $NiO/MgO/CeO_2$ catalyst.

Figure 11 compares the $C_3H_8O_3$ conversion as a function of the reaction temperature during the GSR reaction in the SHFR, AHFR and a conventional FBR which uses as catalyst either the asymmetric or symmetric Al_2O_3 hollow fibres impregnated with 20% $NiO/MgO/CeO_2$ after grinding, A and B, respectively.

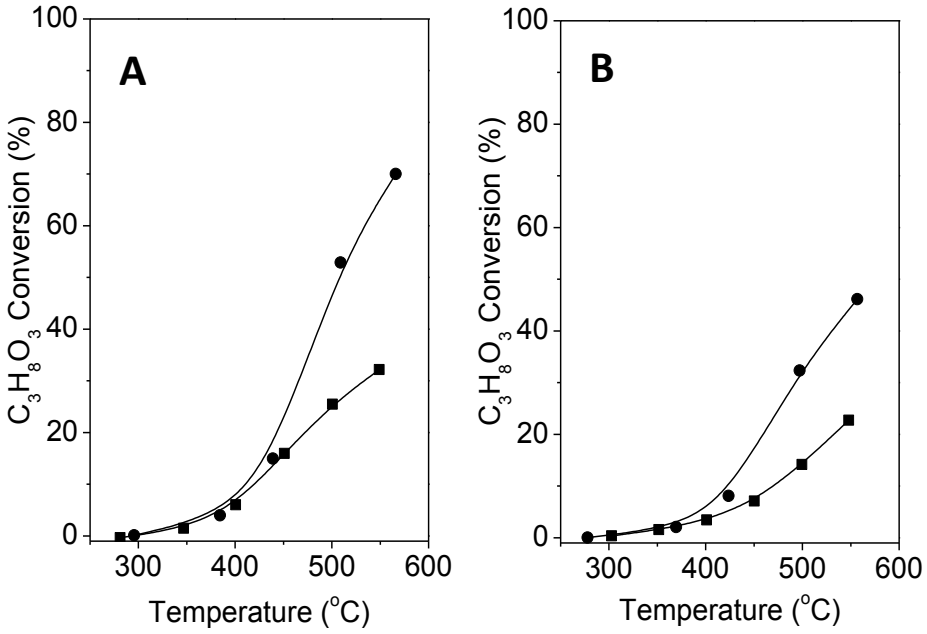

Figure 11. Glycerol conversion as a function of the temperature during the GSR reaction with a WHSV 44.2 h^{-1}: A) (■) FBR using as a catalyst powder ground from asymmetric Al_2O_3 hollow fibre impregnated with 20% NiO/MgO/CeO_2 and (●) AHFR working with an "dead-end" configuration. B) (■) FBR using as a catalyst powder ground from symmetric Al_2O_3 hollow fibre impregnated with 20% NiO/MgO/CeO_2 and (●) SHFR working with a "dead-end" configuration.

Although $C_3H_8O_3$ conversion increased as the temperature increased in both SHFR and AHFR, the catalytic activity of the impregnated symmetric Al_2O_3 hollow fibre is lower than that obtained using the impregnated asymmetric Al_2O_3 hollow fibre. The results obtained at 500°C during the GSR reaction showed that the glycerol conversion using the impregnated symmetric Al_2O_3 hollow fibre as a catalyst was 32%, which was 21% lower than that obtained with the impregnated asymmetric Al_2O_3 hollow fibre. This behaviour suggests that the small catalyst particles deposited in the symmetric Al_2O_3 hollow fibres have lower catalytic activity than the large catalyst particles deposited in the asymmetric Al_2O_3 hollow fibres (see Figure 10). In this respect, Y.F. Yu Yao has found that during the oxidation of hydrocarbon over noble metal based catalysts the reaction rate

decreases as the alkane carbon chain length increases because more adjacent sites are required to achieve the adsorption of the hydrocarbon claims [61]. Thus, the differences in the catalytic activity could be explained due to differences in either the geometry or crystal surface between small and large 20% $NiO/MgO/CeO_2$ catalyst particles, corner/steps vs faces/planes, respectively [62].

Moreover, Figure 11A shows that the AHFR performance during the GSR reaction is higher than that observed in the FBR using as a catalyst powder ground from asymmetric Al_2O_3 hollow fibre impregnated with 20% $NiO/MgO/CeO_2$ (i.e., at 500 ^oC the glycerol conversion in the AHFR working with a "dead-end" configuration was 56%, which was 31% larger than that obtained in a FBR). Likewise, Figure 11B shows that the performance of the FBR using as a catalyst the powder ground from symmetric Al_2O_3 hollow fibre impregnated with 20% $NiO/MgO/CeO_2$ is lower than that observed in the SHFR (i.e., at 500 ^oC the glycerol conversion in the SHFR working with a "dead-end" configuration was 33%, which was 10% larger than that obtained in a FBR). Despise the big differences in the $C_3H_8O_3$ conversion; it is important to note that the light-off starting temperature for the FBR/AHFR (Figure 11A) and FBR/SHFR (Figure 11B) is the same, 314 °C and 374 °C, respectively. This behaviour indicates that the $C_3H_8O_3$ conversion in both FBRs is limited by external and pore diffusion, whereas the configuration of both the AHFR and SHFR intensifies the contact between the catalyst and the reactants resulting in a high catalytic activity [27][30][63][64].

In order to study the stability of the 20%$NiO/MgO/CeO_2$ catalyst deposited in both AHFR and SHFR during the GSR reaction, a second reaction run was carried out under the same reaction conditions. Figure 12 shows both AHFR and SHFR $C_3H_8O_3$ conversion curves during the GSR reaction before and after the second

reaction run. It can be observed that the performance of both hollow fibre reactors decreases during the second reaction run. This behavior could be explained due to either carbon deposition or sintering of the Ni particles. The fact that, during the second run the $C_3H_8O_3$ conversion at 550 ^oC is 50% lower in the AHFR, but 15% in the SHFR, suggests that coke formation and the particle sintering are smaller in the SHFR. Less carbon deposition could be explained due to the shorter residence time in the SHFR compared with the AHFR, thus the polymerization of the intermediate products is less likely. Likewise, the initial Ni particle size in the SHFR is smaller than in the AHFR, which could help to diminish catalyst deactivation due to sintering effect.

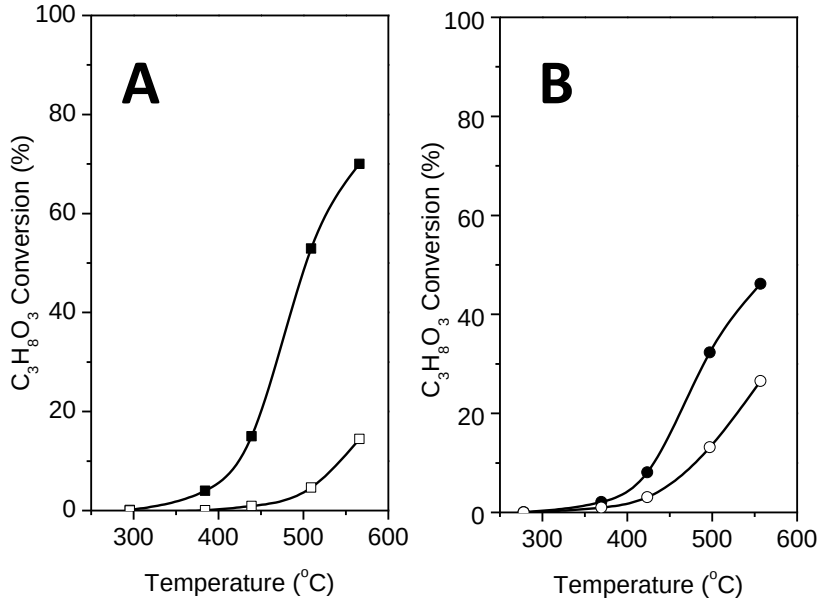

Figure 12. Glycerol conversion as a function of the temperature during the GSR reaction. A) AHFR performance during the (■) first and (□) second reaction run. B) SHFR performance during the (●) first and (o) second reaction run.

5.2.4 CONCLUSIONS

The main conclusions of this work can be summarized as follows:

Among all the catalysts tested, Ni content range from 5% to 30%, the 20% NiO/MgO/CeO_2 catalyst showed the highest catalytic activity in the GSR

reaction, i.e. at 550 °C the $C_3H_8O_3$ conversion for 20% NiO/MgO/CeO_2 catalyst is 82% which is 24%, 32%, 51% and 64% higher than that observed in the 5% 10% 15% and 30% NiO/MgO/CeO_2 catalyst, respectively. The highest catalytic activity of the 20% NiO/MgO/CeO_2 catalyst could be explained due its optimum catalyst particle size, which allow the $C_3H_8O_3$ carbon chain to be adsorbed on the metal surface, and right MgO content, which avoided the carbon deposition without compromising the catalytic activity.

The 20% NiO/MgO/CeO_2 catalyst was effectively deposited in both asymmetric and symmetric hollow fibres substrates by the sol–gel Pechini method in the development of the AHFR and SHFR, respectively. The 20% NiO/MgO/CeO_2 catalyst particle size was determined by the pore dimension of the finger-like and sponge-like regions. Hence, two different catalyst particle size distributions were observed in the asymmetric and symmetric Al_2O_3 hollow fibres, average particle size about 8 nm and 3 nm, respectively.

The reaction results obtained during the GSR reaction in a FBR which uses as catalyst either the asymmetric or symmetric Al_2O_3 hollow fibres impregnated with 20% NiO/MgO/CeO_2 after grinding, showed that the glycerol conversion over the large catalyst particles was higher than that observed on the small catalyst particles. These results support the idea that GSR reaction is sensitive to the structure.

Finally, the performance of both SHFR and AHFR is higher than that observed in a conventional FBR. This behaviour can be explained due to the intensification of the transfer between the catalyst and the reactants during the reaction in the SHFR and AHFR resulting in a high catalytic activity.

5.2.5 REFERENCES

[1] F. Ma, M.A. Hanna, Bioresour. Technol. 70 (1999) 1-70.

[2] S.M. Kim, S.I. Woo, Chemsuschem 5 (2012) 1513-1522.

[3] P. Anand, R.K. Saxena, N. Biotechnol. 29 (2012) 199-205.

[4] S. Fernando, S. Adhikari, C. Chandrapal, N. Murali, Energy & Fuels 20 (2006) 1727-1737.

[5] P.D. Vaidya, A.E. Rodrigues, Chem. Eng. Technol. 32 (2009) 1463-1469.

[6] R. Sundari, P.D. Vaidya, Energy & Fuel 26 (2012) 4195-4204.

[7] T. Hirai, N. Ikenaga, T. Miyake, T. Suzuki, Energy & Fuel 19 (2005) 1761-1762.

[8] V. Chiodo, S. Freni, A. Galvagno, N. Mondello, F. Frusteri, Appl. Catal. A: Gen. 381 (2010) 1-7.

[9] C. Wang, B. Dou, H. Chen, Y. Song, Y. Xu, X. Du, T. Luo, C. Tan, Chem. Eng. J. 220 (2013) 133-142.

[10] A. Iriondo, V.L. Barrio, J.F. Cambra, P.L. Arias, M.B. Guemez, M.C. Sanchez-Sanchez, R.M. Navarro, J.L.G. Fierro, Int. J. Hydrog. Energy 35 (2010) 11622-11633.

[11] H.M. Swaan, V.C.H. Kroll, G.A. Martin, C. Mirodatos, Catal. Today 21 (1994) 571-578.

[12] G. Sadanandam, N. Sreelatha, M.V.P. Sharma, S.K. Reddy, B. Srinivas, K. Venkateswarlu, T. Krishnudu, M. Subrahmanyam, V. D. Kumari, ISRN Chem. Eng. 2012 (2012) 1-10.

[13] J.A. Lercher, J.H. Bitter, W. Hally, W. Niessen, K. Seshan, Stud. Surf. Sci. Catal. 101 (1996) 463-472.

[14] K. Tomishige, Y.-G. Chen, K. Fujimoto, J. Catal. 181 (1999) 91-103.

[15] V.A. Tsipouriari, X.E. Verykios, J. Catal. 187 (1999) 85-94.

[16] Q. Zhuang, Y. Qin, L. Chang, Appl. Catal. 70 (1991) 1–8.

[17] A. Iulianelli, T. Longo, S. Liguori, A. Basile, Asia-Pac. J. Chem. Eng. 5 (2010) 138-145.

[18] A.C.-C. Chang, W.-H. Lin, K.-H. Lin, C.-H. Hsiao, H.-H. Chen, H.-F. Chang, Int. J. Hydrog. Energy 37 (2012) 13110-13117.

[19] F.D. Alvarado, F. Gracia, Int. J. Hydrog. Energy 37 (2012) 14820-14830.

[20] L.He, J.M.S. Parra, E.A. Blekkan, D. Chen, Energy & Environ. Sci. 3 (2010) 1046-1056.

[21] K. Hou, M. Fowles, R. Hughes, Chem. Eng. Sci. **54** (1999) 3783–3791.

[22] M.N. Pedernera, J. Piña, D.O. Borio, Chem. Eng. J. **134** (2007) 138–144.

[23] R. Schafer, M. Noack, P. Kolsch, M. Stohr, J. Caro, Catalysis Today **82** (2003) 15-23.

[24] B. Park, Ph.D. Thesis, University of Southern California, Los Angeles, CA, 2001

[25] S.Y. Lim, B. Park, F. Hung, M. Sahimi, T.T. Tsotsis, Chem. Eng. Sci. 57 (2002) 4933-4946.

[26] B. Park, T.T. Tsotsis, Chem. Eng. Proc. 43 (2004) 1171–1180.

[27] F.R. García-García, M.A. Rahman, B.F.K. Kingsbury, K. Li, Catal. Commun, 12 (2010) 161-164.

[28] F. R. García-García, M. A. Rahman, B. F. K. Kingsbury, K. Li. Appl. Catal. A: Gen. 393 (2011) 71-77.

[29] F.R. García-García, S.C. Tsang, K. Li. J. Membr. Sc.: In press.

[30] M.A. Rahman, F.R. García-García, K. Li, J. Membr. Sci. 390-391 (2012) 68-75.

[31] F.R. García-García, K. Li, Appl. Catal. A: Gen. 456 (2013) 1-10.

[32] F.R. García-García, B.F.K. Kingsbury, M.A. Rahman, K. Li, Catal. Today 193 (2012) 20-30.

[33] B.F.K. Kingsbury, K. Li, A morphological study of ceramic hollow fibre membranes. Journal of Membrane Science 328 (2009) 134-140.

[34] Q. Shi, C. Liu, W. Chen, J. Rare Earths, 27 (2009) 948-954.

[35] J.A. Montoya, E. Romero-Pascual, C. Gimon, P. Del Angel, A. Monzón, Catal. Today 63 (2000) 71-85.

[36] W. Gaowei, Z. Chengxi, L. Shuirong, H. Zhiping, W. Tuo, M. Xinbin, G. Jinlong, *ACS Sustainable Chem. Eng. In press*

[37] R. de Souza Monteiro, F.B. Noronha, L.C. Dieguez, M. Schmal, Appl. Catal. 131 (1995) 89-106.

[38] C.K. Loong, M. Ozawa, J. Alloys Comp. 303-304 (2000) 60-65.

[39] F. Arena, A. Licciardello, A. Parmaliana, Catal. Lett. 6 (1990) 139-149.

[40] A.M. Diskin, R.H. Cunningham, R.M. Ormerod, Catal. Today 46 (1998) 147-154.

[41] S. Tang, J. Lin, K.L. Tan, Catal. Lett., 51 (1998) 169-175.

[42] W.-S. Dong, H.-S. Roh, K.-W. Jun, S.-E. Park, Y.-S. Oh, Appl. Catal. A: Gen. 226 (2002) 63-72.

[43] S. Xu, X. Wang, Fuel 84 (2005) 563-567.

[44] R. Moliner, Y. Echegoyen, I. Suelves, M.J. Lázaro, J.M. Palacios, Int. J. Hydrog. Energy 33 (2008) 1719-1728.

[45] R. Molina, G. Poncelet, J. Catal., 173 (1998) 257-267.

[46] W. Yang, W. Chu, C. Jiang, J. Wen, W. Sun, Chin. J. Catal. 32 (2011) 1323-1328.

[47] Y.X. Li, Y.H. Guo, B. Xue, Fuel Process Technol. 90 (2009) 652-656.

[48] V.R. Choudhary, S. Banerjee, S.G. Pataskar, Appl. Catal. A: Gen. 253 (2003) 65-74.

[49] A. Trovarelli, Catal. Rev.-Sci. Eng. 38 (1996) 439-520.

[50] P. Fornasiero, R. Di Monte, G. Ranga Rao, J. Kaspar, S. Meriani, A. Trovarelli, M. Graziani, J. Catal. 151 (1995) 168-177.

[51] D. Chen, K.O. Christensen, E. Ochoa-Fernandez, Z. Yu, B. Totdal, N. Latorre, A. Monzon, A. Holmen, J. Catal. 229 (2005) 82-96.

[52] J.H. Kim, D.J. Suh, T.J. Park, K.L. Kim. Appl. Catal. A: Gen. 197 (2000) 191-200.

[53] H.S. Bengaard, J.K. Norskov, J. Sehested, B.S. Clausen, L.P. Nielsen, A.M. Molenbroek, J.R. Rostrup-Nielsen, J. Catal. 209 (2002) 365-384.

[54] M.L. Dieuzeide, M. Jobbagy, N. Amadeo, Catal. Today 213 (2013) 50-57.

[55] S. Li, C. Zhang, Z. Huang, G. Wu, J. Gong, Chem. Commun. 49(2013) 4226-4228.

[56] M. Benito, R. Padilla, A. Serrano-Lotina, L. Rodríguez, J.J. Brey, L. Daza, J. Power Sources 192 (2009) 158-164.

[57] F. Wang, Y. Li, W. Cai, E. Zhan, X. Mu, W. Shen, Catal. Today 146 (2009) 31-36.

[58] L. F. Bobadilla, A. Álvarez, M. I. Domínguez, F. Romero-Sarria, M.A. Centeno, M. Montes, J.A. Odriozola, Appl. Catal. B: Environ., 123 (2012) 379-390.

[59] M. Kakihana, J. Sol-Gel Sci. Technol. 6 (1996) 7-55.

[60] S. Koonaphaptleelert, K. Li, J. Membr. Sci. 291 (2007) 70-76.

[61] Y. Y. Yung-Fang, *Ind. Eng. Chem. Prod. Res. Dev.* 19 (**1980)** 293-298.

[62] R.A. Van Santen, M. Neurock, S.G. Shetty, Chem Rev. 110 (2010) 2005-2048.

[63] M.A. Rahman, F.R. García-García, K. Li, Catal. Commun. 16 (2011) 128-132.

[64] F.R. García-García, M.A. Rahman, I. D. González-Jiménez, K. Li, Catal. Today 171 (2011) 281-289.

5.3 Efficient and Stable Ni-Ce Glycerol Reforming Catalysts: Chemical Imaging using X-ray Electron and Scanning Transmission Microscopy

E. Gallegos-Suárez,[1,2] A. Guerrero-Ruiz,[2] M. Fernández-García,[1] I. Rodríguez-Ramos,[1] A. Kubacka[1]

Applied Catalysis B: Environmental 165 (2015) 139-148

[1] Instituto de Catálisis y Petroleoquímica, CSIC, C/Marie Curie 2, 28049-Madrid, Spain
[2] Dpto Química Inorgánica, UNED, Paseo Senda del Rey 9, 28040-Madrid, Spain

5.3.0 ABSTRACT

Nickel-Ceria composite catalysts prepared by a microemulsion method showed outstanding catalytic behavior in hydrogen production by glycerol steam reforming. Contrarily to usual Ni-based catalysts, the system allows long-term stability and nearly absence of by-products, particularly methane and carbon monoxide. With the help of scanning transmission electron microscopy and energy dispersive X-ray spectroscopy we confirmed the key role played by an intimate intermixing of Ni and Ceria components at reaction conditions. In addition, chemical imaging maps as well as more conventional techniques, such as Temperature Programmed Oxidation (TPO) and X-ray Photoelectron Spectroscopy (XPS) were used to identify the carbon containing (including coke) species nature and to establishing their chemical relevance. Combination of these techniques points out that the optimum interphase contact, reached for a specific 20:80 molar Ni:Ce formulation, allows; i) to keep the Ni particle size controlled with absence of significant formation of coke and thus without deleterious effects on the long-term stability of the catalysts; and ii) to eliminate undesirable side reactions such as methanation.

5.3.1 INTRODUCTION

The settlement of a hydrogen economy derived from renewable energy sources may provide significant benefits by solving problems related to the energy crisis and environmental pollution [1, 2] Among numerous renewable candidates, glycerol seems to provide significant advantages. Being a biomass derivative, glycerol is currently produced in large quantities in the process of transesterification of fatty acids into biodiesel [3]. During this process glycerol is normally generated at a rate of 1 mol of glycerol for every 3 mol of methyl ester synthesized, which accounts for approximately 10 wt% of the total product [2, 3]. Other bio-based processes also produce glycerol; for example, up to 4 wt. % of this molecule (with respect to the initial sugar weight) is obtained in fermentation of sugars oriented to ethanol formation [2]. Due to constant increment of biodiesel production it is estimated that by 2015, 1.54 million tons of glycerol will be generated worldwide [3] Thus, in order to make the chemicals obtained from the biomass sector competitive with chemicals from fossil fuels, all of this glycerol should be efficiently processed.

Bio-oils including glycerol have numerous potential applications which includes its usage in boilers for heat and electricity, in engines and turbines for electricity, in chemicals production such as phenols, organic acids, and oxygenates or in transportation fuel production [1-3]. The latter would be the more important from a economic point of view, however bio-oil derived transportation fuels require expensive upgrading techniques, and this route is currently less attractive for motor fuels production. To alleviate this disadvantage, reforming of bio-oil has been proposed and employed to produce hydrogen, a key fuel for the future.

The steam reforming of glycerol appears thus as a potential alternative for producing hydrogen in the near future with significant impact in the viability of numerous bio-refining processes [1-4]. Steam reforming of glycerol is an endothermic process and the offgas composition is governed by the (formal) equilibrium between the decomposition, reaction (1), water gas shift (WGS), reaction (2), and methanation, reaction (3) [5]:

$$C_3H_8O_3 \rightarrow 3\,CO + 4\,H_2 \qquad (1)$$

$$CO + H_2O \leftrightarrow CO_2 + H_2 \qquad (2)$$

$$CO + 3\,H_2 \rightarrow CH_4 + H_2O \qquad (3)$$

The first two provide a H_2/CO_2 ratio of 7/3 which will render the maximum attainable hydrogen yield. The third, methanation, is an almost unavoidable reaction in Ni-based catalysts which can limit such hydrogen yield. High temperatures will shift the decomposition (reaction 1) and methanation (reaction 3) steps to enhance production of H_2. This however has concomitant detrimental effects in catalyst lifetime due to the aggregation of the active metals and carbon deposition [2].

In this context the search of active and stable, low-temperature glycerol reforming catalysts is a field of intense research [2]. Ni-based catalysts are among the best choices for the reaction not only from a catalytic but also from an economic point of view, due to its significantly lower price than other, alternative active metal typically used in this reaction, i.e. Pt [1, 2]. Both metals, Ni and Pt, are active in dehydrogenation and decarbonylation reactions to produce hydrogen although Ni shows enhanced activity toward methanation. Enormous efforts have been made in Ni-based systems to control activity/selectivity in reforming reactions to

favor hydrogen production, and to increase the resistance to carbon formation and sintering of the metal phase. Strategies related to regulating surface composition, tuning particle sizes and shapes, metal "encapsulation" by rigid supports, enhancing metal-support interaction, and fabricating hierarchical structures within the catalysts has been essayed with partial success [6, 7, 8, 9, 10, 11, 12, 13, 14, 15, 16, 17, 18, 19, 20, 21, 22, 23, 24].

In this contribution we exploit the development of a Ni-CeO_2 catalyst system based in a single pot preparation method yielding a fluorite-based mixed oxide. This system has been shown high activity in the WGS and ethanol reforming reactions as it evolves in a "composite" metal-oxide (nickel-ceria) solid with high interaction area among components [8, 25]. In this work, we subjected such system to the more thought glycerol reforming test and founded superior performance in terms of activity/selectivity and stability. Specific nickel-ceria formulations having certain Ni/Ce atomic ratios show activity at relatively low temperatures, e.g. well below 873 K, and presents significant stability under reaction conditions due to the control of the structure/morphology of the solid-state components of the system as well as of the carbon formation process. To interpret the scientific bases of these features at atomic scale we present a scanning transmission electron imaging study with the aim of "chemically" discriminating between elements of the samples [26]. To this end, energy dispersive X-ray maps were obtained for a series of catalysts to track the evolution of metal, oxide and carbon phases present in spent catalysts. Combined with more conventional techniques such as X-ray diffraction, X-ray photoelectron spectroscopy and temperature programmed oxidation reaction, we would provide evidence of the key issues leading to highly active and stable Ni-based glycerol reforming catalysts.

5.3.2 EXPERIMENTAL

The Ce-Ni composite catalysts were prepared by employing reverse microemulsions following using *n*-heptane (Scharlau) as organic media, Triton X-100 (Aldrich) as surfactant and hexanol (Aldrich) as cosurfactant. Ce and Ni nitrates (Aldrich) were used as metal precursors [25]. Water/M (M=Ce+Ni) and water/surfactant molar ratios were, respectively, 110 and 18 for all Ce-Ni samples as well as a CeO_2 support reference. Systems are called Ni20 and Ni30 in correspondence of the molar percentage of Ni on cationic basis (equivalent to a 7.7 and 12.3 wt.% of metallic Ni, respectively) as measured by X-ray Total Reflection Fluorescence (error below 3 %). For the Ni20/CeO_2, the nickel nitrate has been used to impregnated the ceria support with the same loading as the Ni20 sample. Samples were dried overnight as subsequently calcined at 773 K -during 2 h. Prior to reaction, samples were pre-reduced in 10%H_2/He at 773 K during 2 h. For analysis (see below) of samples after reduction, they were transferred to the characterization technique cells in contact with air.

The BET surface area and average pore volume values were measured by nitrogen physisorption (Micromeritics ASAP 2010). XRD profiles were obtained with a Seifert D-500 diffractometer using Ni-filtered Cu Kα radiation with a 0.02^o step and fitted using the Von Dreele approach to the Le Bail method [27]; particle sizes and microstrain were measured with XRD using the Willianson-Hall formalism [28].

TEM analyses were done using a JEOL 2100F field emission electron gun microscope operated at 200 kV and equipped with an Energy-Dispersive X-Ray detector. The sample was ground until powder and a small amount was suspended in ethanol solution using an ultrasonic bath. Some drops were added to the copper

grid (Aname, Lacey carbon 200 mesh) and the ethanol was evaporated at room temperature before introduce in the microscope. The Scanning Transmission Electron Microscopy (STEM) was done using a spot size of 1 nm.

The Temperature Programme Oxidation (TPO) analyses were done in a SDTQ600 5200 Thermogravimetric Analysis system. In this latter, the samples were heated from room temperature to 1173 K, with a heating rate of 8 K/min under pure air.

X-ray photoelectron spectra of the used samples were recorded with an Omicron spectrometer equipped with an EA-125 hemispherical electron multichannel analyser and X-ray source (Mg Kα) operated at 150 W, with a pass energy of 50 eV. Each sample was pressed into a small pellet of 15 mm diameter and placed in the sample holder and fixed with a gold grid. The sample was degassed in the chamber for 6-8 h to achieve a dynamic vacuum below 10-8 Pa before analysis. The spectral data for each sample was analysed using CASA XPS software. The Au 4f7/2 peak at 83.4 eV was used as an internal standard.

The glycerol steam reforming was conducted in a stainless steel fix-bed reactor (Length: 47 cm; inner diameter: 0.95cm), operating at atmospheric pressure. The reactor was filled with 30 mg of catalyst and SiC was added to obtain 4 cm length. Prior to the catalytic test, the catalyst was reduced over 1 h with H_2 flow at 673 K increasing the temperature at 5 K/min. When the catalyst was reduced 50 mL/min of N_2 flow through the reactor and a mixture of 10 wt.% (2.1 mol.%) of glycerol in water (1 g/h) was added using a Controller Evaporator Mixture(CEM) (Bronkhorst) working at 473 K. After the CEM, all the system was heated to prevent condensation until the cooling system situated in the reactor exit. The outlet gas was analyses online with a GC equipped with two thermal conductivity

detectors and one flame ionization detector (Bruker GC-450). The reaction test with water was done using the same experimental conditions and after reaction, the feed was changed to introduce 1 g/h of pure water.

For thermodynamic equilibrium calculations we used the Aspen-Hysys software. The Gibbs reactor was used to calculate the product composition behavior vs. temperature and other experimental variables using the condition of minimization of Gibbs free energy and the Peng-Robinson state equation due to its largest applicability range in terms of temperature, pressure and also because its suitability for systems containing hydrocarbons, water, air and combustion gases [29].

5.3.3 RESULTS AND DISCUSSION

The glycerol steam reforming activity of the Ni-Ce composite catalysts having 20 and 30 mol. Ni % on cation basis (called Ni20 and Ni30) and a reference Ni supported on CeO_2 (called Ni20/CeO_2) having the exact molar composition of the Ni20 catalyst were tested at 773 K. After stabilization on stream, the H_2/CO_2 ratio is 7/3 (within ± 8 %) for the two composite materials indicating that both composite catalysts convert glycerol using an overall reaction close to:

$$C_3H_8O_3 + 3\ H_2O \rightarrow 3\ CO_2 + 7\ H_2 \qquad (4)$$

Only trace amounts of additional products were observed (see below). Stable conditions over an extended period of time (ca. 48 h) were obtained at 773 K. We thus provide a first comparison of the samples at this temperature using two observables, the conversion of glycerol (panel A) and the hydrogen molar yield (panel B) in Figure 1 while a more detail analysis of carbon-containing gas-phase products is presented in Figure 2.

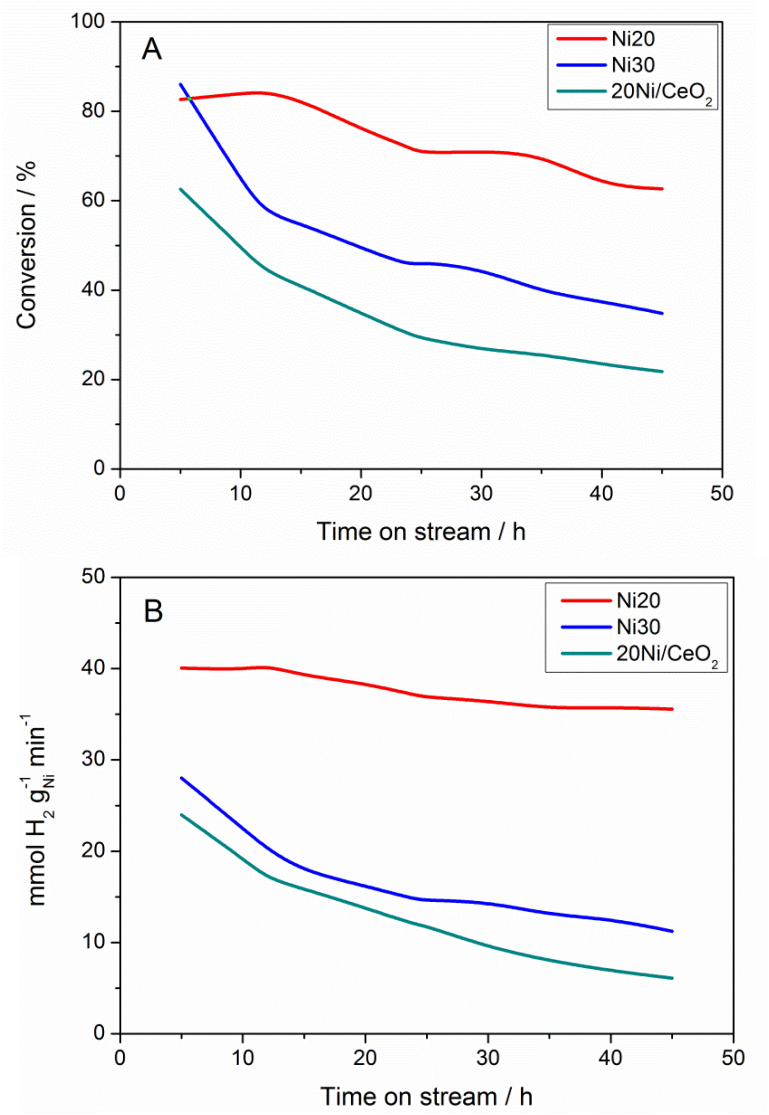

Figure 1. Glycerol reforming conversion (A) and hydrogen molar activity per gram of Ni (B) vs. time on stream for the Ni-Ce samples.

The time on stream performances of the Ni20 and Ni30 catalysts, as well as the sample Ni20/CeO_2, are displayed in Figure 1. In the catalytic runs presented in this figure, conversion was kept below 99 % (thermodynamic equilibrium) but sufficiently high to obtain information about deactivation. The performance of the composite catalysts is clearly better than the one displayed by the two phase, impregnated catalyst.

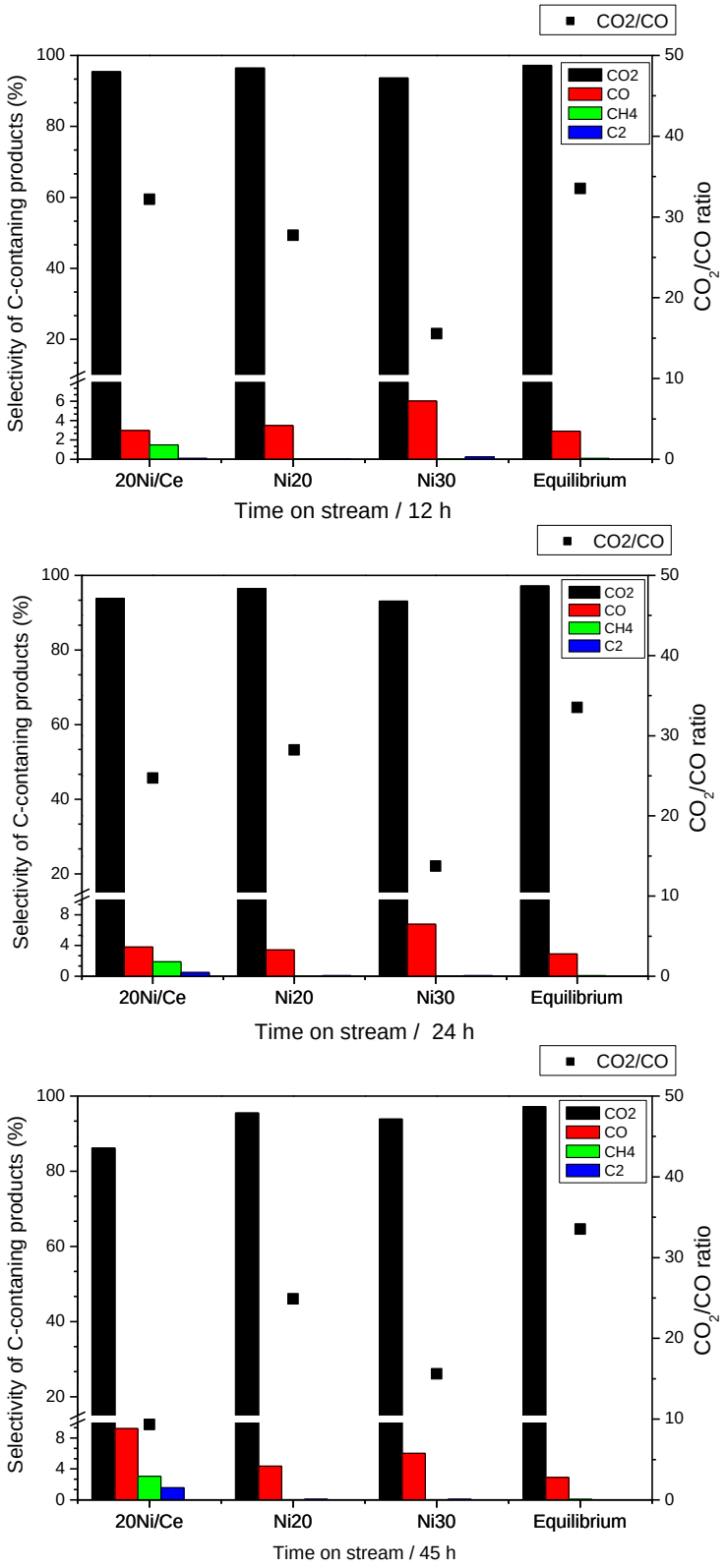

Figure 2. Selectivity of C-containing species gas-phase products for the samples and corresponding thermodynamic equilibrium values for the reaction mixture.

Both composite catalysts achieve hydrogen yields per mol of glycerol reasonably close to the maximum possible (i.e. 7 moles per mol of reactant) after a

few hours from the beginning of the reaction, maintaining such value (very slow decay as can be interpreted from Figure 2; see below) in certain cases throughout the whole experiment. Hydrogen production is, in the Ni20 case, close to the thermodynamic equilibrium of the reaction mixture as it would render an almost selective hydrogen production (98.8%) with rather minor presence of methane as hydrogen-containing product. The maximum or optimum yield of hydrogen per mol of glycerol is usually reached at higher temperatures, over 823 K, in Ni-based catalysts [17, 30, 31, 32, 33]. For the specific case of ceria-promoted catalysts and at the operation temperature of our experiment, hydrogen production presents important shortcomings in previously published works: optimum hydrogen yield is either obtained at 873 K [32, 33], or below that temperature the production of hydrogen is far from optimum as an effect of the poor selectivity control with significant formation of a number of hydrogen-containing products such as methane and C1-C2 oxygenates [32].

Focusing on comparing now our composite samples, the activity of the Ni30 sample is lower than the one of Ni20 and, moreover, shows a temporal behavior relatively similar to the Ni20/CeO_2 sample, indicating that the latter sample has certain similarities with a normal, impregnated ceria-based nickel sample. Still its activity is higher than the Ni20/CeO_2 for all times essayed. In any case, the optimum activity and selectivity is achieved with the Ni20 sample. This sample presents a behavior significantly different from impregnated samples as the reference (Ni20/CeO_2) used here or those presented in the literature [17, 18, 30, 32, 34, 35].

To show this in more detail, the distribution of C-containing products is presented at specific reaction times in Figure 2. The results of the thermodynamic

calculation described in the experimental section are also included in this figure. CO_2/CO molar ratios above 25 are always observed for Ni20 while such ratio decreases up to ca. 15 for the Ni30 case. Both ratios are outstanding ones if compared with Ni-based systems reported in the literature [17, 32, 33]. The plot in Figure 2 also shows that this ratio is not stable for the Ni20/CeO_2 material. In fact, as occurring in many cases in the literature, this Ni20/CeO_2 catalyst does show selectivity evolution with additional production of C2 hydrocarbon chains at time-on-stream values above 24 h. As well known ethylene and other olefins polymerize at the catalyst surface and are initiators of highly detrimental coke [17, 32]. We can also note that a relatively low formation of CO is positive in terms of significant coke production as it is well known that a low temperature (below 873 K – 923 K) path for coke formation is the Boudouard reaction (34). The absence C_2-C_3 oligomers in addition to the relatively low CO production seem thus elements supporting the good selectivity and stability of the Ni20/Ni30 catalysts.

Summarizing, Figure 2 provides evidence of the control of CO, CH_4 and other side molecules production in the composite catalysts and particularly in Ni20. Although the mechanism of the glycerol reforming is not fully elucidated, there are indications that methane and small hydrocarbons are formed by hydrogenolysis (leading to simple alcohols such as methanol as key intermediates) or by dehydratation and further hydrogenation (from hydroxyacetone as key intermediate further evolving in acids such acetic, formic, etc.) [36, 37, 38]. The dehydration pathway is usually important in acid systems and may not be thus a prevalent route in the case of ceria-based materials. In Ni-based materials, the well-known strong activity in methanation also appears as a significant pathway for methane formation [2]. While the almost null activity in methanation of the composite materials was previously proved [8], the results in Figure 2 shown that

both methane formation paths above mentioned are efficiently controlled in Ni20. Similarly, CO production is rather low, in this case, likely as an effect of the rather important water gas shift activity owned by ceria-related catalysts. This has been previously demonstrated for the particular case of the Ni20 material [25]. In our composite catalysts, the overall catalytic performance is controlled by the chemical/oxidation state of the metal and the metal-support interaction. The latter controls the active state of the metal at the interphase between the two components as well as the oxide vacant role in the activation of oxygen-containing molecules [2, 8, 32, 33]. The adequate combination of catalytic properties and, as detailed below, the intimate contact between nickel and ceria would thus provide the basis for the good selectivity performance observed for Ni20, rendering a product distribution rather close to the thermodynamic equilibrium result (Figure 2).

Table S1. Main physicochemical characterization results of samples and support reference.

Sample	BET (m^2/g)	Ceria Particle size fresh sample (nm)	Ceria Particle size used sample (nm)
CeO_2	103.0	5.1	-
Ni20	121.7	4.8	7.4 8.3[a]
Ni30	97.3	4.8	7.6
Ni/CeO_2	85.8	5.1	8.1

a) after water treatment

To interpreting the outstanding catalytic properties of the Ni20 sample, we carried out a scanning transmission electron microscopy (STEM) study of the composite catalysts. As an illustrative example of the state of the materials after reduction pre-treatment Figure 3 displays the Ni20 case. The reduction of the composite catalysts has been examined previously using spectroscopic techniques,

proving key information about the presence of metallic nickel and oxidic ceria (fluorite-type) phases [25]. Here the STEM and chemical mapping images highlights the reasonable chemical homogeneity of the Ni dispersion on the fluorite-type ceria matrix. Ni is barely seem by XRD in the reduced catalysts (small peak near 50 degrees) while the fluorite-type ceria phase is clearly visible with a primary particle size of ca. 5 nm (see Figure S1 and Table S1). We employed microscopy to analyze the Ni-based catalysts after reduction. Due to the strong intermixing of the components, inherent to the preparation method (where Ni metal and ceria oxide evolve from a single phase), and the presence of Ni in all surface and bulk (and not only in the former) parts of the material, we focus on using chemical mapping tools as the optimal analytical choice. Thus the average nickel aggregate size was estimated from STEM chemical mapping, yielding an aggregate size of 3.4 and 4.3 nm for, respectively, Ni20 and Ni30 samples (see Table 1).

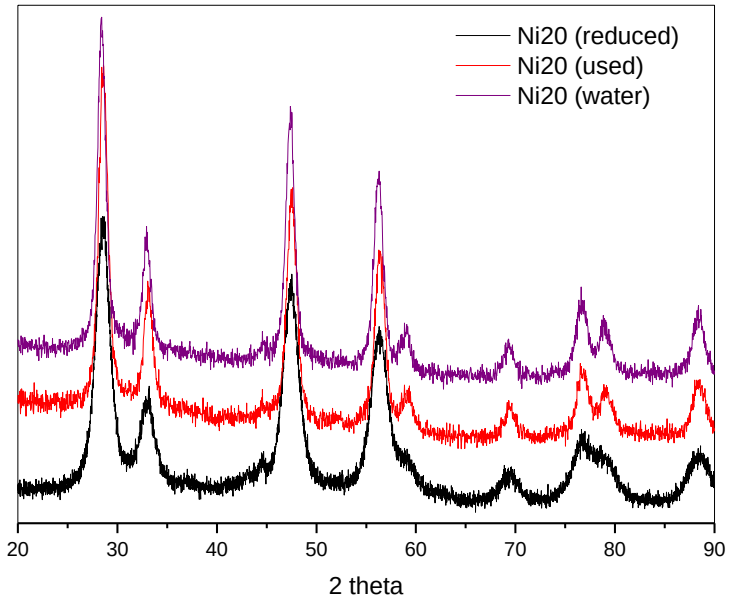

Figure S1. XRD Diffraction profiles of Ni20 fresh, used in reaction and subsequent water treated samples.

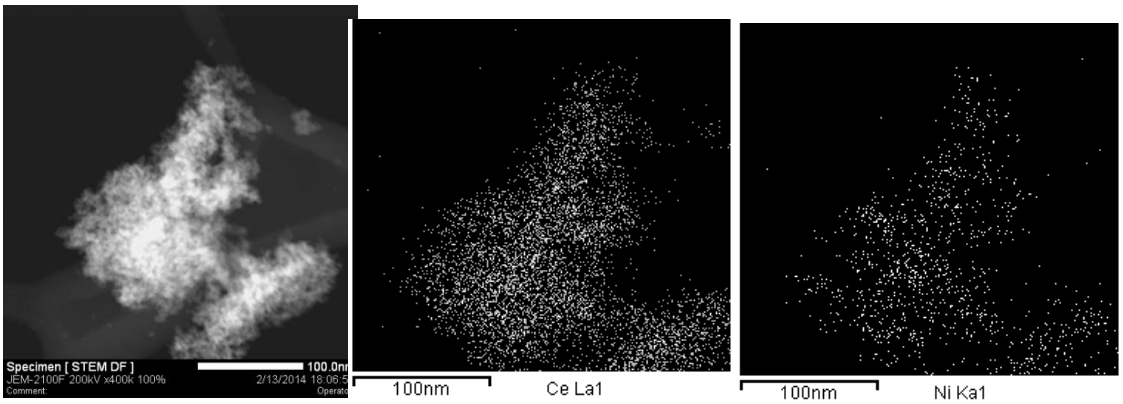

Figure 3. STEM micrographs and corresponding Ce and Ni chemical maps of the pretreated (reduced) Ni20 sample.

After ca. 48 h of reaction the chemical heterogeneity of the materials increases significantly. For the Ni20 sample this is illustrated in Figures 4 to 6. In Figure 4 we present chemical maps displaying the location of ceria and nickel after reaction, together with the micrograph image from which they were taken. The chemical map shows the presence of ceria and nickel rich zones, in contrast with the more homogeneous situation displayed in Figure 3. To make a more quantitative analysis, a line profile analysis is also included in Figure 4. Overall, the zone is nickel-enriched with respect to the chemical composition obtained by chemical analysis (Ni:Ce average atomic relation ca. 3:2 instead of the 1:4 of the material). The uphill line goes from zones with high Ni:Ce ratios near 2 to those near zero. This illustrated the rupture of the nickel-ceria contact expected during reaction in a zone were the intensity of such process appears maximum [8]. Still, the ceria-rich parts show presence of Ni in more than 95 % from individual energy dispersive X-ray spectra (EDXS). As these are taken with a 1 nm beam, it clearly shows that contact between the two components is still present at subnanometric level. Specifically, particle size estimation using chemical mapping STEM tools (using Figures 4 and 6 as well as Figure S2) indicates that Ni aggregates grow for

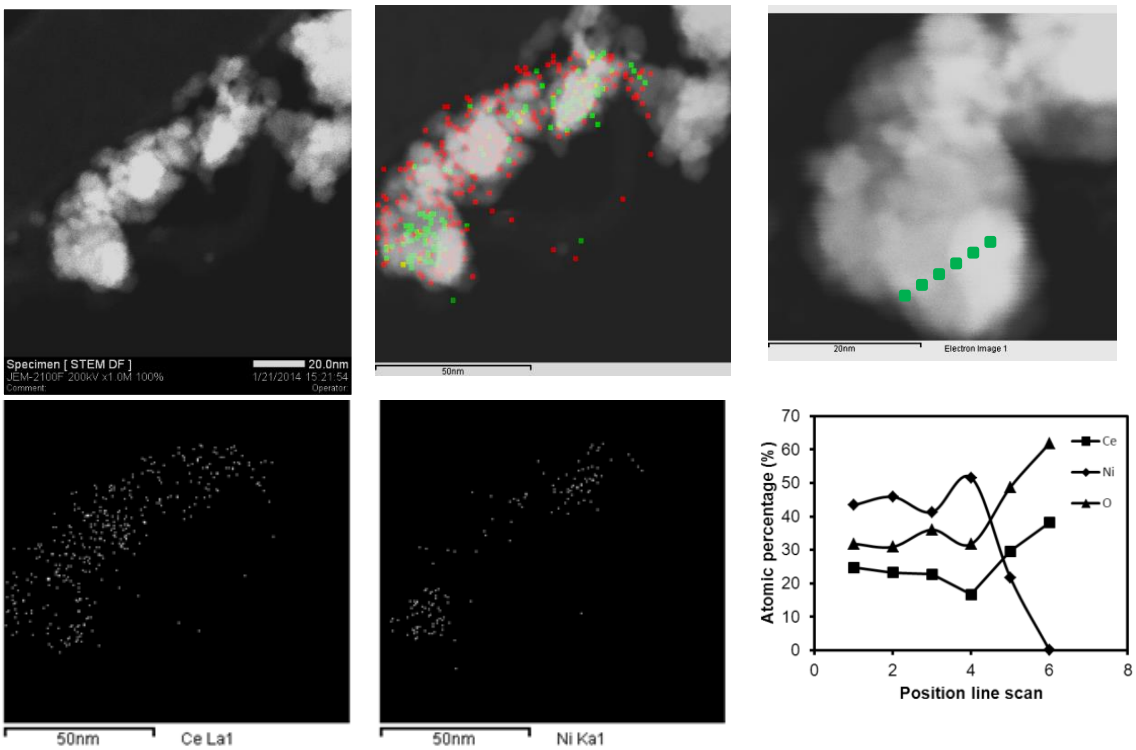

Figure 4. STEM micrograph and corresponding Ce (red), Ni (green) and overlaying (Ce-Ni) chemical maps of the Ni20 sample after reaction. The result of an EDXS line scan is also presented.

Ni20 and Ni30 cases under reaction but to a significantly lower extent in the former case (see Table 1). While the analysis presented in Table 1 is not considered fully quantitative as, among several factors, it is difficult to distinguish between Ni aggregates from Ni present at ceria lattice (we assigned arbitrarily signals below 1.5 nm to lattice entities), the distribution moment values displayed in Table 1 and more precisely, the differences between pre-treated (reduced) and used samples, provide a reasonable quantification of the "disproportion" evolution taking place between the two Ni and Ce components from the pre-reduced solid to the specimen after reaction conditions. For Ni20, Table 1 points out that the Ni aggregate distribution shows strong analogies in the fresh (after reduction) and used (after reaction) states. The control of Ni dispersion and particle size (more generally speaking, morphological properties) has been shown critical to obtain high hydrogen yields through the control of glycerol decomposition handling and

Table 1. Average particle size (first raw order moment), variance (second raw order moment) and higher normalized central moments of Ni aggregates in the Ni20 and Ni30 catalysts. See text for details.

Sample	Size (nm)	Variance (nm^2)	Skewness (a.u.)	Kutuosis (a.u.)
Ni20 red.	3.4	1.0	0.6	0.2
Ni20 used	3.8	1.3	0.4	0.6
Ni30 red.	4.3	3.1	0.8	0.6
Ni30 used	7.8	15.3	1.2	1.0_5

water gas shift activity enhancement [15, 17, 39]. Worth to mention is the fact that analysis of Ni by other bulk averaged techniques like XRD or EXAFS are relatively less informative in this situation where a complex distribution of the active metal takes place throughout the existent phases. This in addition to strong limitations in their in-situ capabilities; to our knowledge no single in operando experiment has been reported in gas phase glycerol reforming due to the high boiling point and viscosity of the reactive.

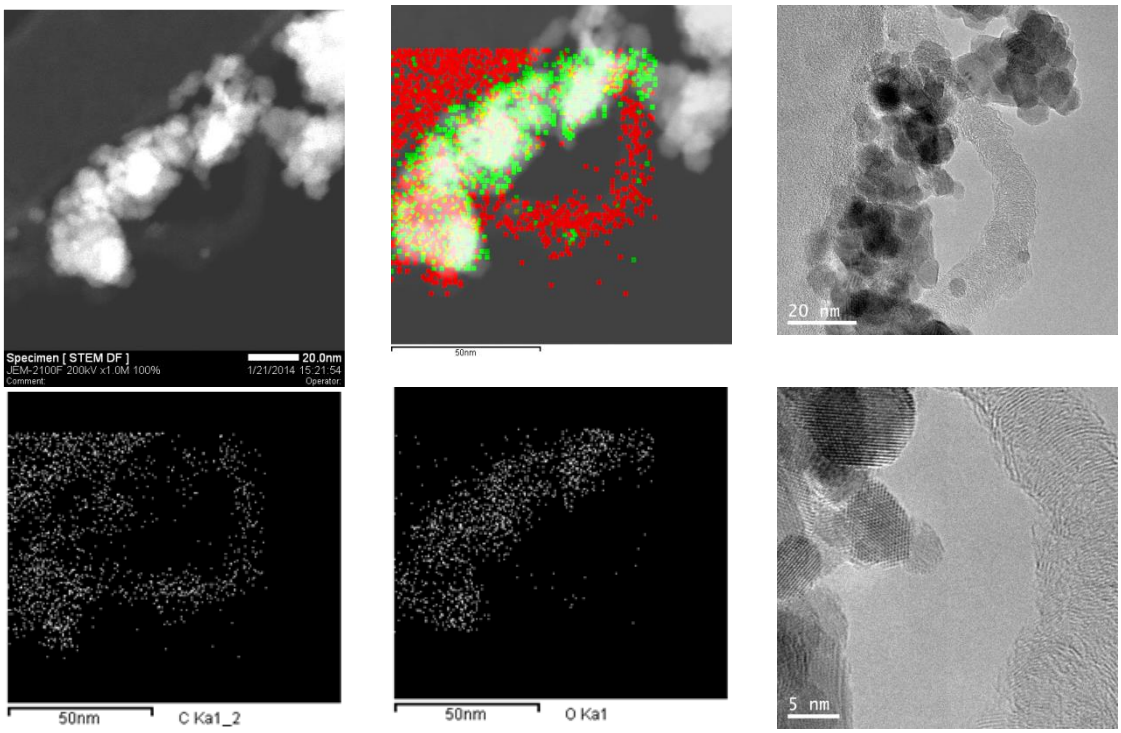

Figure 5. STEM micrograph and corresponding C (red), O (green), and overlaying C-O chemical maps of the Ni20 sample after reaction. Two TEM micrographs are also presented for the same zone at two magnifications.

Figure 5 shows analogous data (to Figure 4) for location of carbon-containing deposits. This figure also presents a normal TEM image at two magnifications. In the latter presence of filamentous carbon is observed [40, 41]. Such carbon structure presents some ill-organized growth with layered graphitic walls in perpendicular direction to that of the growth direction. The presence of such type of carbon structure is relatively low, on average less than 5 on ca. 10^4 nm^2. Moreover, the information enclosed in the mapping indicates that a significant part of carbon is still located near the catalysts, without forming nanofiber or any other typical nanoarchitecture of carbonaceous materials. Figure 6 better illustrates

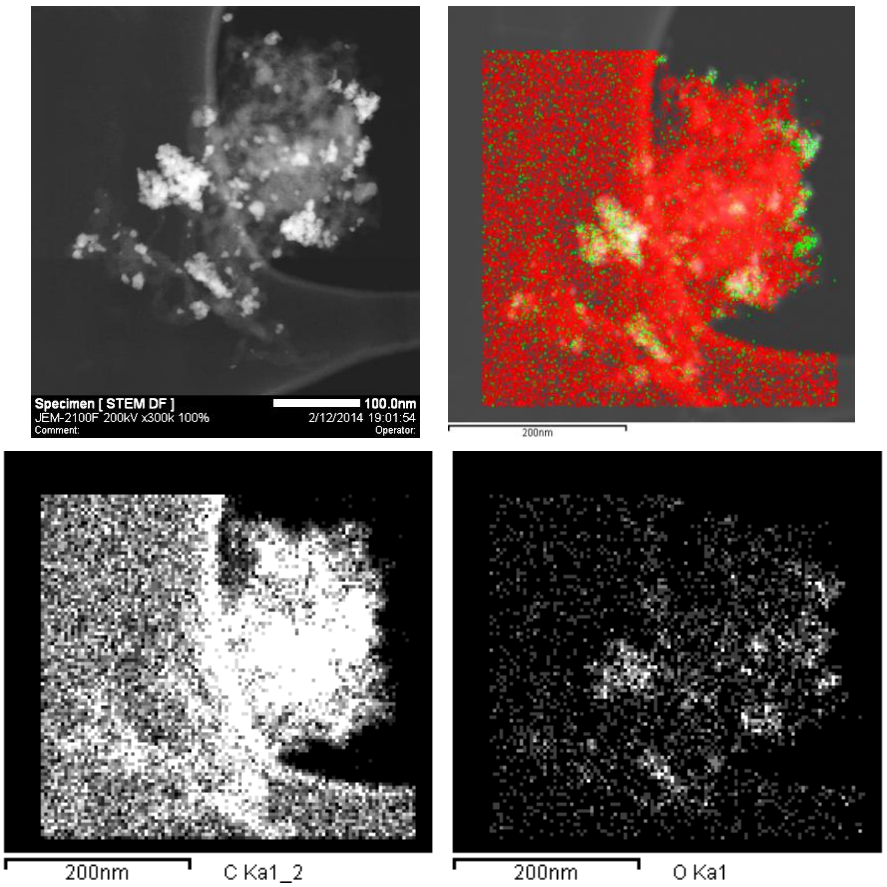

Figure 6. STEM micrograph and corresponding C (red), O (green), and overlaying C-O chemical maps of a second aggregate of the Ni20 sample after reaction.

the nature of such carbon in intimate contact with the catalyst. In this figure, a cloud of carbon-containing material is surrounding the mixed nickel-ceria entities.

Overlaying of the C and O EDXS chemical maps show that this type of carbon deposit contains oxygen to an important level. So, it is expected to be a highly hydrogenated, truly amorphous carbon-containing component with chemical composition far from coke and thus with absence of strong deactivation effects over the catalyst.

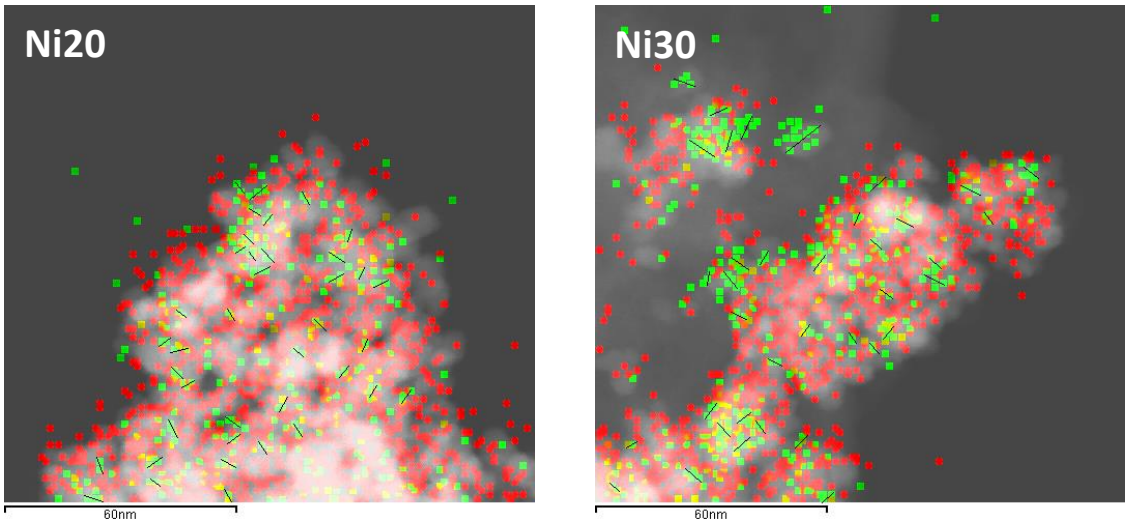

Figure S2. Micrographs of Ni20 and Ni30 catalysts after reaction illustrating the Ni particle size (black lines show the characteristic dimension presented in Table 1 of the main paper for Ni aggregates –in green).

Figures 7 and 8 attempt to illustrate the situation for the Ni30 sample. In Figure 7 (and Figure S2) the overlaying of the nickel and cerium EDX maps show a significantly larger clustering effect, providing a clear clue toward the lower contact between the two phases present in the catalyst under reaction. The important growth of the mean and variance of the Ni aggregate size distribution in going from the pre-treated (reduced) to the final (after reaction) samples supports quantitatively this conclusion (Table 1). The system however, presents evidence of carbon containing species with similar C and O overlaying effects (Figure 8; upper part) as observed for the Ni20 case. Nevertheless, Figure 9 shows the existence of a new Carbon-containing species; in this case we can see numerous filamentous (some of them hollow core) carbon with nickel particles (according to EDXS analysis) at the end. As it shows the last image of Figure 9 such fibers grow from

the solid but separate the metal definitively from ceria. As well known, this is a major concern with regard to the coverage of the active metal sites by carbon species that can lead to deactivation of catalysts in reforming reactions [40, 41, 42, 43, 44, 45]. The initial quantity or loading of nickel in the catalysts would thus control the average particle size of the metal during reaction. Those particles of larger particle size and, consequently, with limited interaction with the support, are finally producing C carbon fibers which encapsulates the metal. While nickel in Ni20 would have a minimum fraction of the metal in such condition, a noticeable fraction is observed at Ni30. Such issue is responsible of the deactivation decay observed in Figure 1 while the remaining nickel in contact with ceria is providing the stable activity observed at large reaction time on stream.

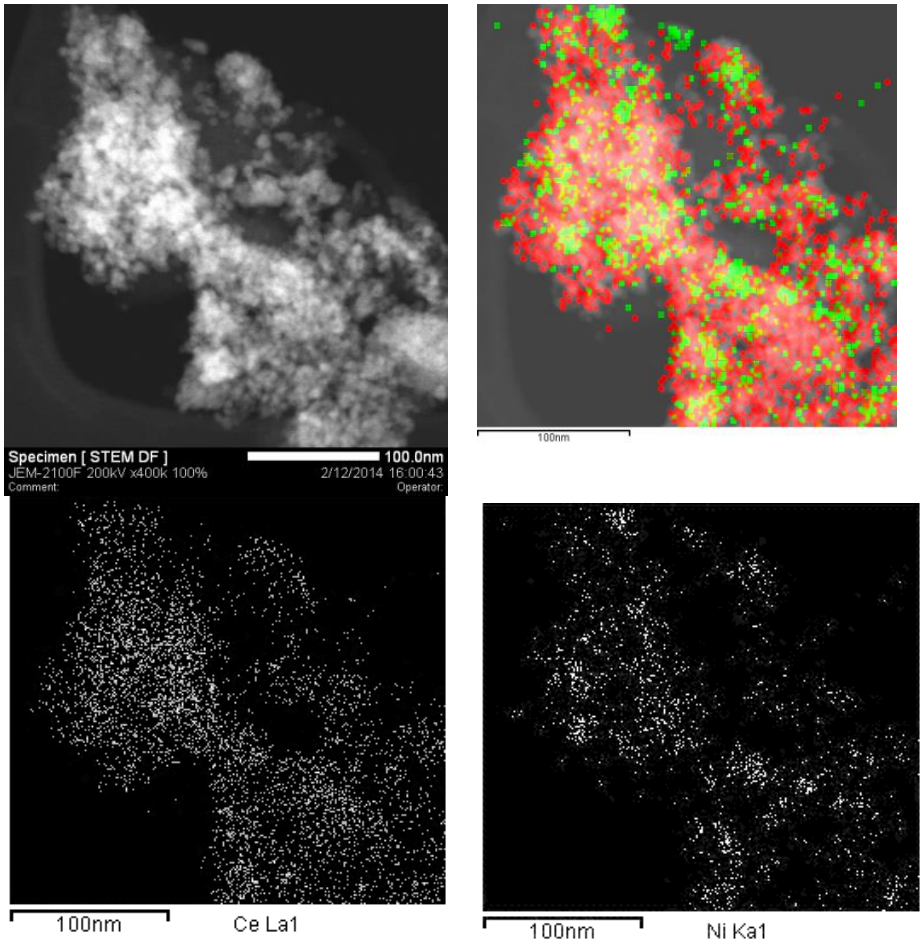

Figure 7. STEM micrograph and corresponding Ce (red), Ni (green), and overlaying Ce-Ni chemical maps of the Ni30 sample after reaction.

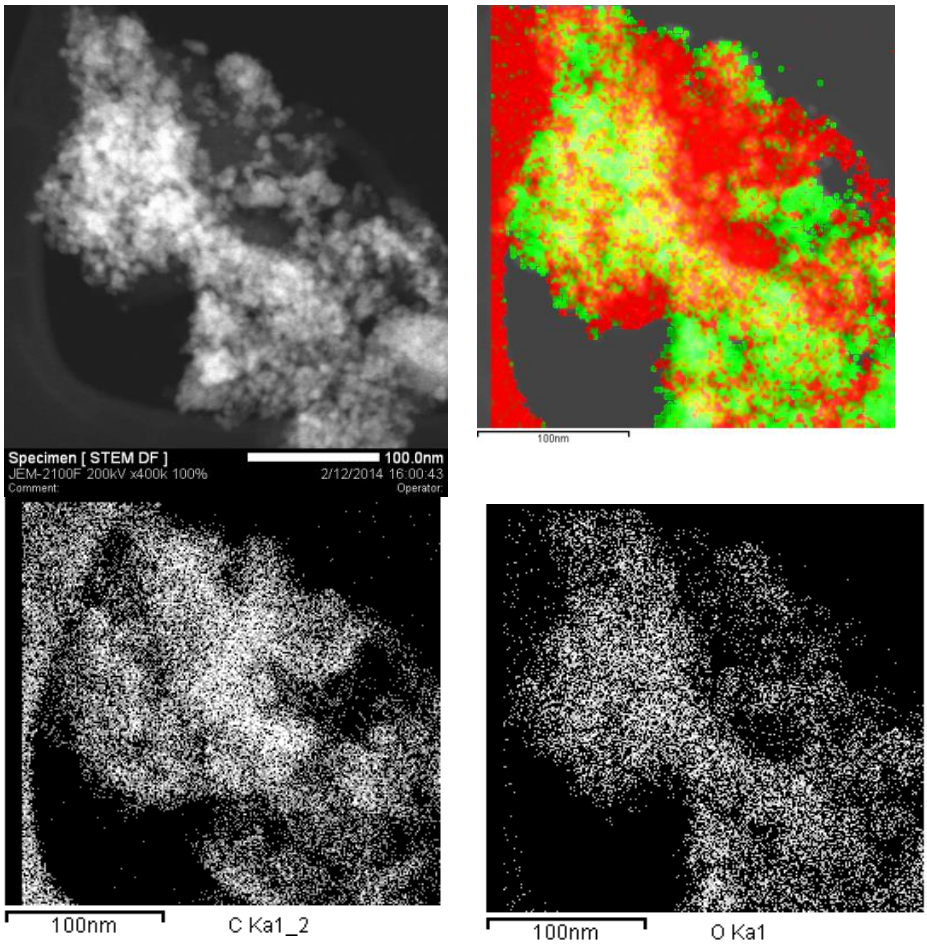

Figure 8. STEM micrograph and corresponding C (red), O (green), and overlaying C-O chemical maps of the Ni30 sample after reaction.

We can thus observe that Ni20 and Ni30 have nickel entities differing essentially in the parts where the contact between nickel and ceria components is lost. The preparation method of the samples thus provides a way to stabilizing the nickel-ceria interface which is fully operative in the Ni20 catalyst. Above that, the excess of nickel, allows a behavior typical of the supported catalysts with carbon structures occluding the active nickel phase at relatively long time on stream, resulting in the strong deactivation profile presented by Ni30 in Figure 1. Note that as summarized recently in the review of Tran et al. [2] the maintenance of the metal-oxide interface in ceria-based systems is critical to hold high activity, particularly in relation with the presence of oxygen vacancies at the interface and the promoting effect on water activation and water gas shift reaction and on the

suppression of the methanation process. As previously discussed, both facts are capital to end up in the control of gas phase products and to provide a "stable" behavior as shown in Figure 1/2. The microscopy study indicates that the significantly developed nickel-ceria interaction coming directly from the preparation method and its stability under reaction has a direct consequence in controlling the carbon-containing phases produced (Figures 5, 6, 8 and 9) as well as the control of growth processes in both nickel (see Table 1) and ceria (Figure S1 and Table S1) phases. The Ni20 sample study thus indicates that the progression of carbon phases is stooped with production of carbon-containing hydroxylated phases which can evolve in the reaction products (CO_2+H_2O) easily. In parallel, Ni aggregates suffer a rather mild growth process during 48 h of reaction (see distribution moment values at Table 1) as a consequence of the stabilizing effect of the ceria contact.

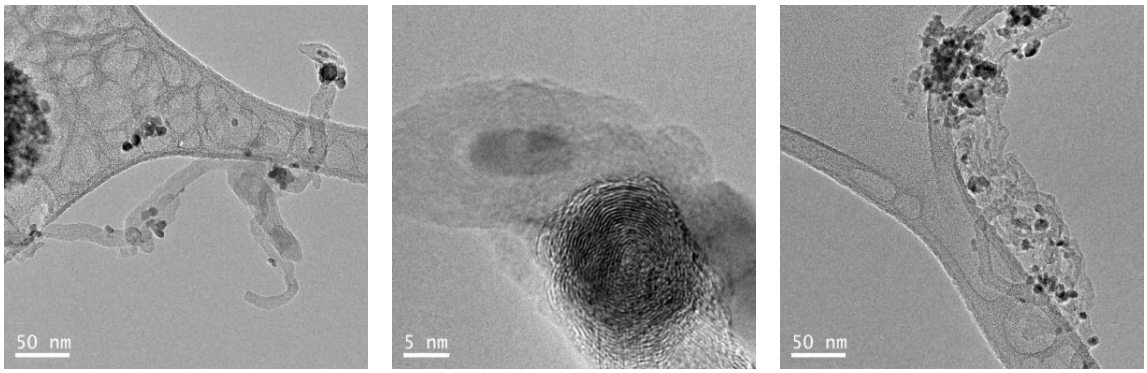

Figure 9. TEM micrographs of the Ni30 sample showing zones with presence of Ni and C structures.

We carried out a simple chemical test to proof the behavior of the highly hydroxylated carbon species by subjecting the spent Ni20 catalyst to water treatment at reaction conditions (e.g. in absence of glycerol, maintain all other experimental reaction variables). The sample after this test was called Ni20-w.

Using Ni20, Ni20-W, and Ni30 we use temperature programmed oxidation (TPO) and X-ray photoelectron spectroscopy (XPS) to further characterize the carbon containing species already analyzed by microscopy. A summary of the TPO results is presented in Table 1 while a representative example of the experimental results in shown in Figure. Table 1 summarizes the contribution of the two main peaks observed in the Derivative TPO profiles. A low temperature peak, which according to its maximum will content glycerol (boiling point at 543 K) and similar small molecules or oligomers, appears as the main component for Ni20 (Table 2). Contrarily, the carbon containing species oxidized at higher temperature dominates in the Ni20-w and Ni30 cases. Such species, evolving above 673 K are usually described as graphitic (see below). More importantly, the TPO experiment shows that the water treatment is able to convert highly hydroxylated carbon species in evolving gases and leaves the graphitic-type at the surface. The latter, graphitic-type species dominates the Ni30 case. The different nature of the post-reaction carbon species are thus in agreement with the microscopy analysis.

Table 2. Summary of carbon content and C species percentage over total carbon as determined by TPO experiments over used (after reaction) samples. See text for details.

Sample	Glycerol-type (423-673 K)	Graphitic (673-1173 K)	g_{carbon}/g_{cat}
Ni20	69	31	0.040
Ni20-w	13	87	0.018
Ni30	15	85	0.057

To further analyze this point, we also carried out a XPS study. Results for the C 1s XPS peak are depicted in Figure 10. A Summary of the C 1s contributions binding energy and relative abundance (%) is presented in Table 3. Three species are detected and correspond to carbon species with dominant sp2 (ca. 284.6 eV),

sp3 (ca. 285.3 eV) electronic character, as well as those with an environment described as C-O bonds (ca. 286.4 eV) [46, 47, 48]. The first contribution mentioned is customarily assigned to graphitic-type deposits. In the context of our work, the second one at 285.3 eV is assigned to hydrogen incorporated carbon species [46, 48].

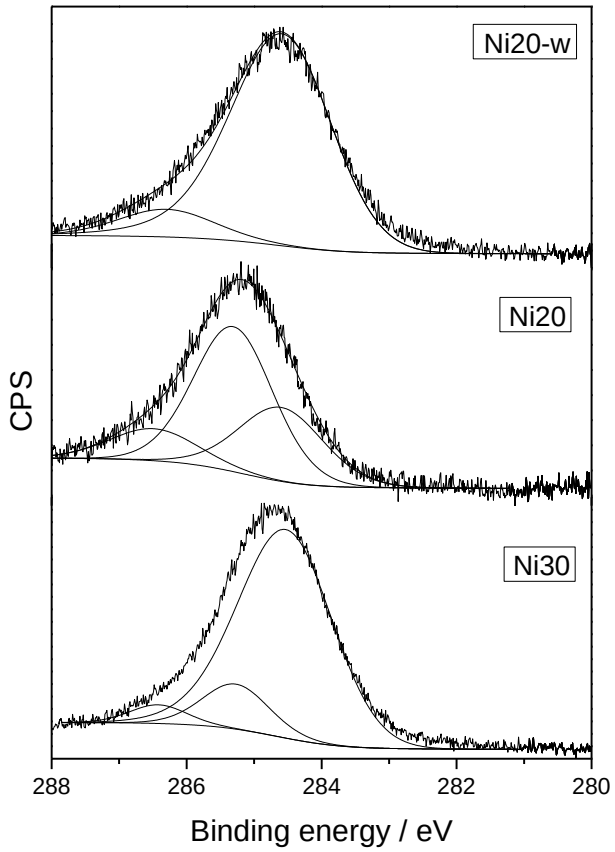

Figure 10. C 1s XPS peak of the Ni20, Ni20-W, and Ni30 samples after reaction.

The joint analysis of Tables 2 and 3 would thus support the conclusions extracted from the microscopy study. An increase of Ni content in the composite catalysts increases the contribution of the carbon species more resistant to chemical oxidation and displaying a graphitic-type chemical identity. This is a direct consequence of the decreasing Ni-Ce interaction uncovered by the STEM-EDXS chemical imaging analysis. In the Ni20 case, oligomeric, hydroxylated carbon species dominates according to these two techniques. A similar conclusion can be

Table 3. C 1s XPS peak analysis of the used (after reaction) samples. See text for details.

Sample	Binding Energy (eV)			Relative C1s peak area (%)		
	Csp^2	Csp^3	C-O	Csp^2	Csp^3	C-O
Ni20	284.6	285.3	286.5	30	56	14
Ni20-w	284.6	-	286.3	88	-	12
Ni30	284.5	285.3	286.4	82	13	5

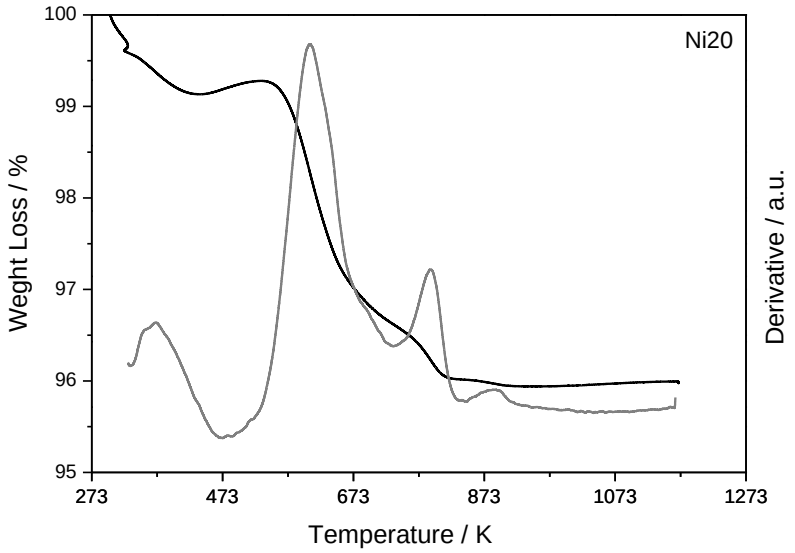

Figure S3. Weight loss (black color) and Derivative (gray color) of the spent Ni20 sample during a TPO experiment.

extracted from the Ni20-w test carried out. In an optimum catalyst, this Ni-Ce interaction prevents the Ni growth and encapsulation by carbon species (effects occurring in Ni30; Figure 9) and the concomitant irreversible deactivation. The Ni20 sample does not suffer these effects by maintaining the interaction between the two main phases of the system, metallic Ni and oxidic ceria, with an efficient supply of oxygen-hydrogen species to the initially formed carbon residues. The outstanding properties of the system derived from the strong interaction between the two main components and affecting the glycerol decomposition are completed with both high water gas shift and low methanation activities [8, 25], providing a

rather good system with limited production of CO and CH_4 by-products (Figure 2). These outstanding catalytic characteristics of the Ni20 material, mainly high activity and stability as well as significant absence of by-products, have not been presented to our knowledge in the literature [5, 9, 17, 18, 30, 32], giving clear indications of the exceptional behavior of this catalyst in the reforming of glycerol, a challenging reaction.

5.3.4 CONCLUSIONS

Using a microemulsion procedure we synthesized Ce-Ni mixed oxides having fluorite-type structure. Following reduction and under reaction conditions, evolve forming separate Ni-metal and Ce-oxide phases. The microscopy study was able to shown the intimacy of the interaction between these two phases and provides significant information to establishing its relationship with the activity, selectivity for hydrogen production and stability of the catalysts under reaction conditions. This was further corroborated with additional, conventional TPO and XPS techniques.

The optimum, stable catalytic performance in the glycerol reforming reaction was achieved with a composite system having a 20 mol. % of Ni in cation basis. Excess Ni over the 20 mol. % is not stabilized by contact with ceria and has thus detrimental effects on catalytic properties. The Ni20 system outperforms the corresponding Ni20/CeO_2 reference system prepared by a conventional impregnation method in terms of activity, selectivity as well as stability. Comparison of the literature shows the reaching of an optimum H_2/CO_2 (7/3) ratio at significantly lower temperatures, being this ratio constant in a long catalytic run (48 h). Consequently, production of by-products like CO and CH_4 was kept to a minimum, contrarily to the usual Ni-based reforming catalysts. The outstanding

properties of Ni20 would represent a proof of concept for the glycerol reforming reaction.

5.3.5 REFERENCES

[1] S. A. Chattanathan, S. Adhikari, N. Abdoulmoumine, Renewable Sustainable Energy Reviews 16 (2012) 2366-2372.

[2] N.H. Tran, G.S.K. Kannangara, Chem. Soc. Rev. 42 (2013) 9454-9479.

[3] W. Huber, S. Iborra, A. Corma, Chem. Rev. 106 (2006) 4044–4098.

[4] Global Industry Analyst, http://www.strategyr.com/Glycerin Market Report.asp; http://www.strategyr.com/Emulsifiers_Market_Report.asp

[5] A. Basagiannis, X. Verykios Catal Today 127 (2007) 256–64.

[6] E. Nikolla, A. Holewinski, J. Schwank, S. Linic, J. Am. Chem. Soc. 128 (2006) 11354-11361.

[7] J.C. Park, J.U. Bang, J. Lee, C.H. Ko, H. Song, J. Mater. Chem. 20 (2010) 1239-1245.

[8] Z. Gong, L. Barrio, S. Agnoli, S.D. Senanayake, J.; Evans, A. Kubacka, M. Estrella, J.C. Hanson, A. Martínez-Arias, M. Fernández-García, J.A. Rodriguez, Angew. Chem., Int. Ed. 49 (2010) 9680-9684.

[9] F. Pompeo, G. Sanhori, N.N. Nichio, Int. J. Hydrogen Energ. 35 (2010) 8912-8920.

[10] N. Luo, K. Ouyang, F. Cao, T. Xiao, Biomass Bioenerg. 34 (2010) 489-495.

[11] C. Pirez, M. Capron, H. Jobic, F. Dumeignil, L. Jalowiecki-Duhamel, Angew. Chem., Int. Ed. 2011, 50, 10193-10197.

[12] J. Guo, C. Xie, K. Lee, N. Guo, J.T. Miller, M. Janik, C. Song, ACS Catal. 1 (2011) 574.

[13] S.M. Kim, S.I. Wo, ChemSusChem 5 (2012) 1513-1522.

[14] L. Li, S. He, Y. Song, J. Zhao, W. Ji, C.-T. Au, J. Catal. 288 (2012) 54.

[15] S, Li, C Zhang, G. Wu, J. Gong, Chem. Comm. 49 (2013) 4226-4228.

[16] C. Zhang, H. Yue, Z. Huang, G. Wu, S. Li, X. Ma, J. Gong, ACS Sustainable Chem. Eng., 2013, 1, 161-168.

[17] G. Wu, C. Zhang, S. Li, Z. Han, T. Wang, X. Ma, J. Gong, ACS Sustainable Chem. Eng., 2013, 1, 1052–1062.

[18] R. Trane-Restrup, S. Dahl, A.D. Jensen, Int. J. Hydrogen Energ. 2013, 38, 15105-15118.

[19] F. Fang, C. Pirez, S. Paul, M. Capron, H. Jobic, F. Dumeignil, L. Jalowiecki-Duhamel, ChemCatchem 2013, 5, 2207-2216.

[20] S. Li, C. Zhang, Z. Huang, G. Wu, J. Gong, Chem. Comm. 2013, 49, 4226-4228.

[21] C. Wang, N. Sun, N. Zhao, W. Wei, Y. Zhang, Y. Sun, C. Sun, H. Liu, C.E. Snape, ChemCatChem 6 (2014) 640-648.

[22] M. El Doukkaki, A. Iriondo, J.F. Cambra, I. Gandarias, L. Jalowiecki-Duhamel, F. Dumeignil, P.L. Arias, Appl. Catal. A 474 (2014) 80-91.

[23] J.Y. Liu, W.-N. Su, J. Rich, J.F. Lee, B.-J. Wang, ChemSusChem 7 (2014) 570-576.

[24] J.-F. Dacquin, D. Sellam, C. Batiot-Dupeyrat, A. Tougerti, D. Duprez, S. Royer, ChemSusChem. 7 (2014) 631-637.

[25] L. Barrio, A. Kubacka, G. Zhou, M. Estrella, A. Martínez-Arias. J.C. Hanson, M. Fernández-García, J.A. Rodríguez, J. Phys Chem C 114 (2010) 12689–12697.

[26] M. Varela, A.R. Lupini, K. Van Bentham, A.Y. Borisevich, M.F. Chrisholm, N. Shibata, E. Abe, S.J. Pennycoook, Annul. Rev. Mater. Res. 35 (2005) 539-569.

[27] A. Le Bail, H. Duroy, J.L. Forquet, Mater. Res. Bull. 23 (1988) 447-453.

[28] G.K. Williamson, W.H. Hall, Acta Metall, 1 (1953) 22-31.

[29] S. Özkara-Aydınoğlu, Int. J. Hydrogen Energy, 35 (2010) 12821-12828.

[30] S. Adhikari, S. Fernandeo, A. Haryanto, Energy Fuels 21 (2007) 2306-2310.

[31] B. Zhang, X. Tang, Y. Li, Y. Xu, W. Shen, Int. J. Hydrogen Energy 32 (2007) 2367-2373.

[32] A. Iriondo, L. Barrio, J.F. Cambra, P.L. Arias, M.B. Guemez, M.C. Sánchez-Sánchez, R.M. Navarro, J.L.G. Fierro, Int. J. Hydrogen Energy 35 (2010) 11622-11633.

[33] C.D. Dare, K.K. Pant, Renewable Energy 36 (2011) 3195-3202.

[34] M. Benito, R. Padilla, A. Serrano-Lotina, L. Rodríguez, J. Brey, L. Daza, J. Power Sources 192 (2009) 158-164.

[35] V. Michele, M. Signoretto, F. Menegazzo, A. Gallo, V. Dal Santo, G. Cruciani, G. Cerrato, Appl. Catal. B 111-112 (2012) 225-232.

[36] P. Laksmanan, P.P. Upare, N.-T. Le, Y.K. Hwang, H.R. Kim, J.-S. Chang, Appl. Catal. A 468 (2013) 260-268.

[37] Y.-C. Lin, Int. J. Hydrogen Energy 38 (2013) 2678-2700.

[38] B.C. Miranda, R.J. Chimentao, J.B.O. Santos, F. Gispert-Guirado, J. Llorca, F. Medina, F. López Borillo, J.E. Sueiras, Appl. Catal. B 147 (2014) 464-480.

[39] K.O. Christensen, D. Chen, R: Lodeng, A. Holmen, Appl. Catal. A 314 (2006) 9-22.

[40] Z. Wang, X. Shao, A. Larcher, K. Xie, D. Dong, C.-Z. Li, Catal. Today 216 (2013) 44-49.

[41] C. Zang, N. Sun, N. Zhao, W. Wei, J. Zhang, T. Zhao, Y. Sun, C. Sun, H. Liu, C.E. Snape, ChemCatChem 6 (2014) 640-648.

[42] M. C. J. Bradford, M. A. Vannice, Catal. Rev. Sci. Eng. 41 (1999) 1 –42.

[43] S. Tang, L. Ji, J. Lin, H. C. Zeng, K. L. Tan, K. Li, J. Catal. 194 (2000) 424 –430.

[44] F. Wang, Y. Li, W. Cai, E. Zhang, X. Zhou, W. Shen, Catal. Today 146 (2009) 31-36.

[45] B. Bachiller-Baeza, C. Mateos-Pedrero, M.A. Soria, A. Guerrero-Ruiz, U. Rodemerck, I. Rodríguez-Ramos. Appl. Catal. B: Environ. 129 (2013) 450-459.

[46] E. Desmoni, G.I. Casella, A. Morone, A.M. Salvi, Surf. Interf. Anal. 15 (1990) 627-634.

[47] H. Estrade-Szwarckopf, Carbon 42 (2004) 1713-1724.

[48] L. Guczi, G: Stefler, O. Geszli, I. Sajó, Z. Pászti, A. Trompos, Z. Schay, Appl. Catal. B 375 (2010) 236-246.

Capítulo 6

Conclusiones generales de la tesis

Contenido del capítulo

6.1 Conclusiones generales de la tesis doctoral

El estudio detallado de la actividad de los distintos catalizadores preparados para la reacción de hidrogenolisis del glicerol y para el reformado del glicerol con vapor de agua, junto con el minucioso trabajo de caracterización de los materiales, unido a la comparación de nuestros resultados con la bibliografía más relevante, nos ha permitido llegar a las siguientes conclusiones.

- En la reacción de hidrogenolisis del glicerol, se ha demostrado que el tratamiento del carbón activado con ácido nítrico genera distintos tipos de grupos oxigenados superficiales. Por otra parte, el carácter oxidante de la sal precursora $Ru(NO)(NO_3)_3$ también modifica la superficie del carbón activado para introducir grupos de oxígeno. Estos grupos de oxígeno aportan cierto carácter ácido al material, pero son térmicamente inestables y durante la reducción del catalizador (523 K) parte de dichos grupos ácidos (carboxílicos, lactónicos y anhídridos) se descomponen.
- La presencia de estos grupos oxigenados superficiales produce un aumento del tamaño de partícula de Ru en el soporte del carbón activado, pero el estudio detallado por microcalorimetría de quimisorción de CO nos muestra que la presencia de estos grupos oxigenados no produce cambios en la distribución energética de los sitios superficiales de las partículas de Ru. Luego la interacción del carbón activado con las partículas metálicas es débil.
- En cuanto al uso de los diferentes precursores de Ru, la microcalorimetría nos muestra que la distribución energética de sitios activos superficiales, cuando usamos el $RuCl_3 \cdot 3H_2O$ como compuesto precursor, es más heterogénea, en comparación con el $Ru(NO)(NO_3)_3$. Al usar el $RuCl_3 \cdot 3H_2O$ algunas especies cloruro quedan ancladas, ya que la reducción se lleva a cabo a baja

temperatura (523 K). Estas especies cloruro bloquean sitios activos para la adsorción del CO y además modifican las propiedades electrónicas de los átomos de Ru cercanos. El enlace sinérgico entre el Ru y el CO se ve interrumpido por la presencia de los cloruros, lo que produce una disminución sistemática de la entalpia de adsorción.

- En cuanto a la reacción de hidrogenolisis del glicerol, la actividad global de los catalizadores soportados en carbón activado se incrementa cuando la concentración de los grupos superficiales ácidos aumenta. Además, se favorece la formación del 1,2-propanodiol por la presencia de dichos grupos, ya que se lleva a cabo el mecanismo bifuncional, donde el ácido deshidrata el glicerol para formar el acetol que tras la hidrogenación, por parte del metal, forma el 1,2-propanodiol.
- En el catalizador Ru(Cl)-AC, con baja concentración de grupos ácidos, la catálisis del glicerol se produce en el metal, el cual favorece la ruptura del enlace C-C siendo el producto mayoritario el etilenglicol o productos de degradación sucesiva.
- Los soportes HSAG y CNT tienen la propiedad de donar electrones a las partículas de Ru estabilizando especies de Ru electronegativas ($Ru^{\delta-}$). Estas especies favorecen la formación del 1,2-propanodiol en la superficie metálica, pero simultáneamente realzan la sucesiva fragmentación del glicerol o subproductos formados mediante la ruptura del enlace C-C, siendo más acentuado este carácter a medida que aumenta la grafitización del soporte (CNT > HSAG).
- El catalizador de Ru/KL tiene centros ácidos Brönsted como consecuencia de la reducción de las especies de $RuCl_3{\cdot}3H_2O$ ancladas a la estructura de la zeolita. Estos centros mejoran la actividad y selectividad de este catalizador para formar el 1,2-propanodiol, siguiendo el mecanismo de la formación del acetol en los centros ácidos.

- En el reformado del glicerol con vapor de agua, se han sintetizado catalizadores activos para dicha reacción mediante dos métodos distintos. En primer lugar se sintetizaron catalizadores formados por un sistema ternario de NiO – MgO – CeO_2 mediante el método de Pechini, variando el contenido en NiO desde 5% al 30%. El segundo lugar se sintetizaron catalizadores formados por un óxido mixto de Ni-Ce con estructura tipo fluorita.

- El catalizador 20%NiO/MgO/CeO_2 presentó el mejor comportamiento catalítico dentro de la serie estudiada como consecuencia de un tamaño de partícula de NiO óptimo, que favorece la adsorción del $C_3H_8O_3$ en la superficie de dichas partículas.

- En los catalizadores de óxidos mixtos se observa, mediante la microscopía electrónica de transmisión, una evolución del catalizador después de ser reducido y testeado en la reacción, apareciendo fases separadas de Ni metálico y CeO_2.

- Se han sintetizado los novedosos reactores catalíticos asimétrico y simétrico *"hollow fibre"* confinando en su porosidad el catalizador 20%NiO/MgO/CeO_2 mediante el método de Pechini. El tamaño de partícula de NiO en el reactor asimétrico y simétrico viene definido por la porosidad de las fibras, siendo el tamaño medio de 8 nm en el caso del reactor asimétrico y de 3 nm para el simétrico.

- El uso de estos reactores molturados y testeados en un reactor de lecho fijo nos muestra que la reacción del reformado de glicerol es sensible a la estructura de la fase activa, siendo favorecida por tamaños de partícula más grandes.

- El uso de los reactores asimétrico y simétrico mejora considerablemente el rendimiento catalítico en comparación con el tradicional

reactor de lecho fijo. Esto es consecuencia de una intensificación de los procesos de transferencia entre el catalizador y los reactivos durante la reacción, con lo que en dichos sistemas catalíticos se origina una mayor actividad catalítica.

- El catalizador con 20%mol Ni en el óxido mixto de Ni y Ce presenta la composición óptima que produce una mayor estabilidad del catalizador, como consecuencia del contacto directo de la fase de Ni con la fase fluorita del CeO_2, lo que le proporciona unas propiedades excepcionales. Mayores contenidos en Ni producen segregación de las fases, lo que lleva al comportamiento como en los tradicionales catalizadores de Ni/CeO_2, preparados por métodos de impregnación a humedad incipiente, los cuales se desactivan también más rápidamente.

- El comportamiento catalítico del catalizador 20%mol Ni presenta una relación H_2/CO_2 de 7/3 a temperaturas más bajas que otros catalizadores encontrados en la bibliografía y durante largos tiempos de reacción (48 h). Además la producción de subproductos como CO y CH_4 es mínima, hecho contrario a lo ocurrido con los catalizadores tradicionales basados en Ni.

6.2 Conclusions

From the studies presented in this thesis and the comparison of our results with the bibliography, the following conclusions can be drawn:

- The treatment of activated carbons with nitric acid produces different superficial oxygen groups. On the other hand, the use of $Ru(NO)(NO_3)_3$ as a metal precursor also introduces superficial oxygen groups, because this precursor has oxidant character. These superficial oxygen groups (carboxylic, carbonylic, cetonic, phenolic, and alcoholic, among others) present acid character, but during the reduction step of the catalysts (at 523 K) these groups partly decompose.
- The Ru catalysts supported on activated carbon are modified by the presence of these oxygen groups, resulting in Ru particles bigger in sizes. In contrast, the energetic distribution of the Ru surface active sites, detected by CO chemisorption coupled with calorimetry, does not change with the presence of these oxygen groups. This fact means that the interaction between oxidized activated carbons and Ru precursors is weak.
- The catalysts synthesized using $RuCl_3 \cdot 3H_2O$ as precursor have a more heterogeneous distribution of surface active sites, as determined by microcalorimetric studies of CO chemisorption. In contrast, the use of $Ru(NO)(NO_3)_3$ as a metal precursor originates a more homogeneous distribution of Ru actives sites. Also some chloride species can remain anchored on the catalysts, when $RuCl_3 \cdot 3H_2O$ is used as a metal precursor, probably because the reduction temperature is too low (523 K). This chloride species block some of the surface active sites, therefore part of the CO chemisorption is inhibited. Moreover, these chloride species alter the electronic properties of Ru atoms, resulting that synergic bonds between Ru and CO are weakened.

- In the glycerol hydrogenolysis reaction, the catalyst activity increases when the concentration of the acid groups on the carbon support increases. Furthermore, the presence of these groups improves the selectivity towards 1,2-propanediol because a bifunctional mechanism takes place. The acid sites dehydrate the glycerol to obtain the intermediate (acetol) followed by successive hydrogenation of this intermediate to produces 1,2-propanediol.
- In the Ru(Cl)-AC (with low concentration of acid groups) the hydrogenolysis of glycerol occurs on the metallic Ru which produces the C-C cleavage. For this reason, the mainly products obtained is ethylene glycol or methane.
- The HSAG and CNT supports have electron donor properties which promote formation of electron-rich metal species ($Ru^{\delta-}$) in Ru/HSAG and Ru/CNT catalysts. These $Ru^{\delta-}$ species favor formations of 1,2-propanediol and also enhances the successive C-C cleavage to obtain undesired products such as methane.
- The Ru/KL catalyst has Brönsted acid sites, resulting from the reduction of the chlorinated ruthenium species bonded to the zeolite framework. This acid sites improve the activity and selectivity through 1,2-propanediol, because a bifunctional mechanism is generated using these acid sites and the metal sites.
- NiO-MgO-CeO_2 catalysts were synthesized using a sol-gel method (Pechini method) with different loading of NiO, between 5 to 30%. Furthermore, Ni-Ce mixed oxide catalyst with fluorite structure was also synthetized. Both catalytic systems were tested in the glycerol steam reforming with good performance.
- In the NiO-MgO-CeO_2 catalysts, the 20%NiO-MgO-CeO_2 shows the best catalytic activity, probably because exhibits an optimum particle size which favors the $C_3H_8O_3$ conversion.

- New catalytic microreactors were synthetized using asymmetric and symmetric hollow fibres. The 20%NiO/MgO/CeO_2 catalyst was confined in the finger-like and sponge-like porosity of these hollow fibre reactors. The average NiO particle sizes in asymmetric and symmetric hollow fibre are 8 nm and 3 nm respectively. The difference in particle size is consequence of the intrinsic porosity of the hollow fibres.
- The use of these asymmetric and symmetric reactors ground and tested in a fixed-bed reactor reveals that glycerol steam reforming reaction is a sensitive particle size reaction.
- The asymmetric and symmetric hollow fibre reactors enhance the catalytic properties compared with the traditional fix-bed reactor. This behavior can be explained due to the intensification of the contact among reactants and the catalyst during the reaction.
- 20% Ni-Ce mixed oxide having fluorite-type structure presents an optimum and stable catalytic performance in the glycerol steam reforming reaction, because the Ni is stabilized by contact with ceria. Increasing the Ni loading implies formation of two Ni phases, one with direct contact with Ce and other without contact. This last Ni phase has similar performance to traditional Ni/CeO_2 catalysts, and consequently suffer fast deactivation process.
- Interestingly the 20% Ni-Ce catalyst produces a H_2/CO_2 molar ratio close to 7/3 at significantly lower temperatures and also this ratio is constant in a long catalytic run (48 h) in comparison with the literature. Consequently, production of by-products such as CO and CH_4 was kept to a minimum, contrarily to usual Ni-based reforming catalysts.

Anexos

Contenido del capítulo

1. Publicaciones presentadas en la tesis doctoral

Applied Surface Science 287 (2013) 108–116

Contents lists available at ScienceDirect

Applied Surface Science

journal homepage: www.elsevier.com/locate/apsusc

Effect of the functional groups of carbon on the surface and catalytic properties of Ru/C catalysts for hydrogenolysis of glycerol

E. Gallegos-Suarez[a,b], M. Pérez-Cadenas[b], A. Guerrero-Ruiz[b,c], I. Rodriguez-Ramos[a,c], A. Arcoya[a,c,*]

[a] Departamento de Química Inorgánica y Técnica, Facultad de Ciencias, UNED, Paseo Senda del Rey nº 9, 28040 Madrid, Spain
[b] Instituto de Catálisis y Petroleoquímica, CSIC, Marie Curie nº 2, L-10, 28049 Madrid, Spain
[c] Unidad Asociada UNED ICP-CSIC, Group Design and Applied Heterogeneous Catalysis, Spain

ARTICLE INFO

Article history:
Received 15 July 2013
Received in revised form 6 September 2013
Accepted 15 September 2013
Available online 25 September 2013

Keywords:
Glycerol hydrogenolysis
1,2-Propanediol
Ethylene glycol
Ru/carbon supported catalysts
Carboxylic groups

ABSTRACT

Ruthenium catalysts supported on activated carbons, original (AC) and treated with nitric acid (AC-Ox) were prepared by incipient wetness impregnation from either chloride (Cl) or nitroxyl nitrate (n) precursors. These catalysts were characterized by TG, XPS, TEM, TPD-MS and CO adsorption microcalorimetry and evaluated in the hydrogenolysis of glycerol in the liquid phase, at 453 K and 8 MPa. Studies by TEM show that ruthenium particles supported on AC-Ox are larger than on AC, without any effect of the nature of the metal precursor. However, adsorption of CO on the ex-chloride catalysts is inhibited in comparison with that of the ex-nitroxyl nitrate catalysts. Catalysts characterization by TG, TPD-MS and XPS reveals that the nitric acid treatment and the nitroxyl nitrate precursor generate oxygenated groups on the carbon surface, which provide acid properties to the catalysts, although they are partly destroyed during the reduction treatment applied to the catalysts. The sequence of the overall TOF, Ru(Cl)/AC < Ru(n)/AC < Ru(Cl)/AC-Ox ≈ Ru(n)/AC-Ox, reasonably parallels the population increase of surface acid groups. Participation of the —COOH groups in the transformation of glycerol into 1,2-propanediol is verified by using the admixture Ru(Cl)/AC+AC-Ox as catalyst. In this case, since AC-Ox was not thermally treated and no loss of oxygenated groups occurred, TOF and selectivity toward 1,2-propanediol improve in comparison with those of the more active catalysts.

1. Introduction

Glycerol is one of the ten top building blocks in the biorefinery feedstocks [1] because it appears as an important byproduct in the biodiesel industry [2]. Since the selectivity of the process toward glycerol is 10% and the biodiesel production is growing, the surplus glycerol needs to be transformed into other more valuable products. With this aim, important catalytic processes, such as dehydration to acrolein [3,4], oxidation for producing dihydroxyacetone [5,6] or glyceric acid [7,8] and degradation until hydrogen production by steam reforming [9–12] among other, have been developed.

In order to obtain raw materials for synthesis of polymers, plastics, pharmaceuticals, farming products and automotive fuels, some glycols such as 1,2-propanediol, 1,3-propanediol and ethylene glycol are highly demanded [13–15]. In this context hydrogenolysis of glycerol for producing those valuable products is an alternative process to the more conventional routes based on the hydration of either propylene or ethylene oxides [16–18]. Hydrogenolysis of glycerol has been performed on various supported noble metals, Rh and Ir-based catalysts being the most active [19–26] as it occurs for other reactions involving hydrogen [27,28]. However, Rh and Ir-based catalysts were not suitable to the glycerol conversion to 1,2-propanediol because of high reaction rate of the consecutive hydrogenolysis of 1,2-propanediol. Regarding the glycerol hydrogenolysis to 1,2-propanediol, ruthenium is one of the most suitable active components for the catalysts [29] but it simultaneously induces the C—C cleavage leading to lower chain products, even methane [30]. In contrast, copper presents low hydrogenolysis activity but it is highly selective toward the target product 1,2-propanediol, due to its intrinsic ability to selectively cleave the C—O bond [31–33]. Selectivity toward 1,2-propanediol over Ru-supported catalyst has been improved by using additives as CaO or NaOH [34], K, Cu and Mo [35] sulfurized metal catalysts [30], bimetal catalysts like Ru—Pt, Ru—Au and Ru—Cu [36,37] or admixtures of Ru and Pt supported catalysts [38]. On the other hand ruthenium supported catalysts over inorganic materials as SiO_2, Al_2O_3, ZrO_2 [39], TiO_2 [40,41], hydrotalcite [42], bentonite [43] and also on carbon nanotubes [44] are reported to be highly active

* Corresponding author at: Instituto de Catálisis y Petroleoquímica, Marie Curie nº 2, L-10, 28049 Madrid, Spain. Fax: +34 915854760.
E-mail address: aarcoya@icp.csic.es (A. Arcoya).

0169-4332/$ – see front matter © 2013 Elsevier B.V. All rights reserved.
http://dx.doi.org/10.1016/j.apsusc.2013.09.087

Thermochimica Acta 567 (2013) 112–117

Contents lists available at SciVerse ScienceDirect

Thermochimica Acta

journal homepage: www.elsevier.com/locate/tca

Surface properties of Ru particles supported on carbon materials: A microcalorimetric study of the effects over the CO chemisorptions of residual anionic species

A. Guerrero-Ruiz[a,b,*], E. Gallegos-Suárez[a,c], L. Gonzalo-Chacón[c], I. Rodríguez-Ramos[c]

[a] Dpto. Química Inorgánica y Técnica, Fac. de Ciencias, UNED, c/Senda del Rey nº9, 28040 Madrid, Spain
[b] Grupo de Diseño y Aplicación de Catalizadores Heterogéneos, Unidad Asociada UNED-CSIC (ICP), Spain
[c] Instituto de Catálisis y Petroleoquímica, CSIC, c/Marie Curie 2, 28049 Madrid, Spain

ARTICLE INFO

Article history:
Received 14 September 2012
Received in revised form 31 October 2012
Accepted 15 November 2012
Available online 23 November 2012

Keywords:
Supported metal catalysts
Carbon supports
CO adsorption
Microcalorimetry

ABSTRACT

Chemisorption of CO combined with microcalorimetry has been applied to study the nature, number and adsorption strength distribution of surface sites exposed by carbon-supported Ru catalysts. A comparative analysis of the CO chemisorption on different Ru catalysts, prepared using two different metal precursors, $RuCl_3 \cdot xH_2O$ and $Ru(NO)(NO_3)_3$, has been carried out. An activated carbon and the corresponding derivative where oxygen surface groups were incorporated, as well as carbon nanotubes and a high surface area graphite, were used as catalytic supports. Based on previous temperature programmed reduction studies, all the catalysts were reduced under hydrogen flow at 523 K or at 573 K. The CO adsorption differential enthalpy profiles show that $Ru(NO)(NO_3)_3$ precursor produces more homogeneous surface site distribution in the Ru nanocrystals, in comparison with those prepared from $RuCl_3$, as well as higher values of enthalpies in the medium range of coverage. As a possible explanation for this effect, residual chloride species remaining after reduction treatment in the ex-chloride catalysts, that can be anchored to the Ru nanoparticles weakening the CO adsorption, have been considered. This behavior occurs for the three studied carbon supports. On the other hand, the oxygen surface groups incorporated on the activated carbon seem not to modify the CO adsorption properties of the catalysts, independently of the precursor employed.

1. Introduction

Adsorption calorimetry has been widely used to measure the energy of interaction of probe molecules with the surface of the catalysts, which is a parameter related with its surface structure [1]. Pioneers studies by Gravelle et al. have employed Tian-Calvet calorimeters to measure heats of hydrogen and CO chemisorptions on supported metal catalysts [2–4]. In this cases Ni and Ni-Cu supported nanoparticles where investigated, being demonstrated that CO chemisorption is an interesting tool for studying active metal surface sites. This is due, among others, to the well known CO molecule binding mechanism of chemisorption, which is highly sensitive to modifications of the electronic properties of the adsorbing sites and to the changes in surface topology [1,5]. In many cases CO chemisorption calorimetric data are complementarily analyzed with spectroscopic techniques [6] [7–9], for instance Fourier-transformed Infrared Spectroscopy (FTIR), but when carbon materials are used as supports, the surface structure of the deposited nanometallic particles can be hardly characterized by these spectroscopic techniques, and chemisorption microcalorimetry rises as the more applicable technique.

On the other hand, the preparation and activation of carbon supported metal catalysts require a series of steps that merit a further understanding. The method of preparation and the metal precursor are some preliminary aspects to be considered, but also the activation steps are important, usually consisting in drying and reduction. Thus, if the reduction temperature is too high we can assure that the metallic surface sites are free of residual adsorbed species, but possibly we are producing particles larger in sizes than when we reduce at an adequate temperature. In general, choosing these reduction temperatures will be based on previous temperature programmed reduction experiments, conducted over the dried materials. In summary, the generation of metallic nanoparticles over carbon materials, with more or less developed porosities and with various graphitic structures at their surface, is a relatively complex process from the chemical point of view [10]. Finally, it

* Corresponding author at: Departamento de Química Inorgánica y Técnica, Facultad de Ciencias, UNED, Senda del rey, s/n, 28040 Madrid. Spain. Fax: +34 915854760.
E-mail addresses: aguerrero@ccia.uned.es, aguerrero@icp.csic.es (A. Guerrero-Ruiz).

0040-6031/$ – see front matter © 2012 Elsevier B.V. All rights reserved.
http://dx.doi.org/10.1016/j.tca.2012.11.019

Chemical Engineering Journal 262 (2015) 326–333

Contents lists available at ScienceDirect

Chemical Engineering Journal

journal homepage: www.elsevier.com/locate/cej

Comparative study of the hydrogenolysis of glycerol over Ru-based catalysts supported on activated carbon, graphite, carbon nanotubes and KL-zeolite

E. Gallegos-Suarez [a,b], A. Guerrero-Ruiz [b,c], I. Rodriguez-Ramos [a,c], A. Arcoya [a,c,*]

[a] Instituto de Catálisis y Petroleoquímica, CSIC, Marie Curie n° 2, L-10, 28049 Madrid, Spain
[b] Departamento de Química Inorgánica y Técnica, Facultad de Ciencias, UNED, Paseo Senda del Rey n° 9, 28040 Madrid, Spain
[c] Unidad Asociada UNED ICP-CSIC, Group Design and Applied Heterogeneous Catalysis, Spain

HIGHLIGHTS

- Activated carbon, graphite, carbon nanotubes and KL-zeolite as Ru-catalyst supports for hydrogenolysis of glycerol.
- Ruthenium supported on activated carbon produces mainly ethylene glycol.
- Reduction of ruthenium generates Brönsted acid sites in the KL-zeolite which enhance the selectivity toward 1,2-PDO.
- Graphite and carbon nanotubes promote formation of Ru^{δ} species and favor largely production of methane and 1,2-propanediol.

GRAPHICAL ABSTRACT

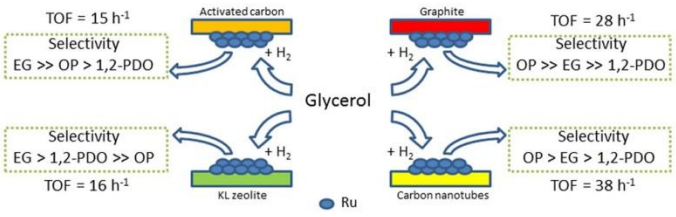

EG – ethyleneglycol ; 1,2-PDO – 1,2-propanediol ; OP – other products

ARTICLE INFO

Article history:
Received 23 July 2014
Received in revised form 25 September 2014
Accepted 30 September 2014
Available online 7 October 2014

Keywords:
Glycerol hydrogenolysis
Ruthenium catalysts
KL-zeolite
Carbon nanotubes
Propanediol
Ethylene glycol

ABSTRACT

Supported ruthenium catalysts were prepared by incipient wetness impregnation of three different carbon materials: activated carbon (AC), high surface area graphite (HSAG) and multiwalled carbon nanotubes (CNT). Another catalyst was prepared by treating KL zeolite with $RuCl_3 \cdot xH_2O$ in aqueous solution. All these samples were characterized by temperature programmed reduction (TPR), CO chemisorption coupled with microcalorimetry and transmission electron microscopy (TEM). The reduced catalysts were tested in the hydrogenolysis of glycerol in the liquid phase, under a reaction pressure of 8 MPa and isothermally at the reaction temperature of 453 K. The CO microcalorimetry measurements evidenced that electron donor properties of graphite and carbon nanotubes promote formation of electron-rich metal species (Ru^{δ}) in Ru/HSAG and Ru/CNT catalysts, which not only favors formation of 1,2-propanediol from glycerol but also enhances the successive C—C cleavage, with formation of undesired products, mainly methane. For Ru/KL the occurrence of Brönsted acid sites, resulting of the reduction of the chlorinated ruthenium species bonded to the zeolite framework, was verified by temperature programmed desorption (TPD) of NH_3. Furthermore, observations by TEM of the Ru/KL catalyst showed an important population of metal nanoparticles lower than 1 nm, part of which exhibits electron deficient character as indicated by the CO microcalorimetry. As a consequence, the transformation of glycerol into 1,2-PDO over Ru/KL seems to be promoted through formation of the intermediate acetol on acid sites,

* Corresponding author at: Instituto de Catálisis y Petroleoquímica, Marie Curie n° 2, L10, 28049 Madrid, Spain. Fax: +34 915854760.
E-mail address: aarcoya@icp.csic.es (A. Arcoya).

http://dx.doi.org/10.1016/j.cej.2014.09.121

Catalysis Today 233 (2014) 21–30

Contents lists available at ScienceDirect

Catalysis Today

journal homepage: www.elsevier.com/locate/cattod

Ceramic hollow fibres catalytic enhanced reactors for glycerol steam reforming

E. Gallegos-Suárez[a,b], F.R. García-García[c,*], I.D. González-Jiménez[d], I. Rodríguez-Ramos[a], A. Guerreo-Ruiz[b], K. Li[c]

[a] Instituto de Catálisis y Petroleoquímica, C/Marie Curie 2, Cantoblanco, Madrid 28049, Spain
[b] Grupo de Diseño y Aplicación de Catalizadores Heterogéneos, UA: UNED-ICP/CSIC, Madrid, Spain
[c] Department of Chemical Engineering, Imperial College London, South Kensington Campus, London SW7 2AZ, UK
[d] Inorganic Chemistry and Catalysis, Debye Institute for Nanomaterial Science, Utrecht University, Sorbonelaan 16, Utrecht 3584 CA, The Netherlands

ARTICLE INFO

Article history:
Available online 16 March 2014

Keywords:
$NiO/MgO/CeO_2$ catalyst
Ceramic hollow fibre reactor
Glycerol steam reforming

ABSTRACT

In this study, $NiO/MgO/CeO_2$ catalysts with Ni content from 5% to 30% were synthetized by sol–gel method and tested in a fixed-bed reactor (FBR) in the glycerol steam reforming (GSR) reaction. The catalysts were characterized by N_2 adsorption isotherms at −196 °C (S_{BET}), X-ray diffraction (XRD), H_2 temperature programmed reduction (H_2-TPR), transmission electron microscopy (TEM) and energy dispersive X-ray (EDX). The 20% $NiO/MgO/CeO_2$ catalyst, which showed the highest catalytic activity in GSR reaction, was selected to be deposited in the finger-like region of the asymmetric Al_2O_3 hollow fibre and the sponge-like region of the symmetric Al_2O_3 hollow fibre in the development of the asymmetric hollow fibre reactor (AHFR) and symmetric hollow fibre reactor (SHFR), respectively. The impregnated ceramic substrates were characterized by scanning electron microscopy (SEM), EDX and TEM. The performances of the AHFR and SHFR were compared with that in a conventional FBR during the GSR reaction. Both AHFR and SHFR were operating at "dead-end" configuration at a temperature range from 250 °C to 550 °C, atmospheric pressure and in a reactant mixture of steam and glycerol (16:1 molar ratio). At 550 °C the glycerol conversion in the AHFR and SHFR was 70% and 46%, respectively, which are 5 and 2 times higher than that obtained in the FBR. The different performances of the AHFR and SHFR could be explained due to the unlike catalyst particle size deposited in the asymmetric and symmetric substrates, 8 nm and 3 nm, respectively.

1. Introduction

The expansion of the biodiesel market involves the development of new approaches such as enhanced hollow fibre reactors which can efficiently transform the glycerol excess into more valuable products. Glycerol is by far the main by-product (10%, w/w) obtained during the manufacturing of biodiesel through transesterification of vegetable oil and animal fats. Although glycerol is used in food, pharmaceutical, cosmetic and tobacco industries, its commercial market has been limited due to its low production a few years ago [1,2]. Nevertheless, since 1990 an increasing interest has been observed in the biodiesel as alternative and renewable fuel which has increased the annual production of glycerol. It is estimated that 4 billion gallons of glycerol will be produced by 2016 [3]. This represents an opportunity for new applications of the glycerol in the current market. In this contest, glycerol has been proposed as a promising renewable source of H_2 since it can be decomposed in the presence of H_2O to produce H_2:

$$C_3H_8O_3 + 3H_2O \longrightarrow 3CO_2 + 7H_2 \Delta H = 128\ kJ/mol \quad (1)$$

In addition, the CO_2 produced during the reaction is consumed for biomass growth which nearly closes the carbon loop. On the other hand, the chemical–physical properties of glycerol, liquid at room temperature and atmospheric pressure along with its non-toxicity possibly make it useful as a "storage-molecule" of H_2 [4].

The glycerol steam reforming (GSR) reaction has been extensively studied in the open literature over both noble and non-noble metal supported catalysts [5–9]. Nevertheless, it is still uncertain which could be the most suitable catalyst for industrial large scale applications. Among all the metal supported catalysts reported, Pt, Ru, Pd and Ni based catalysts show the better catalytic activity and selectivity for hydrogen production due to their ability to cleave

* Corresponding author. Tel.: +44 07 540 865 301.
E-mail address: f.garcia-garcia@imperial.ac.uk (F.R. García-García).

http://dx.doi.org/10.1016/j.cattod.2014.02.040
0920-5861/

Applied Catalysis B: Environmental 165 (2015) 139–148

Contents lists available at ScienceDirect

Applied Catalysis B: Environmental

journal homepage: www.elsevier.com/locate/apcatb

Efficient and stable Ni–Ce glycerol reforming catalysts: Chemical imaging using X-ray electron and scanning transmission microscopy

E. Gallegos-Suárez[a,b], A. Guerrero-Ruiz[b], M. Fernández-García[a,*], I. Rodríguez-Ramos[a,*], A. Kubacka[a,*]

[a] Instituto de Catálisis y Petroleoquímica, CSIC, C/Marie Curie 2, 28049 Madrid, Spain
[b] Dpto Química Inorgánica, UNED, Paseo Senda del Rey 9, 28040 Madrid, Spain

ARTICLE INFO

Article history:
Received 5 August 2014
Received in revised form
29 September 2014
Accepted 3 October 2014
Available online 12 October 2014

Keywords:
Ni
Glycerol
Metal–support interaction
Hydrogen production

ABSTRACT

Nickel–ceria composite catalysts prepared by a microemulsion method showed outstanding catalytic behavior in hydrogen production by glycerol steam reforming. Contrarily to usual Ni-based catalysts, the system allows long-term stability and nearly absence of by-products, particularly methane and carbon monoxide. With the help of scanning transmission electron microscopy and energy dispersive X-ray spectroscopy we confirmed the key role played by an intimate intermixing of Ni and Ceria components at reaction conditions. In addition, chemical imaging maps as well as more conventional techniques, such as Temperature Programmed Oxidation (TPO) and X-ray Photoelectron Spectroscopy (XPS) were used to identify the carbon containing (including coke) species nature and to establishing their chemical relevance. Combination of these techniques points out that the optimum interphase contact, reached for a specific 20:80 molar Ni:Ce formulation, allows; (i) to keep the Ni particle size controlled with absence of significant formation of coke and thus without deleterious effects on the long-term stability of the catalysts; and (ii) to eliminate undesirable side reactions such as methanation.

1. Introduction

The settlement of a hydrogen economy derived from renewable energy sources may provide significant benefits by solving problems related to the energy crisis and environmental pollution [1,2]. Among numerous renewable candidates, glycerol seems to provide significant advantages. Being a biomass derivative, glycerol is currently produced in large quantities in the process of transesterification of fatty acids into biodiesel [3]. During this process glycerol is normally generated at a rate of 1 mol of glycerol for every 3 mol of methyl ester synthesized, which accounts for approximately 10 wt% of the total product [2,3]. Other bio-based processes also produce glycerol; for example, up to 4 wt% of this molecule (with respect to the initial sugar weight) is obtained in fermentation of sugars oriented to ethanol formation [2]. Due to constant increment of biodiesel production it is estimated that by 2015, 1.54 million tons of glycerol will be generated worldwide [3]. Thus, in order to make the chemicals obtained from the biomass sector competitive with chemicals from fossil fuels, all of this glycerol should be efficiently processed.

Bio-oils including glycerol have numerous potential applications which includes its usage in boilers for heat and electricity, in engines and turbines for electricity, in chemicals production such as phenols, organic acids, and oxygenates or in transportation fuel production [1–3]. The latter would be the more important from a economic point of view, however bio-oil derived transportation fuels require expensive upgrading techniques, and this route is currently less attractive for motor fuels production. To alleviate this disadvantage, reforming of bio-oil has been proposed and employed to produce hydrogen, a key fuel for the future.

The steam reforming of glycerol appears thus as a potential alternative for producing hydrogen in the near future with significant impact in the viability of numerous bio-refining processes [1–4]. Steam reforming of glycerol is an endothermic process and the offgas composition is governed by the (formal) equilibrium between the decomposition, reaction (1), water gas shift (WGS), reaction (2), and methanation, reaction (3) [5]:

$$C_3H_8O_3 \rightarrow 3CO + 4H_2 \quad (1)$$

$$CO + H_2O \leftrightarrow CO_2 + H_2 \quad (2)$$

$$CO + 3H_2 \rightarrow CH_4 + H_2O \quad (3)$$

* Corresponding authors. Tel.: +34 915854939; fax: +34 915854760.
E-mail addresses: mgf@icp.csic.es (M. Fernández-García), irodriguez@icp.csic.es (I. Rodríguez-Ramos), ak@icp.csic.es (A. Kubacka).

http://dx.doi.org/10.1016/j.apcatb.2014.10.007
0926-3373/

2 Índice de figuras

Capítulo 1

Capítulo 3

Capítulo 4

4.2. Effect of the functional groups of carbon on the surface and catalytic properties of Ru/C catalysts for hydrogenolysis of glycerol.

4.3 Surface properties of Ru particles supported on carbon materials: a microcalorimetric study of the effects over the CO chemisorptions of residual anionic species

4.4 Comparative study of the hydrogenolysis of glycerol over Ru-based catalysts supported on activated carbon, graphite, carbon nanotubes and KL-zeolite

Capítulo 5

5.2 Ceramic hollow fibres catalytic enhanced reactors for glycerol steam reforming

5.3 Efficient and Stable Ni-Ce Glycerol Reforming Catalysts: Chemical Imaging using X-ray Electron and Scanning Transmission Microscopy

3 Índice de tablas

Capítulo 4

4.2. Effect of the functional groups of carbon on the surface and catalytic properties of Ru/C catalysts for hydrogenolysis of glycerol.

4.3 Surface properties of Ru particles supported on carbon materials: a microcalorimetric study of the effects over the CO chemisorptions of residual anionic species

4.4 Comparative study of the hydrogenolysis of glycerol over Ru-based catalysts supported on activated carbon, graphite, carbon nanotubes and KL-zeolite

Capítulo 5

5.2 Ceramic hollow fibres catalytic enhanced reactors for glycerol steam reforming.

5.3 Efficient and Stable Ni-Ce Glycerol Reforming Catalysts: Chemical Imaging using X-ray Electron and Scanning Transmission Microscopy

4 Breve Curriculum Vitae

Esteban Gallegos Suárez nació en 1985 en Lanjarón (Granada). En 2008 se licenció en Ciencias Químicas por la Universidad de Granada. En 2009 obtuvo el título de Máster en Ciencias Químicas impartido por la Universidad de Granada. Ese mismo año fue contratado con cargo a proyecto por la Universidad Nacional de Educación a Distancia (UNED) lo que le permitió iniciar su carrera investigadora en el grupo de Diseño Molecular de Catalizadores Heterogéneos, unidad asociada entre dicha universidad y el Instituto de Catálisis y Petroleoquímica (CSIC). Trabajó bajo la dirección del Dr. Antonio Guerrero Ruiz y la Dra. Inmaculada Rodríguez Ramos. En 2011 consiguió una beca FPU propia de la UNED lo que le permitió desarrollar la tesis doctoral en el mismo grupo. En el año 2012 realizó una estancia predoctoral en el Imperial College en Londres durante 3 meses bajo la supervisión del Profesor Kan Li. En 2013 realizó otra estancia predoctoral en Queen University en Belfast durante 2 meses bajo la supervisión del Profesor Alexandre Goguet. Ha participado además en numerosos congresos nacionales e internacionales relacionados con sus temas de investigación y es coautor de 16 publicaciones (5 derivadas de esta tesis doctoral). En ese período ha codigirido junto a la Dra. Inmaculada Rodríguez trabajos fin de grado de estudiantes de máster y ha impartido clases prácticas de microscopía electrónica de transmisión.